

*Bridging the gap between in vitro and in vivo*

an MRI toolkit  
for milk protein  
digestion studies

Momwarid Mayar



## Propositions

1. The capabilities of MRI for studying human intra-gastric digestion render animal experiments in this field unnecessary.  
(this thesis)
2. Measuring pH during intra-gastric milk protein digestion is more informative than measuring protein hydrolysis.  
(this thesis)
3. Relying on male-female comparisons in biomedical research oversimplifies the complex relationship between sex-related factors and health status.
4. Integrating environmental impact assessment when designing experiments is crucial for sustainable laboratory research.
5. Abolishing different levels in secondary education in the Netherlands will result in more equal opportunities.
6. Implementation of a dual-status system for refugees is an inefficient approach for addressing the refugee crisis.

Propositions belonging to the thesis, entitled

Bridging the gap between *in vitro* and *in vivo*: an MRI toolkit for milk protein digestion studies

Morwarid Mayar  
Wageningen, 14 May 2024







Bridging the gap between *in vitro* and *in vivo*:  
an MRI toolkit for milk protein digestion studies

Morwarid Mayar







## **Thesis committee**

### **Promotor**

Prof. Dr J.P.M. van Duynhoven

Special professor, Magnetic Resonance in Relation to Food

Wageningen University & Research

### **Co-promotors**

Dr P.A.M. Smeets

Senior researcher, Human Nutrition and Health

Wageningen University & Research

Dr C. Terenzi

Assistant professor, Biophysics

Wageningen University & Research

### **Other members**

Prof. Dr T. Huppertz, Wageningen University & Research

Prof. Dr P. Gowland, University of Nottingham, United Kingdom

Dr G. Pagès, French National Institute for Agriculture, Food and Environment, Paris, France

Prof. Dr T. Scheenen, Radboud University Medical Center, Nijmegen

This research was conducted under the auspices of VLAG graduate school (Biobased, Biomolecular, Chemical Food, and Nutrition Sciences)

Bridging the gap between *in vitro* and *in vivo*:  
an MRI toolkit for milk protein digestion studies

Morwarid Mayar

**Thesis**

submitted in fulfilment of the requirements for the degree of doctor

at Wageningen University

by the authority of the Rector Magnificus,

Prof. Dr C. Kroeze,

in the presence of the

Thesis committee appointed by the Academic Board

to be defended in public

on Tuesday 14 May 2024

at 1.30 p.m. in the Omnia Auditorium.



Morwarid Mayar

Bridging the gap between *in vitro* and *in vivo*: an MRI toolkit for milk protein digestion studies,

244 pages.

PhD thesis, Wageningen University, Wageningen, the Netherlands (2024)

With references, with summaries in English and Dutch

DOI: <https://doi.org/10.18174/649771>

# Contents

	<b>Page</b>
Chapter 1. Introduction	7
Chapter 2. Non-invasive monitoring of <i>in vitro</i> gastric milk protein digestion kinetics by <sup>1</sup> H NMR magnetization transfer	47
Chapter 3. <i>In vitro</i> <sup>1</sup> H MT and CEST MRI mapping of gastrointestinal milk protein breakdown	81
Chapter 4. MRI assessment of pH and coagulation during semi-dynamic <i>in vitro</i> gastric digestion of milk proteins	113
Chapter 5. Magnetization Transfer MRI of intra-gastric milk digestion: a feasibility study in humans	153
Chapter 6. General Discussion	187
Chapter 7. Summary	222
Samenvatting	226
Acknowledgements/Dankwoord	234
List of publications	241
Overview of completed training activities	242
About the author	243

**CHAPTER**

# 1



# Introduction



## 1.1. Dietary proteins

Proteins are indispensable building blocks of life; they serve numerous structural and biochemical functions in our bodies, such as growing and repairing tissues, driving metabolic processes, and supporting the immune system. Proteins are synthesized in our cells from amino acids (AAs), which can be divided into essential and non-essential AAs. Essential AAs must be obtained through the consumption of dietary proteins, which are broken down into absorbable and bioavailable AAs in our digestive tract. Protein digestion is not an isolated process, but encompasses several complex interrelated physiological processes at multiple length scales (Bornhorst et al., 2016). Gaining a better understanding of the complex processes involved in digestion can help food researchers optimize our food and its processing for optimal protein digestion, thereby enhancing nutritional benefits (Mackie et al., 2020). Furthermore, a better understanding of digestion can aid identifying the root causes of digestive disorders and diseases, leading to more effective diagnostic and treatment approaches.

Protein intake and digestion are especially critical for infants to support their rapid growth and their developing immune system. Milk is the only source of nutrients, including proteins, right after birth and it remains one of the main protein sources throughout the first year of life. Although mother's milk is considered the ideal food for infants during the first year of life (World Health Organization, 2001), it is not always available, and it is commonly substituted by infant formulas mainly produced from cow's milk.

## 1.2. Cow's milk: source of high-quality proteins

Cow's milk is an important source of high-quality proteins in the human diet. The major proteins in milk are caseins and whey proteins (WPs), constituting approximately 80% and 20%, respectively. Both caseins and WPs are considered complete proteins, meaning that they contain high levels of all essential AAs required by the human body. Additionally, these proteins have excellent digestibility, as evaluated by the digestible indispensable amino acid score (DIAAS), leading to their high bioavailability (Dupont & Tomé, 2019).



Caseins and WPs possess different physicochemical characteristics. Whey proteins are globular proteins with an isoelectric point (pI) of 4.2 and 5.1 for  $\alpha$ -lactalbumin and  $\beta$ -lactoglobulin, respectively. The casein fraction consists of  $\alpha$ s1-,  $\alpha$ s2-,  $\beta$ -, and  $\kappa$ -casein, which lack a tertiary structure and are present in milk as large casein micelles (100-200 nm). Caseins have an isoelectric point (pI) of 4.6. Both WPs and caseins have a negative surface charge at the neutral pH of milk. The processing of milk includes heat treatment, which can impact the structure of milk proteins and subsequently affect their digestion (van Lieshout et al., 2020; Walstra et al., 2006).

### 1.2.1. Milk processing

Industrial milk processing (Fig. 1.1) is required to ensure microbiological safety, and to extend the shelf life of the product. Milk processing includes filtration to remove large particles, followed by milk skimming or homogenization to reduce fat content and to improve texture and taste. Heat treatment may be applied before or after homogenization. The two most common heat treatments in milk processing are pasteurization and sterilization.

Pasteurization can be low (typically 72 °C for around 15 s or 63 °C for 30 min) or high (>80 °C, several min). High pasteurization can lead to partial or full denaturation of the WPs. Caseins are not directly affected by pasteurization due to their lack of a tertiary structure. However, denatured WPs can aggregate on the casein micelles: this process is mainly driven by the formation of disulphide bridges between  $\beta$ -lactoglobulin and  $\kappa$ -casein (Kethireddipalli & Hill, 2015; van Lieshout et al., 2020).

Sterilization is performed at higher temperatures, leading to a longer shelf life compared to pasteurized milk. Sterilization methods include in-bottle sterilization and ultra-high temperature (UHT) treatment. In-bottle sterilization has a very high cumulative heat load, causing full WP denaturation and extensive glycation of lysine, leading to undesired browning and flavour changes in the finished product.

On the other hand, UHT treatment at 130 °C for a few seconds results in limited chemical modifications while preserving the colour and flavour of the original product. Therefore, UHT treatment is currently the most common sterilization method (Borad et al., 2017; van Lieshout et al., 2020; Walstra et al., 2006).

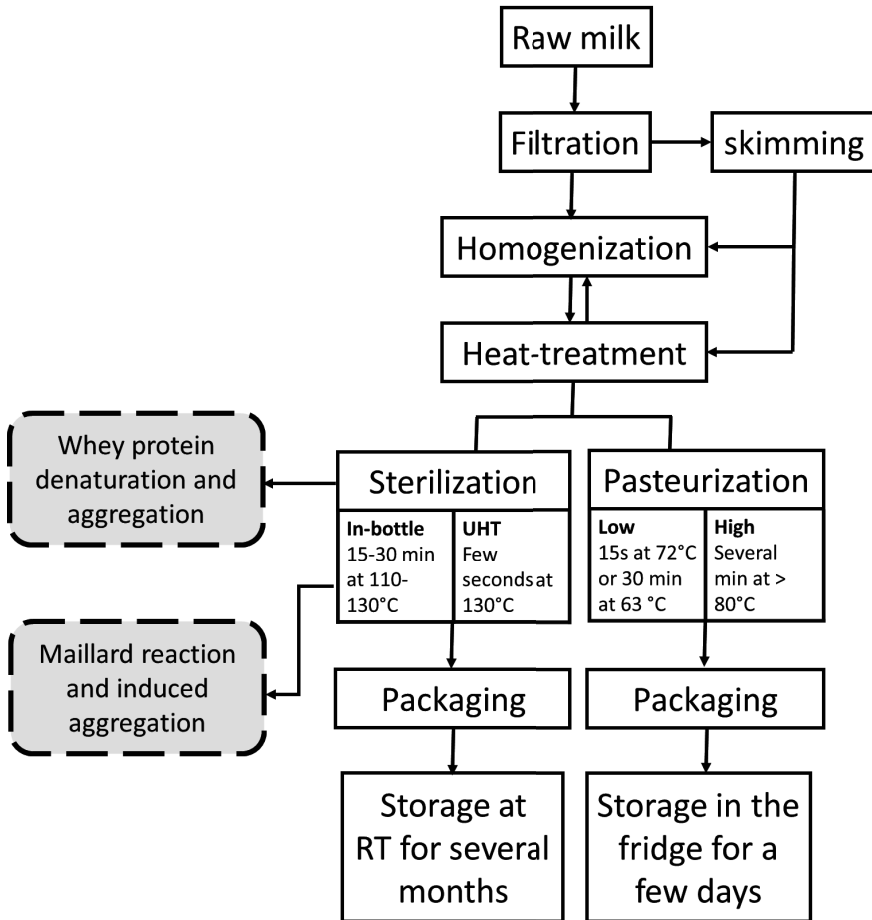


**Figure 1.1.** Liquid processing of milk, including the different types of heating conditions applied and their effect on the protein structure. RT = room temperature.

## 1.3. Milk protein digestion

### 1.3.1. The digestive tract

As shown in Fig. 1.2a, digestion starts in the oral phase, during which the food is mixed with saliva, and solid foods are broken down into small particles by mastication to form a bolus that can be swallowed. Saliva also contains the enzyme amylase, which initiates the hydrolysis of carbohydrates. For liquid foods, such as milk, the oral phase does not play a significant role, and only results in a slight dilution of the food with saliva (Sensoy, 2021).

The second phase is gastric digestion, which involves mechanical and biochemical breakdown and structuring of the food bolus into a partially digested semi-solid mass called the chyme. The stomach (Fig 1.2b), is a J-shaped muscular organ that consists of four major parts: the fundus, corpus (body), antrum, and pylorus. The fundus stores swallowed air or gas produced during digestion. The corpus is the largest section of the stomach, and serves as a reservoir for ingested food. It is also responsible for mixing the food bolus with gastric juice, resulting in partially digested food. Mixing is achieved by the peristaltic contractions of the stomach, made possible by the action of the longitudinal, circular, and oblique muscles in the stomach wall. The antrum lies below the corpus and stores the chyme until it is delivered to the intestines, a process known as gastric emptying (GE), which is regulated by hormonal and neural feedback responses (Camilleri, 2019; Goyal et al., 2019). The antral grinding reduces the size of solid particles down to less than 1-2 mm, enabling these to bypass pyloric sieving and enter the duodenum (Mackie et al., 2020; Sensoy, 2021).

Protein hydrolysis starts in the stomach, during which pepsin cleaves the peptide bonds of non-terminal AAs. The content of the stomach varies both spatially and temporally. Initially, after the bolus enters the stomach, the pH is relatively high, and pepsin activity is low. However, in response to, and in anticipation of the meal, the gastric mucosa secretes acidic gastric juice, lowering the pH and activating pepsinogen, the inactive zymogen of pepsin. pH plays a crucial role in gastric digestion of proteins, because pepsin becomes active at pH 5.5 with maximum peptic activity at pH 2 (Piper & Fenton, 1965). The rate at which the

stomach pH decreases and, hence, the pepsin activity increases, depends on the buffering capacity of the food. For example, milk, which is high in proteins, has a high buffering capacity, leading to a relatively slow decrease in gastric pH (Wang et al., 2018).

The third phase takes place in the small intestines, which comprise the duodenum, the jejunum, and the ileum. In the duodenum, the pH is neutralized, and the chyme is mixed with bile and pancreatic enzymes. The pancreatic enzymes secreted into the duodenum include proteases, lipases, and amylase, which are present at relatively high enzyme activities. This, combined with strong intestinal mixing leads to the production of hydrolysis products that are taken up in the epithelium of the jejunum and ileum for further hydrolysis and absorption into the bloodstream (Erickson & Kim, 1990; Sensoy, 2021).



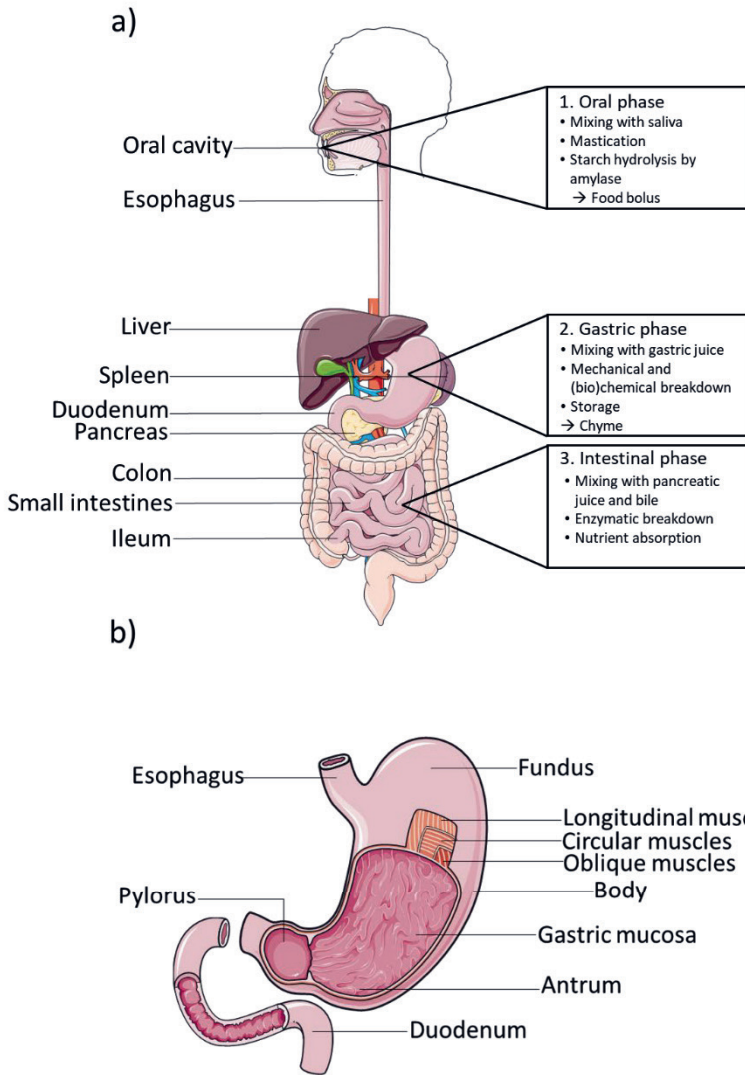


**Figure 1.2.** Schematic overview of a) the digestive tract and a description of the three phases of food digestion (oral, gastric and intestinal). b) The anatomy of the stomach. Adapted from Servier Medical Art.

### 1.3.2. Zooming in on gastric milk protein digestion

Caseins and WPs behave differently during gastric digestion because of their different physicochemical characteristics. Native WPs remain largely intact during gastric digestion due to the inaccessibility of the cleavage sites. Their breakdown primarily takes place in the small intestines (Huppertz & Chia, 2021).

During gastric digestion, the acidic gastric juice and pepsin will, respectively, neutralize the negative charge, and hydrolyse the  $\kappa$ -caseins at the surface of the casein micelles. As a result, the casein micelles aggregate and form a semi-solid coagulum (Fig. 1.3a) (Horstman & Huppertz, 2023; Huppertz & Chia, 2021). This is followed by solubilization and hydrolysis of the semi-solid protein coagulum into soluble proteins and relatively large peptides. These proteins and peptides are then transported into the intestinal phase, where they are further hydrolysed into tri- and di-peptides (Dupont & Tomé, 2019). Gastric coagulation of caseins has been linked to regulating the passage of proteins from the stomach into the intestine which, in turn, may facilitate a sustained release of AAs into the bloodstream, maximizing the utilization of the proteins (Lacroix et al., 2006; Soop et al., 2012). Moreover, it ensures that the digestive capacity of the intestines does not become overloaded, which is especially important for infants, the elderly and groups with digestive disorders. However, gastric coagulation and further breakdown of milk proteins are highly affected by milk processing. For example, heat-induced modification of milk proteins can influence the accessibility of the cleavage sites to digestive proteases and, as a result, these modifications may affect the overall digestion of milk proteins. Generally, protein denaturation increases, while aggregation and glycation reduce, the accessibility of the cleavage sites in WPs to proteases (van Lieshout et al., 2020). Research on the effect of heat treatment on milk protein digestion primarily rely on *in vitro* and animal models.

These studies have demonstrated that casein and WP aggregation during heat treatment leads to the formation of a looser and softer milk protein coagulum during gastric digestion, as shown in Fig. 1.3b (Ahlborn et al., 2023; Ye et al., 2016, 2019)

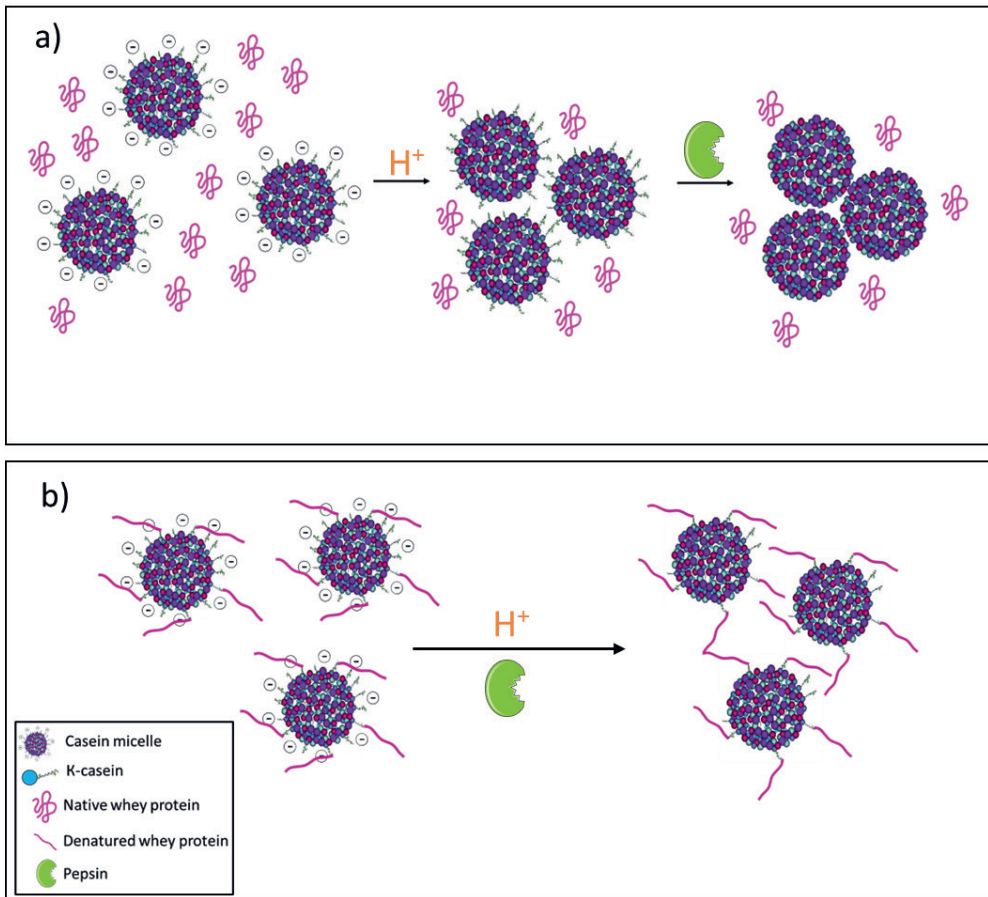


**Figure 1.3.** Schematic representation of: a) casein micelles and their acid- and pepsin-induced aggregation in unheated milk under gastric conditions, and consequent formation of a semi-solid coagulum; b) the effect of heat treatment on casein coagulation. Heating results in denatured WPs, which aggregate onto the casein micelle via s-s bridges with the  $\kappa$ -caseins, leading to a looser casein coagulum during gastric digestion. Adapted from (Villa et al., 2018).

## 1.4. Current state-of-the-art in digestion research

Various approaches have been developed and employed to study food digestion. These include: *in vitro* models, that simulate human digestion; animal models and, to a lesser extent, *in vivo* methods. These various approaches, along with their strengths and limitations, are summarized in Table 1.1.

### 1.4.1. *In vitro* digestion models

The use of *in vitro* models of human digestion has become widespread due to their ease of sampling for biochemical and physical analysis, their simplicity, controllability, reproducibility, and lack of ethical constraints. *In vitro* digestion models can range from simple static models, to complex and highly sophisticated dynamic models. Static models have the advantage of being cost-effective, readily available, and adaptable to simulate digestion in different age groups.

These models are particularly useful for investigating structure breakdown, mass transport, hydrolysis kinetics under controlled conditions (Mackie et al., 2020). The INFOGEST international network on food digestion has developed static *in vitro* models that simulate digestion in adults (Brodkorb et al., 2019), full-term 1 month old infants (Ménard et al., 2018), and the elderly population (Ménard et al., 2023). However, static models do not fully replicate the complexity of the digestive tract, as the digestive fluids and food materials remain constant, and the digestion parameters, such as meal-to-digestive fluid ratio, pH, and enzyme activity, are often based on the digestion conditions at the emptying halftime or endpoint.

*In vivo* gastric digestion is a complex and dynamic process that involves many feedback controls. For instance, the secretion of digestive fluids in response to, and, in anticipation of a meal is automatically regulated through hormonal and neural responses. Additionally, the pH, ionic strength, and enzyme activity change over time as gastric fluid is secreted, and food is emptied from the stomach into the intestines. Sophisticated dynamic models, such as the TNO gastro-Intestinal model (TIM), the Dynamic Gastric Model (DGM) (Thuenemann et al., 2015), and the Human Gastric Simulator (HGS) (Kong & Singh, 2010), are physiologically

more realistic than static models, because they include gastric secretion and emptying, they consider the shape of the stomach or intestines, and they even simulate gastric and intestinal motility. Despite providing valuable insights, these models are highly complex, time-consuming, expensive, and not readily available. In this regard, semi-dynamic models are advantageous as they incorporate the transient nature of gastric secretions and emptying, while being relatively simple and easily usable in any laboratory (Deng et al., 2022; Mulet-Cabero et al., 2020).

*In vitro* models are typically combined with biochemical and physical analysis of the digesta samples to monitor digestion. Common analysis techniques include DUMAS or bicinchoninic acid assay (BCA) for protein content measurements, o-phthalaldehyde assay for determining the degree of hydrolysis, and SDS-PAGE or high-performance liquid chromatography (HPLC) for assessing the size of peptides that are formed during digestion. Liquid chromatography coupled to mass spectrometry (LC-MS) is used to identify specific peptides that are formed during digestion, which can be useful for assessing their subsequent immunological responses (Liang et al., 2022; Macierzanka et al., 2012; Sousa et al., 2020). To assess the digesta's physical characteristics, photographs are paired with rheology, texture analysis, confocal laser scanning microscopy (CLSM), and electron microscopy (EM) (Li et al., 2022; Ye et al., 2016).

#### 1.4.2. *In vivo* animal models

Animal models are typically used for determining protein digestibility. These studies are mostly conducted in rats or pigs, with pigs being a more suitable model for human digestion because their GI tract and diet is similar to that of humans. The digestible indispensable amino acid score (DIAAS) (Mathai et al., 2017) is determined at the ileal level in pigs and is currently recommended by the Food and Agricultural Organization (FAO) for assessing protein quality and digestibility of foods for human consumption. Animal models have also been used to study gastric milk protein coagulation *in vivo* (Ahlborn et al., 2023; Roy et al., 2022; Ye et al., 2019). These studies include sampling of the gastric content after sacrificing the animals. The samples are analysed using techniques typically employed to monitor *in vitro* digestion, which enables comparing *in vivo* and *in vitro* results.

However, animal models, while being more physiologically realistic compared to *in vitro* models, are costly, resource demanding and, most importantly, ethically controversial. Therefore, innovative tools are required to enable non-invasive monitoring of digestion in humans. This, in turn, can aid in optimizing and verifying *in vitro* digestion models.

### 1.4.3. *In vivo* methods to study digestion in humans

*In vivo* protein digestion studies in humans can be challenging due to practical constraints, biological complexity, and ethical obstacles. Most *in vivo* studies in humans involve indirect measurements of endpoints, such as the concentration of AAs in the blood (Horstman et al., 2021; Lacroix et al., 2008; Nyakayiru et al., 2020; Trommelen et al., 2020), faecal nitrogen levels, and AA in the ileal digesta (Bandyopadhyay et al., 2022). The latter is only possible in patients with an ileostomy due to its invasiveness. While these endpoint measures can provide useful information about protein digestibility and bioavailability, they do not provide information on the preceding digestive processes.




Specific knowledge on food digestion mechanisms and kinetics at different locations within the GI tract may provide more useful insights than endpoints. However, sampling the gastric content through gastric aspirates is highly invasive and burdensome for participants, and it only provides a sample of a small part of the liquid fraction at an unknown location due to the heterogeneity of the gastric chyme. Due to its invasiveness, this approach has only been used to study gastric milk digestion in pre-term infants who already have a nasogastric tube in place (de Oliveira et al., 2017; Demers-Mathieu et al., 2018).

An emerging technology that could overcome some of the challenges of *in vivo* research involves the use of ingestible camera and sensing capsules. These capsules can record videos and conduct measurements of pH, temperature, and pressure in the gastrointestinal tract (Cheng et al., 2021; Qureshi, 2004; Wang et al., 2005). However, these devices are limited to the location at which they are placed, which cannot be controlled.

To gain a better understanding of *in vivo* digestion in humans and to aid in the validation of *in vitro* digestion models, novel non-invasive measurement techniques that can be used to monitor changes in space and time during *in vitro* and *in vivo* digestion are required. Magnetic Resonance Imaging (MRI) can be utilized to obtain detailed anatomical images, and contrast based on the local composition and structure of tissues. Therefore, MRI has the potential to provide spatially-resolved information about the gastric content and its changes during digestion, and may ultimately aid in bridging the gap between *in vitro* digestion models and real-life digestion physiology in a non-invasive manner (Smeets, Deng, Van Eijnatten, & Mayar, 2020).



**Table 1.1.** Overview of *in vitro* and *in vivo* approaches for studying gastric food digestion, including the level of information that they provide, and their strengths and limitations. BP = blood parameters and GA = gastric aspirates.

	<i>In vitro</i> models	<i>In vivo</i> animal models	<i>In vivo</i> human studies
			
	<b>Static</b>	<b>Semi-dynamic</b>	<b>Dynamic</b>
<b>Information</b>	<ul style="list-style-type: none"> <li>• End-point biochemical and structural characteristics</li> </ul>	<ul style="list-style-type: none"> <li>• Dynamic biochemical and structural characteristics</li> </ul>	<ul style="list-style-type: none"> <li>• Dynamic (bio)chemical and structural characteristics</li> </ul>
<b>Strengths</b>	<ul style="list-style-type: none"> <li>✓ Simple, cheap, adaptable and controllable</li> <li>✓ Relatively simple, cheap, adaptable and controllable</li> <li>✓ Simulates biochemical dynamics</li> </ul>	<ul style="list-style-type: none"> <li>✓ Simulates biochemical and mechanical dynamics</li> <li>✓ Similar physiology as humans</li> </ul>	<ul style="list-style-type: none"> <li>• Blood nutrient and hormone levels (BP)</li> <li>• Biochemical and structural characteristics (GA)</li> <li>• Gastric emptying and motility</li> <li>• Subjective ratings of appetite and wellbeing</li> <li>✓ May provide physiologically significant outcomes</li> </ul>
<b>Limitations</b>	<ul style="list-style-type: none"> <li>- Lacks physiological complexity</li> <li>- Lacks gastric motility and hormone response</li> </ul>	<ul style="list-style-type: none"> <li>- Complex and expensive</li> <li>- Lacks hormone response</li> <li>- Ethical constraints</li> <li>- Complex and expensive</li> </ul>	<ul style="list-style-type: none"> <li>- Indirect (BP)</li> <li>- End-point information (BP)</li> <li>- Invasive (GA)</li> <li>- Complex and expensive</li> </ul>

## 1.5. MRI: an emerging tool in digestion research

MRI is a non-invasive and non-ionizing medical imaging technology that is based on the principles of Nuclear Magnetic Resonance (NMR). In NMR, a combination of a strong magnet and radio frequency (RF) pulses is used to generate RF signals arising from certain nuclei of interest. Protons ( $^1\text{H}$ ) are the most frequently investigated nuclei due to their high natural abundance and widespread presence in most materials: these factors are both responsible for the typically high signal-to-noise ratio (SNR) and sensitivity of  $^1\text{H}$  NMR measurements. The  $^1\text{H}$  NMR signals can be utilized to obtain information on various properties of molecules, including their structure, conformation, dynamics and quantity. In MRI, magnetic field gradients are included to encode spatial information in the RF signal, allowing the construction of detailed cross-sectional images of different parts of the object studied or human body, such as the abdomen in the latter case (Fig. 1.4). In the clinic, MRI is widely used to diagnose diseases, monitor disease progression, and assess treatment effectiveness.

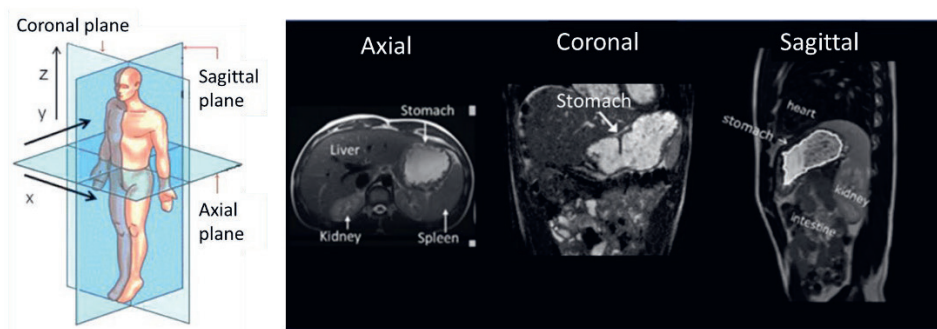


**Figure. 1.4.** Schematic representation of the slice directions in MRI (left-most figure) and corresponding images of the abdominal area reproduced from (Camps et al., 2018; Carneiro et al., 2022; Deng et al., 2023) with permission. Note that images are from different studies, and differ in the meal given to participants, explaining the difference in the intensities of the stomach contents.

In gastric digestion research, MRI is predominantly used to measure GE by obtaining gastric content volumes over time (Camps et al., 2016, 2021). The most common approaches for measuring GE involve indirect tracer-based methods like C-isotope breath analysis, paracetamol absorption tests, and gamma scintigraphy. The latter involves the use of ionizing radiation (Abell et al., 2008; Glerup et al., 2007). MRI offers distinct advantages over these methods: it is less dependent on the food matrix, does not use ionizing radiation, provides anatomical detail, and it has shown lower inter-observer variability compared to C-isotope breath analysis, making it the preferred method for measuring GE (Camps et al., 2018). In addition MRI has been used to assess gastric motility (de Jonge et al., 2018; de Zwart & de Roos, 2010; Lu et al., 2022) and for assessment of phase separation (Camps et al., 2021; Hoad et al., 2004). While measuring GE is useful, complementing it with structural- and molecular-level information is necessary for a more comprehensive understanding of gastric digestion in humans.

## **1.6. Potential $^1\text{H}$ NMR/MRI techniques for monitoring gastric protein digestion**

NMR and MRI are highly versatile techniques and can offer a diverse range of specialized scan sequences tailored to meet specific clinical or research needs. These scan sequences include methods capable of providing structural and molecular information. By integrating data on GE with quantitative MRI markers, a more comprehensive evaluation of gastric digestion and the effects of heat-induced changes on digestion might be obtained. A selection of NMR/MRI techniques, which are promising for studying gastric protein digestion, is discussed below.

### 1.6.1. Spectroscopy

$^1\text{H}$  NMR spectroscopy is commonly used in chemistry, biology, food sciences, and clinical research to identify and quantify molecular properties. In NMR/MRI experiments, an RF pulse is applied to rotate the net longitudinal magnetization vector,  $M_z$ , from its equilibrium along a  $z$ -axis towards the  $xy$ - or transverse plane. The magnetization vector starts to precess around the  $B_0$ -field with a characteristic frequency, known as the Larmor frequency:  $\omega_0 = \gamma B_0$ , where  $\gamma$  is the gyromagnetic ratio of the nucleus. The precession induces an oscillating signal known as the free induction decay (FID). To obtain a 1D  $^1\text{H}$  spectrum, this FID signal is converted into the frequency-domain NMR spectrum using the Fourier Transformation (FT). In reality, the precession frequency is dependent on the effective magnetic field experienced by the nucleus, which is affected by magnetic field inhomogeneities and the electron density around the nucleus. The latter gives rise to the chemical shift ( $\delta$ ) in parts per million (ppm), which forms the basis of NMR spectroscopy. In an NMR spectrum, the  $\delta$  of the peaks provides molecular structure information, and their areas are proportional to the number of nuclei giving rise to the peaks, allowing identification and quantification of several components in samples or tissues (Keeler, 2010).

The combination of molecular-level and quantitative information that can be obtained with NMR spectroscopy makes it an interesting technique for examining food digestion. It has previously been used to monitor *in vitro* protein (Bordoni et al., 2011; Vidal et al., 2016) and lipid digestion (Nieva-Echevarría et al., 2016). However, the application of NMR spectroscopy for *in vivo* monitoring of gastric digestion is not feasible because its typical acquisition time of several minutes is too long to enable monitoring of a dynamic process, and the acquisition of spectra is limited to a single voxel, which is not ideal due to the heterogenous composition of the digesta.

Additionally, the sensitivity of MR spectroscopy at the field strength of clinical scanners (0.2 to 3T) is not sufficient to detect low-abundant proteins, and their breakdown products. Moreover, *in vivo* NMR spectroscopy is highly sensitive to motion (breathing, patient movement, organ contractions), due to motion-related issues during signal averaging, which is necessary for obtaining sufficient SNR (Alger, 2010).

### 1.6.2. Diffusion

NMR enables the measurement of, among other molecular properties, the self-diffusion coefficient of  $^1\text{H}$  nuclei within one or several molecular constituents of a sample. The self-diffusion coefficient is sensitive to the radius and molecular/structural environment of the molecule under study. This technique is extensively used in material science studies, including food applications, *e.g.* to probe the microstructure of heterogenous matrices indirectly via characterizing the molecular mobility of water or solutes therein (Dai & Matsukawa, 2012; Mariette, 2017; Schork et al., 2020). Applications related to gastric milk protein digestion include the monitoring of acid- and rennet-induced casein coagulation, and measurements of WP solutions and gels using water or polyethylene glycol (PEG) as a probe (Colsenet et al., 2005; Le Feunteun et al., 2012; Mariette, 2017; Mariette et al., 2002).

In the context of clinical MRI, diffusion-weighted imaging (DWI) is used to generate imaging contrast based on differences in the water diffusion between the different biological tissues. Quantitative Apparent Diffusion Coefficient (ADC) maps can be obtained by fitting of diffusion weighted signals, which can be used as a tool to assess disease progression and treatment response (Baliyan et al., 2016; Bozzali et al., 2020; Lee et al., 2021). Diffusion tensor imaging (DTI) is an advanced MRI technique used for measuring structural anisotropy in muscle and brain tissue (Alexander et al., 2007; Heemskerk & Damon, 2007). While *in vitro* experiments have proven that self-diffusion coefficients can be used to probe

casein coagulation, such self-diffusion measurements of gastric digestion *in vivo* would be, in analogy to spectroscopy (section 1.6.1), too challenging.

Due to their limitations with regards to gastric food digestion research, spectroscopy and diffusion methods were deemed impractical and, thus, not pursued further. However, in addition to these techniques, there are several other MR techniques, such as relaxometry and saturation transfer, which are promising for monitoring different aspects of gastric food digestion. These techniques are summarized in Table 1.2 and elaborated upon in the subsequent sections.

### 1.6.3. Relaxometry

Relaxometry refers to measurements of the longitudinal ( $T_1$ ), transverse ( $T_2$ ) and rotating frame ( $T_{1\rho}$ ) NMR relaxation times. Following the application of an RF pulse, two relaxation processes take place: the longitudinal and transverse relaxation. Longitudinal relaxation refers to the return of the net magnetization to its equilibrium state, aligned with the magnetic field, after being perturbed by an RF pulse. The time constant associated with this longitudinal relaxation is referred to as  $T_1$ . Transverse relaxation is the process by which the  $xy$ -components of the net magnetization decay back to zero, as in the initial state before application of the RF pulse, by losing their phase coherence, and the time constant associated with this transverse relaxation process is  $T_2$ . The  $T_1$ - and  $T_2$ -values are influenced by re-orientational dynamics, as opposed to translational motion in diffusion NMR/MRI. The re-orientational dynamics of molecules are affected by sample-related factors like viscosity, molecular size, and macromolecular environment, leading to distinct NMR relaxation times. Longitudinal and transverse relaxation are, in some cases, described in terms of the relaxation rates, namely  $R_{1,2} = 1/T_{1,2}$ .

NMR relaxation times are utilized in, among others, clinical and food science applications to create  $T_1$ - or  $T_2$ -weighted contrast images, allowing the visualization of different tissues or phases in food systems. Specialized scan sequences, based on Carr-Purcell-Meiboom-Gill (CPMG) or Multi-Slice-Multi-Echo

(MSME) sequences, can be used to quantify the  $T_2$ -values. The  $T_1$ -values can be quantified using Inversion Recovery (IR) or Saturation Recovery (SR) pulse sequences. Because the  $T_1$ - and  $T_2$ -values can provide information on the state of water protons in food systems, they are commonly used to study food structure and composition, including those of dairy systems (Duynhoven et al., 2010; Mariette et al., 2012). In the context of digestion research,  $T_2$ -measurements have been used to study physico-chemical changes in WP hydrogels under static *in vitro* digestion conditions (Ozel et al., 2018). Deng et al. have explored both  $T_1$ - and  $T_2$ -measurements for monitoring gastric digestion of WP gels in static (Deng et al., 2020) and semi-dynamic (Deng et al., 2022) *in vitro* models as well as in a human trial (Deng et al., 2023). In the latter studies it was demonstrated that the  $T_2$ -values of the supernatant phase decreased during gastric digestion due to the release of proteins and large peptides from the gel matrix.  $T_2$ -mapping, combined with fat quantification, has recently been utilized to assess semi-dynamic *in vitro* digestion of a bread- and cheese meal (Musse et al., 2023). These studies showed that measurements of the  $T_2$ -values are valuable for monitoring digestion-mediated changes in the liquid phase of the digesta. However, conventional  $T_2$ -mapping cannot be used to directly detect (semi-solid) macromolecular protons with a short transverse relaxation time due to the long dead times of clinical MRI scanners of typically a few ms.

Ultra-short Echo Time (UTE) and Zero-Echo Time (ZTE) MRI techniques are designed to overcome this limitation, and can be used to capture signals from components with short transverse relaxation times of  $\geq 300 \mu\text{s}$  (Tyler et al., 2007; Weiger & Pruessmann, 2019). However, these techniques are still not capable of measuring the transverse magnetization decay for (semi-)solid macromolecular protons with  $T_2$ -values as short as 15-20  $\mu\text{s}$  (Hinrichs et al., 2007; Morrison et al., 1995). Furthermore, both conventional- and short- $T_2$  MRI techniques lack the sensitivity to detect low-abundant proteins and peptides.

The transverse relaxation time of water is also sensitive to macromolecular dynamics via  $^1\text{H}$  chemical exchange between macromolecules and water and diffusional averaging (Hills et al., 1989; Hills & Duce, 1990). CPMG dispersion measurements can be used to quantify the macromolecular dynamics by measuring the  $T_2$ -value at varying echo times. In the presence of chemical exchange, a variation of  $T_2$  as a function of the inverse of the echo time will be observed, resulting in a  $T_2$ -dispersion curve. This curve can be fitted with a two-site chemical exchange model to obtain parameters such as the exchange rate ( $R_{ex}$ ), the macromolecular proton fraction ( $p_m$ ), and the  $R_2$  of the macromolecular fraction ( $R_2^m$ ) (Carver & Richards, 1972). CPMG dispersion measurements have mainly been used in *in vitro* studies of macromolecular dynamics, including dairy systems (Gottwald et al., 2005; Hills et al., 1990), and currently there are no *in vivo* applications of this technique.

Another relaxometry technique is the measurement of  $T_{1\rho}$ -values, in which a spin-lock pulse with varying duration is applied after the first RF pulse to lock the magnetization in the transverse plane, resulting in a slower decay of the transverse magnetization component (Gilani & Sepponen, 2016). Measurements of  $T_{1\rho}$  have been applied in studies of cartilage depletion (Keenan et al., 2011; Stahl et al., 2009), liver fibrosis (Sirlin, 2011), Alzheimer's disease (Borthakur et al., 2008) and Parkinson's disease (Nestrasil et al., 2010). In analogy to  $T_2$ ,  $T_{1\rho}$ -dispersion measurements can be conducted by varying the amplitude of the spin-lock RF pulse. The obtained dispersion curves can be fitted with models of two- or three-site exchange to obtain  $R_{ex}$ ,  $p_m$ , and  $R_2^m$  (Palmer, 2014).  $T_{1\rho}$ -dispersion has been applied in *in vivo* human studies to assess chemical exchange in cartilage, skeletal muscle and brain (Adelnia et al., 2021; Wang et al., 2015). However, *in vivo* applications of this technique are limited due to long acquisition times of several minutes up to an hour, hardware limitations, and high specific absorption rates (SAR).



**Table 1.2.** Overview of potential NMR/MRI techniques for monitoring protein digestion with a summary of the markers/parameters that can be obtained, the information they provide, the *in vivo* applicability, and relevant applications. The colours of the cells classify the techniques as applicable (green), not applicable (red), and limited applicability (orange) for *in vivo* human studies. The applicable techniques that have already been explored for protein digestion are coloured in blue and those that are not yet explored for digestion research in green, highlighting the current research gap.

NMR/MRI techniques	Markers/Parameters	Information	In vivo applicability	Relevant <i>in vitro</i> and <i>in vivo</i> applications
<b>Relaxometry</b>				
Carr-Purcell-Meiboom-Gill (CPMG) Inversion/saturation recovery	Transverse relaxation rate of water ( $R_2^w$ ) Longitudinal relaxation rate of water ( $R_1^w$ )	Sensitive to: <ul style="list-style-type: none"> <li>water content and mobility</li> <li>macromolecular dynamics</li> </ul>	Yes	<i>In vitro</i> digestion of a bread and cheese meal (Muse et al., 2023) <i>In vitro</i> and <i>in vivo</i> WP gel digestion (Deng et al., 2020, 2022, 2023) <i>In vitro</i> digestion of WP and polysaccharide gels (Ozel et al., 2018)
CPMG dispersion	Exchange rate ( $R_{ex}$ ) Fraction of exchangeable solute protons ( $P_{ex}$ ) Transverse relaxation rate of the solute ( $R_2^s$ )	Quantification of: <ul style="list-style-type: none"> <li>slow to fast macromolecular dynamics</li> <li>can potentially be linked to macromolecular structure, concentration and pH</li> </ul>	No <i>in vivo</i> applications	None
Spin-lock	$R_1$ in the rotating frame ( $R_{1\rho}$ )	Sensitive to: <ul style="list-style-type: none"> <li>slow macromolecular dynamics</li> <li>macromolecular content</li> </ul>	Limited (hardware and SAR limitations)	Enzymatic degradation of proteoglycans in ex vivo cartilage (Collins et al., 2019)
Spin-lock dispersion	$R_{ex}$ $P_{ex}$ $R_2^s$	Quantification of: <ul style="list-style-type: none"> <li>slow macromolecular dynamics</li> <li>macromolecular content</li> <li>can potentially be linked to changes in macromolecular structure, concentration and pH</li> </ul>	Limited (hardware and SAR limitations)	<i>In vivo</i> proteoglycan and collagen depletion in cartilage (Wang et al., 2015)
<b>Saturation Transfer</b>				
MT	<b>Quantitative two-pool exchange fitting parameters</b> $R_{ex}$ $R_{ex}M_0^s / R_1^w$ $R_{SS}^s$ $R_{1\rho}^w$ $R_1^w$ <b>Semi-quantitative parameter</b> $MTTR$	Quantification of: <ul style="list-style-type: none"> <li>macromolecular mobility</li> <li>(semi)solid macromolecular content:</li> </ul>	Yes	None
CEST	<b>Quantitative multipool Lorentzian fitting</b> ss MT, NOE Solute amine, amide and hydroxyl CE <b>Semi-quantitative parameter</b> $MTTR_{ss,ym}$	Quantification of: <ul style="list-style-type: none"> <li>chemical exchange processes between macromolecules/metabolites and water</li> <li>can potentially be linked to macromolecular structure, concentration and pH</li> </ul>	Yes	<i>In vitro</i> BSA aggregation and enzymatic hydrolysis (Longo et al., 2014) pH mapping in phantoms (Longo, Sun, et al., 2014), in mice (Chen et al., 2017) and in human liver (Tang et al., 2020)

#### 1.6.4. Saturation Transfer NMR/MRI

Saturation Transfer (ST) techniques, which include Magnetization Transfer (MT) and Chemical Exchange Saturation Transfer (CEST), are specialized NMR/MRI techniques that enable the indirect detection of semi-solid or low-abundant soluble (macro)molecules by probing their interactions with surrounding water molecules (Ward et al., 2000; Wolff & Balaban, 1989). As depicted in Fig. 1.5a, these interactions include (i)  $^1\text{H}$  dipolar coupling between semi-solid macromolecules and water, (ii)  $^1\text{H}$  chemical exchange between amine, amide, and hydroxyl groups of (macro)molecules and water, and (iii) intra-molecular  $^1\text{H}$  dipolar coupling followed by  $^1\text{H}$  chemical exchange. The latter is referred to as the relayed Nuclear Overhauser Effect (rNOE) (Zhou et al., 2023).

ST measurements involve selectively saturating the (macro)molecular protons of interest by applying an RF pulse at their resonance frequency relative to that of water ( $\Delta$ ). This saturation pulse, characterized by a low amplitude ( $B_1$ ) and long duration ( $T_{sat}$ ), is applied preceding the image encoding and acquisition (Fig. 1.5b,c). As depicted in Fig. 1.5b, the saturation pulse can either be a continuous wave (CW) pulse or a train of RF pulses, with the latter approach reducing RF power deposition. Commonly utilized image encoding and acquisition schemes include the Rapid Acquisition with Refocused Echoes (RARE), also known as the Turbo Spin Echo (TSE), Echo Planar Imaging (EPI), and Gradient Recalled Echo (GRE) sequences (Zhang et al., 2023). The saturation is subsequently transferred from the (macro)molecular protons to bulk water protons via  $^1\text{H}$  dipolar coupling, chemical exchange, or a combination of both, causing a slight attenuation of the water signal. A single saturation transfer is insufficient to produce a detectable effect on the water signal. However, since the water pool is much larger than the (macro)molecular pool, each saturated (macro)molecular proton is replaced by a non-saturated water proton, which is again subjected to saturation. If the transfer is sufficiently fast, *e.g.* in the millisecond range, and the saturation time ( $T_{sat}$ ) is long enough, *e.g.* in the seconds range, prolonged saturation can lead to a substantial enhancement of the saturation effect, ultimately becoming visible in the water signal (Fig. 1.5c, right) (Van Zijl & Yadav, 2011; Wu et al., 2016).

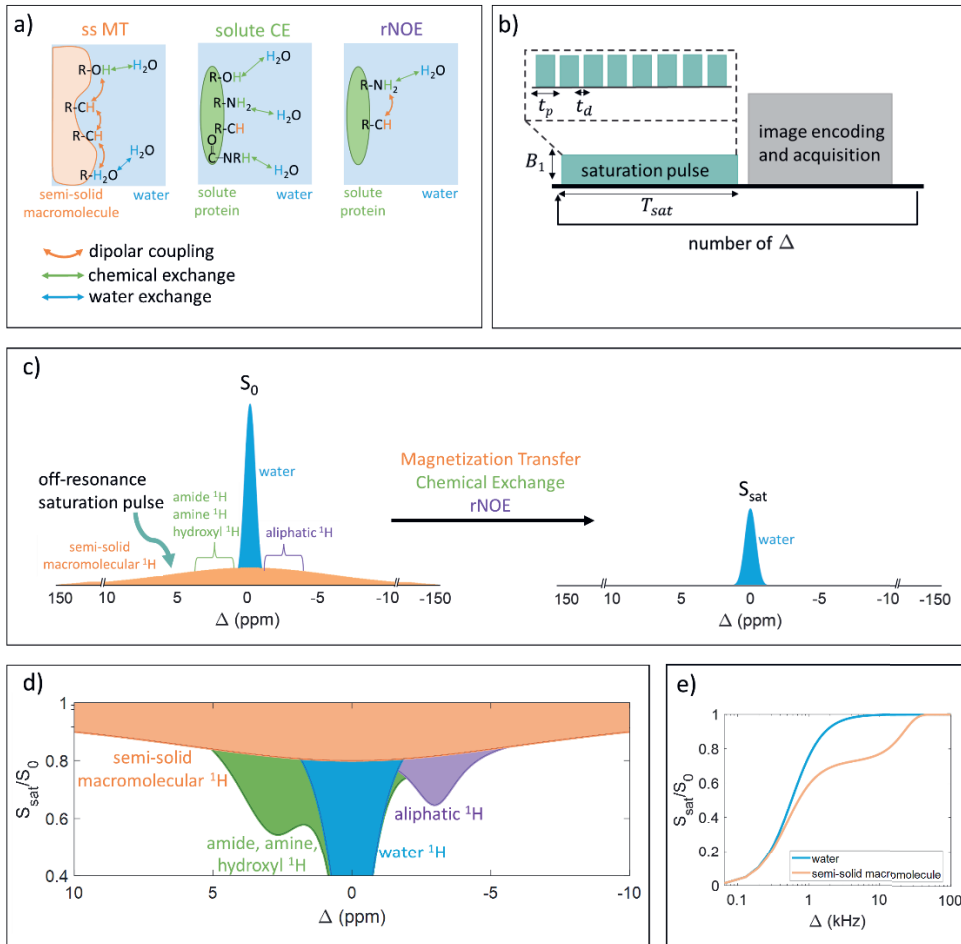


**Figure 1.5.** (a) Examples of possible ST pathways in MT and CEST MRI. (b) MT/CEST pulse sequence consisting of a selective RF pulse applied at a specific frequency offset ( $\Delta$ ) with a low amplitude ( $B_1$ ) and long duration ( $T_{sat}$ ) to saturate the  $^1H$  magnetization at the specific  $\Delta$  values, followed by the image encoding and acquisition. The saturation pulse can be a CW pulse or a train of RF pulses with a specific pulse length ( $t_p$ ) and inter-pulse delay ( $t_d$ ). (c) An example of a liquid state  $^1H$  NMR spectrum of a sample consisting of, besides mobile water, immobile semi-solid macromolecules and mobile proteins in solution, which are not detectable respectively due to their broad signal or low abundance (left). Reduction of the water signal intensity (right) as a result of magnetization transfer, chemical exchange or relayed NOE. (d) ST signals of different (macro)molecular entities plotted as a CEST spectrum, where the normalized water proton signal is reported vs. the  $\Delta$  values (ppm), relative to water ( $\Delta = 0$ ), used for selective saturation. (e) Common representation of ST data in MT MRI literature, where the normalized water proton signal is reported vs. the positive  $\Delta$  values (kHz) on a logarithmic scale.

The saturation pulse can be applied at various  $\Delta$  relative to the bulk water frequency, yielding a ST spectrum (Fig. 1.5d) that represents the ratio of the saturated ( $S_{sat}$ ) over unsaturated ( $S_0$ ) water  $^1\text{H}$  NMR signal as a function of  $\Delta$ . This spectrum may contain multiple contributions, including a direct water saturation peak, chemical exchange peaks originating from amine ( $\Delta = 2\text{-}3$  ppm), amide ( $\Delta = 3.5$  ppm), and hydroxyl ( $\Delta = 0.6\text{-}2$  ppm) protons, a broad semi-solid MT peak, and a rNOE peak ( $\Delta = -1.6\text{-}4.0$  ppm) (van Zijl et al., 2018). In MT literature, it is common to present the ST spectrum as shown in Fig. 1.5e, where the  $S_{sat}/S_0$  values are plotted vs. the positive  $\Delta$  values (KHz) on a logarithmic scale. This representation demonstrates that for pure water, where no magnetization transfer takes place, a sigmoid curve is observed, reflecting the direct saturation of the water signal. In contrast, for a semi-solid macromolecular system, magnetization transfer causes a distinct shape that deviates from the sigmoid shape observed for pure water. This distinct shape reflects the exchange rate, as well as the size and relaxation rates of the macromolecular proton pool (Henkelman et al., 1993).

The CEST effect relies on several key factors, including the chemical exchange rate, relaxation rates, chemical shift difference with water, magnetic field strength ( $B_0$ ), and the accessibility of the labile (macro)molecular protons to water. Notably, for proteins, their state, e.g. intact, denatured, aggregated, or hydrolysed, can influence the accessibility of amine, amide, and hydroxyl groups to water. The exchange rate is further influenced by factors such as pH, temperature and (macro)molecular concentration (van Zijl et al., 2018). The main applications of  $^1\text{H}$  CEST MRI are focused on detecting changes in pH (Chen et al., 2017; Longo, Sun, et al., 2014; Tang et al., 2020), (macro)molecular structure (Goerke et al., 2015), and concentrations (Chan et al., 2016). It has previously been used to study *in vitro* aggregation and hydrolysis of bovine serum albumin (BSA)(Longo et al., 2014).

The semi-solid MT effect observed in the CEST spectrum arises from the transfer of magnetization between semi-solid macromolecular protons and bulk water protons. This transfer is predominantly facilitated by  $^1\text{H}$  dipolar coupling, but chemical exchange and water exchange may also be involved (Fig. 1.5a) (Zhou et al., 2023).  $^1\text{H}$  dipolar coupling refers to the magnetic interactions between protons that are close to each other in space; when two protons are in close

proximity to each other, their magnetic dipolar fields interact, resulting in the transfer of magnetization between these nuclei. It is to be noted that the semi-solid MT signal at  $\Delta \leq 5$  ppm (Fig. 1.5d), in addition to  $^1\text{H}$  dipolar coupling effects, may contain contributions from  $^1\text{H}$  chemical exchange between labile (macro)molecular protons and water from both the semi-solid and solute phase. Hence, to ensure selectivity for semi-solid macromolecules, a  $\Delta \geq 5$  ppm should be chosen. Overall, MT MRI can provide information on the interactions between protons bound to the semi-solid macromolecules and the surrounding water molecules, which is expected to change upon variations in the semi-solid macromolecular mobility and content (Henkelman et al., 2001; van Zijl et al., 2018; Zhou et al., 2023). This technique is used, in clinical research, to detect myelin content and assess structural integrity in the brain (Bourbon-Teles et al., 2019; Chen et al., 2022; Van Obberghen et al., 2018), or to evaluate cartilage structural integrity (Welsch et al., 2008).

In MT and CEST research, there are two main data acquisition and analysis approaches. The first approach involves measuring, at varying  $\Delta$  values, the full spectrum and fitting it with multipool exchange, or Lorentzian, models to extract quantitative parameters (Henkelman et al., 1993; Zaiß et al., 2011). Alternatively, for more rapid measurements, the saturation pulse is applied using few selected  $\Delta$  values, depending on the molecules or functional groups of interest. This targeted approach provides information about specific components within the sample while reducing the acquisition time (Van Zijl & Yadav, 2011).

An important advantage of CEST and MT MRI lies in their capability to detect and quantify low-abundant solute molecules or semi-solid macromolecules, enabling a more targeted assessment with high sensitivity compared to NMR/MRI relaxometry and diffusion techniques, which measure the molecular mobility of, primarily, water molecules. Due to the sensitivity and specificity of CEST, this technique can be used at magnetic field strengths of clinical scanners ( $\leq 3\text{T}$ ) lower than those typically required for NMR/MRI spectroscopy measurements, and its acquisition times may be shorter for measurements at selected  $\Delta$ . Another advantage of MT and CEST is their widespread application in *in vivo* research involving human participants.

Therefore, these techniques are either readily available or can be implemented on NMR spectrometers as well as clinical scanners, while this is not the case for  $T_2$ - and  $T_{1\rho}$ - dispersion measurements.

Overall, CEST and MT are expected to be sensitive to variations in pH, protein/peptide concentration, and modifications in protein states, including aggregation, solubilization, and hydrolysis. These changes are all expected to occur during gastric milk protein digestion. Moreover, MT and CEST offer several key advantages over spectroscopy, diffusion, and relaxometry. Therefore, they were selected as potential MRI markers for monitoring both *in vitro* and *in vivo* gastric milk protein digestion in this thesis.

## 1.7. Aim and outline of the thesis

As demonstrated in this chapter, MRI is a non-invasive and highly versatile imaging technique with the potential to monitor both *in vitro* and *in vivo* gastric protein digestion. By combining  $T_2$ -weighted MRI, commonly utilized for assessing GE, with quantitative and molecular MRI techniques like MT and CEST, a more comprehensive and detailed overview of gastric milk protein digestion may be obtained. This integrated approach could offer valuable insights into different aspects of gastric protein digestion, including structural, concentration and pH changes, and may bridge the gap between *in vitro* models and *in vivo* digestion in humans. As a result, this information could be utilized to optimize industrial food processing methods and food properties for enhanced protein digestion. Therefore, the overall aim of this thesis was to explore  $^1\text{H}$  MT and CEST NMR/MRI for monitoring *in vitro* and *in vivo* human gastric milk protein digestion.

An outline of the topics covered in this thesis is schematically illustrated in Fig. 1.6. **Chapters 2 and 3** describe MT and CEST MRI measurements of static *in vitro* samples on a 7 T vertical bore NMR spectrometer, chosen for its greater availability and flexibility in optimizing measurement parameters compared to clinical scanners.

In **Chapter 4**, the measurements on the 7 T vertical bore NMR spectrometer are supplemented with *in situ* measurements of *in vitro* gastric digestion on a 3 T clinical MRI scanner, which is subsequently utilized in the *in vivo* study outlined in **Chapter 5**.

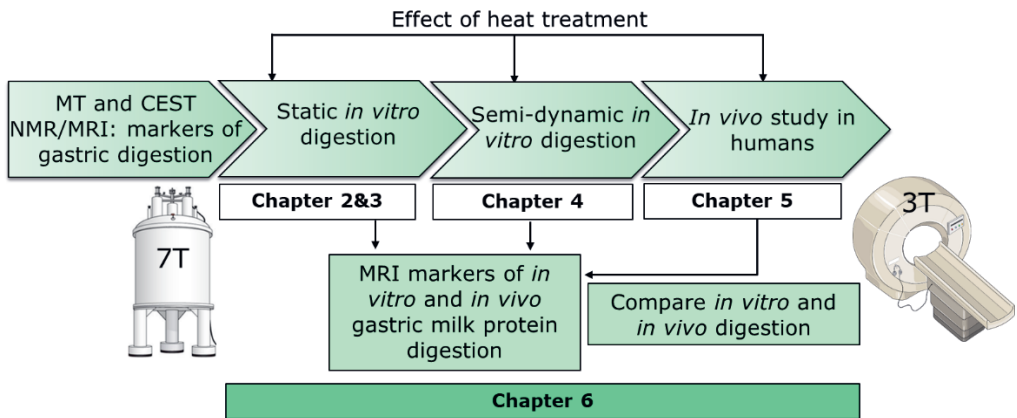


**Figure 1.6.** Schematic outline of the thesis, illustrating its overarching scope and the connection between the different chapters.

First, **Chapter 2** describes the implementation of bulk  $^1\text{H}$  MT NMR measurements on the 7 T vertical bore NMR spectrometer for monitoring gastric digestion of raw and heated skim milk in static *in vitro* samples. This includes optimization of the saturation pulse amplitudes and offsets for reliable fitting of MT spectra with a two-pool exchange model. Additionally, the faster acquisition of the MT ratio is presented, in view of the forthcoming planned *in vivo* study. The outcomes from the MT measurements are compared with conventional protein content analysis.

Building upon this, **Chapter 3** describes spatially-resolved  $T_2$ -weighted MT and CEST MRI measurements on the 7 T vertical bore NMR spectrometer, which were deployed to assess changes in both the semi-solid and soluble milk protein fractions of static *in vitro* digestion samples.

Moving to the dynamic complexity of *in vivo* protein digestion in **Chapter 4**, MT and CEST MRI are explored for monitoring pH and milk protein coagulation during semi-dynamic *in vitro* gastric digestion of low- (15 s at 72 °C) and high- (30 min at 80 °C) pasteurized skim milk using both the 7 T NMR spectrometer and a 3 T

clinical MRI scanner. These MRI markers are verified against bulk pH, protein concentration, and rheology measurements.

**Chapter 5**, describes a randomized cross-over trial to investigate the feasibility of using MT MRI for monitoring gastric milk protein digestion *in vivo* in humans, using the same milk products as in Chapter 4. The MT MRI measurements are complemented with total, semi-solid and liquid gastric content volumes estimated from  $T_2$ -weighted MRI images.

Finally, **Chapter 6** offers a discussion of the main findings presented in this thesis, places the research within a broader context, and identifies directions for future research. By comparing the outcomes from the *in vivo* human study with those from the *in vitro* experiments, this chapter explores the potential of MRI in bridging the gap between *in vitro* digestion models and *in vivo* digestion in humans.



## References

- Abell, T. L., Camilleri, M., Donohoe, K., Hasler, W. L., Lin, H. C., Maurer, A. H., McCallum, R. W., Nowak, T., Nusynowitz, M. L., Parkman, H. P., Shreve, P., Szarka, L. A., Snape, W. J., & Ziessman, H. A. (2008). Consensus Recommendations for Gastric Emptying Scintigraphy: A Joint Report of the American Neurogastroenterology and Motility Society and the Society of Nuclear Medicine. *The American Journal of Gastroenterology*, *103*(3), 753–763. <https://doi.org/10.1111/j.1572-0241.2007.01636.x>
- Adelnia, F., Zu, Z., Spear, J. T., Wang, F., Harkins, K. D., & Gore, J. C. (2021). Tissue characterization using R1rho dispersion imaging at low locking fields. *Magnetic Resonance Imaging*, *84*, 1–11. <https://doi.org/10.1016/j.mri.2021.05.006>
- Ahlborn, N. G., Montoya, C. A., Hodgkinson, S. M., Dave, A., Ye, A., Samuelsson, L. M., Roy, N. C., & McNabb, W. C. (2023). Heat treatment and homogenization of bovine milk loosened gastric curd structure and increased gastric emptying in growing pigs. *Food Hydrocolloids*, *137*, 108380. <https://doi.org/10.1016/j.foodhyd.2022.108380>
- Alger, J. R. (2010). Quantitative Proton Magnetic Resonance Spectroscopy and Spectroscopic Imaging of the Brain. *Topics in Magnetic Resonance Imaging*, *21*(2), 115–128. <https://doi.org/10.1097/RMR.0b013e31821e568f>
- Baliyan, V., Das, C. J., Sharma, R., & Gupta, A. K. (2016). Diffusion weighted imaging: Technique and applications. *World Journal of Radiology*, *8*(9), 785. <https://doi.org/10.4329/wjr.v8.i9.785>
- Bandyopadhyay, S., Kashyap, S., Calvez, J., Devi, S., Azzout-Marniche, D., Tomé, D., Kurpad, A. V., & Gaudichon, C. (2022). Evaluation of Protein Quality in Humans and Insights on Stable Isotope Approaches to Measure Digestibility – A Review. *Advances in Nutrition*, *13*(4), 1131–1143. <https://doi.org/10.1093/advances/nmab134>
- Borad, S. G., Kumar, A., & Singh, A. K. (2017). Effect of processing on nutritive values of milk protein. *Critical Reviews in Food Science and Nutrition*, *57*(17), 3690–3702. <https://doi.org/10.1080/10408398.2016.1160361>
- Bordoni, A., Picone, G., Babini, E., Vignali, M., Danesi, F., Valli, V., Di Nunzio, M., Laghi, L., & Capozzi, F. (2011). NMR comparison of *in vitro* digestion of *Parmigiano Reggiano* cheese aged 15 and 30 months. *Magnetic Resonance in Chemistry*, *49*, S61–S70. <https://doi.org/10.1002/mrc.2847>
- Bornhorst, G. M., Gouseti, O., Wickham, M. S. J., & Bakalis, S. (2016). Engineering Digestion: Multiscale Processes of Food Digestion. *Journal of Food Science*, *81*(3), R534–R543. <https://doi.org/10.1111/1750-3841.13216>
- Borthakur, A., Sochor, M., Davatzikos, C., Trojanowski, J. Q., & Clark, C. M. (2008). T1p MRI of Alzheimer's disease. *NeuroImage*, *41*(4), 1199–1205. <https://doi.org/10.1016/j.neuroimage.2008.03.030>
- Bourbon-Teles, J., Bells, S., Jones, D. K., Coulthard, E., Rosser, A., & Metzler-Baddeley, C. (2019). Myelin Breakdown in Human Huntington's Disease: Multi-Modal Evidence from Diffusion MRI and Quantitative Magnetization Transfer. *Neuroscience*, *403*, 79–92. <https://doi.org/10.1016/j.neuroscience.2017.05.042>
- Bozzali, M., Barritt, A. W., & Serra, L. (2020). *Diffusion MRI: Applications in the Brain* (pp. 605–636). <https://doi.org/10.1016/B978-0-12-817057-1.00025-1>
- Brodkorb, A., Egger, L., Alminger, M., Alvito, P., Assunção, R., Ballance, S., Bohn, T., Bourliou-Lacanal, C., Boutrou, R., Carrière, F., Clemente, A., Corredig, M., Dupont, D., Dufour, C., Edwards, C., Golding, M., Karakaya, S., Kirkhus, B., Le Feunteun, S., ... Recio, I. (2019). INFOGEST static *in vitro* simulation of gastrointestinal food digestion. *Nature Protocols*, *14*(4), 991–1014. <https://doi.org/10.1038/s41596-018-0119-1>

- Camilleri, M. (2019). Gastrointestinal hormones and regulation of gastric emptying. *Current Opinion in Endocrinology, Diabetes & Obesity*, 26(1), 3–10. <https://doi.org/10.1097/MED.0000000000000448>
- Camps, G., Mars, M., de Graaf, C., & Smeets, P. A. (2016). Empty calories and phantom fullness: a randomized trial studying the relative effects of energy density and viscosity on gastric emptying determined by MRI and satiety. *The American Journal of Clinical Nutrition*, 104(1), 73–80. <https://doi.org/10.3945/ajcn.115.129064>
- Camps, G., Mars, M., Witteman, B. J. M., de Graaf, C., & Smeets, P. A. M. (2018). Indirect vs direct assessment of gastric emptying: A randomized crossover trial comparing C-isotope breath analysis and <scp>MRI</scp>. *Neurogastroenterology & Motility*, 30(7). <https://doi.org/10.1111/nmo.13317>
- Camps, G., van Eijnatten, E. J., van Lieshout, G. A., Lambers, T. T., & Smeets, P. A. (2021). Gastric Emptying and Intra-gastric Behavior of Breast Milk and Infant Formula in Lactating Mothers. *The Journal of Nutrition*, 151(12), 3718–3724. <https://doi.org/10.1093/jn/nxab295>
- Carneiro, L., White, J., Parker, H., Hoad, C., Tucker, E., Marciani, L., Gowland, P., Gazis, T., Walker, M., & Fox, M. (2022). Pilot Double-Blind Randomised Controlled Trial: Effects of Jejunal Nutrition on Postprandial Distress in Diabetic Gastropathy (J4G Trial). *Nutrients*, 14(7), 1321. <https://doi.org/10.3390/nu14071321>
- Carver, J. P., & Richards, R. E. (1972). A general two-site solution for the chemical exchange produced dependence of T2 upon the carr-Purcell pulse separation. *Journal of Magnetic Resonance* (1969), 6(1), 89–105. [https://doi.org/10.1016/0022-2364\(72\)90090-X](https://doi.org/10.1016/0022-2364(72)90090-X)
- Chan, K. W. Y., Jiang, L., Cheng, M., Wijnen, J. P., Liu, G., Huang, P., van Zijl, P. C. M., McMahon, M. T., & Glunde, K. (2016). CEST-MRI detects metabolite levels altered by breast cancer cell aggressiveness and chemotherapy response. *NMR in Biomedicine*, 29(6), 806–816. <https://doi.org/10.1002/nbm.3526>
- Chen, G., Fu, S., Chen, P., Zhong, S., Chen, F., Qian, L., Luo, Z., Pan, Y., Tang, G., Jia, Y., Huang, L., & Wang, Y. (2022). Reduced myelin density in unmedicated major depressive disorder: An inhomogeneous magnetization transfer MRI study. *Journal of Affective Disorders*, 300, 114–120. <https://doi.org/10.1016/j.jad.2021.12.111>
- Chen, M., Chen, C., Shen, Z., Zhang, X., Chen, Y., Lin, F., Ma, X., Zhuang, C., Mao, Y., Gan, H., Chen, P., Zong, X., & Wu, R. (2017). Extracellular pH is a biomarker enabling detection of breast cancer and liver cancer using CEST MRI. *Oncotarget*, 8, 45759–45767. [www.impactjournals.com/oncotarget](http://www.impactjournals.com/oncotarget)
- Cheng, C., Wu, Y., Li, X., An, Z., Lu, Y., Zhang, F., Su, B., & Liu, Q. (2021). A wireless, ingestible pH sensing capsule system based on iridium oxide for monitoring gastrointestinal health. *Sensors and Actuators B: Chemical*, 349, 130781. <https://doi.org/10.1016/j.snb.2021.130781>
- Colsenet, R., Mariette, F., & Cambert, M. (2005). NMR Relaxation and Water Self-Diffusion Studies in Whey Protein Solutions and Gels. *Journal of Agricultural and Food Chemistry*, 53(17), 6784–6790. <https://doi.org/10.1021/jf050162k>
- Dai, B., & Matsukawa, S. (2012). NMR studies of the gelation mechanism and molecular dynamics in agar solutions. *Food Hydrocolloids*, 26(1), 181–186. <https://doi.org/10.1016/j.foodhyd.2011.04.021>
- de Jonge, C. S., Smout, A. J. P. M., Nederveen, A. J., & Stoker, J. (2018). Evaluation of gastrointestinal motility with MRI: Advances, challenges and opportunities. *Neurogastroenterology & Motility*, 30(1), e13257. <https://doi.org/10.1111/nmo.13257>
- de Oliveira, S. C., Bellanger, A., Ménard, O., Pladys, P., Le Gouar, Y., Dirson, E., Kroell, F., Dupont, D., Deglaire, A., & Bourlieu, C. (2017). Impact of human milk pasteurization on gastric digestion in preterm infants: a randomized controlled trial. *The American Journal of Clinical Nutrition*, 105(2), 379–390. <https://doi.org/10.3945/ajcn.116.142539>

- de Zwart, I. M., & de Roos, A. (2010). MRI for the evaluation of gastric physiology. *European Radiology*, 20(11), 2609–2616. <https://doi.org/10.1007/s00330-010-1850-3>
- Demers-Mathieu, V., Qu, Y., Underwood, M. A., & Dallas, D. C. (2018). The preterm infant stomach actively degrades milk proteins with increasing breakdown across digestion time. *Acta Paediatrica*, 107(6), 967–974. <https://doi.org/10.1111/apa.14244>
- Deng, R., Janssen, A. E. M., Vergeldt, F. J., Van As, H., de Graaf, C., Mars, M., & Smeets, P. A. M. (2020). Exploring in vitro gastric digestion of whey protein by time-domain nuclear magnetic resonance and magnetic resonance imaging. *Food Hydrocolloids*, 99(August 2019), 105348. <https://doi.org/10.1016/j.foodhyd.2019.105348>
- Deng, R., Mars, M., Janssen, A. E. M., & Smeets, P. A. M. (2023). Gastric digestion of whey protein gels: A randomized cross-over trial with the use of MRI. *Food Hydrocolloids*, 108689. <https://doi.org/10.1016/j.foodhyd.2023.108689>
- Deng, R., Seimys, A., Mars, M., Janssen, A. E. M., & Smeets, P. A. M. (2022). Monitoring pH and whey protein digestion by TD-NMR and MRI in a novel semi-dynamic in vitro gastric simulator (MR-GAS). *Food Hydrocolloids*, 125, 107393. <https://doi.org/10.1016/j.foodhyd.2021.107393>
- Dupont, D., & Tomé, D. (2019). Milk proteins: Digestion and absorption in the gastrointestinal tract. In *Milk Proteins* (3rd ed., pp. 701–714). Academic Press. <https://doi.org/10.1016/B978-0-12-815251-5.00020-7>
- Duynhoven, J. van, Voda, A., Witek, M., & Van As, H. B. T. (2010). *Chapter 3 - Time-Domain NMR Applied to Food Products* (Vol. 69, pp. 145–197). Academic Press. [https://doi.org/https://doi.org/10.1016/S0066-4103\(10\)69003-5](https://doi.org/https://doi.org/10.1016/S0066-4103(10)69003-5)
- Egger, L., Schlegel, P., Baumann, C., Stoffers, H., Guggisberg, D., Brügger, C., Dürr, D., Stoll, P., Vergères, G., & Portmann, R. (2017). Physiological comparability of the harmonized INFOGEST in vitro digestion method to in vivo pig digestion. *Food Research International*, 102, 567–574. <https://doi.org/10.1016/j.foodres.2017.09.047>
- Erickson, R. H., & Kim, Y. S. (1990). Digestion and Absorption of Dietary Protein. *Annual Review of Medicine*, 41(1), 133–139. <https://doi.org/10.1146/annurev.me.41.020190.001025>
- Gilani, I. A., & Sepponen, R. (2016). Quantitative rotating frame relaxometry methods in MRI. *NMR in Biomedicine*, 29(6), 841–861. <https://doi.org/10.1002/nbm.3518>
- Glerup, H., Bluhme, H., Villadsen, G. E., Rasmussen, K., Ejskjaer, N., & Dahlerup, J. F. (2007). Gastric emptying: a comparison of three methods. *Scandinavian Journal of Gastroenterology*, 42(10), 1182–1186. <https://doi.org/10.1080/00365520701370922>
- Goerke, S., Zaiss, M., Kunz, P., Klika, K. D., Windschuh, J. D., Mogk, A., Bukau, B., Ladd, M. E., & Bachert, P. (2015). Signature of protein unfolding in chemical exchange saturation transfer imaging. *NMR in Biomedicine*, 28(7), 906–913. <https://doi.org/10.1002/nbm.3317>
- Gottwald, A., Creamer, L. K., Hubbard, P. L., & Callaghan, P. T. (2005). Diffusion, relaxation, and chemical exchange in casein gels: A nuclear magnetic resonance study. *The Journal of Chemical Physics*, 122(3). <https://doi.org/10.1063/1.1825383>
- Goyal, R. K., Guo, Y., & Mashimo, H. (2019). Advances in the physiology of gastric emptying. *Neurogastroenterology & Motility*, 31(4). <https://doi.org/10.1111/nmo.13546>
- Henkelman, R. M., Huang, X., Xiang, Q. -S, Stanisz, G. J., Swanson, S. D., & Bronskill, M. J. (1993). Quantitative interpretation of magnetization transfer. *Magnetic Resonance in Medicine*, 29(6), 759–766. <https://doi.org/10.1002/mrm.1910290607>
- Henkelman, R. M., Stanisz, G. J., & Graham, S. J. (2001). Magnetization transfer in MRI: A review. *NMR in Biomedicine*, 14(2), 57–64. <https://doi.org/10.1002/nbm.683>
- Hills, B. P., & Duce, S. L. (1990). The influence of chemical and diffusive exchange on water proton transverse relaxation in plant tissues. *Magnetic Resonance Imaging*, 8(3), 321–331. [https://doi.org/10.1016/0730-725X\(90\)90106-C](https://doi.org/10.1016/0730-725X(90)90106-C)

- Hills, B. P., Takacs, S. F., & Belton, P. S. (1989). The effects of proteins on the proton N.M.R. transverse relaxation times of water. *Molecular Physics*, *67*(4), 903–918. <https://doi.org/10.1080/00268978900101531>
- Hills, B. P., Takacs, S. F., & Belton, P. S. (1990). A new interpretation of proton NMR relaxation time measurements of water in food. *Food Chemistry*, *37*(2), 95–111. [https://doi.org/10.1016/0308-8146\(90\)90084-H](https://doi.org/10.1016/0308-8146(90)90084-H)
- Hinrichs, R., Bulca, S., & Kulozik, U. (2007). Water mobility during renneting and acid coagulation of casein solutions: a differentiated low-resolution nuclear magnetic resonance analysis. *International Journal of Dairy Technology*, *60*(1), 37–43. <https://doi.org/10.1111/j.1471-0307.2007.00290.x>
- Hoad, C. L., Marciani, L., Alonso, B. de C., Traynor, C., Gowland, P. A., Rayment, P., Spiller, R. C., Mela, D. J., & Peters, H. P. F. (2004). In Vivo Imaging of Intragastric Gelation and Its Effect on Satiety in Humans. *The Journal of Nutrition*, *134*(9), 2293–2300. <https://doi.org/10.1093/jn/134.9.2293>
- Horstman, A. M. H., Ganzevles, R. A., Kudla, U., Kardinaal, A. F. M., van den Borne, J. J. G. C., & Huppertz, T. (2021). Postprandial blood amino acid concentrations in older adults after consumption of dairy products: The role of the dairy matrix. *International Dairy Journal*, *113*, 104890. <https://doi.org/10.1016/j.idairyj.2020.104890>
- Huppertz, T., & Chia, L. W. (2021). Milk protein coagulation under gastric conditions: A review. *International Dairy Journal*, *113*, 104882. <https://doi.org/10.1016/j.idairyj.2020.104882>
- Keeler, J. (2010). *Understanding NMR Spectroscopy* (2nd ed.). John Wiley And Sons Ltd.
- Keenan, K. E., Besier, T. F., Pauly, J. M., Han, E., Rosenberg, J., Smith, R. L., Delp, S. L., Beaupre, G. S., & Gold, G. E. (2011). Prediction of glycosaminoglycan content in human cartilage by age, T1ρ and T2 MRI. *Osteoarthritis and Cartilage*, *19*(2), 171–179. <https://doi.org/10.1016/j.joca.2010.11.009>
- Kethireddipalli, P., & Hill, A. R. (2015). Rennet Coagulation and Cheesemaking Properties of Thermally Processed Milk: Overview and Recent Developments. *Journal of Agricultural and Food Chemistry*, *63*(43), 9389–9403. <https://doi.org/10.1021/jf504167v>
- Kong, F., & Singh, R. P. (2010). A Human Gastric Simulator (HGS) to Study Food Digestion in Human Stomach. *Journal of Food Science*, *75*(9), E627–E635. <https://doi.org/10.1111/j.1750-3841.2010.01856.x>
- Lacroix, M., Bon, C., Bos, C., Léonil, J., Benamouzig, R., Luengo, C., Fauquant, J., Tomé, D., & Gaudichon, C. (2008). Ultra High Temperature Treatment, but Not Pasteurization, Affects the Postprandial Kinetics of Milk Proteins in Humans. *The Journal of Nutrition*, *138*(12), 2342–2347. <https://doi.org/10.3945/jn.108.096990>
- Le Feunteun, S., Ouethrani, M., & Mariette, F. (2012). The rennet coagulation mechanisms of a concentrated casein suspension as observed by PFG-NMR diffusion measurements. *Food Hydrocolloids*, *27*(2), 456–463. <https://doi.org/10.1016/j.foodhyd.2011.09.008>
- Lee, M. K., Choi, Y., & Jung, S.-L. (2021). Diffusion-weighted MRI for predicting treatment response in patients with nasopharyngeal carcinoma: a systematic review and meta-analysis. *Scientific Reports*, *11*(1), 18986. <https://doi.org/10.1038/s41598-021-98508-5>
- Li, S., Pan, Z., Ye, A., Cui, J., Dave, A., & Singh, H. (2022). Structural and rheological properties of the clots formed by ruminant milks during dynamic in vitro gastric digestion: Effects of processing and species. *Food Hydrocolloids*, *126*, 107465. <https://doi.org/10.1016/j.foodhyd.2021.107465>
- Longo, D. L., Di Gregorio, E., Abategiovanni, R., Ceccon, A., Assfalg, M., Molinari, H., & Aime, S. (2014). Chemical exchange saturation transfer (CEST): an efficient tool for detecting molecular information on proteins' behaviour. *The Analyst*, *139*(11), 2687–2690. <https://doi.org/10.1039/C4AN00346B>

- Longo, D. L., Sun, P. Z., Consolino, L., Michelotti, F. C., Uggeri, F., & Aime, S. (2014). A general MRI-CEST ratiometric approach for pH imaging: Demonstration of in vivo pH mapping with iobitridol. *Journal of the American Chemical Society*, *136*(41), 14333–14336. <https://doi.org/10.1021/ja5059313>
- Lu, K., Liu, Z., Jaffey, D., Wo, J. M., Mosier, K. M., Cao, J., Wang, X., & Powley, T. L. (2022). Automatic assessment of human gastric motility and emptying from dynamic 3D magnetic resonance imaging. *Neurogastroenterology & Motility*, *34*(1). <https://doi.org/10.1111/nmo.14239>
- Macierzanka, A., Böttger, F., Lansonneur, L., Groizard, R., Jean, A.-S., Rigby, N. M., Cross, K., Wellner, N., & Mackie, A. R. (2012). The effect of gel structure on the kinetics of simulated gastrointestinal digestion of bovine  $\beta$ -lactoglobulin. *Food Chemistry*, *134*(4), 2156–2163. <https://doi.org/10.1016/j.foodchem.2012.04.018>
- Mackie, A., Mulet-Cabero, A.-I., & Torcello-Gómez, A. (2020). Simulating human digestion developing our knowledge to create healthier and more sustainable foods. *Food & Function*, *11*, 9397–9431.
- Mariette, F. (2017). NMR Relaxometry and Imaging of Dairy Products. In *Modern Magnetic Resonance* (pp. 1–23). Springer International Publishing. [https://doi.org/10.1007/978-3-319-28275-6\\_38-1](https://doi.org/10.1007/978-3-319-28275-6_38-1)
- Mariette, F., Collewet, G., Davenel, A., Lucas, T., & Musse, M. (2012). Quantitative MRI in food science & food engineering. *EMagRes*, *1*(1), 205–214. <https://doi.org/10.1002/9780470034590.emrstm1272>
- Mariette, F., Topgaard, D., Jönsson, B., & Soderman, O. (2002).  $^1\text{H}$  NMR Diffusometry Study of Water in Casein Dispersions and Gels. *Journal of Agricultural and Food Chemistry*, *50*(15), 4295–4302. <https://doi.org/10.1021/jf0115948>
- Mathai, J. K., Liu, Y., & Stein, H. H. (2017). Values for digestible indispensable amino acid scores (DIAAS) for some dairy and plant proteins may better describe protein quality than values calculated using the concept for protein digestibility-corrected amino acid scores (PDCAAS). *British Journal of Nutrition*, *117*(4), 490–499. <https://doi.org/10.1017/S0007114517000125>
- Ménard, O., Bourlieu, C., De Oliveira, S. C., Dellarosa, N., Laghi, L., Carrière, F., Capozzi, F., Dupont, D., & Deglaire, A. (2018). A first step towards a consensus static in vitro model for simulating full-term infant digestion. *Food Chemistry*, *240*(2017), 338–345. <https://doi.org/10.1016/j.foodchem.2017.07.145>
- Menard, O., Lesmes, U., Shani-Levi, C. S., Araiza Calahorra, A., Lavoisier, A., Morzel, M., Rieder, A., Feron, G., Nebbia, S., Mashiah, L., Andres, A., Bornhorst, G., Carrière, F., Egger, L., Gwala, S., Heredia, A., Kirkhus, B., Macierzanka, A., Portman, R., ... Dupont, D. (2023). Static *in vitro* digestion model adapted to the general older adult population: an INFOGEST international consensus. *Food & Function*, *14*(10), 4569–4582. <https://doi.org/10.1039/D3FO00535F>
- Morrison, C., Stanis, G., & Henkelman, R. M. (1995). Modeling Magnetization Transfer for Biological-like Systems Using a Semi-solid Pool with a Super-Lorentzian Lineshape and Dipolar Reservoir. In *Journal of Magnetic Resonance* (Vol. 108, Issue 2, pp. 103–113). <https://doi.org/10.1006/jmrb.1995.1111>
- Mulet-Cabero, A. I., Egger, L., Portmann, R., Ménard, O., Marze, S., Minekus, M., Le Feunteun, S., Sarkar, A., Grundy, M. M. L., Carrière, F., Golding, M., Dupont, D., Recio, I., Brodkorb, A., & Mackie, A. (2020). A standardised semi-dynamic: in vitro digestion method suitable for food-an international consensus. *Food and Function*, *11*(2), 1702–1720. <https://doi.org/10.1039/c9fo01293a>
- Musse, M., Le Feunteun, S., Collewet, G., Ravilly, M., Quellec, S., Ossemond, J., Morzel, M., Challoy, S., Nau, F., & Lucas, T. (2023). Quantitative magnetic resonance imaging of in vitro gastrointestinal digestion of a bread and cheese meal. *Food Research International*, *169*, 112821–112833.

- Nestrasil, I., Michaeli, S., Liimatainen, T., Rydeen, C. E., Kotz, C. M., Nixon, J. P., Hanson, T., & Tuite, P. J. (2010). T1p and T2p MRI in the evaluation of Parkinson's disease. *Journal of Neurology*, 257(6), 964–968. <https://doi.org/10.1007/s00415-009-5446-2>
- Nieva-Echevarría, B., Goicoechea, E., Manzanos, M. J., & Guillén, M. D. (2016). A study by 1H NMR on the influence of some factors affecting lipid in vitro digestion. *Food Chemistry*, 211, 17–26. <https://doi.org/10.1016/j.foodchem.2016.05.021>
- Nyakayiru, J., van Lieshout, G. A. A., Trommelen, J., van Kranenburg, J., Verdijk, L. B., Bragt, M. C. E., & van Loon, L. J. C. (2020). The glycation level of milk protein strongly modulates post-prandial lysine availability in humans. *British Journal of Nutrition*, 123(5), 545–552. <https://doi.org/10.1017/S0007114519002927>
- Ozel, B., Aydin, O., Grunin, L., & Oztop, M. H. (2018). Physico-Chemical Changes of Composite Whey Protein Hydrogels in Simulated Gastric Fluid Conditions. *Journal of Agricultural and Food Chemistry*, 66(36), 9542–9555. <https://doi.org/10.1021/acs.jafc.8b02829>
- Palmer, A. G. (2014). Chemical exchange in biomacromolecules: Past, present, and future. *Journal of Magnetic Resonance*, 241(1), 3–17. <https://doi.org/10.1016/j.jmr.2014.01.008>
- Piper, D. W., & Fenton, B. H. (1965). pH stability and activity curves of pepsin with special reference to their clinical importance. *Gut*, 6(5), 506–508. <https://doi.org/10.1136/gut.6.5.506>
- Qureshi, W. A. (2004). Current and future applications of the capsule camera. *Nature Reviews Drug Discovery*, 3(5), 447–450. <https://doi.org/10.1038/nrd1385>
- Roy, D., Moughan, P. J., Ye, A., Hodgkinson, S. M., Stroebinger, N., Li, S., Dave, A. C., Montoya, C. A., & Singh, H. (2022). Structural changes in milk from different species during gastric digestion in piglets. *Journal of Dairy Science*, 105(5), 3810–3831. <https://doi.org/10.3168/jds.2021-21388>
- Schork, N., Schuhmann, S., Gruschke, O., Groß, D., Zick, K., Nirschl, H., & Guthausen, G. (2020). *Recent MRI and diffusion studies of food structures* (pp. 203–264). <https://doi.org/10.1016/bs.arnmr.2020.02.002>
- Sensoy, I. (2021). A review on the food digestion in the digestive tract and the used in vitro models. *Current Research in Food Science*, 4, 308–319. <https://doi.org/10.1016/j.crfcs.2021.04.004>
- Sirlin, C. B. (2011). Science to Practice: Can T1p Imaging Be Used to Diagnose and Assess the Severity of Hepatic Fibrosis? *Radiology*, 259(3), 619–620. <https://doi.org/10.1148/radiol.11110547>
- Smeets, P. A. M., Deng, R., Van Eijnatten, E. J. M., & Mayar, M. (2020). Monitoring food digestion with magnetic resonance techniques. *Proceedings of the Nutrition Society*, 3, 1–11. <https://doi.org/10.1017/S0029665120007867>
- Sousa, R., Portmann, R., Dubois, S., Recio, I., & Egger, L. (2020). Protein digestion of different protein sources using the INFOGEST static digestion model. *Food Research International*, 130, 108996. <https://doi.org/10.1016/j.foodres.2020.108996>
- Stahl, R., Luke, A., Li, X., Carballido-Gamio, J., Ma, C. B., Majumdar, S., & Link, T. M. (2009). T1rho, T2 and focal knee cartilage abnormalities in physically active and sedentary healthy subjects versus early OA patients—a 3.0-Tesla MRI study. *European Radiology*, 19(1), 132–143. <https://doi.org/10.1007/s00330-008-1107-6>
- Tang, Y., Xiao, G., Shen, Z., Zhuang, C., Xie, Y., Zhang, X., Yang, Z., Guan, J., Shen, Y., Chen, Y., Lai, L., Chen, Y., Chen, S., Dai, Z., Wang, R., & Wu, R. (2020). Noninvasive Detection of Extracellular pH in Human Benign and Malignant Liver Tumors Using CEST MRI. *Frontiers in Oncology*, 10(November), 1–10. <https://doi.org/10.3389/fonc.2020.578985>
- Thuenemann, E. C., Mandalari, G., Rich, G. T., & Faulks, R. M. (2015). Dynamic Gastric Model (DGM). In *The Impact of Food Bioactives on Health* (pp. 47–59). Springer International Publishing. [https://doi.org/10.1007/978-3-319-16104-4\\_6](https://doi.org/10.1007/978-3-319-16104-4_6)

- Trommelen, J., Weijzen, M. E. G., van Kranenburg, J., Ganzevles, R. A., Beelen, M., Verdijk, L. B., & van Loon, L. J. C. (2020). Casein Protein Processing Strongly Modulates Post-Prandial Plasma Amino Acid Responses In Vivo in Humans. *Nutrients*, *12*(8), 2299. <https://doi.org/10.3390/nu12082299>
- Tyler, D. J., Robson, M. D., Henkelman, R. M., Young, I. R., & Bydder, G. M. (2007). Magnetic resonance imaging with ultrashort TE (UTE) PULSE sequences: Technical considerations. *Journal of Magnetic Resonance Imaging*, *25*(2), 279–289. <https://doi.org/10.1002/jmri.20851>
- van Lieshout, G. A. A., Lambers, T. T., Bragt, M. C. E., & Hettinga, K. A. (2020). How processing may affect milk protein digestion and overall physiological outcomes: A systematic review. *Critical Reviews in Food Science and Nutrition*, *60*(14), 2422–2445. <https://doi.org/10.1080/10408398.2019.1646703>
- Van Obberghen, E., Mchinda, S., le Troter, A., Prevost, V. H., Viout, P., Guye, M., Varma, G., Alsop, D. C., Ranjeva, J.-P., Pelletier, J., Girard, O., & Duhamel, G. (2018). Evaluation of the Sensitivity of Inhomogeneous Magnetization Transfer (ihMT) MRI for Multiple Sclerosis. *American Journal of Neuroradiology*, *39*(4), 634–641. <https://doi.org/10.3174/ajnr.A5563>
- van Zijl, P. C. M., Lam, W. W., Xu, J., Knutsson, L., & Stanisz, G. J. (2018). Magnetization Transfer Contrast and Chemical Exchange Saturation Transfer MRI. Features and analysis of the field-dependent saturation spectrum. *NeuroImage*, *168*, 222–241. <https://doi.org/10.1016/j.neuroimage.2017.04.045>
- Van Zijl, P. C. M., & Yadav, N. N. (2011). Chemical exchange saturation transfer (CEST): What is in a name and what isn't? *Magnetic Resonance in Medicine*, *65*(4), 927–948. <https://doi.org/10.1002/mrm.22761>
- Vidal, N. P., Picone, G., Goicoechea, E., Laghi, L., Manzanos, M. J., Danesi, F., Bordoni, A., Capozzi, F., & Guillén, M. D. (2016). Metabolite release and protein hydrolysis during the in vitro digestion of cooked sea bass fillets. A study by <sup>1</sup>H NMR. *Food Research International*, *88*, 293–301. <https://doi.org/10.1016/j.foodres.2016.01.013>
- Villa, C., Costa, J., Oliveira, M. B. P. P., & Mafra, I. (2018). Bovine Milk Allergens: A Comprehensive Review. *Comprehensive Reviews in Food Science and Food Safety*, *17*(1), 137–164. <https://doi.org/10.1111/1541-4337.12318>
- Walstra, P., Wouters, J. T. M., & Geurts, T. J. (2005). *Dairy science and technology* (2nd ed.). CRC Press.
- Wang, P., Block, J., & Gore, J. C. (2015). Chemical exchange in knee cartilage assessed by R1p (1/T1p) dispersion at 3T. *Magnetic Resonance Imaging*, *33*(1), 38–42. <https://doi.org/10.1016/j.mri.2014.07.008>
- Wang, X., Ye, A., Lin, Q., Han, J., & Singh, H. (2018). Gastric digestion of milk protein ingredients: Study using an in vitro dynamic model. *Journal of Dairy Science*, *101*(8), 6842–6852. <https://doi.org/10.3168/jds.2017-14284>
- Wang, Yan, G. Z., Sun, F., Jiang, P. P., Zhang, W. Q., & Zhang, G. F. (2005). A non-invasive method for gastrointestinal parameter monitoring. *World Journal of Gastroenterology*, *11*(4), 521. <https://doi.org/10.3748/wjg.v11.i4.521>
- Ward, K. M., Aletras, A. H., & Balaban, R. S. (2000). A New Class of Contrast Agents for MRI Based on Proton Chemical Exchange Dependent Saturation Transfer (CEST). *Journal of Magnetic Resonance*, *143*(1), 79–87. <https://doi.org/10.1006/jmre.1999.1956>
- Weiger, M., & Pruessmann, K. P. (2019). Short-T2 MRI: Principles and recent advances. *Progress in Nuclear Magnetic Resonance Spectroscopy*, *114–115*, 237–270. <https://doi.org/10.1016/j.pnmrs.2019.07.001>
- Welsch, G. H., Trattnig, S., Scheffler, K., Szomonanyi, P., Quirbach, S., Marlovits, S., Domayer, S., Bieri, O., & Mamsch, T. C. (2008). Magnetization transfer contrast and T2 mapping in the

evaluation of cartilage repair tissue with 3T MRI. *Journal of Magnetic Resonance Imaging*, 28(4), 979–986. <https://doi.org/10.1002/jmri.21516>

Wolff, S. D., & Balaban, R. S. (1989). Magnetization transfer contrast (MTC) and tissue water proton relaxation in vivo. *Magnetic Resonance in Medicine*, 10(1), 135–144. <https://doi.org/10.1002/mrm.1910100113>

Wu, B., Warnock, G., Zaiss, M., Lin, C., Chen, M., Zhou, Z., Mu, L., Nanz, D., Tuura, R., & Delso, G. (2016). An overview of CEST MRI for non-MR physicists. *EJNMMI Physics*, 3(1). <https://doi.org/10.1186/s40658-016-0155-2>

Ye, A., Cui, J., Dalgleish, D., & Singh, H. (2016). Formation of a structured clot during the gastric digestion of milk: Impact on the rate of protein hydrolysis. *Food Hydrocolloids*, 52, 478–486. <https://doi.org/10.1016/j.foodhyd.2015.07.023>

Ye, A., Weilin, L., Cui, J., Kong, Z., Roy, D., Kong, Y., Han, J., & Singh, H. (2019). Coagulation behaviour of milk under gastric digestion: Effect of pasteurization and ultra-high temperature treatment. *Food Chemistry*, 286, 216–225.

Zaiß, M., Schmitt, B., & Bachert, P. (2011). Quantitative separation of CEST effect from magnetization transfer and spillover effects by Lorentzian-line-fit analysis of z-spectra. *Journal of Magnetic Resonance*, 211(2), 149–155. <https://doi.org/10.1016/j.jmr.2011.05.001>

Zhang, Y., Zu, T., Liu, R., & Zhou, J. (2023). Acquisition sequences and reconstruction methods for fast chemical exchange saturation transfer imaging. *NMR in Biomedicine*, 36(6). <https://doi.org/10.1002/nbm.4699>

Zhou, Y., Bie, C., van Zijl, P. C. M., & Yadav, N. N. (2023). The relayed nuclear Overhauser effect in magnetization transfer and chemical exchange saturation transfer MRI. *NMR in Biomedicine*, 36(6). <https://doi.org/10.1002/nbm.4778>





**CHAPTER**

# 2

# Non-invasive monitoring of *in vitro* gastric milk protein digestion kinetics by $^1\text{H}$ NMR magnetization transfer

A version of this chapter has been published as:  
Mayar, M., Miltenburg, J. L., Hettinga, K., Smeets, P. A. M., van Duynhoven, J. P. M., & Terenzi, C. (2022). Non-invasive monitoring of *in vitro* gastric milk protein digestion kinetics by  $^1\text{H}$  NMR magnetization transfer. *Food Chemistry*, 383, 132545.

## Abstract

Processing of milk involves heating, which can modify the structure and digestibility of its proteins. *In vitro* models are useful for studying protein digestion. However, validating these models with *in vivo* data is challenging. Here, we non-invasively monitor *in vitro* gastric milk protein digestion by probing the protein-water interactions detected by  $^1\text{H}$  nuclear magnetic resonance (NMR) magnetization transfer (MT). We obtained either a fitted composite exchange rate (*CER*) with a relative standard error of  $\leq 10\%$  or the MT ratio (*MTR*) of the intensity without or with an off-resonance saturation pulse. Both *CER* and *MTR*, affected by the variation in the amount of semi-solid protons, decreased during *in vitro* gastric digestion in agreement with standard protein content analyses. The decrease was slower in heated milk, indicating slower breakdown of the coagulum. Our results open the way to future quantification of protein digestion *in vivo* by MRI.

## 2.1. Introduction

Protein intake is essential for the growth and repair of body cells, muscle function and development of the immune system. Milk is one of the main food sources of protein in the human diet. Gastric digestion is the first step in the breakdown of milk proteins, namely casein and whey proteins, and in the subsequent absorption of amino acids (Walstra, Wouters, Geurts, 2006). However, industrial preparation of milk products includes heating, which can modify the structure and the gastric digestibility of the proteins. Understanding the effect of heating on protein digestion can ultimately aid in optimizing the industrial processing of milk proteins. During gastric digestion, gastric acid and pepsin cause aggregation of the casein micelles into a semi-solid casein coagulum, followed by subsequent hydrolysis of the proteins by pepsin (Egger et al., 2019; Nakai & Li-Chan, 1987). Due to their open structure, caseins are almost completely broken down into peptides in the gastric phase, while native whey proteins are more resistant to hydrolysis due to their globular structure, and are still largely intact after gastric digestion (van Lieshout, Lambers, Bragt, & Hettinga, 2020). The modifications imposed on the proteins during heating can affect both the structure of the coagulum and the digestion of caseins and whey proteins (Mulet-Cabero, Mackie, Wilde, Fenelon, & Brodkorb, 2019).

Protein digestion is commonly studied using static or dynamic *in vitro* digestion models that in turn mimic either adult (Brodkorb et al., 2019; Dupont et al., 2019) or infant digestion (Ménard et al., 2018). During *in vitro* digestion studies, samples are taken at different digestion time points, and are typically analyzed with the o-phthalaldehyde (OPA) assay, sodium dodecyl sulphate–polyacrylamide gel electrophoresis (SDS-PAGE), high performance liquid chromatography (HPLC) and liquid chromatography coupled to mass spectrometry (LC-MS) (Egger et al., 2019; Macierzanka et al., 2012). These methods, limited to *in vitro* applications, typically only measure the supernatant instead of the whole digestion sample including the coagulum formed during phase separation. Whereas *in vitro* digestion studies can provide valuable insights into protein digestion kinetics and the chemical composition of the digesta, they do not fully capture the complexity of the digestive tract. *In vivo* studies provide a biological environment that is hard to replicate *in vitro* because the digestive tract is within a complex biological system

containing delicate feedback controls. For instance, secretion of digestive juice in response to a meal is automatically controlled *in vivo* but are difficult to reproduce through *in vitro* experiments (Bornhorst & Paul Singh, 2014). Moreover, the physicochemical conditions, such as pH, ionic strength and enzyme concentration evolve with time and influence digestion. Static *in vitro* digestion models do not take these evolutions over time into account. Protein digestion may be better understood through *in vivo* monitoring in humans, which can help optimize and validate the *in vitro* digestion models. herefore, non-invasive techniques must be developed to monitor both *in vitro* and *in vivo* digestion.

Magnetic resonance imaging (MRI) is promising for studying *in vivo* protein digestion, because it can be used to study physiological processes in a non-invasive manner (Smeets, Deng, Van Eijnatten, & Mayar, 2020). MRI is based on nuclear magnetic resonance (NMR), which has been applied widely to characterize a variety of food systems, including milk and milk products (Bordoni et al., 2011; Duynhoven, Voda, Witek, & Van As, 2010; Le Dean, Mariette, & Marin, 2004). MRI is currently used to study gross changes in digesta, linked to changes in food structure and possible phase separation, by visual assessment of anatomical images of the stomach (De Zwart & De Roos, 2010; Spiller & Marciani, 2019). Yet, such images do not provide a local molecular-scale measure of the degree of protein coagulation and subsequent protein hydrolysis. It has already been established that it is possible to indirectly monitor the *in vitro* gastric digestion of whey protein gels by measuring the  $^1\text{H}$  transverse relaxation time ( $T_2$ ) of the supernatant, which changes during digestion due to a release of proteins and peptides from the gel (Deng et al., 2020). Contrarily to standard biochemical methods, all these NMR/MRI measurements are suitable for non-invasive studies in humans, and of whole digestion samples, in principle including both liquid and semi-solid phases. Yet, with  $T_2$  measurements it is not possible to capture the breakdown of coagulated caseins, especially in the early stages of digestion. This is because NMR spectrometers and clinical scanners cannot directly assess the short ( $\mu\text{s}$ - $\text{ms}$  range)  $T_2$  NMR relaxation times associated with semi-solid proteins. Magnetization Transfer (MT) is an NMR/MRI technique that is used to quantify low-abundant semi-solids dispersed in aqueous food matrices as a complementary method to  $T_2$  relaxometry (Chinachoti, Vittadini, Chatakanonda, & Vodovotz, 2008; Duynhoven, Kulik, Jonker, & Haverkamp, 1999). This technique found

widespread use in both pre-clinical and clinical MRI because of its potential to improve tissue contrast, compared to conventional MRI techniques, and its capacity to quantitatively characterize tissues in which biopolymers form semi-solid networks (Guo, Erickson, Trouard, Galons, & Gillies, 2003; Sled, 2018; Van Zijl et al., 2003).

In conventional NMR and MRI, only signals from mobile protons are detected that have sufficiently long  $T_2$ -values and are present at high concentrations. The  $T_2$ -values of motion-restricted protons from semi-solid macromolecules, such as proteins, is too short to be detected directly by NMR spectrometers with long dead times of typically a few ms. MT MRI enables indirect detection of protons from low-abundance semi-solid macromolecules, with short  $T_2$ -values, through the signal of the more mobile water protons.

In MT measurements, a radio frequency (RF) pulse with a specific amplitude and frequency is applied to saturate the magnetization of the protons associated with the semi-solid macromolecules by equilibrating the populations of the  $^1\text{H}$  energy levels. The saturation is then transferred to the more mobile water  $^1\text{H}$  via a combination of through-space dipolar interactions and  $^1\text{H}$  exchange between the semi-solid macromolecules and water. The saturation transfer can then be detected as a suppression of the water signal. The magnitude of the signal suppression is mainly dependent on the  $^1\text{H}$  magnetization transfer rate and on the population of the semi-solid pool (Henkelman, Stanisz, & Graham, 2001). Since changes in the semi-solid protein pool occur during gastric milk protein digestion, which involves casein coagulation and digestion of both casein and whey proteins, we hypothesize that MT can be used to monitor these changes *in vitro*, on the whole digestion sample, via the  $^1\text{H}$  protein-water exchange kinetics. The latter can be quantified by multi-parameter fitting of MT spectra recorded with different saturation pulse amplitudes and frequency offsets with respect to the signal of water. This approach enables the quantification of exchange and relaxation parameters of the liquid and semi-solid components (Henkelman et al., 1993). However, these measurements are time-consuming and, hence, not applicable to dynamic *in vivo* studies, where fast measurements are desired to meet safety requirements and avoid breathing motion artefacts in the images. Therefore, in clinical MRI, mostly a semi-quantitative rapid measurement of the MT ratio (*MTR*)

is performed. Signal saturation with at least one pulse amplitude and two frequency offsets is required in order to obtain the *MTR*. The *MTR* is a semi-quantitative parameter, because it depends not only on the rate of magnetization transfer, but also on the amplitude and duration of the saturation pulse (Henkelman et al., 2001; Sinclair et al., 2010). In this study of *in vitro* gastric milk protein digestion, we validate and assess the quantification of protein-water exchange kinetics by MT during digestion, as well as the respective faster semi-quantitative *MTR* measurements, in view of their ultimate feasibility under *in vivo* conditions using MRI.

## 2.2. Materials and methods

### 2.2.1. Materials

Pepsin from porcine gastric mucosa (631 activity units/mg), pepstatin A, HCl, KCl, NaHCO<sub>3</sub>, NaCl, Bis-Tris buffer, DL-dithiothreitol (DTT) and guanidine hydrochloride (GdnHCl) were purchased from Sigma Aldrich, Inc. (St. Louis, USA). o-phthaldehyde (OPA), disodiumtetraborate decahydrate, sodiumdodecyl sulfate, trisodium citrate dihydrate, trifluoroacetic acid (TFA) were purchased from Merck (Darmstadt, Germany). HPLC ultra-gradient grade acetonitrile was purchased from Biosolve Chemicals (Valkenswaard, The Netherlands). Milli-Q water (resistivity 18.2 MΩ.cm at 25 °C, Merck Millipore, Billerica, USA) was used in all experiments.

### 2.2.2. Preparation of raw and heated skim milk

Raw cow's milk was provided by FrieslandCampina (Wageningen, The Netherlands). To obtain skim milk (SM), the raw milk was centrifuged at 6000 *g* for 20 min at 4 °C. The cream that was formed on top was removed and the remaining SM was stored at -20 °C. The heated SM samples were prepared by heating SM in a water bath at 80 °C or 70 °C for 30 min.



### 2.2.3. *In vitro* infant gastric protein digestion protocol

*In vitro* gastric digestion of raw and heated SM was conducted based on a digestion protocol for 1 month old infants (Ménard et al., 2018). This digestion protocol was chosen because milk protein digestion, and the effect of heating on digestion, is most poorly understood in infants. The methodology described in this paper can however directly be applied to other digestion models, such as Infogest (Brodkorb et al., 2019). First, simulated gastric fluid (SGF) and SM were separately heated in a water bath at 37 °C for 5 min. SGF was composed of NaCl and KCl with a concentration of 94 and 13 mM, respectively, and a pH of 5.3. Next, 1 mL of digestion sample was prepared by mixing SM and SGF containing pepsin in a 10-mm NMR tube in a 63:37 (v/v) ratio. The activity of pepsin in the digestion sample was 268 U/mL. The pH was adjusted to 5.3 with 1 M HCl. The samples were incubated in a water bath at 37 °C for  $t = 0, 1, 5, 15, 30$  and 60 min. These time points were based on Ménard et al. (2018) with the addition of  $t = 1$  min to better capture the fast disappearance of the coagulum in raw SM. The activity of pepsin was stopped by adding 10  $\mu$ L of a 60  $\mu$ mol/mL Pepstatin A solution to each of the prepared samples. The samples were measured by NMR without any further sample preparation.

### 2.2.4. NMR measurements

All the  $^1\text{H}$  MT NMR measurements were conducted at a magnetic field strength of 7 T, corresponding to a  $^1\text{H}$  frequency of 300.13 MHz, on an Avance III spectrometer (Bruker Biospin, Fällanden, Switzerland) equipped with a 10-mm diff30 probe.  $^1\text{H}$  NMR spectra were acquired at room temperature with an MT pulse sequence, consisting of a continuous-wave (CW) saturation pulse followed by a  $90^\circ$  RF excitation pulse and acquisition of the free induction decay (FID) during the time  $acq(CW(5s) - 90_x(13.5 \mu s) - acq(0.4s))$ . The recycle delay was set to 5 s, and 8 acquisitions were recorded with 8-step phase cycling. To obtain quantitative data, MT NMR spectra were measured using 29 different values of the frequency offset ( $\Delta$ ), ranging from 90 Hz to 130 kHz, and 3 values of the saturation pulse amplitude ( $\omega_1/2\pi$ ), resulting in a total measurement time of 2 hours.

Single-point MT measurements were performed with  $(\omega_1/2\pi) = 0.50$  kHz and  $\Delta = 130$  and 7.5 kHz, resulting in a total acquisition time of 2.6 min.

### 2.2.5. Two-pool exchange model

The two-pool exchange model (Eq. 2.1), consisting of a free water pool (A) and a semi-solid macromolecular pool (B), was used to fit the MT spectra obtained at different  $\omega_1$  and  $\Delta$ :

$$\frac{M_Z^A}{M_0^A} = \frac{R_1^B \cdot \left[ \frac{R_{ex} M_0^B}{R_1^A} \right] + (R_1^B + R_{rfB} + R_{ex})}{\left[ \frac{R_{ex} M_0^B}{R_1^A} \right] \cdot (R_1^B + R_{rfB}) + \left( 1 + \left( \frac{\omega_1}{2\pi\Delta} \right)^2 \cdot \left[ \frac{R_2^A}{R_1^A} \right] \right) \cdot (R_1^B + R_{rfB} + R_{ex})} \quad \text{Eq. 2.1}$$

where  $R_1$  and  $R_2$  are the longitudinal and transverse relaxation rates, respectively,  $R_{ex}$  is the chemical exchange rate constant and  $M_0^B$  is the population of the semi-solid pool. The  $R_{rfB}$  parameter is the RF absorption rate of the semi-solid pool and it depends on the absorption line shape of the restricted pool, which is typically described by a Gaussian function:

$$R_{rfB} = \omega_1^2 \cdot \sqrt{\frac{\pi}{2}} \cdot T_2^B \cdot e^{-\frac{(2\pi\Delta T_2^B)^2}{2}} \quad \text{Eq. 2.2}$$

Four parameters were obtained from the fitting, namely:  $R_{ex} M_0^B / R_1^A$ ,  $T_2^B$ ,  $R_{ex}$ , and  $R_2^A / R_1^A$ . It is known from the literature that the model is weakly dependent on  $R_1^B$  and that it is not possible to obtain a precise estimate of this parameter from the model. Therefore,  $R_1^B$  was fixed to  $1 \text{ s}^{-1}$  (Morrison, Stanisz, & Henkelman, 1995). The  $R_{ex} M_0^B / R_1^A$  and  $R_{ex}$  parameters are of particular interest for monitoring protein digestion, because they describe the  $^1\text{H}$  protein-water exchange kinetics, which is expected to change during protein digestion. For simplicity and in analogy to *MTR*, in the following the  $R_{ex} M_0^B / R_1^A$  parameter will be referred to as the composite exchange rate (*CER*).

### 2.2.6. Data processing and calculations

All processing and calculations were done in MATLAB R2019b (MathWorks, Massachusetts, USA). Each magnitude spectrum was obtained as the absolute value of the respective complex spectrum after Fourier transformation of the free induction decays (FIDs). The maximum intensity of the water peak was calculated for the different  $\omega_1$  and  $\Delta$ , which were subsequently used to calculate the  $S_{sat}/S_0$  ratio. Global fitting of the  $S_{sat}/S_0$  ratios was performed with the two-pool exchange model using the non-linear least squares method with the trust-region algorithm. The 95% confidence interval (CI) for each model parameter was determined via a bootstrap procedure with residual re-sampling and included 1000 repetitions (Efron & Tibshirani, 1993). To obtain a good estimate of the 95% CI for the  $CER$  from the one-datapoint fit, a Gaussian distribution of 1000 samples was simulated for the  $S_{sat}/S_0$  obtained with  $\omega_1/2\pi = 0.50$  and  $\Delta = 7.5$  kHz. The standard deviation for the simulation was estimated from triplicate measurements of the  $S_{sat}/S_0$ . The simulated  $S_{sat}/S_0$  ratios were separately fitted with the two-pool exchange model, resulting in 1000 values for  $CER$  from which the 95% CIs were calculated. All parameters in the model, except the  $CER$ , were fixed to their respective average value across the different digestion samples.

### 2.2.7. Protein content quantification

First the supernatant was separated from the coagulum by centrifuging the digestion sample at 10000 *g* for 30 min. The white semi-solid protein coagulum was obtained as a result of phase separation occurring during *in vitro* protein digestion. Next, the soluble nitrogen content in the supernatant was quantified using a DUMAS Flash EA 1112 Protein analyzer (Thermo Fisher Scientific, Massachusetts, USA). A conversion factor of 6.38 was used to obtain the protein content from the nitrogen content. The coagulated protein fraction was calculated by subtracting the protein content in the supernatant from the total known amount of protein in the sample.

### 2.2.8. RP-HPLC

The total amount of caseins in the supernatant of the digestion samples was determined by RP-HPLC (Thermo Scientific™UltiMate 3000, Massachusetts, USA) equipped with an Aeris Widepore 3.6  $\mu\text{m}$  XB-C18 column, 250  $\times$  4.6 mm (Phenomenex, the Netherlands), according to the method described by de Vries et al. (2015). Two solvents (A and B), consisting of 0.1% TFA in milliQ water (Millipore, Billerica, MA) and 0.1% TFA in acetonitrile, respectively, were used as the mobile phase for protein elution. The resulting chromatograms were analyzed with Chromeleon 7.1.2. (Thermo Fisher Scientific, Massachusetts, USA). The sum of the peak areas of  $\alpha_{s1}$ -,  $\alpha_{s2}$ -,  $\beta$ -, and  $\kappa$ -casein in the supernatant were determined for each of the digestion samples.

## 2.3. Results and discussion

### 2.3.1. MT spectra of raw and heated SM during *in vitro* gastric protein digestion

*In vitro* gastric digestion of SM was followed by recording MT spectra as a function of the frequency offset with  $\omega_1/2\pi = 0.50$  kHz. Especially in the frequency offset range 2-10 kHz, the MT spectra of both raw (Fig. 2.1a) and heated (Fig. 2.1c) SM deviated from the reference sigmoid curve expected for a system, such as bulk water, devoid of MT effects. The observed shape was characteristic of a system containing a semi-solid macromolecular pool, similar to what has been observed for agar gels and membrane mixtures (Morrison et al., 1995). In such a system, MT is expected to occur between the NMR signal of semi-solid macromolecules and that of water via  $^1\text{H}$  dipolar coupling.

A shift from high to low frequency offsets was observed in the MT spectra of raw SM with increasing digestion times (Fig. 2.1a). Large differences were observed between the MT spectra at  $t = 0$  min and  $t = 1$  min as well as between  $t = 1$  min and  $t = 5$  min. The shift in the MT spectra indicates that both the semi-solid proteins and the exchange rate decreased with increasing digestion time. The decrease in the amount of semi-solid proteins was also visible in the digestion

samples (Fig. 2.1b). The photographs of the digestion samples showed that a physical separation occurred between a semi-solid pool that consisted of coagulated caseins and a supernatant that consisted of soluble proteins and peptides. Initially, casein coagulation takes place because the acidic environment during gastric digestion neutralizes the negative charge on the surface of the casein micelles. These neutralized casein micelles will interact with each other and aggregate to form small flocs (Fig. 2.1b,  $t = 0$  min) that can aggregate further to form a coagulum once pepsin is added (Fig. 2.1b,  $t = 1$  min).

Pepsin cleaves, amongst others, the  $\kappa$ -casein tails on the surface of the casein micelles, which leads to the formation of a tighter coagulum that can be macroscopically observed as a clot (Fig. 2.1b,  $t = 1$  min). As the digestion continues, the casein coagulum is broken down by pepsin through hydrolysis of peptide bonds (Didier Dupont & Tomé, 2014). This was observed in both the MT spectra and the photographs of the digestion samples. After  $t = 5$  min, the MT spectra largely overlapped, with only small differences observed in the intermediate range of frequency offsets, namely 2-10 kHz, where the  $^1\text{H}$  protein-water exchange is mostly captured. We note that the MT spectra were different from those of water, which indicates that even at  $t = 60$  min still some semi-solid protein was present in the sample.

The protein coagulum in heated SM consists of both caseins and denatured WP. The MT spectra of heated SM (Fig. 2.1c) were notably different from those of raw SM (Fig. 2.1a). Lower  $S_{sat}/S_0$  values and smaller differences between  $t = 0$  and 30 min were observed for heated SM than for raw SM, especially in the frequency offset range 2-10 kHz. The most significant variation in the MT spectra of heated SM was observed between  $t = 30$  and 60 min. This indicates that heating slows down the *in vitro* gastric digestion of the protein coagulum under infant digestion conditions, which is in agreement with the photographs of the digestion samples (Fig. 2.1d). After 60 min of digestion, only a small amount of casein coagulum was present for raw SM, whereas for heated SM the amount of protein coagulum was similar to that of raw SM at  $t = 5$  min.

The heated SM sample was prepared by heating raw SM for 30 min at 80°C, resulting in 90% WP denaturation, which is quite high. To explore whether MT can distinguish raw SM from heated SM with a lower WP denaturation level, we also

measured heated SM with 27% WP denaturation (Fig. S2.1). These results showed that from  $t = 1$  min onwards, the MT spectra of the three milk samples are distinctly different from each other. At  $t = 60$  min, the MT spectra of the two heated milk samples overlap, but can still be distinguished from the respective spectrum of raw milk. Therefore, it is possible to study the effect of heating at different temperatures on the breakdown of the protein coagulum with MT.

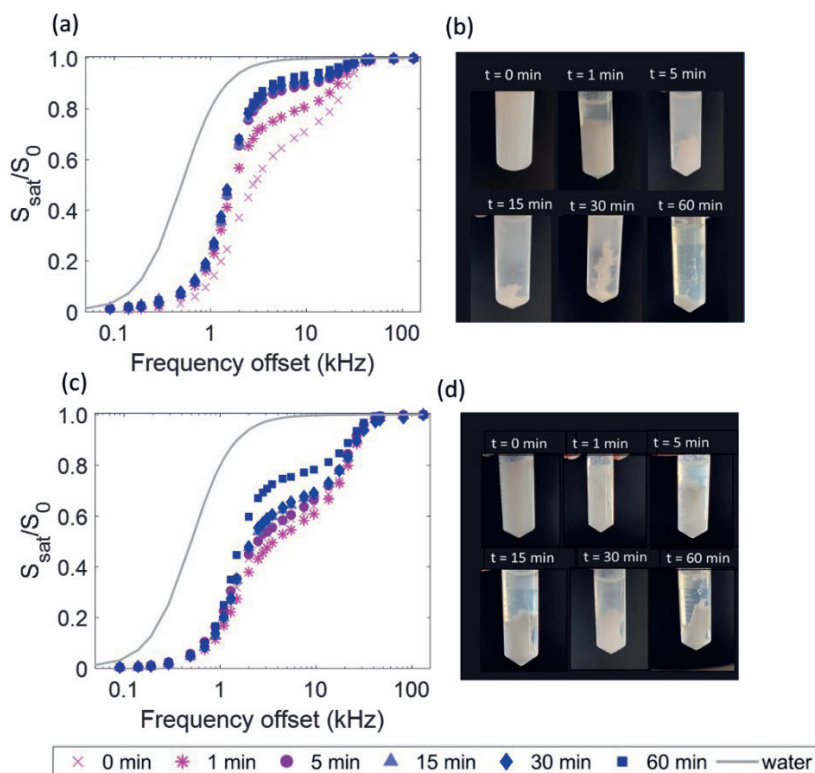


**Figure 2.1.** Left:  $^1\text{H}$  MT NMR spectra acquired with  $\omega_1/2\pi=0.50$  kHz for (a) raw skim milk and (c) skim milk heated at  $80^\circ\text{C}$  (90% Whey protein denaturation) digested in the *in vitro* infant gastric digestion model for  $t=0, 1, 5, 15, 30$  and  $60$  min. Right: photographs of the digestion samples of (b) raw and (d) heated skim milk, in which two phases can be distinguished, namely a precipitate consisting of the coagulum and a supernatant consisting of soluble proteins and peptides.

### 2.3.2. Multi-parameter fitting of MT spectra

Protein digestion was quantitatively monitored by fitting MT spectra obtained at different  $\omega_1/2\pi$  and  $\Delta$  values with the two-pool exchange model (Henkelman et al., 1993). We also assessed the performance of three- and two-pool exchange

with the inclusion of a dipolar order models, respectively containing 10 and 5 fitting parameters (data not shown) (Ceckler, Maneval, & Melkowits, 2001). As expected, fitting errors with the three-pool exchange model were very large, even for simulated data. The two-pool exchange model with inclusion of a dipolar order contains one extra fitting parameter, given by the relaxation time of the dipolar order. The latter, although significant for systems with strong molecular order and immobility, such as lipid bilayers, is expected to be negligible for coagulated milk proteins (Morrison et al., 1995). Hence, these examined models with inclusion of a dipolar reservoir either reduced, or did not improve, the quality of the fit. Based on the above considerations, we decided to adopt the four-parameter two-pool exchange model, from which the dimensionless composite parameters,  $CER (R_{ex}M_0^B/R_1^A)$  and  $R_2^A/R_1^A$ , and the single parameters,  $T_2^B$  and  $R_{ex}$ , were obtained. The  $CER$  and  $R_{ex}$  are of particular interest for monitoring protein digestion because they describe the  $^1\text{H}$  protein-water exchange kinetics.

First, the number of measurements at distinct  $\omega_1/2\pi$  and  $\Delta$  values was optimized for obtaining accurate and precise fitting of MT spectra of SM with the two-pool exchange model, yet minimizing the measurement time. We found that reducing the number of saturation pulse powers from seven to three values, namely  $\omega_1/2\pi = 1.40, 0.78$  and  $0.50$  kHz, did not have an effect on the fitting value and error. The optimal values for the saturation pulse power depended on the exchange rate of the sample under study, and for raw SM these values gave the best fit. With 29 offsets, it was possible to include sufficient points in the intermediate offset range while also sampling the two plateaus, which was essential for accurate fitting of the data (Fig. S2.2 and Table S2.1).

Next, the MT spectra recorded with the optimized acquisition parameters for raw and heated SM samples at different time points during *in vitro* gastric digestion were fitted with the two-pool exchange model. In general, the fitting successfully described the MT spectra of the digestion samples (Fig. 2.2 and Fig. S2.3). However, in a few cases, at  $\omega_1/2\pi=0.5$  kHz and low-frequency offsets, the fitting line deviated from the data. This became more evident for the longer digestion time points, especially from  $t = 5$  min onwards for raw SM. In these cases, a super-Lorentzian line shape provided a better fit than the Gaussian line shape

(Fig. S2.4 and Table S2.2), but in view of a uniform fitting procedure, we chose to fit all MT spectra with a Gaussian line shape.

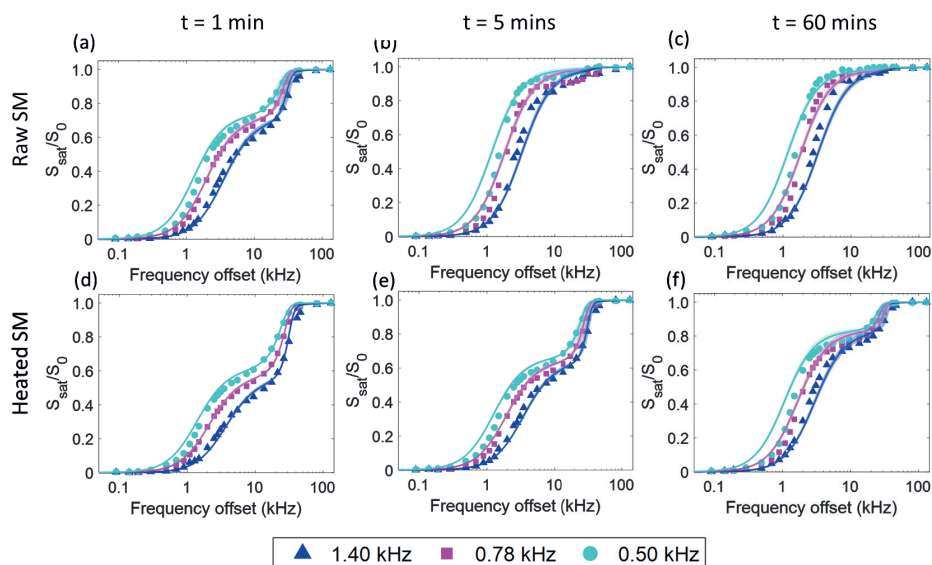


**Figure 2.2.**  $^1\text{H}$  MT NMR spectra measured with  $\omega_1/2\pi = 1.40, 0.78$  or  $0.50$  kHz for raw skim milk (top panel) or heated skim milk with 90% whey protein denaturation (bottom panel) digested in the *in vitro* infant gastric digestion model at  $t = 1$  (a and d),  $t = 5$  (b and e) and  $t = 60$  min (c and f). The solid line represents the multiparameter fitting of the two-pool exchange model to the MT data. The thickness of the line represents the 95% confidence intervals that were calculated via bootstrapping (see section 2.2.6).

Fitting the data with the two-pool exchange model provided plausible values for the model parameters (Fig. 2.3 and Table S2.3). The parameters are shown with 95% CIs as derived via bootstrapping. The obtained CIs indicate that all parameters, except  $R_{ex}$ , can be obtained with a relative standard error of  $\leq 10\%$ . For  $R_{ex}$ , the estimated relative standard error is 10-55%. With the larger errors corresponding to the later digestion time points for raw SM. These errors enable quantitative assessment of the impact of digestion on  $T_2^B$ ,  $R_2^A/R_1^A$ ,  $CER$ . As shown in Fig. 2.3a, the  $T_2^B$  and  $R_2^A/R_1^A$  parameter did not notably vary during *in vitro* digestion, but were useful for verifying fitting performance and plausibility of returned values. Since both the  $T_2^B$  and  $R_2^A/R_1^A$  do not largely vary during *in vitro* digestion, fixing these parameters in the model could be considered for increasing the confidence levels for  $CER$  and  $R_{ex}$ . Indeed, fixing  $T_2^B$  and  $R_2^A/R_1^A$  to their average



value across the digestion duration resulted in a  $\sim 2.5$  and 4-fold decrease in the error of the  $CER$  and  $R_{ex}$  respectively.

However, a one-way ANOVA revealed that there was still a statistically significant variation over the digestion duration for  $T_2^B$  for both raw SM ( $F(5,12) = [357.4]$ ,  $P = <0.001$ ) and heated SM ( $F(5,12) = [59.70]$ ,  $P = <0.001$ ).

The same was found for  $R_2^A/R_1^A$  for both raw SM ( $F(5,12) = [1905]$ ,  $P = <0.001$ ) and heated SM ( $F(5,12) = [2165]$ ,  $P = <0.001$ ). Therefore, we decided to treat the  $T_2^B$  and  $R_2^A/R_1^A$  as free parameters in the fitting. The  $T_2^B$  remained short, around 14-19  $\mu\text{s}$ , due to the restricted molecular motion of  $^1\text{H}$  in the coagulum. This is in agreement with the expected short value of  $T_2^B$  for semi-solid macromolecules, with 9-20  $\mu\text{s}$  being the range typically reported in the literature, which is too short to be measured by conventional NMR (Graham, Stanisiz, Kecojevic, Bronskill, & Henkelman, 1999; Jerban et al., 2018). Therefore, the semi-solid protein pool ( $M_0^B$ ) can only be detected indirectly, by making its signal cross-relax with that of water by, for example, magnetization transfer. The  $R_2^A/R_1^A$  ratio is expected to be larger than 1 for water molecules with restricted mobility, which is the case when a large amount of semi-solid protein is present in the sample. For the digestion samples, the  $R_2^A/R_1^A$  was between 5-13. The mobility of the water molecules is expected to increase during digestion due to a decrease in the amount of coagulum. This explains the decrease observed in the  $R_2^A/R_1^A$  from  $t = 0$  to 5 min and  $t = 0$  to 60 min for raw and heated SM, respectively. Both the composite parameter  $CER$  (Fig. 2.3c) and the chemical exchange rate  $R_{ex}$  (Fig. 2.3d) increased with the amount of semi-solid proteins present in the sample due to correspondingly more efficient protein-water magnetization transfer. The caseins in the coagulum are broken down into insoluble peptides that remain in the coagulum but also soluble peptides that move into the supernatant, thereby leading to a decrease in the  $CER$  and  $R_{ex}$ . While both of these parameters are promising for monitoring protein digestion, the  $CER$  was determined with a smaller error than  $R_{ex}$ . In addition, the  $CER$  depends not only on the exchange rate but also on the amount of semi-solid protein, which is known to change during protein digestion; furthermore, the  $CER$  proved comparably more sensitive to heat treatment. Therefore,  $CER$  will be considered as the most informative MT fitting parameter for studying the breakdown of the protein coagulum.

The  $CER$  for raw SM largely decreased from  $t = 0$  to 5 min, followed by a plateau towards values close to zero (Fig. 2.3c). This indicates that most of the breakdown of the casein coagulum occurred within the first 5 min. The  $CER$  for heated SM increased slightly from  $t = 0$  to  $t = 1$  min followed by a decrease from  $t = 1$  to  $t = 60$  min (Fig. 2.3c), which is in agreement with the photographs in section 2.3.1 (Fig. 2.1b). The  $CER$  values at all digestion time points were higher for heated SM due to its larger semi-solid protein content compared to raw SM. The observed difference between raw and heated SM in the decrease of  $CER$  during gastric digestion indicates that heating may cause slower digestion of the protein coagulum. These results show that the  $CER$  parameter can be used to monitor both *in vitro* gastric digestion and changes in the digestion caused by heating.

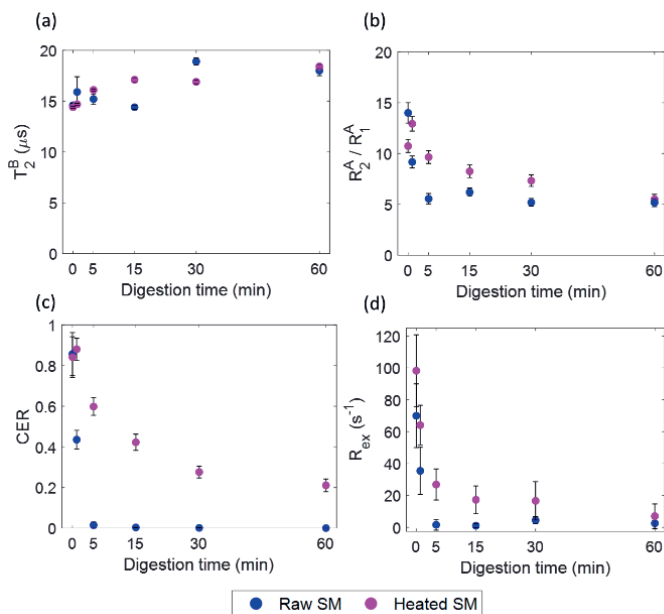


**Figure 2.3.** Evolution of relaxation parameters (a)  $T_2^B$ , (b)  $R_2^A/R_1^A$  and MT parameters (c)  $CER$  and (d)  $R_{ex}$  obtained from the multi-parameter fit of the two-pool exchange model to the MT spectra for raw SM and heated SM with 90% WP denaturation during *in vitro* gastric protein digestion.

### 2.3.3. Rapid MT measurements for monitoring digestion

While the *CER* can successfully be used to monitor *in vitro* gastric protein digestion, the experimental conditions required to acquire multiple MT spectra and, thus, estimate *CER*, are not compatible with dynamic studies of *in vivo* protein digestion. This is because the overall measurement time and RF irradiation power, respectively, exceed the duration of the digestion process itself and the specific absorption rate (SAR) limitations on clinical MRI scanners. In addition, faster measurements that fit within one breath hold are preferred in order to avoid motion-related artifacts. Therefore, we explored whether the *CER* could be obtained from a single MT measurement, at a single combination of  $\omega_1/2\pi$  and  $\Delta$  values, if all other parameters in the two-pool exchange model were fixed. The data point at  $\omega_1/2\pi = 0.50$  and  $\Delta = 7.50$  kHz was chosen because, with this combination, the difference in  $S_{sat}/S_0$  for the different digestion samples was maximized, while the effect of direct saturation of the water signal was minimized. For estimation of the fitting error of *CER*, a Gaussian distribution with 1000 samples of the  $S_{sat}/S_0$  was simulated. The fitting was performed with 1000 repetitions, resulting in 1000 values for the *CER* for each digestion sample from which the 95% CIs were calculated. All other parameters in the model were fixed to their average value across the different digestion time points. The *CER* values obtained from the single-datapoint fit (Fig. 2.4a) were comparable to the values obtained from the multiparameter fit of 87 data points (Fig. 2.4b) and, as expected, the fitting error was larger. Overall, the single-datapoint fit of *CER* for both raw (Fig. 2.4c) and heated (Fig. 2.4d) SM allows for the assessment of the impact of the digestion time. The larger errors observed for the longer digestion times are in agreement with the results from the multi-parameter global fit (Fig. 2.2a-c). This approach was based on the assumption that the values of the other model parameters did not significantly affect the outcome of the single-datapoint fit. This was justified because fixing those parameters to other physically realistic values, for example values within the 95% CI obtained from the multiparameter global fitting, did not affect the value of *CER* obtained from the one-datapoint fit. (Fig. S2.5). This demonstrates that the *CER* can be obtained reliably from a single-shot measurement if all other model parameters are fixed to physically realistic values.

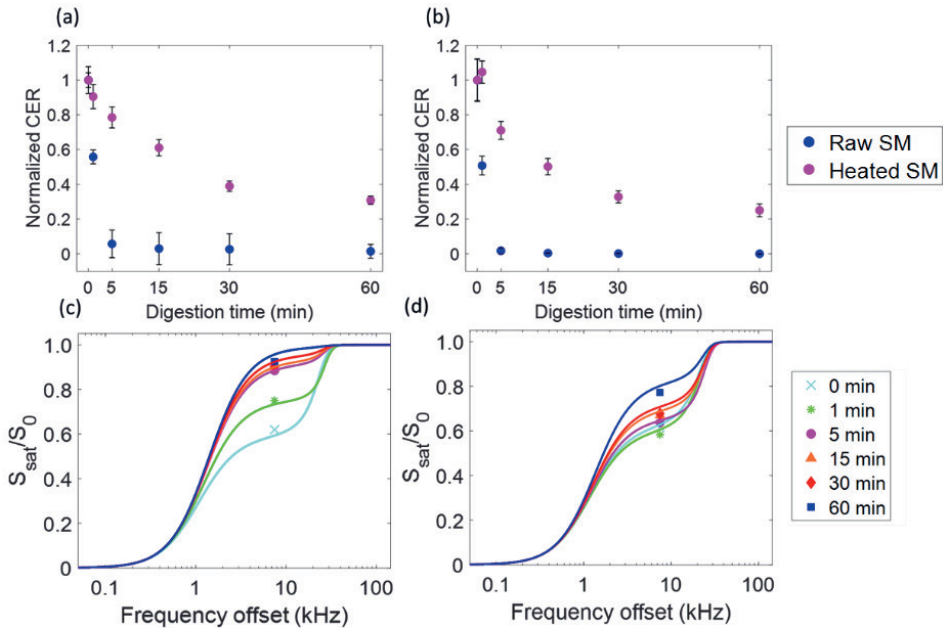


**Figure 2.4.** Evolution of CER during *in vitro* infant gastric digestion obtained from (a) fitting a single-data point at  $\omega_1/2\pi = 0.50$  and  $\Delta = 7.5$  kHz with the two-pool exchange model in which all parameters except for the CER were fixed to the average value from the multiparameter fit (b) multiparameter global fitting of MT data at  $\omega_1/2\pi = 1.40, 0.78$  and  $0.50$  kHz. Fitting of one datapoint for  $\omega_1/2\pi = 0.50$  and  $\Delta = 7.5$  kHz for (c) raw and (d) heated SM (90% WP denaturation) at different time points during *in vitro* infant gastric digestion. The CER is normalized to the value at  $t = 0$ . The error bars in (a) represent the 95% confidence intervals, which were calculated via bootstrapping, the error bars in (b) represent the 95% CI interval based on simulating a Gaussian distribution of the single-datapoint with  $n=1000$  and then fitting the simulated datapoints with the two-pool exchange model.

A feasible approach for *in vivo* monitoring of protein digestion is to use the MT ratio (*MTR*), which can simply be calculated as  $1 - S_{sat}/S_0$ . The *MTR* is semi-quantitative and does not provide information on the magnetization transfer kinetics. However, the advantage of using the *MTR* over the *CER* obtained from the one-datapoint fit is that the former does not rely on assumptions nor fitting, and is already an established method in *in vivo* MRI (Geeraert et al., 2018).

The *MTR* and the *CER* both depend on the amount of MT that takes place between the semi-solid protein and the water pool. Therefore, they are expected to follow the same trend during *in vitro* gastric protein digestion. To collect data with optimal MT effect for the digestion samples, the same  $\omega_1/2\pi$  and  $\Delta$  were used as for the single-datapoint fitting approach. The *MTR* for both raw and heated SM decreased with increasing digestion times (Fig. 2.5a). Higher *MTR* values and a slower variation in the *MTR* were observed for heated SM as compared to raw SM during *in vitro* gastric digestion. These observations are in agreement with the trends observed for the *CER*. However, the variation in the *MTR* for both raw and heated SM was smaller in the first 5 min of *in vitro* gastric digestion, and, in contrast to the *CER* no clear plateau was reached after 5 min for raw SM. Whether the *MTR* follows the trend of *CER* depends on the choice of  $\omega_1/2\pi$  and  $\Delta$ . For our selection of these parameters, Pearson correlation coefficient of *MTR* and *CER* showed a significant positive correlation for both raw SM,  $r = 0.92$ ,  $n = 5$ ,  $P = 0.001$  and heated SM,  $r = 0.95$ ,  $n = 5$ ,  $p = 0.003$ . This shows that both parameters follow the same trend and, hence, that the *MTR* can be used as a semi-quantitative alternative for the *CER* to interpret MT contrast in MRI images acquired during gastric protein digestion.

To validate *MTR* as a marker for protein digestion, we benchmarked it against commonly used reference methods, such as the OPA assay, which measures the number of free amino groups, often described as the degree of hydrolysis. This method is mainly applied to study *in vitro* gastric and intestinal digestion (Mulet-Cabero et al., 2019). However, infant gastric digestion is slow due to the low pepsin activity, and the caseins are mainly broken down into relatively large peptides (Ménard et al., 2018). The difference in the number of free amino groups between the intact proteins and large peptides is small and difficult to detect with the OPA assay. In our study, no variation was found in the number of free amino groups during *in vitro* gastric digestion for both raw and heated SM (Fig. S2.6).

Next, the total protein content and the amount of caseins in the supernatant were determined by DUMAS and RP-HPLC, respectively. The protein content in the supernatant, as determined by DUMAS, was used to calculate the protein fraction in the coagulum. It should be noted that with DUMAS, as opposed to the Bradford or Bicinchoninic Acid (BCA) assay, the total nitrogen content is measured, which

includes also the non-protein nitrogen (NPN) fraction. The NPN in milk mainly consists of urea and makes up only 5% of the total nitrogen. However, because the contribution from the NPN fraction does not vary during protein digestion, DUMAS can be reliably used for protein content analysis of our digestion samples. Furthermore, DUMAS is expected to yield less over-estimation of protein content in milk (Wu, Jackson, Khan, Ahuja, & Pehrsson, 2018) or protein-protein variability (Hayes, 2020) as compared to colorimetric methods. In the results of our DUMAS analysis shown in Fig. 2.5a, the protein fraction was higher, and the variation during *in vitro* gastric digestion was smaller, for heated SM than for raw SM. The initial protein fraction in the coagulum was smaller than for the subsequent digestion times, because the coagulum at  $t = 0$  min consisted of small flocs that were formed by acid-induced coagulation and the majority of proteins in the sample were at that point still in the supernatant. This was in contrast with the *MTR* and *CER* results, for which the bulk sample was measured and, therefore, contributed to the MT process. At  $t = 0$  min, the caseins were mainly present as micelles in milk, whereas at later digestion time points a separation into a liquid and semi-solid phase was observed. In these bulk measurements, the contribution from the liquid phase affects the overall *MTR*, resulting in lower values as digestion progresses during which the liquid phase increases.

The *MTR* results were further benchmarked by comparing the *MTR* of the supernatant (Fig. 2.5b with the sum of the peak areas for caseins obtained from RP-HPLC analysis of the supernatant. The *MTR* of the supernatant at  $t = 1$  and 5 min was higher for heated than for raw SM. After 15 min the *MTR* is the same for both raw and heated SM. At  $t = 1$  and 5 min, the supernatant of heated SM contained some coagulated particles, explaining the higher *MTR* measured for those samples. The sum of peak areas of caseins for heated SM were always lower or the same as those for raw SM, indicating that the supernatant from heated SM contained less or the same amount of intact casein as that of raw SM. A difference was observed between the *MTR* and RP-HPLC analysis for  $t = 0$  and 5 min, which can be explained by the fact that all solid particles had to be removed from the sample for the RP-HPLC analysis, while this was not needed for the *MTR* measurements. As there was nearly no intact casein in the supernatant, RP-HPLC analysis of the supernatant alone is not sufficient to get a complete picture of the digestion.

Overall, the MT results are in agreement with the reference methods and a positive significant correlation was found between the *MTR* and protein fraction in the clot ( $r = 0.95$ ,  $P < 0.001$ ,  $n = 10$ ; Fig 2.5c). It should be noted that an additional advantage of the MT-NMR methods is that the *MTR* is more sensitive to gastric protein digestion compared to protein content measurements. The decrease in the *MTR* between  $t = 1$  min and 60 min is 60% and 45% for raw and heated SM, respectively, while the corresponding decrease in the protein content is 10% for both milk samples.

The MT results are further supported by previous observations (Sánchez-Rivera, Ménard, Recio, & Dupont, 2015) of a difference in casein digestion kinetics between raw and heated SM. Sánchez-Rivera and co-workers found a decrease in the amount of caseins after 4 min of digestion of 80% and 8%, respectively for raw and heated SM. This is comparable with the *MTR* and *CER* results in our study. The decrease in the *MTR* was 50% and 10%, and the decrease in the *CER* was 90% and 20% for raw and heated SM, respectively. Heating can cause the caseins and denatured whey protein to aggregate together, thereby leading to slower pepsin penetration of the coagulum, which may explain the slower gastric digestion of the protein coagulum in heated SM.

In this work, we focused solely on gastric digestion because it is the first step in the digestion process, and it is well known to be affected by heat treatment. Protein digestion continues in the intestines, where the solubilized proteins and relatively large peptides, produced during gastric digestion, are further hydrolyzed into small peptides and amino acids that can be absorbed. Gastric digestion may have an influence on intestinal digestion, and thereby on subsequent absorption of small peptides and amino acids (Mulet-Cabero, Mackie, Brodkorb, & Wilde, 2020). In future works, it would be interesting to link the effect of processing on gastric digestion to the absorption of peptides and amino acids.

Our results show that  $^1\text{H}$  MT NMR can be used to monitor *in vitro* protein digestion and that the *MTR* is a promising marker for monitoring *in vivo* gastric protein digestion in humans. The current duration of the *MTR* measurements is 2.6 min, but this could be further reduced by reducing the saturation pulse length and the number of scans, to make the measurement fit within one breath hold.

The next step will be to make the MT measurements spatially-resolved and to assess the capability of MT to monitor protein digestion under conditions more similar to *in vivo* digestion, e.g. by using a dynamic *in vitro* digestion model.

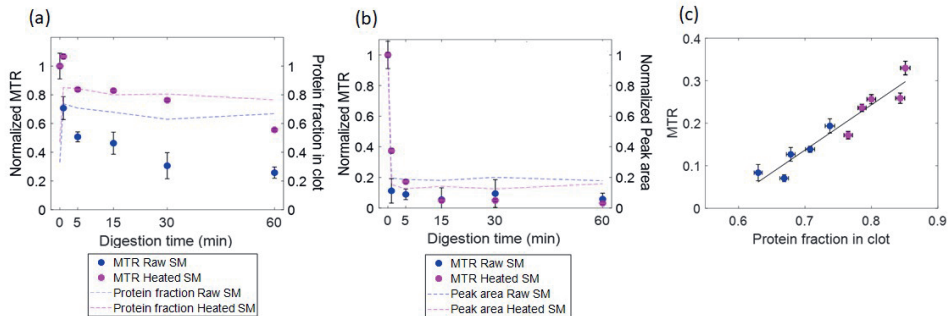


**Figure 2.5.** (a) Evolution of normalized MTR of coagulum and supernatant calculated as  $1 - S_{\text{sat}}/S_0$  for  $\omega_1/2\pi = 0.50 \pm 0.05$  kHz and  $\Delta = 7.5$  kHz at different time points during *in vitro* infant gastric digestion of raw and heated SM. The protein fraction in the coagulum is plotted in the same figure and was calculated by subtracting the amount of protein in the supernatant determined by DUMAS from the total amount of protein in the sample. (b) normalized MTR of the supernatant and normalized sum of peak areas of caseins determined by RP-HPLC analysis of the supernatant. The MTR and peak areas were normalized to their respective values at  $t = 0$  min. (c) The MTR plotted against the protein fraction in the clot. The Pearson correlation coefficient of the MTR and the protein fraction in the clot for both samples showed a significant positive correlation ( $r = 0.95$ ,  $P < 0.001$ ,  $n = 10$ ). The first time point, at  $t = 0$  min, has been left out of the correlation analysis.



## 2.4. Conclusions

$^1\text{H}$  MT NMR was successfully applied, and benchmarked against reference methods, to non-invasively study *in vitro* gastric protein digestion of raw and heated SM. The MT spectra are sensitive to changes in the  $^1\text{H}$  protein-water interactions, which occurred during protein digestion. The quantitative composite parameter, *CER*, can be determined as a function of digestion time with a relative standard error of  $\leq 10\%$ , both by MT spectra and single-point MT measurements. The decrease in the *CER* is in line with the literature and reference data of *in vitro* gastric digestion of SM. Therefore, the *CER* is a suitable parameter for monitoring *in vitro* gastric protein digestion. For a more rapid MT measurement that does not require data fitting, the semi-quantitative *MTR* can be used, which is more feasible for *in vivo* studies on clinical MRI systems. Heating of SM results in a slower decrease of the *CER* and *MTR* with digestion, indicating a difference in protein coagulum digestion kinetics between heated and raw SM. Therefore, MT could also be applied to study the effect of processing on protein digestion. Our results pave the way for future *in vivo* quantification of protein digestion by means of MT-MRI.

### Authorship contribution statement

Morwarid Mayar: Conceptualization, Investigation, Methodology, Validation, Writing original draft; Julie Miltenburg: Investigation, Validation; Kasper Hettinga: Reviewing the manuscript, Funding acquisition; John van Duynhoven: Conceptualization, Reviewing all versions of the manuscript, Paul Smeets: Conceptualization, Reviewing all versions of the manuscript; Camilla Terenzi: Conceptualization, Methodology, Reviewing all versions of the manuscript.

## Acknowledgements

Gert-Jan Goudappel is gratefully acknowledged for providing the MT-NMR pulse sequence and for help with setting up the measurements. We thank BSc thesis student Dirk Wevers for his contribution to optimizing the MT acquisition parameters. Ewoud van Velzen is gratefully acknowledged for his expert advice on modelling and bootstrapping. Camilla Terenzi acknowledges funding from the 4TU Precision Medicine program supported by High Tech for a Sustainable Future: ([https://www.4tu.nl/en/news/!/393/awarding\\_hightech/](https://www.4tu.nl/en/news/!/393/awarding_hightech/)).

## References

- Balaban, R., & Ceckler, T. (1992). Magnetization transfer contrast in magnetic resonance imaging. *Magn Reson Q*, 8(2), 116–137.
- Bordoni, A., Picone, G., Babini, E., Vignali, M., Danesi, F., Valli, V., ... Capozzi, F. (2011). NMR comparison of in vitro digestion of Parmigiano Reggiano cheese aged 15 and 30 months. *Magnetic Resonance in Chemistry*, 49, 61–70. <https://doi.org/10.1002/mrc.2847>
- Bornhorst, G. M., & Paul Singh, R. (2014). Gastric Digestion In Vivo and In Vitro: How the Structural Aspects of Food Influence the Digestion Process. *Annual Review of Food Science and Technology*, 5(1), 111–132. <https://doi.org/10.1146/annurev-food-030713-092346>
- Brodkorb, A., Egger, L., Alminger, M., Alvito, P., Assunção, R., Ballance, S., ... Recio, I. (2019). INFOGEST static in vitro simulation of gastrointestinal food digestion. *Nature Protocols*, 14(4), 991–1014. <https://doi.org/10.1038/s41596-018-0119-1>
- Ceckler, T., Maneval, J., & Melkowitz, B. (2001). Modeling magnetization transfer using a three-pool model and physically meaningful constraints on the fitting parameters. *Journal of Magnetic Resonance*, 151(1), 9–27. <https://doi.org/10.1006/jmre.2001.2326>
- Chinachoti, P., Vittadini, E., Chatakanonda, P., & Vodovotz, Y. (2008). Characterization of Molecular Mobility in Carbohydrate Food Systems by NMR. In *Modern Magnetic Resonance* (Webb G.A., pp. 1703–1712). Dordrecht: Springer. [https://doi.org/10.1007/1-4020-3910-7\\_191](https://doi.org/10.1007/1-4020-3910-7_191)
- de Vries, R., van Kneysel, A., Johansson, M., Lindmark-Månsson, H., van Hooijdonk, T., Holtenius, K., & Hettinga, K. (2015). Effect of shortening or omitting the dry period of Holstein-Friesian cows on casein composition of milk. *Journal of Dairy Science*, 98(12), 8678–8687. <https://doi.org/10.3168/jds.2015-9544>
- De Zwart, I. M., & De Roos, A. (2010). MRI for the evaluation of gastric physiology. *European Radiology*, 20(11), 2609–2616. <https://doi.org/10.1007/s00330-010-1850-3>
- Deng, R., Janssen, A. E. M., Vergeldt, F. J., Van As, H., de Graaf, C., Mars, M., & Smeets, P. A. M. (2020). Exploring in vitro gastric digestion of whey protein by time-domain nuclear magnetic resonance and magnetic resonance imaging. *Food Hydrocolloids*, 99(2019), 105348–105358. <https://doi.org/10.1016/j.foodhyd.2019.105348>
- Dupont, D., Alric, M., Blanquet-Diot, S., Bornhorst, G., Cueva, C., Deglaire, A., ... Van den Abbeele, P. (2019). Can dynamic in vitro digestion systems mimic the physiological

- reality? *Critical Reviews in Food Science and Nutrition*, 59(10), 1546–1562.  
<https://doi.org/10.1080/10408398.2017.1421900>
- Dupont, Didier, & Tomé, D. (2014). Milk Proteins: Digestion and Absorption in the Gastrointestinal Tract. In M. Boland & H. Singh (Eds.), *Milk Proteins From Expression to Food* (3rd ed., pp. 701–714). Cambridge Massachusetts: Academic Press.  
<https://doi.org/10.1016/B978-0-12-405171-3.00020-9>
- van Duynhoven, J., Voda, A., Witek, M., & Van As, H. B. T. (2010). Chapter 3 - Time-Domain NMR Applied to Food Products (Vol. 69, pp. 145–197). Academic Press.  
[https://doi.org/https://doi.org/10.1016/S0066-4103\(10\)69003-5](https://doi.org/https://doi.org/10.1016/S0066-4103(10)69003-5)
- Efron, B., & Tibshirani, R. J. (1993). *An Introduction to the Bootstrap*. Boca Raton, FL, USA: Chapman and Hall/CRC.
- Egger, L., Ménard, O., Baumann, C., Duerr, D., Schlegel, P., Stoll, P., ... Portmann, R. (2019). Digestion of milk proteins: Comparing static and dynamic in vitro digestion systems with in vivo data. *Food Research International*, 118(December 2017), 32–39.  
<https://doi.org/10.1016/j.foodres.2017.12.049>
- Geeraert, B. L., Lebel, R. M., Mah, A. C., Deoni, S. C., Alsop, D. C., Varma, G., & Lebel, C. (2018). A comparison of inhomogeneous magnetization transfer, myelin volume fraction, and diffusion tensor imaging measures in healthy children. *NeuroImage*, 182(2017), 343–350. <https://doi.org/10.1016/j.neuroimage.2017.09.019>
- Graham, S. J., Stanisiz, G. J., Kecojevic, A., Bronskill, M. J., & Henkelman, R. M. (1999). Analysis of changes in MR properties of tissues after heat treatment. *Magnetic Resonance in Medicine*, 42(6), 1061–1071. [https://doi.org/10.1002/\(SICI\)1522-2594\(199912\)42:6<1061::AID-MRM10>3.0.CO;2-T](https://doi.org/10.1002/(SICI)1522-2594(199912)42:6<1061::AID-MRM10>3.0.CO;2-T)
- Guo, J., Erickson, R., Trouard, T., Galons, J. P., & Gillies, R. (2003). Magnetization transfer contrast imaging in Niemann pick type C mouse liver. *Journal of Magnetic Resonance Imaging*, 18(3), 321–327. <https://doi.org/10.1002/jmri.10404>
- Hayes, M. (2020). Measuring protein content in food: An overview of methods. *Foods*, 9(10). <https://doi.org/10.3390/foods9101340>
- Henkelman, R. M., Huang, X., Xiang, Q. -S, Stanisiz, G. J., Swanson, S. D., & Bronskill, M. J. (1993). Quantitative interpretation of magnetization transfer. *Magnetic Resonance in Medicine*, 29(6), 759–766. <https://doi.org/10.1002/mrm.1910290607>
- Henkelman, R. M., Stanisiz, G. J., & Graham, S. J. (2001). Magnetization transfer in MRI: A review. *NMR in Biomedicine*, 14(2), 57–64. <https://doi.org/10.1002/nbm.683>
- Jerban, S., Ma, Y., Nazaran, A., Dorthe, E. W., Cory, E., Carl, M., ... Du, J. (2018). Detecting stress injury (fatigue fracture) in fibular cortical bone using quantitative ultrashort echo time-magnetization transfer (UTE-MT): An ex vivo study. *NMR in Biomedicine*, 31(11), 1–11. <https://doi.org/10.1002/nbm.3994>
- Le Dean, A., Mariette, F., & Marin, M. (2004). <sup>1</sup>H nuclear magnetic resonance relaxometry study of water state in milk protein mixtures. *Journal of Agricultural and Food Chemistry*, 52(17), 5449–5455. <https://doi.org/10.1021/jf030777m>
- Macierzanka, A., Böttger, F., Lansonneur, L., Groizard, R., Jean, A. S., Rigby, N. M., ... MacKie, A. R. (2012). The effect of gel structure on the kinetics of simulated gastrointestinal digestion of bovine β-lactoglobulin. *Food Chemistry*, 134(4), 2156–2163.  
<https://doi.org/10.1016/j.foodchem.2012.04.018>
- Ménard, O., Bourlieu, C., De Oliveira, S. C., Dellarosa, N., Laghi, L., Carrière, F., ... Deglaire, A. (2018). A first step towards a consensus static in vitro model for simulating full-term infant digestion. *Food Chemistry*, 240(2017), 338–345.  
<https://doi.org/10.1016/j.foodchem.2017.07.145>
- Morrison, C., Stanisiz, G., & Henkelman, R. M. (1995). Modeling Magnetization Transfer for

- Biological-like Systems Using a Semi-solid Pool with a Super-Lorentzian Lineshape and Dipolar Reservoir. *Journal of Magnetic Resonance*.  
<https://doi.org/10.1006/jmrb.1995.1111>
- Mulet-Cabero, A. I., Mackie, A. R., Brodkorb, A., & Wilde, P. J. (2020). Dairy structures and physiological responses: a matter of gastric digestion. *Critical Reviews in Food Science and Nutrition*, 60(22), 3737–3752. <https://doi.org/10.1080/10408398.2019.1707159>
- Mulet-Cabero, A. I., Mackie, A. R., Wilde, P. J., Fenelon, M. A., & Brodkorb, A. (2019). Structural mechanism and kinetics of in vitro gastric digestion are affected by process-induced changes in bovine milk. *Food Hydrocolloids*, 86, 172–183.  
<https://doi.org/10.1016/j.foodhyd.2018.03.035>
- Nakai, S., & Li-Chan, E. (1987). Effect of Clotting in Stomachs of Infants on Protein Digestibility of Milk. *Food Structure*, 6(2), 161–170.
- Sánchez-Rivera, L., Ménard, O., Recio, I., & Dupont, D. (2015). Peptide mapping during dynamic gastric digestion of heated and unheated skimmed milk powder. *Food Research International*, 77, 132–139.  
<https://doi.org/https://doi.org/10.1016/j.foodres.2015.08.001>
- Sinclair, C. D. J., Samson, R. S., Thomas, D. L., Weiskopf, N., Lutti, A., Thornton, J. S., & Golay, X. (2010). Quantitative magnetization transfer in in vivo healthy human skeletal muscle at 3 T. *Magnetic Resonance in Medicine*, 64(6), 1739–1748.  
<https://doi.org/10.1002/mrm.22562>
- Sled, J. G. (2018). Modelling and interpretation of magnetization transfer imaging in the brain. *NeuroImage*, 182(2017), 128–135. <https://doi.org/10.1016/j.neuroimage.2017.11.065>
- Smeets, P. A. M., Deng, R., Van Eijnatten, E. J. M., & Mayar, M. (2020). Monitoring food digestion with magnetic resonance techniques. *Proceedings of the Nutrition Society*, (3), 1–11. <https://doi.org/10.1017/S0029665120007867>
- Spiller, R., & Marciari, L. (2019). Intraluminal impact of food: New insights from MRI. *Nutrients*, 11(5), 1147–1161. <https://doi.org/10.3390/nu11051147>
- van Duynhoven, J. P. M., Kulik, A. S., Jonker, H. R. A., & Haverkamp, J. (1999). Solid-like components in carbohydrate gels probed by NMR spectroscopy. *Carbohydrate Polymers*, 40(3), 211–219. [https://doi.org/10.1016/S0144-8617\(99\)00056-9](https://doi.org/10.1016/S0144-8617(99)00056-9)
- van Lieshout, G. A. A., Lambers, T. T., Bragt, M. C. E., & Hettinga, K. A. (2020). How processing may affect milk protein digestion and overall physiological outcomes: A systematic review. *Critical Reviews in Food Science and Nutrition*, 60(14), 2422–2445.  
<https://doi.org/10.1080/10408398.2019.1646703>
- Van Zijl, P. C. M., Zhou, J., Mori, N., Payen, J. F., Wilson, D., & Mori, S. (2003). Mechanism of magnetization transfer during on-resonance water saturation. A new approach to detect mobile proteins, peptides, and lipids. *Magnetic Resonance in Medicine*, 49(3), 440–449.  
<https://doi.org/10.1002/mrm.10398>
- Walstra, Pieter, Wouters, Jan T. M., Geurts, T. J. (2006). *Dairy science and technology* (2nd ed.). Boca Raton, FL: CRC Press.
- Wu, X., Jackson, R. T., Khan, S. A., Ahuja, J., & Pehrsson, P. R. (2018). Human milk nutrient composition in the United States: Current knowledge, challenges, and research needs. *Current Developments in Nutrition*, 2(7), 1–18. <https://doi.org/10.1093/cdn/nzy025>

## 2.5. Supplementary Information

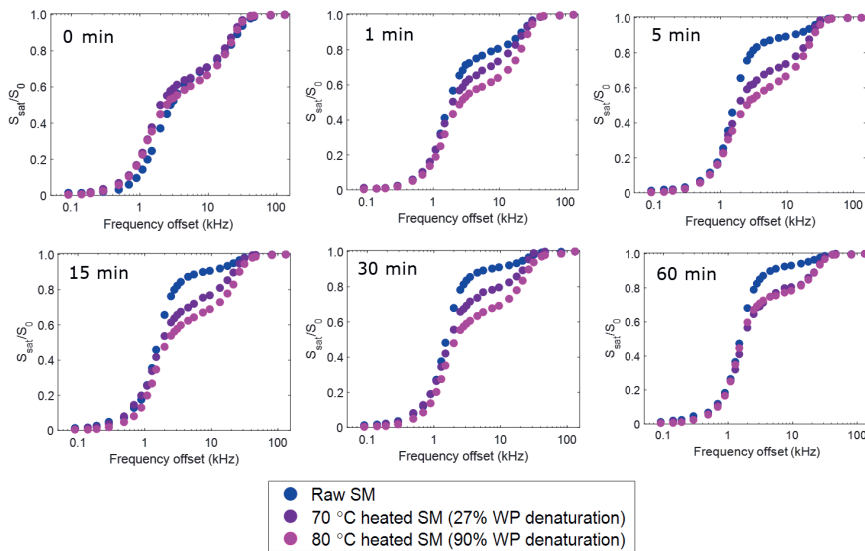


**Figure S2.1.**  $^1\text{H}$  MT NMR spectra acquired with  $\omega_1/2\pi=0.50$  kHz for raw SM (blue) and SM heated at 70°C (purple) and 80 °C (pink) digested in the *in vitro* infant gastric digestion model for  $t=0, 1, 5, 15, 30$  and 60 minutes. The digestion was stopped at each time point by adding Pepstatin A.

### 2.5.1. Optimization of $\omega_1/2\pi$ and $\Delta$ for accurate and reliable fitting of MT spectra with the two-pool exchange model

First, the number of  $\omega_1$  and  $\Delta$  were optimized for accurate and reliable fitting of MT spectra of skim milk with the two-pool exchange model. We started with a data set of 7  $\omega_1/2\pi$  and 37  $\Delta$  (Fig. S2.2a), which took 5 hours and 45 minutes to measure, and incrementally decreased this to 4  $\Delta$ . We found that the number of  $\Delta$  could be reduced to 22 without having a significant impact on the fitting value (Fig S2.2b) and error (Fig S2.2c). Moreover, the best fit was obtained when a large number of  $\Delta$  was included in the center of the MT spectrum ( $\Delta = 0.5 - 50$  kHz). Next, the number of  $\omega_1$  was systematically decreased and we found that using three  $\omega_1/2\pi$  values was sufficient to obtain an accurate fit of the MT spectra. The optimal values for  $\omega_1/2\pi$  depends on the exchange rate (Fig S2.2d) of the system under study and for raw skim milk (pH 6.7), intermediate to low values for  $\omega_1/2\pi$  gave the best fit and the parameter values and errors did not

significantly differ from those obtained from the complete data set (Fig. S2.2e; Table S2.1). With the optimized MT acquisition parameters, the measurement time was reduced to less than 2 hours.

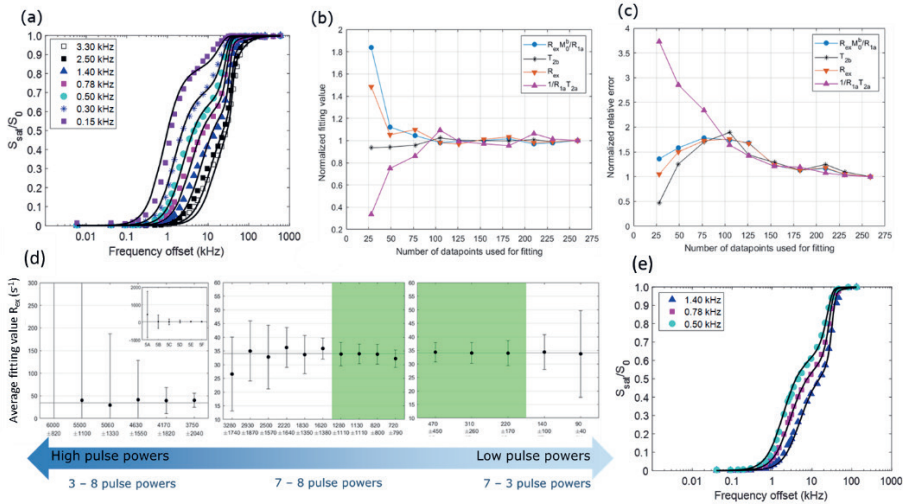


**Figure S2.** (a) MT spectra of skimmed milk at  $7 \omega_1/2\pi$  and  $37 \Delta$  forming a data set consisting of 259 data points in total. (b) Normalized fitting value as function of number of data points used for fitting, in which the number of  $\Delta$  per  $\omega_1/2\pi$  was systematically decreased. (c) Normalized fitting value as function of number of data points. (d) MT spectra of skimmed milk with the optimized MT acquisition parameters consisting of  $3 \omega_1/2\pi$  and  $29 \Delta$  resulting in a total data set size of 87. (e) The fitting value of  $R_{\text{ex}}$  with the 95% confidence interval shown as an error bar obtained from fitting simulated data with an  $R_{\text{ex}}$  of  $35 \text{ s}^{-1}$ .

## 2.5.2. Multiparameter fitting of MT data

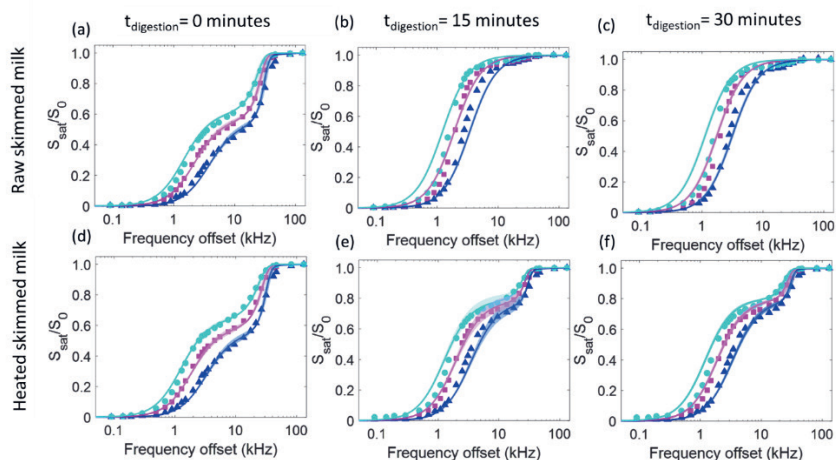


**Figure S2.3.** MT spectra obtained with saturation pulse powers,  $\omega_1/2\pi = 1.40$ ,  $0.78$  and  $0.50$  kHz at a magnetic field strength of  $7$  T for raw skim milk digested in the *in vitro* infant gastric digestion model at (a)  $t = 0$ , (b)  $t = 15$  and (c)  $t = 30$  minutes. The MT spectra under the same conditions for heated skim milk are shown in (d)  $t = 0$ , (e)  $t = 15$  and (f)  $t = 30$  minutes. The  $R_1^{\beta}$  was fixed to  $1$  s $^{-1}$ . The solid line represents the multiparameter fitting of the two-pool exchange model to the MT data. The thickness of the line represents the 95% confidence intervals that were calculated via bootstrapping (see materials and methods).

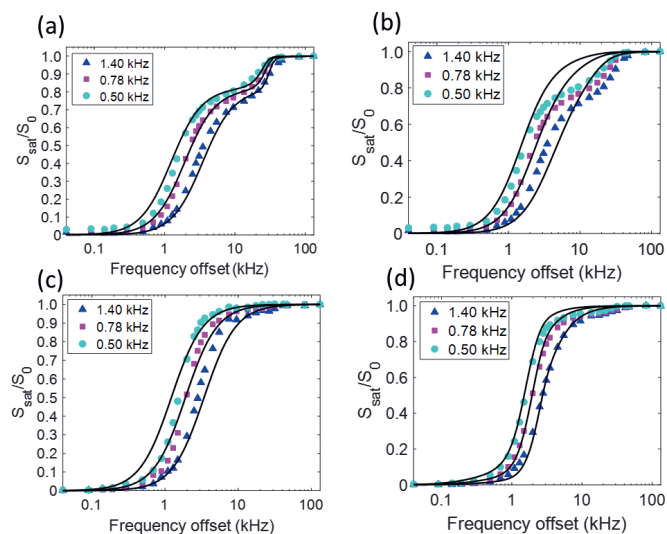


**Figure S2.4.** Left: Fitting of  $^1\text{H}$  MT NMR spectra acquired with  $\omega_1/2\pi = 0.50$ ,  $0.78$  and  $1.40$  kHz with the two-pool exchange model using a gaussian function to describe the lineshape of the semi-solid pool for raw skim milk digested in the *in vitro* infant gastric digestion model for (a)  $t = 1$  min and (c)  $t = 60$  mins. Right: same as left but with a super-Lorentzian lineshape.

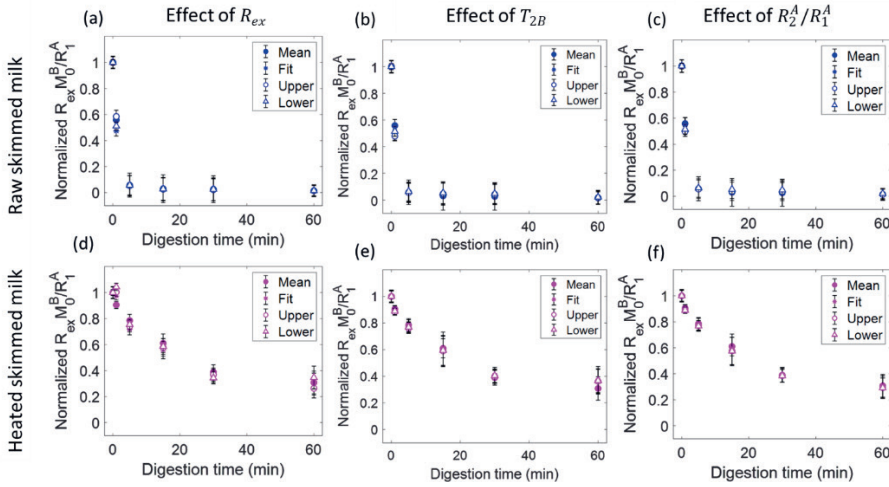


**Figure S2.5.** Effect of different physically plausible values for  $R_{ex}$ ,  $T_{2B}$  and  $R_2^A/R_1^A$  on the value obtained for the composite parameter,  $R_{ex}^B M_0^B / R_1^A$ , from the one-datapoint fit.

### 2.5.3. OPA assay during static *in vitro* digestion of SM

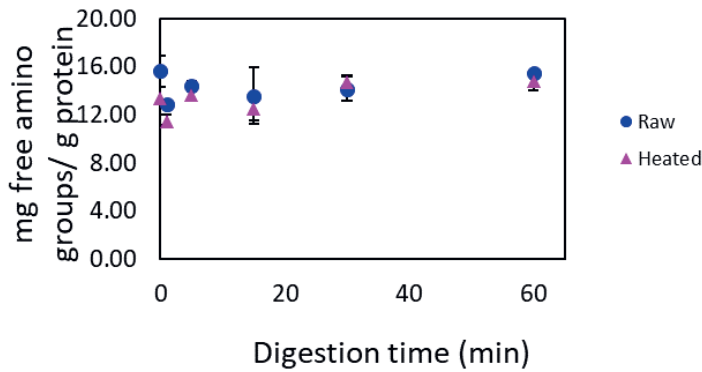


**Figure S2.6.** Free amino group per gram of protein determined by the OPA assay for raw SM and heated SM with 90% WP denaturation.



**Table S2.1.** Physical parameters obtained by global fitting of the original data set consisting of 259 data points in total and of the optimized data set consisting of 87 data points in total.

Fit parameter	Full data set	Optimized data set
$(R_{ex}M_0^B)/R_{1A}$	$0.8 \pm 0.1$	$0.9 \pm 0.1$
$T_{2B}$ ( $\mu s$ )	$14.5 \pm 0.2$	$14.1 \pm 0.1$
$R_{ex}$ ( $s^{-1}$ )	$60 \pm 15$	$75 \pm 20$
$R_{2A}/R_{1A}$	$27 \pm 1$	$24 \pm 2$

**Table S2.2.** Model parameters obtained from the global fit of the two-pool exchange model to the MT spectra using either a gaussian or super-Lorentzian (SL) function to describe the lineshape of the semi-solid pool.  $R_1^B$  was fixed to  $1 s^{-1}$ .

Fit parameter	Gaussian	SL	Gaussian	SL
	1 minute	1 minute	60 minutes	60 minutes
$R_{ex}M_0^B/R_{1A}$	$0.5 \pm 0.1$	$50 \pm 200$	$1 \cdot 10^{-3} \pm 3 \cdot 10^{-3}$	$45 \pm 12$
$T_{2B}$ ( $\mu s$ )	$16 \pm 2$	$190 \pm 190$	$14 \pm 60$	$140 \pm 10$
$R_{ex}$ ( $s^{-1}$ )	$40 \pm 15$	$300 \pm 150$	$1 \pm 40$	$150 \pm 20$
$R_{2A}/R_{1A}$	$10 \pm 0.5$	$350 \pm 200$	$6 \pm 10$	$160 \pm 20$

**Table S2.3.** Physical parameters obtained from the multiparameter global fit of the two-pool exchange model to the MT spectra of raw and heated skimmed milk at different time points during *in vitro* gastric protein digestion.  $R_1^B$  was fixed to  $1 \text{ s}^{-1}$ . The 95% confidence intervals were calculated via bootstrapping.

	0 min	1 min	5 min	15 min	30 min	60 min
<b>Raw skimmed milk</b>						
$R_{ex} M_B^B / R_1^A$	0.86±0.01	0.45±0.01	0.020±0.001	$3 \cdot 10^{-3} \pm 7 \cdot 10^{-7}$	$1 \cdot 10^{-3} \pm 6 \cdot 10^{-6}$	$2 \cdot 10^{-14} \pm 3 \cdot 10^{-17}$
$T_2^B$ (μs)	14.6±0.1	15.9±0.9	15.2±0.3	14.4±0.1	18.9±0.2	18.0±0.3
$R_{ex}$ (s <sup>-1</sup> )	70±2	40±2	1.6±0.3	1.0±0.2	4.2±0.5	2.5±0.4
$R_2^A / R_1^A$	13.4±0.2	9.1±0.1	6.2±0.1	5.6±0.1	5.1±0.1	5.1±0.1
<b>Heated skimmed milk</b>						
$R_{ex} M_B^B / R_1^A$	0.85±0.01	0.89±0.01	0.59±0.01	0.42±0.01	0.28±0.01	0.21±0.01
$T_2^B$ (μs)	14.4±0.1	14.7±0.1	16.1±0.1	17.4±0.1	16.6±0.2	18.4±0.2
$R_{ex}$ (s <sup>-1</sup> )	100±3	65±2	25±1	18±1	16±2	7±1
$R_2^A / R_1^A$	10.8±0.1	12.5±0.1	9.7±0.1	8.2±0.1	7.3±0.1	5.5±0.1



**CHAPTER**

# 3

# *In vitro* $^1\text{H}$ MT and CEST MRI mapping of gastro-intestinal milk protein breakdown

A version of this chapter has been published as:  
Mayar, M., Smeets, P., Duynhoven, J., & Terenzi, C. (2023). *In vitro*  $^1\text{H}$  MT and CEST MRI mapping of gastro-intestinal milk protein breakdown. *Food Structure*, 36, 100314–100324

## Abstract

Protein digestion is commonly studied using *in vitro* models. Validating these models with more complex *in vivo* observations remains challenging, in particular due to the need for non-invasive techniques. Here, we explore Magnetization Transfer (MT) and Chemical Exchange Saturation Transfer (CEST) MRI for non-invasive monitoring of protein solubilization and hydrolysis during static *in vitro* digestion using skim milk (SM). We measured CEST spectra of unheated and heated SM during gastric digestion, from which a measure for soluble proteins/peptides was obtained by calculating the asymmetric MT ratio ( $MTR_{asym}$ ). We also obtained the semi-solid volumes ( $v_{ss}$ ), MT ratio ( $MTR$ ) and  $MTR_{asym}$  from the same measurement, within 1.3 min. The  $MTR_{asym}$  area increased with gastric digestion, due to solubilization of the initially-formed coagulum, yielding a mean difference of  $20\pm 7\%$  between unheated and heated SM ( $p < 0.005$ ). The  $v_{ss}$  and  $MTR$  decreased during gastric digestion and can be used to monitor changes in the coagulum, but not for assessment of soluble proteins/peptides. The  $MTR_{asym}$  increased during gastro-intestinal digestion, proving sensitive to protein solubilization and hydrolysis. Future steps will include similar MT and CEST studies under complex dynamic conditions.

### 3.1. Introduction

Protein intake is essential for the growth and repair of body cells, muscle function and development of the immune system. Milk is one of the main sources of protein in the human diet and is the only source of protein for infants. Milk proteins, namely casein and whey, are digested in the gastro-intestinal tract, which is a complex dynamic system and is crucial for the breakdown of milk proteins and for the subsequent absorption of amino acids (Dupont & Tomé, 2020).

Milk protein digestion starts in the gastric phase (GP), where first a semi-solid protein coagulum is formed by a combination of acid- and pepsin-induced aggregation of the casein micelles or, in the case of heated milk, of casein micelles and denatured whey proteins (Huppertz & Chia, 2021). This is followed by solubilization and hydrolysis of the semi-solid protein coagulum into soluble proteins and relatively large peptides. Next, these proteins and peptides are transported into the intestinal phase (IP), where they are hydrolysed into small peptides and amino acids (Dupont & Tomé, 2020). Processing of milk products includes heating, which in turn can modify the structure, gastric coagulation, and overall digestibility of the proteins (Huppertz & Chia, 2021; van Lieshout et al., 2020). Protein digestion is currently studied using either animal models (Barbé et al., 2014), static (Brodkorb et al., 2019; Ménard et al., 2018) or (semi)-dynamic *in vitro* digestion models (Dong et al., 2021; Mulet-Cabero, Egger, et al., 2020; Mulet-Cabero et al., 2017), gastric aspirates in infants (Nielsen et al., 2020), ileal sampling (Gaudichon et al., 1999) or by measuring the appearance of amino acids in blood in humans (Bos et al., 2003; Horstman et al., 2021).

*In vitro* digestion models are useful because they are simple, well controlled, do not impose any ethical constraints, and can provide insights into the digestion kinetics and chemical composition of the digesta. However, they need to be validated using *in vivo* data. This requires the use of non-invasive measurement techniques that can monitor both *in vitro* and *in vivo* digestion.

Magnetic Resonance Imaging (MRI) has great potential for investigating *in vivo* protein digestion because it can be used to acquire detailed images of the gastro-intestinal tract in a non-invasive manner (Smeets, Deng, Van Eijnatten, & Mayar, 2020). MRI is currently mainly used to assess gastric processes, such as gastric

emptying and phase separation, at a macroscopic level (Spiller & Marciani, 2019). While such macroscopic MRI images provide some information on the degree of coagulation, as apparent visually (Camps et al., 2017, 2021), they do not provide a local molecular-scale measure of the degree of milk protein coagulation and protein breakdown.

Previous studies have shown that the  $^1\text{H}$  longitudinal ( $R_1$ ) and transverse ( $R_2$ ) Nuclear Magnetic Resonance (NMR) relaxation rates can be used to monitor the digestion of whey protein gels in a static (Deng et al., 2020) and semi-dynamic (Deng et al., 2022) *in vitro* gastric digestion model. The  $R_1$  and  $R_2$  parameters provide information on the molecular mobility of water in food systems, but their translation into quantitative chemically-specific or molecular-level parameters is not trivial.

Magnetization Transfer (MT) and Chemical Exchange Saturation Transfer (CEST) are promising for monitoring milk protein coagulation and breakdown on a macroscopic- and (supra-)molecular level. MT is a magnetic resonance technique that can be used to quantify low-abundant semi-solid proteins in aqueous (food)-systems via through-space dipolar couplings between the semi-solid protein and water (Henkelman et al., 1993; van Duynhoven et al., 1999).

CEST is based on the same principle as MT, but instead it can be used to measure the  $^1\text{H}$  chemical exchange between amide, amine and hydroxyl protons of dissolved mobile proteins/peptides and water (Van Zijl & Yadav, 2011). CEST is known to be dependent on solute concentration (Chan et al., 2014), molecular conformation (e.g. protein folding/unfolding and structural rearrangements) (Goerke et al., 2015; Longo et al., 2014) and pH (Sun et al., 2016). Therefore, a combination of MT and CEST MRI is promising for the assessment of both semi-solid and soluble proteins during gastric digestion. MT and CEST measurements are performed using the same MRI pulse sequence.

First a radio-frequency (RF) saturation pulse is applied at a frequency offset relative to the water signal. This pulse selectively saturates the magnetization of protons associated with the semi-solid macromolecules or solutes by equalizing the populations of the respective  $^1\text{H}$  energy levels.



The obtained saturation is then transferred to the water protons via a combination of through-space  $^1\text{H}$  dipolar couplings and/or  $^1\text{H}$  chemical exchange. The saturation transfer can then be detected as a suppression of the water signal. The saturation pulse can be applied at both positive and negative frequency offsets ( $\Delta$ ) relative to the water proton frequency to acquire a CEST spectrum. In the CEST spectrum the water signal intensity with the saturation pulse applied at a given  $\Delta$  value ( $S_{sat}(\Delta)$ ) is normalized to the signal intensity without any saturation ( $S_0$ ), and is plotted as a function of the frequency offset  $\Delta$ . The CEST spectrum includes contributions from  $^1\text{H}$  chemical exchange with mobile low-molecular-weight molecules, MT with semi-solid molecules and direct water saturation (DS) (Van Zijl & Yadav, 2011; Wu et al., 2016). From the CEST spectrum, the MT ratio ( $MTR$ ) (Eq. 3.1) and the  $MTR_{asym}$  (Eq. 3.2) can be obtained, as follows:

$$MTR = 1 - (S_{sat}(\Delta)/S_0) \quad \text{Eq. 3.1}$$

$$MTR_{asym} = (S_{sat}(-\Delta) - S_{sat}(+\Delta))/S_0 \quad \text{Eq. 3.2}$$

The  $MTR$  parameter is mainly dependent on the amount of semi-solid protein and the chemical exchange rate. We have previously shown that bulk NMR measurements of the  $MTR$  can be used to monitor the *in vitro* gastric coagulation and breakdown of milk proteins and to study the effect of heating on this process (Mayar et al., 2022). The chemical exchange of soluble proteins/peptides can be characterized by the  $MTR_{asym}$  calculation, which removes the additional semi-solid MT and DS contributions from the CEST spectrum. This calculation is based on the assumption that the MT and DS contributions are symmetric around the water signal, but the chemical exchange effect is asymmetric (Van Zijl & Yadav, 2011).

*In vitro* gastro-intestinal protein digestion includes changes in the state of proteins, such as coagulation, solubilization and hydrolysis (Huppertz & Chia, 2021; Mulet-Cabero, Egger, et al., 2020). Therefore, we hypothesize that a combination of CEST and MT MRI can be used to monitor these changes during static *in vitro* infant gastro-intestinal digestion of milk. In the present study, we combine CEST and MT measurements with imaging to obtain spatially-resolved information on *in vitro* milk protein coagulation and breakdown. The infant *in vitro* digestion protocol was chosen because milk is the only source of protein for infants but the effect of heating on gastric protein digestion is still poorly understood in

this group. Gaining a better understanding of the effect of processing on digestion can aid in optimizing the production process of infant formula for optimal protein digestion. The methodology described in this paper can however directly be applied to other digestion models, such as INFOGEST (Brodkorb et al., 2019).

## 3.2. Materials and methods

### 3.2.1. Materials

Whey Protein Isolate (WPI) was purchased from Davisco Food International, Inc. (USA). Pepsin (631 activity units/mg), pancreatin (trypsin activity 3.13 U/mg) from porcine origin, trypsin (10000 U/mg) and bile from bovine origin, trypsin inhibitor (Pefabloc), calcium chloride hexahydrate, hydrochloric acid, L-serine, potassium chloride, sodium bicarbonate, sodium chloride, sodium hydroxide and tris(hydroxymethyl)-aminomethane hydrochloride all purchased from Sigma Aldrich, Inc. (USA). Pepsin inhibitor (pepstatin A) was purchased from Thermo Scientific, Inc. (USA). o-phthaldehyde (OPA), disodium tetraborate decahydrate, sodium dodecyl sulfate (SDS), dithiothreitol (DTT) were purchased from Merck (Germany). Milli-Q water (resistivity 18.2 M $\Omega$ .cm at 25 °C, Merck Millipore, USA) was used in all experiments.

### 3.2.2. Preparation of WPI solutions

WPI powder was dissolved in Milli-Q water at different concentrations (1, 3, 6, 12 wt%) and stirred at room temperature for 1 h. The pH of the solutions was adjusted to pH 2, 3.5, 4.5, 5.5 and 7 using either 1 M hydrochloric acid or 0.1 M sodium hydroxide. The protein solutions were stored in the fridge at 5 °C and were used within one day. The WPI solutions were prepared and measured in duplicate.

### 3.2.3. Preparation of whey protein hydrolysate

Whey protein concentrate (WPC) powder was obtained from raw skim milk (SM) from bovine origin. The SM was acidified with 1 M hydrochloric acid to a pH of 4.6 to precipitate the casein micelles, followed by centrifugation for 20 min at 4 °C and 6000 *g*. The supernatant containing the soluble whey proteins was separated from the pellet and was dialyzed to remove salts and lactose. The dialysis was performed against a solution of lactic acid in Milli-Q at pH 4.6 and 4 °C using a dialysis membrane with a molecular weight cutoff of 10 kDa. The demineralized whey protein was freeze dried to obtain the WPC powder. The WPC powder was dissolved in TRIS-HCl (3.4 wt%) and the pH was adjusted to pH 7.5 using 0.1 M sodium hydroxide. The WPC solution was incubated with 5 mg of trypsin per gram of protein at 45 °C for 2.5 and 5.5 hours to obtain the whey protein hydrolysate. The WPC hydrolysate samples were prepared and measured in duplicate.

### 3.2.4. Preparation of simulated digestion fluids

Simulated gastric fluid (SGF) was composed of sodium chloride and potassium chloride with a concentration of 94 and 13 mM, respectively, and adjusted to pH 5.3. Pepsin was added to SGF right before the digestion experiment. Simulated intestinal fluid (SIF) was composed of 164 mM sodium chloride, 10 mM potassium chloride and 85 mM of sodium bicarbonate and adjusted to pH 7. Calcium chloride was added separately before the beginning of the intestinal phase at a concentration of 3 mM within the volume of the intestinal fluid.

### 3.2.5. *In vitro* digestion

Unheated and heated SM (USM and HSM, respectively) were obtained following a procedure described elsewhere (Mayar et al., 2022). *In vitro* gastric and intestinal digestion was conducted based on a digestion protocol for 1 month old infants (Ménard et al., 2018). To prepare 1 mL of gastric digestion sample, SM and SGF containing pepsin were mixed in a 10-mm NMR tube in a 63:37 (v/v) ratio. The

activity of pepsin in the digestion sample was 268 U/mL of gastric content. The pH was adjusted to 5.3 with 1 M hydrochloric acid. The samples were incubated in a water bath at 37 °C for  $t = 0, 1, 5, 15, 30$  and 60 min. These time points were based on (Ménard et al., 2018) with the addition of  $t = 1$  min to better capture the fast disappearance of the coagulum of raw SM. The activity of pepsin was inhibited by adding 10  $\mu\text{L}$  of a 0.72  $\mu\text{M}$  Pepstatin A solution. The samples were measured by MRI without any further sample preparation. For intestinal digestion, first 5 mL of  $t = 60$  min gastric digestion sample was prepared. The pH was adjusted to pH 6.6 and the sample was mixed with SIF in a 62:38 (v/v) ratio to obtain intestinal digestion samples composed of 39% SM, 23% SGF and 38% SIF. The SIF contained pancreatin with a trypsin activity of 16 U/mL of intestinal content. The samples were incubated in a water bath at 37 °C for  $t = 0, 1, 5, 15, 30$  and 60 min. The activity of trypsin was stopped by adding 10  $\mu\text{L}$  of a 0.5 M Pefabloc solution. Both gastric and intestinal digestion experiments were performed in triplicate.

### 3.2.6. MRI measurements

$^1\text{H}$  CEST MRI measurements were conducted at room temperature at a magnetic field strength of 7 T, corresponding to a  $^1\text{H}$  frequency of 300.13 MHz, on an Avance III spectrometer (Bruker Biospin, Fallanden, Switzerland) equipped with the Micro 2.5 radiofrequency (RF) coil with an inner diameter of 30 mm and the Micro 2.5 microimaging gradient system with maximum gradient intensity of 1.5  $\text{T}\cdot\text{m}^{-1}$  along all three axes.

Measurements were conducted using a CEST-Rapid Acquisition with Refocused Echoes (RARE) sequence. The CEST module consisted of a train of 10 block pulses with a pulse length ( $t_p$ ) of 100 ms and an interpulse delay ( $t_d$ ) of 10  $\mu\text{s}$ , resulting in a saturation time ( $T_{sat}$ ) of 1 s. The  $B_1$  amplitude was set to 3  $\mu\text{T}$ .  $^1\text{H}$  CEST spectra were measured for 61  $\Delta$  values equally spaced from -10 to 10 ppm, yielding a CEST spectral resolution of 0.33 ppm. Water saturation shift referencing (WASSR) (Kim et al., 2009) spectra were measured to construct a  $B_0$ -map for  $B_0$ -inhomogeneity correction of the CEST spectra. For the WASSR measurement, a  $T_{sat}$  of 50 ms and a  $B_1$  of 0.2  $\mu\text{T}$  was used. The saturation pulse consisted of 10

block pulses with a  $t_p$  of 5 ms and a  $t_{delay}$  of 10  $\mu$ s. WASSR spectra were measured using 31  $\Delta$  values ranging between -1.5 and 1.5 ppm with a resolution of 0.1 ppm. In addition, two reference  $S_0$  images were acquired, respectively at  $\Delta = -450$  and 450 ppm.

The RARE imaging parameters were as follows: field-of-view of 25 x 25 mm, matrix size of 128x128, three axial slices with thickness of 2 mm, distance of 3 mm and offset set to -3 mm. Sinc3 pulses were used for excitation and refocusing with a flip angle of 90° and 180°, respectively. A repetition time ( $TR$ ) of 5 s, echo time ( $TE$ ) of 9.8 ms and a RARE-factor of 32 was used, resulting in a total measurement time of 21 min and 11 min for the CEST and WASSR measurement, respectively. The effective  $TE$  was 78 ms, leading to a  $T_2$ -weighted image in which the signal of semi-solid protons with a short transverse relaxation time ( $T_2$ ) is suppressed.

### 3.2.7. Data processing and analysis

All processing and calculations were done in MATLAB R2019b (MathWorks, Massachusetts, USA). First, WASSR spectra were constructed for each voxel by calculating  $S_{sat}/S_0$  as a function of  $\Delta$ . The WASSR spectra were interpolated with cubic-spline fitting on a voxel-by-voxel basis and the frequency shift,  $\delta\Delta^{WASSR} = \Delta_{min} - \Delta_0$ , was determined for each voxel as the difference between the position for the minimum of the interpolated spectrum,  $\Delta_{min}$ , and the reference position of the water signal,  $\Delta_0 = 0$  ppm. The WASSR  $B_0$ -map was constructed by plotting  $\delta\Delta^{WASSR}(x, y)$  for each voxel. Next, the CEST saturation frequencies were corrected voxel-wise by using the WASSR  $B_0$ -map and the  $S_{sat}$  were then interpolated with cubic-spline fitting to obtain the  $S_{sat}$  signal intensity at the desired  $\Delta$ . Region-of-Interest (ROI) masks of the sample tube were drawn manually, and the mean signal intensity within the ROI was used to construct the CEST spectra, where  $S_{sat}/S_0$  is plotted as a function of  $\Delta$ . The  $MTR$  and  $MTR_{asym}$  were calculated according to equations 3.1 and 3.2. The  $MTR_{asym}$  area was calculated as the area under the curve between 1.2 and 4 ppm. For WPI, WPC and milk digestion samples, the mean CEST and corresponding  $MTR_{asym}$  were calculated per slice over the whole sample tube.

The WPI and WPC samples were homogenous solutions, therefore, calculating the mean CEST and  $MTR_{asym}$  spectra over the sample tube is adequate and gives a good representation of the local  $MTR_{asym}$ . For the milk digestion samples, which are heterogenous, additional semi-solid and liquid content masks were obtained by intensity thresholding of the  $T_2$ -weighted  $S_0$  images using the multithresh function with two levels in MATLAB (Otsu's method). Masks for the semi-solid or the liquid phases in the sample were applied to the unsaturated and saturated images in order to calculate the  $MTR$  and  $MTR_{asym}$  maps of the coagulum and supernatant, respectively. The masks for the solid-phase sample components were also used to calculate the semi-solid volume ( $v_{ss}$ ) by multiplying the voxel volume by the total number of semi-solid-containing voxels. The mean  $MTR$  and  $MTR_{asym}$  values were calculated by taking the sum over either the solid- or liquid-containing voxels, and averaging it over the total number of voxels within the respective ROIs.

### 3.2.8. OPA assay

The degree of hydrolysis of WPC hydrolysate samples was determined using the OPA method (Nielsen et al., 2001). First the OPA reagent solution was prepared by dissolving 3.8 g disodium tetraborate decahydrate in 80 mL of MilliQ while stirring at 35-40 °C. Next, 88 mg DTT and 100 mg SDS were added. Then, 80 mg OPA was dissolved in 3 mL ethanol and transferred to the above-mentioned solution and the volume was adjusted to 100 mL with MilliQ. The WPC samples were centrifuged at 10000g for 30 minutes and diluted 10 times. The calibration curve consisted of L-serine standards of 0.5, 1.25, 2.5, 5, 7.5, 10 and 15 mM in MilliQ. To prepare the samples for measurement, 10  $\mu$ L of the blank (MilliQ), L-serine standard or diluted WPC sample was added to a well of a transparent 96-well polystyrene plate (Greiner) and was mixed with 200  $\mu$ L of OPA reagent. The well-plate was covered with aluminium foil and kept at RT for 15 mins. The absorbance was measured at 340 nm using a Spectramax M2 microplate reader. The degree of hydrolysis (DH) was calculated using the method described by Spellman et al. (2003).

### 3.2.9. Statistical analysis

The means and standard deviations were calculated based on duplicate or triplicate experiments. The error bars in the figures represent the standard deviations. The regression analysis for the  $MTR_{asym}$  area with the pH and protein concentration were performed in MATLAB R2019b (MathWorks, Massachusetts, USA) using the “fit linear regression model”. Repeated measures analysis of variance (repeated measures ANOVA) followed by a Post-hoc Tukey’s honestly significant difference (HSD) test was performed in MATLAB to determine whether there was a significant effect of digestion time and heat treatment on the  $MTR_{asym}$  area. The significance level for all analyses was set at  $p = 0.05$ .

## 3.3. Results and discussion

### 3.3.1. $^1\text{H}$ CEST of WPI and WPC solutions: effect of pH, concentration and hydrolysis

The effect of pH and protein concentration on the chemical exchange was studied using WPI solutions at varying pH (Fig. 3.1 a-c) and concentration (Fig. 3.1 d-f). The CEST spectra at different pH (Fig. 3.1a) contained a broad and symmetric direct saturation (DS) of the water signal around 0 ppm and a CEST signal around 3 ppm. The CEST signal resulted from chemical exchange between water protons and the exchangeable protein protons, such as hydroxyl ( $\sim\Delta = 1$  ppm), amine ( $\Delta = 2-3$  ppm) and amide ( $\Delta = 3.5$  ppm) protons (DeBrosse et al., 2016; Pardi et al., 1983).

The  $MTR_{asym}$  spectra were calculated for better quantification of the chemical exchange effect (Fig. 3.1b): their amplitude increased with pH, most significantly between pH 2 and 3.5 and pH 5.5 and 7. The  $MTR_{asym}$  spectra at pH 3.5-5.5 had a similar shape and intensity with two overlapping peaks at  $\sim 1$  and 2.5 ppm, and were notably different as compared to the spectrum at pH 7. We note that the samples at pH 3.5-5.5 were more turbid as compared to those prepared at pH 2 and 7 (Fig. S3.1), indicating a correspondingly lower solubility and/or aggregation of the whey proteins. The pH range 3.5-5.5 is near the iso-electric point (pI) of

bovine whey proteins, namely around pH 4.2 or 5.1 for  $\alpha$ -lactalbumin or  $\beta$ -lactoglobulin, respectively. Proteins are known to aggregate, and are less soluble at their pI (Cornacchia et al., 2014), which might explain the distinct shape and low intensity of the  $MTR_{asym}$  spectrum in this pH range. These observations are in agreement with CEST data of bovine serum albumin, where a decrease in the  $MTR_{asym}$  and a separation into two peaks was observed upon heat-induced aggregation (Longo et al., 2014).

The area under the  $MTR_{asym}$  spectrum between  $\Delta = 1.2 - 4$  ppm was calculated to quantify the pH dependence of the bulk chemical exchange. We note that  $\Delta \leq 1$  ppm ranges were excluded in this calculation because, at  $\Delta$  values close to the direct water saturation around 0 ppm, the  $MTR_{asym}$  analysis becomes unreliable and the  $MTR_{asym}$  intensity depends on the slice position, even for homogenous whey protein solutions (Fig. S3.2). We found that the area under the  $MTR_{asym}$  spectrum followed a linearly increasing trend with pH (Fig. 3.1c), with smaller differences and overlapping error bars observed in the pH range around the pI of the whey proteins. Chemical exchange of amine is a dominantly base-catalyzed reaction, which explains the increase of the  $MTR_{asym}$  with pH.

The CEST signal and  $MTR_{asym}$  also increased with concentration (Figs. 3.1d-f), while the shape of the  $MTR_{asym}$  remained the same for all concentrations. These results showed that the  $MTR_{asym}$  is sensitive to variations in pH and protein concentration, which can occur during *in vivo* protein digestion (Gan et al., 2018). However, protein hydrolysis is also expected to occur during gastric digestion.



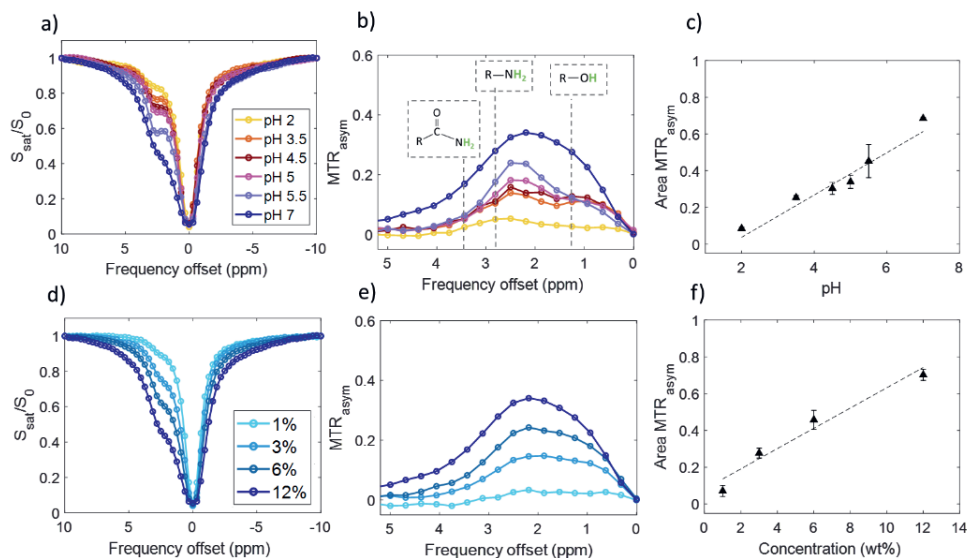


**Figure 3.1.** For WPI solutions at (a-c) 12% concentration and varying pH or at (d-f) pH 7 and varying concentration. (a,d)  $^1\text{H}$  CEST and (b,e)  $\text{MTR}_{\text{asym}}$  spectra, alongside the respective correlation plots for the  $\text{MTR}_{\text{asym}}$  areas ( $\Delta=1.2\text{-}4$  ppm) as a function of either (c) pH ( $y = 0.11x - 0.16$ ,  $R^2 = 0.94$ ) or (f) concentration ( $y = 0.07x + 0.05$ ,  $R^2 = 0.94$ ). The  $\text{MTR}_{\text{asym}}$  area values are plotted as the mean  $\pm$  SD of duplicate experiments.

To verify whether CEST is sensitive to protein hydrolysis, a whey protein hydrolysate was prepared by incubating an unheated intact WPC solution with trypsin at pH 7.5 at 45 °C for 2.5 and 5.5 hours. Unheated WPC was used to avoid whey protein denaturation and aggregation, which could both cause variations in the chemical exchange.

As shown in Fig. 3.2a, the CEST spectra for the intact or hydrolyzed samples were very similar, with only a small difference observed in the  $\Delta=0.6\text{-}3.5$  ppm range. This difference is more clearly visualized in Fig. 3.2b in the  $\text{MTR}_{\text{asym}}$  spectral representation, where a gradual increase was observed with the hydrolysis time. During protein hydrolysis, the peptide bonds are broken and more free -OH ( $\sim 1$  ppm) and  $-\text{NH}_2$  (2-3 ppm) groups are formed, thus yielding an increased abundance of exchangeable protons. This explains the increase in the  $\text{MTR}_{\text{asym}}$  occurring between 1 and 3 ppm. The increase in the  $\text{MTR}_{\text{asym}}$  area was  $22\pm 1\%$  and  $35\pm 1\%$  for 2.5 and 5.5 hours of hydrolysis, respectively, which was in agreement with the trend observed for the degree of hydrolysis (Fig. 3.2c).

The degree of hydrolysis after 5.5 hours was extensive for WPIC ( $26\pm 1\%$ ), which was expected considering the extreme hydrolysis conditions used. The results shown in Figs. 3.1 and 3.2 demonstrate that CEST is sensitive not only to pH and protein concentration, but also to protein hydrolysis.

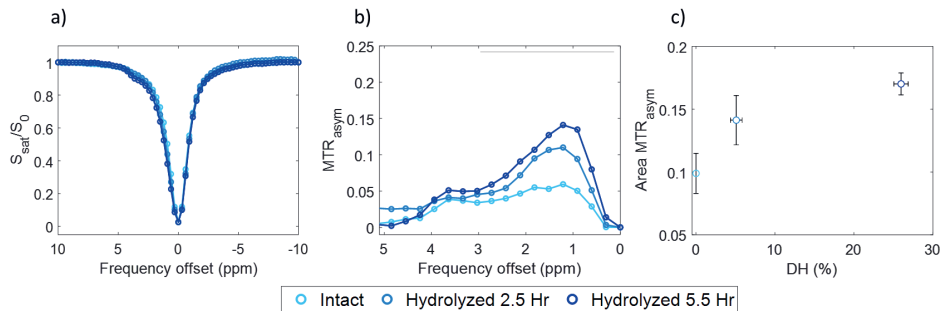


**Figure 3.2.** (a) CEST, (b)  $MTR_{\text{asy}}$  spectra, and (c) the DH (%) determined with the OPA assay for intact 3.4% WPC solution and after 2.5 and 5.5 Hr of hydrolysis. The hydrolysis was performed with trypsin (0.5%) at pH 7.5 and 45 °C.

### 3.3.2. $^1\text{H}$ CEST MRI of gastric milk protein digestion

Next, CEST was used to monitor the *in vitro* digestion of USM and HSM, which contain both whey proteins and caseins. During gastric digestion, phase separation between the milk protein coagulum and its supernatant was observed. This can be detected also in Figure 3.3, where the sagittal and axial  $^1\text{H}$   $T_2$ -weighted  $S_0$ -images of the CEST measurement for both USM (a-d) and HSM (e-h) are shown. Water molecules in the protein coagulum are less mobile and, hence, have a shorter transverse relaxation time compared to those in the supernatant. As a consequence, the protein coagulum and the supernatant have a, respectively, lower (red) or higher (yellow)  $^1\text{H}$  signal intensity in the  $T_2$ -weighted images. We note that semi-solid proteins cannot be detected directly in the  $T_2$ -weighted images, because of their very short  $T_2$ -values in the order of 12-20  $\mu\text{s}$  (Mayar et al., 2022).

The CEST and  $MTR_{\text{asy}}$  spectra were averaged over the whole slice to obtain information on the global changes occurring during *in vitro* digestion for the whole sample composition (coagulum and supernatant). There was no clear trend as function of the digestion time for the CEST spectra of the digestion samples,

shown in supplementary figures S3.3 and S3.4. The  $MTR_{asym}$  spectra for the bottom slice, whose  $^1H$  signal mainly arises from the protein coagulum, remain unchanged during digestion, with a slight intensity increase occurring only between  $t = 0$  and 1 min. Unlike for the coagulum, the middle and top slice exhibited an observable increase in the  $MTR_{asym}$  spectral intensity during digestion, with a difference in peak intensity of 0.2 between  $t = 0$  and  $t = 60$  min. As shown in Figs. 3.3i-3l, these variations are better visualized by monitoring the evolution of the  $MTR_{asym}$  area with digestion. The  $MTR_{asym}$  area for the bulk sample and the bottom slice (Fig. 3.3i,j) remain unchanged as digestion progressed, with only a slight variation observed between  $t = 0$  and 1 min in the bottom slice for USM. A clearer variation with digestion is observed for the middle and top slice (Fig. 3.3k,l).

The largest variation with digestion and heat treatment was observed for the top slice, which mainly consists of the supernatant. During digestion, the  $MTR_{asym}$  spectra of the supernatant (Fig. S3.3 and S4) increased between  $\Delta = 1-4$  ppm, corresponding to the resonance positions of hydroxyl, amine and amide protons. Bovine milk mainly consists of caseins, which lack a well-defined secondary structure and are mainly present as random coils in aqueous solutions (Bhat et al., 2016). Moreover, the pH of the samples over the different digestion time points ( $pH = 5.43 \pm 0.04$ ) and the measurement temperature (RT) were constant. Therefore, conformational changes in the secondary structure are unlikely (Bhat et al., 2016; Markoska et al., 2021; Pardi et al., 1983) and can be ruled out as a cause of variations in the chemical exchange.

The observed increase in the  $MTR_{asym}$  can therefore be attributed to solubilization of the protein coagulum, which leads to more proteins and, hence, to more exchangeable protons in the liquid phase. The larger increase observed specifically at 1.2 ppm and 2-3 ppm could be due to hydrolysis of the peptide bonds, which leads to more free  $-NH_2$  and  $-OH$  groups. The increase in the  $MTR_{asym}$  area between  $t = 1$  and 60 min was 20% and 35% for USM and HSM, respectively. During gastric digestion, pepsin hydrolyzes the peptide-bonds in the semi-solid protein coagulum, which results in proteins and peptides being released from the coagulum into the supernatant. This is expected to lead to a higher concentration of proteins and peptides and, hence, of exchangeable protons in the supernatant,

which explains the observed increase in the  $MTR_{asym}$  area within the top imaging slice. There were main effects of digestion time ( $F(5,2) = 80, p < 0.001$ ) and heat treatment ( $F(1,2) = 200, p < 0.005$ ) on the  $MTR_{asym}$  of the top slice as found by a repeated measures ANOVA. A post hoc comparison with Tukey's HSD test showed that the mean value of the  $MTR_{asym}$  was significantly different between USM and HSM for all digestion time points ( $p < 0.05$ ). The variation in the bottom and middle slices is smaller, potentially due to the minimal change in the net protein concentration

Overall these results show that the  $MTR_{asym}$  area is an MRI parameter sensitive to static *in vitro* digestion and, hence, is potentially useful for monitoring *in vivo* protein digestion. However, the acquisition of a full CEST spectrum is time consuming, here taking up to about 21 min for sampling a total of 61 frequency offset values, including 2 reference images (see Section 3.2.5). Such long measurement times prohibit the implementation of CEST measurements on a clinical scanner for dynamic studies of *in vivo* protein digestion. To address this limitation, we investigated whether the  $MTR_{asym}$  obtained from one set of  $\pm \Delta$  values could be used to construct  $MTR_{asym}$  contrast maps as a function of digestion time, which would require 1 min and 20s of acquisition time and thus enable a  $\sim 16$ -fold faster measurement. Moreover, the measurement of each  $\Delta$  is 20s, and hence, fits within one breath hold, which is important for avoiding breathing-related artifacts in the images.

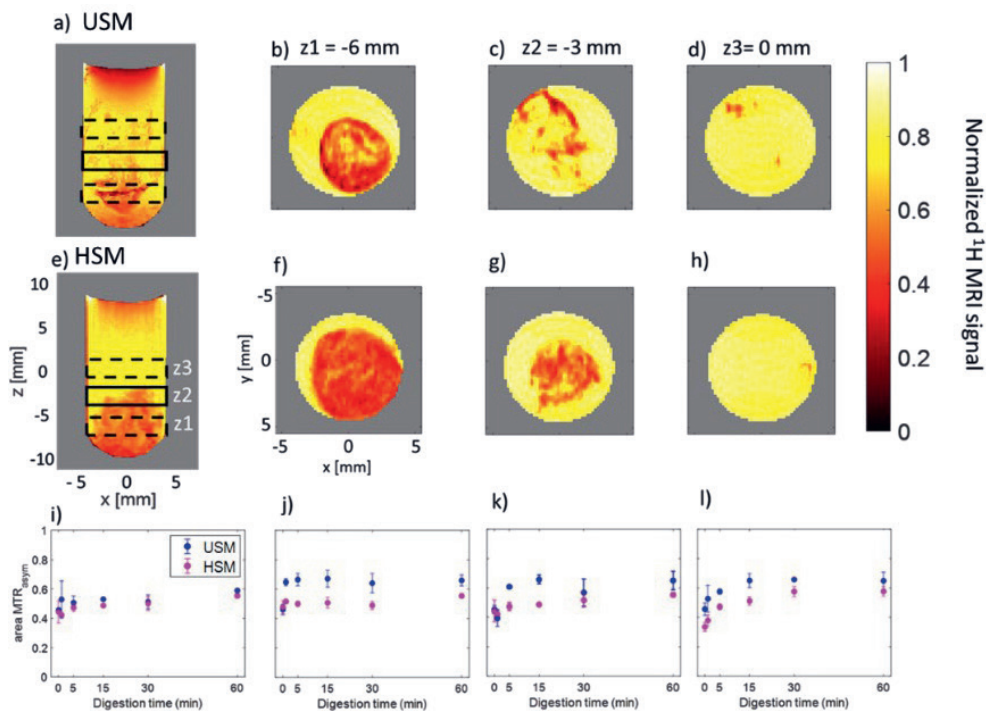


**Figure 3.3.**  $T_2$ -weighted  $^1\text{H}$  MRI intensity images at  $t = 15$  min of USM (a-d) and HSM (e-h) acquired for a sagittal slice (a and e) or for three axial slices (b-d and f-h) at z-coordinate set to  $-6$  mm (b and f),  $-3$  mm (c and g) or  $0$  mm (d and h), alongside the digestion time evolution for the  $MTR_{asyM}$  area for the bulk sample (i) or for three axial slices (j-l). The slice thickness was  $2$  mm for the sagittal and axial measurements. The coagulum is visible in red and the supernatant in yellow. The  $MTR_{asyM}$  area was calculated from the CEST spectrum between  $1.2$  and  $4$  ppm, and is plotted as the mean  $\pm$  SD of triplicate digestion experiments.

In Fig. 3.3. we observed that changes in the  $MTR_{asyM}$  during protein digestion were best detected in the supernatant. Therefore,  $MTR_{asyM}$  maps of the supernatant in the middle slice ( $z = -3$  mm) were constructed for the exchangeable hydroxyl ( $\Delta = 1.2$  ppm) or amine ( $\Delta = 2$  and  $2.7$  ppm) protons (Fig. 3.4a). The  $T_2$ -weighted images shown in Fig. 3.3 were used as a reference to obtain an image mask for the supernatant and coagulum  $^1\text{H}$  MRI signals by intensity thresholding. The values in the  $MTR_{asyM}$  maps of the supernatant were normalized to the highest value in the respective map. The contrast maps show that the  $MTR_{asyM}$  for the supernatant at  $\Delta \pm 2.7$  ppm exhibited the largest variation upon digestion, as indicated by the clear shift from low (red) to high (yellow)  $MTR_{asyM}$  values. Fig. 3.4b shows the mean  $MTR_{asyM}$  for the supernatant calculated

using the respective image mask. At  $\Delta \pm 2.7$  ppm the mean  $MTR_{asym}$  exhibited only a slightly higher variation with digestion as compared to  $\pm 1.2$  and  $\pm 2.0$  ppm. Nevertheless,  $\Delta = \pm 2.7$  is a more optimal offset for monitoring digestion due to the larger difference with respect to the water saturation signal at 0 ppm, which is especially important for application on clinical scanners with a lower magnetic field of 3 T. Therefore,  $\pm 2.7$  ppm was chosen for monitoring *in vitro* protein digestion of USM and HSM in the gastric phase (GP) and of HSM in the intestinal phase (IP).

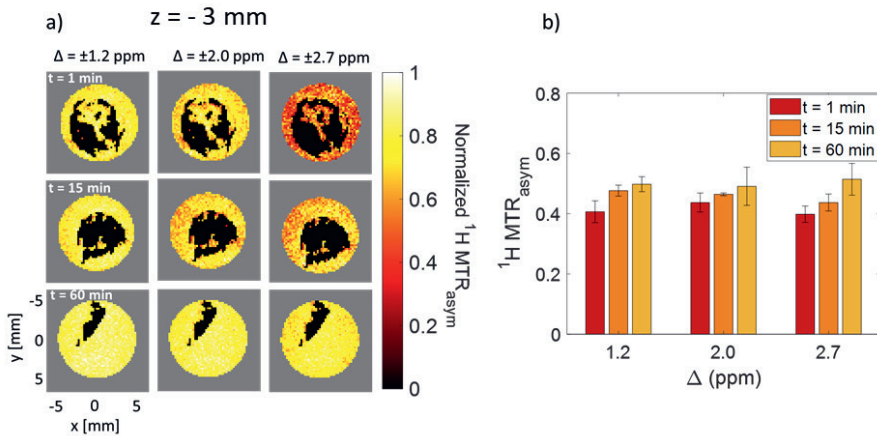


**Figure 3.4.** (a) Normalized axial ( $z = -3$  mm)  $MTR_{asym}$  contrast maps at  $\Delta = 1.2$  (left), 2.0 (middle), or 2.7 ppm (right) and at  $t = 1$  (top), 15 (middle) and 60 min (bottom) gastric digestion times; (b) mean  $MTR_{asym} \pm SD$  ( $n = 3$ ) for each  $\Delta$  and timepoint calculated over the voxels containing the supernatant. The values in (b) are the mean  $MTR_{asym}$  values whereas the maps in (a) show the  $MTR_{asym}$  values, normalized to the maximum value within each map, for the voxels containing the supernatant as obtained by thresholding of the  $T_2$ -weighted images shown in Fig. 3.3.

### 3.3.3. $T_2$ -weighted, MTR and $MTR_{asym}$ imaging of protein digestion

In the following, the use of  $T_2$ -weighted,  $MTR$ - and  $MTR_{asym}$ -contrast ( $\Delta = 2.7$  ppm) images is tested for monitoring protein digestion in the gastric phase for USM (GP-USM) and HSM (GP-HSM), as well as in the intestinal phase for HSM (IP-HSM) (Fig. 3.5a-c). The coagulum and supernatant can clearly be distinguished in the  $T_2$ -weighted images of Fig. 3.5a, and it is possible to visually trace the breakdown of the protein coagulum during gastric digestion for USM and HSM. We note that, as expected, the coagulum in IP-HSM was absent even at the start of intestinal

digestion. These images could be used to estimate changes in the apparent semi-solid volume,  $v_{ss}$ , within the samples, which in turn could be used as a measure of the changes in the amount of protein coagulum. Here, we refer to the coagulum as a semi-solid, because this is a term commonly used in MT and CEST MRI literature to refer to hydrated (bio)-polymers, akin to the casein coagulum (Mayar et al., 2022; van Zijl et al., 2018). It is important to note that exact measurements of the semi-solid volume are not possible, due to partial volume effects in the slice direction and the image acquisition parameters used, namely slice thickness and interslice gap of 2 and 1 mm, respectively. As shown in Fig. 3.5d, for both USM and HSM,  $v_{ss}$  decreased during gastric digestion, due to the breakdown of the protein coagulum.

The  $MTR$  maps in Fig. 3.5b are clearly affected by variations in the amount of semi-solid protons, and can be used to selectively characterize the protein coagulum and to trace its breakdown. The mean  $MTR$  (Fig. 3.5e) decreased with digestion in a similar fashion as the semi-solid volume. We note that for the present goal of jointly measuring MT and CEST effects under acquisition conditions suitable for *in vivo* scanning, we have used different values of  $B_1$  amplitude,  $T_{sat}$  and  $\Delta$  (see Section 3.2.5) compared to those reported in our previous work (Mayar et al., 2022) for obtaining the  $MTR$  parameter. However, as the  $MTR$  is semi-quantitative and its value depends on the acquisition parameters (Henkelman et al., 2001), based on our previous work (Mayar et al., 2022) we estimate that a stronger distinction between USM and HSM systems could be achieved by using higher  $B_1$ , longer  $T_{sat}$  and larger  $\Delta$  values.

The  $MTR$  maps of the bottom slice, shown in supplementary figure S3.5 which consisted mainly of protein coagulum, showed that for HSM the total amount of coagulum and the average  $MTR$  inside the coagulum increased between  $t = 1$  and 15 min and decreased from  $t = 15$  to 60 min. This suggests that during the digestion process, the protein coagulum changed from a loose and porous structure at  $t = 1$  min to a more compact structure at  $t = 15$  min, followed by consequent pepsin-induced solubilization. Moreover, a better distinction between USM and HSM can be made based on the  $MTR$  of the bottom slice. This is especially evident at  $t = 15$  min, at which a two-fold higher  $MTR$  and more compact coagulum was found for HSM compared to USM. Therefore, spatially-resolved measurements

of the  $MTR$  can be used to monitor the coagulum volume as well as changes in the coagulum consistency during the digestion process. In our previous work we have shown that the  $MTR$  is governed by the amount of semi-solid protons and the exchange rate (Mayar et al., 2022). This also implies that the  $MTR$  does not provide any information on protein digestion in the absence of a semi-solid component, which is evident from the data for intestinal digestion (Figs. 3.5a and b, bottom).

To monitor digestion of soluble proteins/peptides, a different contrast from  $T_2$ -weighting or  $MTR$  is needed. The  $MTR_{asym}$  maps for USM during gastric digestion (Fig. 3.5c, top) mainly showed an increase in the supernatant volume with digestion, but no increase in the  $MTR_{asym}$  of the supernatant was observed. However, for HSM during both gastric and intestinal digestion, a clear increase in the  $MTR_{asym}$  of the supernatant was observed in the contrast maps (Fig. 5c, middle and bottom) and in the evolution of the  $MTR_{asym}$  with the digestion time (Fig. 3.5f). This increase could be the result of protein solubilization and hydrolysis. The latter is expected to occur only for heated milk, in which the whey proteins are denatured and, therefore, more susceptible to protein hydrolysis by pepsin. This was previously reported by Sánchez-Rivera et al (2015), who showed that the amount of intact  $\beta$ -lactoglobulins decreased more rapidly during dynamic *in vitro* digestion for HSM compared to USM (Sánchez-Rivera et al., 2015). A combination of semi-solid protein solubilization and whey protein hydrolysis is expected to result in more exchangeable protons, including  $-NH_2$  protons, thereby explaining the higher variation of the  $MTR_{asym}$  at  $\Delta = \pm 2.7$  ppm observed for HSM compared to USM during *in vitro* gastric digestion.

The  $MTR_{asym}$  values of intestinal digestion were lower than those of gastric digestion because for the intestinal phase, the last time point of the gastric phase ( $t = 60$  min) was mixed with SIF, resulting in a dilution of the total amount of protein in the sample. The solubilized proteins and large peptides produced during gastric digestion are further hydrolyzed into smaller peptides during intestinal digestion (Zenker et al., 2020). The  $MTR_{asym}$  increased by 80% over the first 15 min of intestinal digestion, and thereafter slightly decreased.



The observed increase in the  $MTR_{asym}$  could be attributed to protein hydrolysis, because both  $pH \sim 6.6 \pm 0.3$  and protein concentration remained constant during the static intestinal digestion experiment, during which no phase separation had occurred and the full digestion sample was measured.

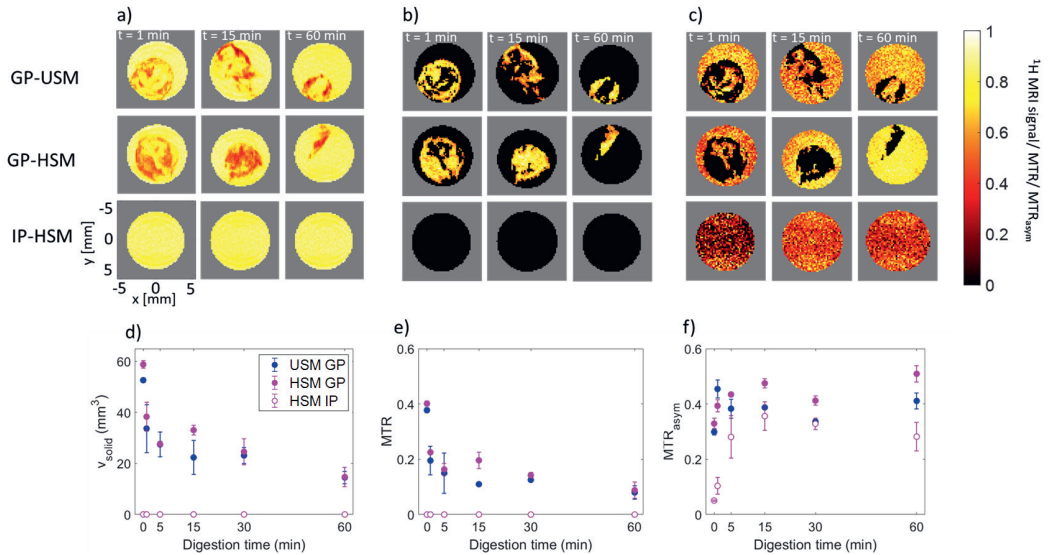


**Figure 3.5.** For GP-USM (top a-c or filled blue circles d-f), GP-HSM (middle a-c or filled pink circles d-f) and IP-HSM (bottom a-c or empty pink circles d-f): normalized axial ( $z = -3$  mm)  $T_2$ -weighted  $^1H$  intensity images (a), alongside MTR (b) and  $MTR_{asym}$  maps both at  $\Delta = 2.7$  ppm (c); digestion time evolution for  $v_{ss}$  (d), mean MTR (e) and mean  $MTR_{asym}$  (f). In d-f, the mean  $\pm$  SD from triplicate digestion experiments is shown.

Overall, these results demonstrate that  $T_2$ -, MTR and  $MTR_{asym}$  contrast are complementary and can be used to probe different events that occur during protein digestion, respectively changes in the semi-solid volume, formation and degradation of the protein coagulum, and molecular-level hydrolysis of soluble proteins. The latter makes the  $MTR_{asym}$  suitable for monitoring protein hydrolysis at later stages of digestion.

Measurements of water relaxation rates have also shown great potential for monitoring digestion of protein gels (Deng et al., 2020, 2022). However, the major limitation of  $^1H$  relaxometry is that it cannot measure low-abundant and semi-solid macromolecules, because it lacks dynamic range, short (sub-ms) relaxation times cannot be assessed with clinical scanners and/or their fitting error is too

high.  $^1\text{H}$  MT and CEST, although affected by relaxation, enable circumventing this limitation, are inherently chemically-specific and the acquisition of semi-quantitative parameters ( $MTR$  and  $MTR_{asym}$ ) is fast enough to be feasible *in vivo*. In addition, obtaining  $MTR$  and  $MTR_{asym}$  values does not require any fitting procedures. While relaxometry can be made chemically specific, this would lengthen the measurement time, thereby hindering *in vivo* feasibility. In addition, it has been shown that the  $R_2$  is not sensitive to the hydrolysis of whey proteins in solution (Deng et al., 2020), while in this article we have shown that the  $MTR_{asym}$  is sensitive to protein breakdown in solution during the hydrolysis of a WPC solution (Fig. 3.2) and during intestinal digestion of skim milk (Fig. 3.5).

The work presented here, as well as our previous work (Mayar et al., 2022), were the first steps in exploring the potential of  $^1\text{H}$  CEST and MT measurements for monitoring *in vitro* and *in vivo* protein digestion. The next step is to apply these methods to monitor milk protein digestion under dynamic *in vitro* and *in vivo* digestion conditions, where in addition to protein solubilization and hydrolysis, large variations in pH and protein concentration (Mulet-Cabero, Egger, et al., 2020; Mulet-Cabero, Mackie, et al., 2020) are expected to occur due to gastric secretion and emptying. Moreover, the measurement temperature for dynamic *in vitro* and *in vivo* studies will be 37 °C compared to room temperature used in this work.

A more complete validation of the method for monitoring dynamic gastric digestion would need to additionally account for pH, concentration and temperature effects on the chemical exchange. For future dynamic *in vitro* and *in vivo* applications, the optimized  $^1\text{H}$  MT and CEST characterization methods must be validated on a clinical MRI scanner, where inhomogeneities in both static ( $B_0$ ) and radio frequency ( $B_1$ ) magnetic fields are expected to affect the saturation and, hence, the MT and CEST response. In this work, we used the WASSR approach to determine the absolute water frequency per voxel, which was subsequently used for voxel-wise centering of the CEST spectra, which is too time consuming for dynamic applications. We foresee that fast  $B_0$ - and  $B_1$ -mapping procedures combined with regression- or two-pool Lorentzian modelling-based approaches for correction of sparsely sampled CEST data (Chen et al., 2022; Sun, 2020) will be a key requirement for robust analysis and interpretation of the CEST data. Another

challenge of *in vivo* measurements is that breathing can cause breathing-related artifacts in the images, therefore, each scan should be conducted within one breath hold ( $\leq 20$ s), which is possible with the acquisition parameters presented here. Moreover, we expect that image registration of all scans obtained at each digestion time point ( $S_{sat}(\pm \Delta)$ ,  $S_0$ ,  $B_0$  and  $B_1$  map) will be crucial to avoid motion induced artifacts in the calculated  $MTR$  and  $MTR_{asym}$  maps.

### 3.4. Conclusions

In this work, we successfully applied  $^1\text{H}$  CEST MRI measurements to monitor the *in vitro* digestion of milk proteins. More specifically, we showed that the  $MTR_{asym}$  area can be used for probing the static *in vitro* gastric digestion of unheated and heated skim milk. There was an effect of digestion time ( $p < 0.001$ ) and heat treatment ( $p < 0.005$ ) on the  $MTR_{asym}$  area. The  $MTR_{asym}$  area increased during digestion, indicating an increase in free  $-\text{NH}_2$  and  $-\text{OH}$  groups due to protein solubilization and hydrolysis. In addition, we showed that a combination of  $T_2$ -,  $MTR$ - and  $MTR_{asym}$ -contrast maps obtained within a short (1.3 min) measurement time can be used to monitor macroscopic changes in the protein coagulum and hydrolysis of soluble proteins during static *in vitro* gastro-intestinal digestion. Our findings open the way to non-invasive monitoring of *in vitro* and *in vivo* protein digestion in the future by MRI.

#### Authorship contribution statement

Morwarid Mayar: Conceptualization, Methodology, Formal analysis, Investigation, Data curation, Visualization, Validation, Writing – original draft; John van Duynhoven, Paul Smeets and Camilla Terenzi: Conceptualization, Methodology, Validation, Writing – review & editing, Supervision.

## Acknowledgements

Luisa Ciobanu and Julien Flament are gratefully acknowledged for providing the CEST-RARE pulse sequence. Camilla Terenzi acknowledges funding from the 4TU Precision Medicine program supported by High Tech for a Sustainable Future. We also acknowledge the support of NWO for the MAGNEFY centre, which is part of the uNMR-NL national facility.

## References

- Barbé, F., Le Feunteun, S., Rémond, D., Ménard, O., Jardin, J., Henry, G., Laroche, B., & Dupont, D. (2014). Tracking the in vivo release of bioactive peptides in the gut during digestion: Mass spectrometry peptidomic characterization of effluents collected in the gut of dairy matrix fed mini-pigs. *Food Research International*, 63(September 2014), 147–156. <https://doi.org/10.1016/j.foodres.2014.02.015>
- Bhat, M. Y., Dar, T. A., & Singh, L. R. (2016). Casein Proteins: Structural and Functional Aspects. In *Milk Proteins - From Structure to Biological Properties and Health Aspects* (1st ed., Issue September, pp. 1–18). IntechOpen. <https://doi.org/10.5772/64187>
- Bos, C., Metges, C. C., Gaudichon, C., Petzke, K. J., Pueyo, M. E., Morens, C., Everwand, J., Benamouzig, R., & Tomé, D. (2003). Postprandial kinetics of dietary amino acids are the main determinant of their metabolism after soy or milk protein ingestion in humans. *Journal of Nutrition*, 133(5), 1308–1315. <https://doi.org/10.1093/jn/133.5.1308>
- Brodkorb, A., Egger, L., Alminger, M., Alvito, P., Assunção, R., Ballance, S., Bohn, T., Bourlieu-Lacanal, C., Boutrou, R., Carrière, F., Clemente, A., Corredig, M., Dupont, D., Dufour, C., Edwards, C., Golding, M., Karakaya, S., Kirkhus, B., le Feunteun, S., ... Recio, I. (2019). INFOGEST static in vitro simulation of gastrointestinal food digestion. *Nature Protocols*, 14(4), 991–1014. <https://doi.org/10.1038/s41596-018-0119-1>
- Camps, G., Eijnatten, E. J. M. Van, Lieshout, G. A. A. Van, Lambers, T. T., & Smeets, P. A. M. (2021). *Gastric Emptying and Intra-gastric Behavior of Breast Milk and Infant Formula in Lactating Mothers Gastric Emptying and Intra-gastric Behavior of Breast Milk and Infant Formula in Lactating*. September. <https://doi.org/10.1093/jn/nxab295>
- Camps, G., Mars, M., de Graaf, C., & Smeets, P. A. M. (2017). A tale of gastric layering and sieving: Gastric emptying of a liquid meal with water blended in or consumed separately. *Physiology and Behavior*, 176(December 2016), 26–30. <https://doi.org/10.1016/j.physbeh.2017.03.029>
- Chan, K. W. Y., Yu, T., Qiao, Y., Liu, Q., Yang, M., Patel, H., Liu, G., Kinzler, K. W., Vogelstein, B., Bulte, J. W. M., Van Zijl, P. C. M., Hanes, J., Zhou, S., & McMahon, M. T. (2014). A diaCEST MRI approach for monitoring liposomal accumulation in tumors. *Journal of Controlled Release*, 180(1), 51–59. <https://doi.org/10.1016/j.jconrel.2014.02.005>
- Chen, Y., Dang, X., Zhao, B., Zheng, Z., He, X., & Song, X. (2022). B0 Correction for 3T Amide Proton Transfer (APT) MRI Using a Simplified Two-Pool Lorentzian Model of Symmetric Water and Asymmetric Solutes. *Tomography*, 8, 1974–1986.

- Cornacchia, L., Forquenot De La Fortelle, C., & Venema, P. (2014). Heat-induced aggregation of whey proteins in aqueous solutions below their isoelectric point. *Journal of Agricultural and Food Chemistry*, 62(3), 733–741. <https://doi.org/10.1021/jf404456q>
- DeBrosse, C., Nanga, R. P. R., Bagga, P., Nath, K., Haris, M., Marincola, F., Schnall, M. D., Hariharan, H., & Reddy, R. (2016). Lactate Chemical Exchange Saturation Transfer (LATEST) Imaging in vivo A Biomarker for LDH Activity. *Scientific Reports*, 6(January), 1–10. <https://doi.org/10.1038/srep19517>
- Deng, R., Janssen, A. E. M., Vergeldt, F. J., van As, H., de Graaf, C., Mars, M., & Smeets, P. A. M. (2020). Exploring in vitro gastric digestion of whey protein by time-domain nuclear magnetic resonance and magnetic resonance imaging. *Food Hydrocolloids*, 99(August 2019), 105348. <https://doi.org/10.1016/j.foodhyd.2019.105348>
- Deng, R., Seimys, A., Mars, M., Janssen, A. E. M., & Smeets, P. A. M. (2022). Monitoring pH and whey protein digestion by TD-NMR and MRI in a novel semi-dynamic in vitro gastric simulator (MR-GAS). *Food Hydrocolloids*, 125, 107393. <https://doi.org/10.1016/j.foodhyd.2021.107393>
- Dong, L., Wu, K., Cui, W., Fu, D., Han, J., & Liu, W. (2021). Tracking the digestive performance of different forms of dairy products using a dynamic artificial gastric digestive system. *Food Structure*, 29(May), 100194. <https://doi.org/10.1016/j.foostr.2021.100194>
- Dupont, D., & Tomé, D. (2020). Milk proteins: Digestion and absorption in the gastrointestinal tract. In *Milk Proteins* (pp. 701–714). Elsevier. <https://doi.org/10.1016/B978-0-12-815251-5.00020-7>
- Gan, J., Bornhorst, G. M., Henrick, B. M., & German, J. B. (2018). Protein Digestion of Baby Foods: Study Approaches and Implications for Infant Health. *Molecular Nutrition and Food Research*, 62(1), 1–11. <https://doi.org/10.1002/mnfr.201700231>
- Gaudichon, C., Mahé, S., Benamouzig, R., Luengo, C., Fouillet, H., Daré, S., Van Oycke, M., Ferrière, F., Rautureau, J., & Tomé, D. (1999). Net postprandial utilization of [15N]-labeled milk protein nitrogen is influenced by diet composition in humans. *Journal of Nutrition*, 129(4), 890–895. <https://doi.org/10.1093/jn/129.4.890>
- Goerke, S., Zaiss, M., Kunz, P., Klika, K. D., Windschuh, J. D., Mogk, A., Bukau, B., Ladd, M. E., & Bachert, P. (2015). Signature of protein unfolding in chemical exchange saturation transfer imaging. *NMR in Biomedicine*, 28(7), 906–913. <https://doi.org/10.1002/nbm.3317>
- Henkelman, R. M., Huang, X., Xiang, Q. -S, Stanisz, G. J., Swanson, S. D., & Bronskill, M. J. (1993). Quantitative interpretation of magnetization transfer. *Magnetic Resonance in Medicine*, 29(6), 759–766. <https://doi.org/10.1002/mrm.1910290607>
- Henkelman, R. M., Stanisz, G. J., & Graham, S. J. (2001). Magnetization transfer in MRI: A review. *NMR in Biomedicine*, 14(2), 57–64. <https://doi.org/10.1002/nbm.683>
- Horstman, A. M. H., Ganzevles, R. A., Kudla, U., Kardinaal, A. F. M., van den Borne, J. J. G. C., & Huppertz, T. (2021). Postprandial blood amino acid concentrations in older adults after consumption of dairy products: The role of the dairy matrix. *International Dairy Journal*, 113, 104890. <https://doi.org/10.1016/j.idairyj.2020.104890>
- Huppertz, T., & Chia, L. W. (2021). Milk protein coagulation under gastric conditions: A review. *International Dairy Journal*, 113, 104882. <https://doi.org/10.1016/j.idairyj.2020.104882>
- Kim, M., Gillen, J., Landman, B. A., Zhou, J., & Van Zijl, P. C. M. (2009). Water saturation shift referencing (WASSR) for chemical exchange saturation transfer (CEST) experiments. *Magnetic Resonance in Medicine*, 61(6), 1441–1450. <https://doi.org/10.1002/mrm.21873>
- Longo, D. L., Di Gregorio, E., Abategiovanni, R., Ceccon, A., Assfalg, M., Molinari, H., & Aime, S. (2014a). Chemical exchange saturation transfer (CEST): An efficient tool for detecting

- molecular information on proteins' behaviour. *Analyst*, 139(11), 2687–2690.  
<https://doi.org/10.1039/c4an00346b>
- Markoska, T., Daniloski, D., Vasiljevic, T., & Huppertz, T. (2021). Structural changes of  $\beta$ -casein induced by temperature and pH analysed by nuclear magnetic resonance, fourier-transform infrared spectroscopy, and chemometrics. *Molecules*, 26(24).  
<https://doi.org/10.3390/molecules26247650>
- Mayar, M., Miltenburg, J. L., Hettinga, K., Smeets, P. A. M., van Duynhoven, J. P. M., & Terenzi, C. (2022). Non-invasive monitoring of in vitro gastric milk protein digestion kinetics by <sup>1</sup>H NMR magnetization transfer. *Food Chemistry*, 383(February), 132545.  
<https://doi.org/10.1016/j.foodchem.2022.132545>
- Ménard, O., Bourlieu, C., de Oliveira, S. C., Dellarosa, N., Laghi, L., Carrière, F., Capozzi, F., Dupont, D., & Deglaire, A. (2018). A first step towards a consensus static in vitro model for simulating full-term infant digestion. *Food Chemistry*, 240(2017), 338–345.  
<https://doi.org/10.1016/j.foodchem.2017.07.145>
- Mulet-Cabero, A. I., Egger, L., Portmann, R., Ménard, O., Marze, S., Minekus, M., le Feunteun, S., Sarkar, A., Grundy, M. M. L., Carrière, F., Golding, M., Dupont, D., Recio, I., Brodkorb, A., & Mackie, A. (2020). A standardised semi-dynamic: in vitro digestion method suitable for food-an international consensus. *Food and Function*, 11(2), 1702–1720.  
<https://doi.org/10.1039/c9fo01293a>
- Mulet-Cabero, A. I., Mackie, A. R., Brodkorb, A., & Wilde, P. J. (2020). Dairy structures and physiological responses: a matter of gastric digestion. *Critical Reviews in Food Science and Nutrition*, 60(22), 3737–3752. <https://doi.org/10.1080/10408398.2019.1707159>
- Mulet-Cabero, A. I., Rigby, N. M., Brodkorb, A., & Mackie, A. R. (2017). Dairy food structures influence the rates of nutrient digestion through different in vitro gastric behaviour. *Food Hydrocolloids*, 67, 63–73. <https://doi.org/10.1016/j.foodhyd.2016.12.039>
- Nielsen, P. M., Petersen, D., & Dambmann, C. (2001). Improved method for determining food protein degree of hydrolysis. *Journal of Food Science*, 66(5), 642–646.  
<https://doi.org/10.1111/j.1365-2621.2001.tb04614.x>
- Nielsen, S. D., Beverly, R. L., Underwood, M. A., & Dallas, D. C. (2020). Differences and Similarities in the Peptide Profile of Preterm and Term Mother's Milk, and Preterm and Term Infant Gastric Samples. *Nutrients*, 12, 2825–2839.
- Pardi, A., Wagner, G., & Wutrich, K. (1983). Protein conformation and proton nuclear-magnetic-resonance chemical shifts. *European Journal of Biochemistry*, 137(3), 445–454.  
<https://doi.org/10.1111/j.1432-1033.1983.tb07848.x>
- Sánchez-Rivera, L., Ménard, O., Recio, I., & Dupont, D. (2015). Peptide mapping during dynamic gastric digestion of heated and unheated skimmed milk powder. *Food Research International*, 77, 132–139.  
<https://doi.org/https://doi.org/10.1016/j.foodres.2015.08.001>
- Smeets, P. A. M., Deng, R., van Eijnatten, E. J. M., & Mayar, M. (2020). Monitoring food digestion with magnetic resonance techniques. *Proceedings of the Nutrition Society*, 3, 1–11. <https://doi.org/10.1017/S0029665120007867>
- Spellman, D., McEvoy, E., O'Cuinn, G., & FitzGerald, R. J. (2003). Proteinase and exopeptidase hydrolysis of whey protein: Comparison of the TNBS, OPA and pH stat methods for quantification of degree of hydrolysis. *International Dairy Journal*, 13(6), 447–453.  
[https://doi.org/10.1016/S0958-6946\(03\)00053-0](https://doi.org/10.1016/S0958-6946(03)00053-0)
- Spiller, R., & Marciani, L. (2019). Intraluminal impact of food: New insights from MRI. *Nutrients*, 11(5), 1147–1161. <https://doi.org/10.3390/nu11051147>
- Sun, P. Z. (2020). Fast correction of B0 field inhomogeneity for pH-specific magnetization transfer and relaxation normalized amide proton transfer imaging of acute ischemic stroke

- without Z-spectrum. *Magnetic Resonance in Medicine*, 83(5), 1688–1697. <https://doi.org/10.1002/mrm.28040>
- Sun, P. Z., Xiao, G., Zhou, I. Y., Guo, Y., & Wu, R. (2016). A method for accurate pH mapping with chemical exchange saturation transfer (CEST) MRI. *Contrast Media and Molecular Imaging*, 11(3), 195–202. <https://doi.org/10.1002/cmimi.1680>
- van Duynhoven, J. P. M., Kulik, A. S., Jonker, H. R. A., & Haverkamp, J. (1999). Solid-like components in carbohydrate gels probed by NMR spectroscopy. *Carbohydrate Polymers*, 40(3), 211–219. [https://doi.org/10.1016/S0144-8617\(99\)00056-9](https://doi.org/10.1016/S0144-8617(99)00056-9)
- van Lieshout, G. A. A., Lambers, T. T., Bragt, M. C. E., & Hettinga, K. A. (2020). How processing may affect milk protein digestion and overall physiological outcomes: A systematic review. *Critical Reviews in Food Science and Nutrition*, 60(14), 2422–2445. <https://doi.org/10.1080/10408398.2019.1646703>
- van Zijl, P. C. M., Lam, W. W., Xu, J., Knutsson, L., & Stanisz, G. J. (2018). Magnetization Transfer Contrast and Chemical Exchange Saturation Transfer MRI. Features and analysis of the field-dependent saturation spectrum. *NeuroImage*, 168, 222–241. <https://doi.org/10.1016/j.neuroimage.2017.04.045>
- Van Zijl, P. C. M., & Yadav, N. N. (2011). Chemical exchange saturation transfer (CEST): What is in a name and what isn't? *Magnetic Resonance in Medicine*, 65(4), 927–948. <https://doi.org/10.1002/mrm.22761>
- Wu, B., Warnock, G., Zaiss, M., Lin, C., Chen, M., Zhou, Z., Mu, L., Nanz, D., Tuura, R., & Delso, G. (2016). An overview of CEST MRI for non-MR physicists. *EJNMMI Physics*, 3(1). <https://doi.org/10.1186/s40658-016-0155-2>
- Zenker, H. E., Van Lieshout, G. A. A., Van Gool, M. P., Bragt, M. C. E., & Hettinga, K. A. (2020). Lysine blockage of milk proteins in infant formula impairs overall protein digestibility and peptide release. *Food and Function*, 11(1), 358–369. <https://doi.org/10.1039/c9fo02097g>

### 3.5. Supplementary Information



Figure S3.1. Photographs of 12% WPI solutions at different pH.

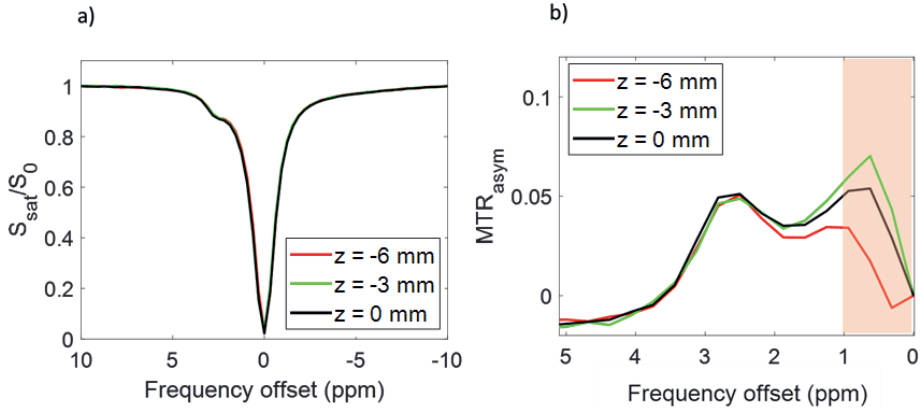
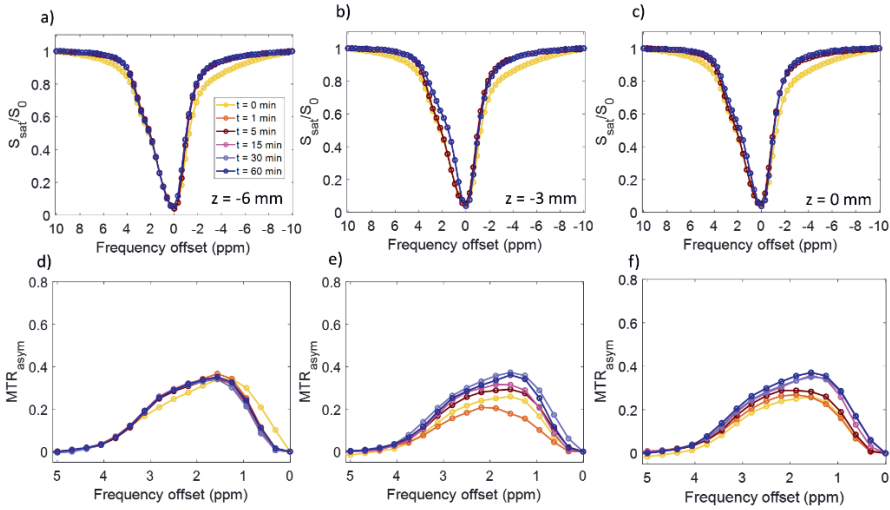
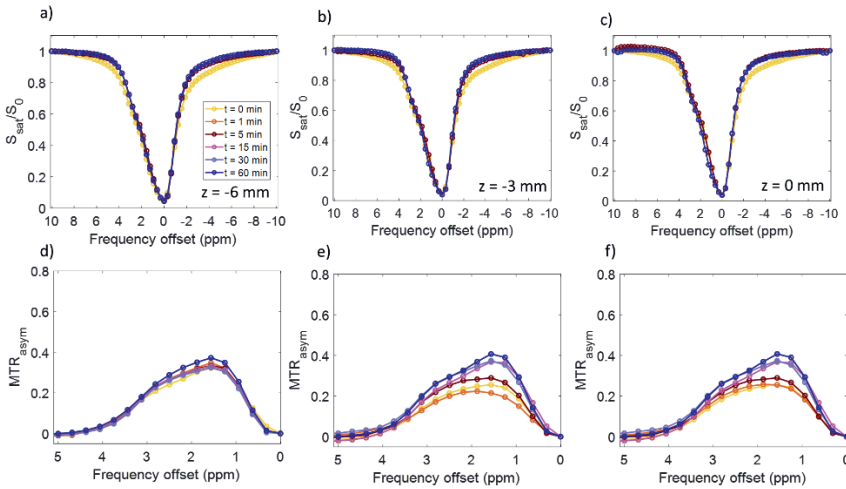


Figure S3.2.  $^1H$  CEST spectra of 1% WPI at pH 7 of three different slices (a) and the corresponding  $MTR_{asym}$  spectra showing the slice-dependence of the  $MTR_{asym}$  in the  $\Delta = 0-1$  ppm range (b).





**Figure S3.3.**  $^1\text{H}$  CEST spectra of USM during in vitro gastric digestion of three different slices (a-c) and the corresponding  $\text{MTR}_{\text{asym}}$  spectra (d-f). A description and visual representation of the slice positions can be found in section 2.5 of the materials and methods and Fig. 3 of the manuscript.



**Figure S3.4.**  $^1\text{H}$  CEST spectra of heated SM during in vitro gastric digestion of three different slices (a-c) and the corresponding  $\text{MTR}_{\text{asym}}$  spectra (d-f). A description and visual representation of the slice positions can be found in section 2.5 of the materials and methods and Fig. 3 of the manuscript.

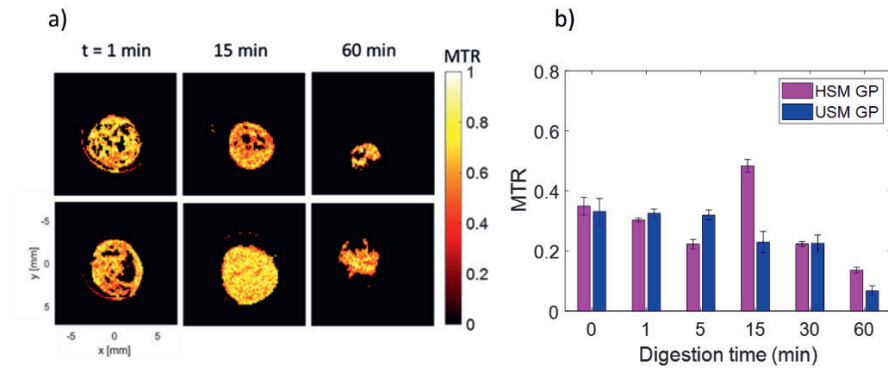


**Figure S3.5.** MTR maps of USM (top) and HSM at  $t = 1, 15,$  and  $60$  min during *in vitro* gastric digestion (a) and the corresponding mean MTR values as a function of the digestion time (b).



**CHAPTER**

**4**

# MRI assessment of pH and coagulation during semi-dynamic *in vitro* gastric digestion of milk proteins

A version of this chapter is published as:

Mayar, M., de Vries, M. Smeets, P.A.M., van Duynhoven, J.P.M., Terenzi, C. MRI assessment of pH and coagulation during semi-dynamic *in vitro* gastric digestion of milk proteins. *Food Hydrocolloids*, 152, 109866-109878

## Abstract

Gastric digestion is essential for protein breakdown, which is commonly studied *in vitro*. However, validating *in vitro* models with *in vivo* data is necessary.  $^1\text{H}$  MRI techniques, including Chemical Exchange Saturation Transfer (CEST) and Magnetization Transfer (MT), are promising for non-invasive assessment of *in vitro* and *in vivo* digestion. We previously demonstrated the ability of these techniques for monitoring *in vitro* milk protein digestion in static conditions. Here, we investigated CEST and MT for detecting pH and milk protein coagulation in semi-dynamic *in vitro* conditions using either whey protein isolate solution (WPIS), low- or high-pasteurized skim milk (LPSM and HPSM). The asymmetric MT ratio ( $MTR_{asym}$ ), reflecting the soluble proteins/peptides, decreased in accordance with the pH and protein concentration during digestion, with distinct trends observed for the different products. The dual-power CEST method allowed accurate estimation of the pH for WPIS within a pH range of 4.5-7 (normalized root mean square deviation = 0.04) on a 7 T NMR spectrometer. *In situ* pH mapping was achieved using a 3 T clinical MRI scanner.  $T_2$ -weighted images combined with MT ratio ( $MTR$ ) maps, reflecting semi-solid proteins, enabled assessment of coagulum volume and structure during digestion. The  $MTR$  allowed differentiation of the coagulation behaviour of LPSM and HPSM due to the heat treatment. In conclusion, CEST and MT can be used to monitor milk protein digestion, and the effect of milk heat treatment in semi-dynamic gastric conditions. Future work will investigate the feasibility of these techniques for *in vivo* gastric milk protein digestion studies.

## 4.1. Introduction

Proteins are essential nutrients, and their nutritional benefits rely on how well they are digested in the gastro-intestinal tract. Gastric digestion plays a crucial role in breaking down proteins, and it involves de- and re-structuring of foods to facilitate further breakdown in the intestinal tract (Mackie et al., 2020). Cow's milk is an important source of high-quality proteins in the human diet (Tome, 2012). The digestion of milk proteins (MP), namely casein and whey, starts in the gastric phase, during which acid- and pepsin-induced aggregation of casein micelles leads to the formation of a semi-solid coagulum. Intact whey proteins (WPs) remain mostly in solution or form small aggregates (Huppertz & Chia, 2021). Heat treatment is a common procedure in milk processing, and may lead to changes in protein structure, thereby affecting gastric protein digestion (van Lieshout et al., 2019). The effect of heat treatment on protein digestion has been studied using static (Tunick et al., 2016) or (semi-)dynamic *in vitro* digestion models (Mulet-Cabero et al., 2019; Wang et al., 2018) that simulate human gastro-intestinal digestion.

Static *in vitro* digestion models (Brodkorb et al., 2019; Ménard et al., 2018) are useful because they are simple, well controlled, and can provide insights into the digestion kinetics and chemical composition of the digesta. However, static models do not fully mimic the complexity of the digestive tract, because they do not incorporate gastric secretion, emptying and motility as well as hormonal responses. In comparison to static *in vitro* digestion models, dynamic models are physiologically more realistic: they include gastric secretion, emptying and motility, and the stomach shape is taken into consideration (Dupont & Mackie, 2015; Mackie et al., 2020). However, such models are highly complex, time-consuming and more expensive than static models. Therefore, semi-dynamic *in vitro* models have been developed, in which gastric secretion and emptying are mimicked by inflow of gastric juice and removal of gastric content (Deng et al., 2022; Mulet-Cabero et al., 2020). The gastric compartment in these models is simply a glass beaker kept at 37 °C, and mixing is achieved either using an overhead stirrer or by flow of air bubbles. Data from these models need be verified with *in vivo* data on intra-gastric digestion from humans. Such data can, in turn, be used to improve *in vitro* digestion models. However, the conventional methods

used to analyze *in vitro* digestion samples, including measurements of pH, coagulum weight, protein content, and degree of hydrolysis cannot be directly utilized *in vivo* because they require invasive sampling of digesta. Consequently, these methods become impractical for *in vivo* studies and raise ethical concerns. Therefore, non-invasive methods that can be used to study both *in vitro* and *in vivo* digestion in humans need to be developed.

Magnetic Resonance Imaging (MRI) holds great potential for studying *in vivo* protein digestion in humans because it can be used to non-invasively acquire detailed images of the chyme inside the gastro-intestinal tract (Smeets, Deng, Van Eijnatten, & Mayar, 2020). MRI has been mainly used to assess macroscopic gastric processes, such as gastric emptying and phase separation *in vivo* (Spiller & Marciani, 2019). However, the anatomical images used in these studies do not provide a quantitative and molecular-scale measurement of gastric protein digestion, which is crucial for monitoring gastric MP structuring and breakdown over time, studying the effect of heat treatment on gastric digestion, and for comparison of *in vitro* and *in vivo* data.

Previous studies have demonstrated that the transverse Nuclear Magnetic Resonance (NMR) relaxation time ( $T_2$ ) of water can be used to monitor the digestion of WP gels in static (Deng et al., 2020) and semi-dynamic (Deng et al., 2022) *in vitro* gastric digestion models, as well as *in vivo* (Deng et al., 2023).  $T_2$  MRI mapping combined with fat quantification has recently been utilized to assess semi-dynamic *in vitro* digestion of a meal containing bread and cheese (Musse et al., 2023). These studies have proven that  $T_2$  measurements via spin-echo based MRI methods are useful for observing digestion-mediated changes in the molecular mobility of water. However, such measurements cannot be used to directly detect semi-solid macromolecular protons with a short  $T_2$ -value of 15-20  $\mu\text{s}$  (Hinrichs et al., 2007; Mayar et al., 2022), due to the long dead times, typically around few ms, of clinical MRI scanners. Specific MRI techniques have been developed for detecting short- $T_2$  components, including Ultra-short Echo Time (UTE) and Zero Echo Time (ZTE) MRI. However, these techniques are typically restricted to measuring  $T_2$  values  $> 300 \mu\text{s}$ , which is too long to observe immobile coagulated proteins. Moreover, these measurements require hardware that is not readily available on most clinical MRI scanners (Weiger & Pruessmann, 2019). In



addition, aforementioned  $T_2$  MRI measurements lack the sensitivity to detect low-abundant proteins and peptides. Although the transverse spin relaxation time of water is sensitive to macromolecular dynamics through diffusional averaging and/or chemical exchange with macromolecules, quantifying exchange rates and macromolecular proton fractions requires, *e.g.*, measurements of  $T_2$ -values at different echo times to obtain  $T_2$ -dispersion curves (Carver & Richards, 1972). While such measurements have been used for characterizing food systems in a laboratory setting (Gottwald et al., 2005; Hills et al., 1990), applying these methods *in vivo* is challenging due to the long measurement times of  $T_2$ -dispersion experiments.

Saturation Transfer MRI techniques, Magnetization Transfer (MT) and Chemical Exchange Saturation Transfer (CEST) (Ward et al., 2000; Wolff & Balaban, 1989) offer several advantages over  $T_2$ -mapping: MT and CEST can be used to indirectly detect semi-solid or low-abundant solute (macro)molecules through their interaction with water. Moreover, these techniques are already widely applied in clinical human research and do not require specialized hardware. Additionally, semi-quantitative parameters, namely the MT ratio ( $MTR$ ) and  $MTR_{asym}$ , can be measured rapidly in 1.3 min (Mayar et al., 2023). In MT and CEST measurements, a radio-frequency (RF) pulse is employed to selectively saturate the magnetization of the semi-solid or low-abundant solute protons of interest. The saturated magnetization is subsequently transferred to the mobile water protons, resulting in a reduction of the detected water signal intensity. The saturation transfer processes in MT and CEST measurements are predominantly driven by  $^1\text{H}$  dipolar coupling and chemical exchange, respectively (Balaban & Ceckler, 1992; van Zijl et al., 2018; Zhou et al., 2023). The  $MTR$  parameter can provide insights into the (semi-)solid macromolecular mobility and content (Henkelman et al., 2001). Clinical applications of MT MRI have demonstrated its ability to detect even subtle alterations in semi-solid tissues, *e.g.* in terms of macromolecular content or structural integrity (Van Obberghen et al., 2018; Welsch et al., 2008).

CEST MRI is designed to measure the chemical exchange of labile protons between specific solute molecules, including proteins and peptides, and bulk water. The  $MTR_{asym}$  parameter obtained from CEST measurements is a measure of  $^1\text{H}$  chemical exchange, and is sensitive to changes in solute concentration and pH

(Wu et al., 2016). CEST MRI has gained increasing recognition as a non-invasive technique for *in vivo* pH mapping (Chen et al., 2017; Tang et al., 2020). Various processes that are essential for gastric protein digestion, such as gastric emptying, and MP coagulation and hydrolysis, depend on pH. Gastric pH evolves over time, due to gastric juice secretion, gastric emptying and the buffering capacity of the proteins.

In addition to pH evolutions, gastric digestion involves alterations in protein/peptide concentration, and modifications in the state of proteins, including coagulation, solubilization, and hydrolysis (Huppertz & Chia, 2021; Mulet-Cabero et al., 2020). As such, MT and CEST MRI are highly promising for assessing these concomitant changes during *in vitro* and *in vivo* gastric protein digestion. Accordingly, we have previously demonstrated that MT and CEST MRI can be used to detect protein hydrolysis and gastric breakdown of the MP coagulum in a static *in vitro* digestion model (Mayar et al., 2022, 2023). The next step is to apply these techniques to study MP digestion under more complex dynamic digestion conditions, including gastric secretion and emptying. Therefore, the aim of this work was to investigate the potential of CEST and MT MRI for monitoring pH and MP coagulation in semi-dynamic *in vitro* gastric digestion conditions. A WP isolate (WPI) solution (WPIS), low pasteurized skim milk (LPSM) and high pasteurized skim milk (HPSM) were used as test products to evaluate the sensitivity of CEST and MT for gastric MP digestion, and the effect of heat treatment on the digestion. The MRI measurements were carried out in the laboratory using a 7 T vertical bore NMR spectrometer, and inside a 3 T clinical MRI scanner. The 7 T vertical bore NMR spectrometer allows for freedom in setting acquisition parameters and was therefore used for developing and testing of the methods. Although compromised in setting acquisition parameters, the 3 T clinical scanner allows *in situ* measurements in the semi-dynamic digestion model, and was therefore utilized to evaluate the feasibility for future *in vivo* studies.

## 4.2. Materials and methods

### 4.2.1. Materials

Commercially available WPI with 87 wt% protein, 0.5 wt% fat, 2 wt% carbohydrates, and 0.5 wt% salt was purchased from Bulk™ (Essex, UK). Commercially available LPSM (3.6 wt% protein, 0.1 wt% fat, 4.7 wt% carbohydrates and 0.13 wt% salt) was purchased from a grocery store. Pepsin (631 activity units/mg), calcium chloride hexahydrate, hydrochloric acid, L-serine, potassium chloride, sodium bicarbonate, sodium chloride, sodium hydroxide, Rhodamin B, and tri tris(hydroxymethyl)-aminomethane hydrochloride were purchased from Sigma Aldrich, Inc. (USA). Pepstatin A and Pierce™ BCA Protein Assay Kit (Thermo Scientific, Inc., USA). Milli-Q water (resistivity 18.2 MΩ.cm at 25 °C, Merck Millipore, USA) was used in all experiments.

### 4.2.2. Preparation of WPI solutions and HPSM

WPIS were prepared according to Mayar et al. (2023). The pH of the solutions was adjusted to pH values ranging between 3-7 using 0.1 M sodium hydroxide (NaOH), and 0.1 and 1 M hydrochloric acid (HCl). The protein solutions were stored at 5 °C and were used within one day. The WPIS were prepared and measured in duplicate. HPSM was prepared from a commercially available LPSM, with a WP denaturation level of 3%, by heating the latter in a water bath for 30 min after reaching a temperature of 80 °C, resulting in a WP denaturation level of 90%. The WP denaturation level in the milk products was measured using SDS-PAGE (data not shown),

### 4.2.3. Preparation of simulated gastric fluid

The simulated gastric fluid (SGF) composition was based on the INFOGEST protocol (Brodkorb et al., 2019) and was prepared at pH 2. To determine the volume of HCl required to lower the pH during digestion, SGF (pH 2) and the WPIS or SM were mixed in a 50:50 ratio in a test tube. Slow titration with 1 M HCl was performed until pH 2 was reached, and the required volume of HCl was noted as an indicator of the amount of 1 M HCl to be added to the SGF for gastric secretion as suggested by Mulet-Cabero et al. (2020). Pepsin was added to the SGF at an activity of 4000 U/mL to ensure a pepsin activity of 2000 U/mL when mixed with the WPIS or SM at a 50:50 meal to SGF ratio.

### 4.2.4. Semi-dynamic *in vitro* gastric digestion

Semi-dynamic *in vitro* gastric digestion was conducted using an MRI-compatible semi-dynamic digestion model (Fig. S4.1) established by Deng et al. (2022). The set-up has several components, including a syringe pump to simulate gastric secretion (NE-500 Programmable OEM Syringe Pump, New Era Pump Systems, Inc., USA), a water-jacketed beaker acting as the stomach chamber, and a circulating water bath (Julabo GmbH, Germany) to maintain the temperature at 37 °C. Mixing was performed manually because magnetic stir bars are not MRI compatible, and the previously described method of mixing with air bubbles (Deng et al., 2022) was impractical due to foaming of the WPIS and SM. Stirring was performed using a stirring rod right before the MRI acquisition. The digestion conditions were based on the standardized semi-dynamic *in vitro* digestion parameters reflecting adult digestion (Mulet-Cabero et al., 2020).

To initiate digestion, 200 mL of 12% WPIS, LPSM or HPSM was placed in the beaker containing 20 mL of pre-heated SGF at 37 °C. The gastric secretion was started with a rate of 2 mL/min. The gastric emptying rate was based on the caloric content of the food and was 4 or 4.3 mL/min for 12% WPIS or SM, respectively. Gastric emptying was performed manually by removing gastric content every 10 min using a 50 mL syringe with a tip that had an inner diameter of ~2 mm, simulating the emptying of food particles through the pylorus

(Bornhorst & Paul Singh, 2014). The activity of pepsin in the removed gastric content was inhibited by adding 400  $\mu\text{L}$  of a 0.72  $\mu\text{M}$  Pepstatin A solution and the samples were stored in the freezer at  $-20\text{ }^{\circ}\text{C}$ . These samples were used for CEST measurements on the 7 T NMR spectrometer, along with pH and protein concentration analysis. For the *in situ* MRI measurements at 3 T, gastric content was removed after each set of MRI acquisitions for each digestion time.

#### 4.2.5. 7 T MRI measurements

$^1\text{H}$  CEST MRI measurements of WPIS and gastric content samples were conducted at room temperature in a vertical bore magnet with a magnetic field strength of 7 T, corresponding to a  $^1\text{H}$  frequency of 300.13 MHz. The spectrometer comprised an Avance NEO console (Bruker Biospin, Fallanden, Switzerland) and was equipped with a Micro 2.5 RF coil with an inner diameter of 30 mm and a Micro 2.5 microimaging gradient system. To enable simultaneous measurements of multiple samples, 2 mL of WPIS or gastric content samples was transferred to a 10 mm NMR tube, and three of these tubes were placed inside a larger 25 mm tube. An additional 5 mm NMR tube containing a glucose solution was included as a reference tube. The sample tubes were surrounded by an aqueous solution containing 5 mM sodium chloride and 10 mM copper sulphate.

Measurements were conducted using a Rapid Acquisition with Relaxation Enhancement (RARE) sequence combined with the saturation transfer module in Paravision 360. The saturation pulse consisted of a train of 10 block pulses (BP) with a pulse length ( $t_p$ ) of 100 ms and an inter-pulse delay ( $t_{\text{delay}}$ ) of 10  $\mu\text{s}$ , resulting in a saturation time ( $T_{\text{sat}}$ ) of 1 s. The  $B_1$  amplitude was set to 1.5 or 3  $\mu\text{T}$ . To obtain  $^1\text{H}$  CEST spectra, saturated images ( $S_{\text{sat}}$ ) (Eq. 4.1 in 4.2.8) were acquired using 67 frequency offset ( $\Delta$ ) values equally spaced from -10 to 10 ppm, resulting in a CEST spectral resolution of 0.3 ppm. In addition, a reference image without saturation ( $S_0$ ) was acquired (Eq. 4.1 in 4.2.8). Water Saturation Shift Referencing (WASSR) (Kim et al., 2009) spectra were measured with the same parameters as described in Mayar et al. (2023), to construct a  $B_0$ -map for  $B_0$ -inhomogeneity correction of the CEST spectra. The imaging parameters for both CEST and WASSR measurements were as follows: field-of-view (FOV) of 30 mm

x 30 mm, in-plane resolution of 0.23 x 0.23 mm, three axial slices with thickness of 2 mm and interslice gap of 1 mm were acquired. Sinc3 pulses were used for excitation and refocusing with a flip angle of 90° and 180°, respectively. A repetition time ( $TR$ ) of 5 s, effective echo time ( $TE_{eff}$ ) of 78 ms, and RARE factor of 32 were used, resulting in a total measurement time of 21 min and 11 min for the CEST and WASSR measurements, respectively.

#### 4.2.6. 3 T MRI measurements

For *in situ* monitoring of digestion, the stomach chamber of the semi-dynamic model was placed inside a 3 T clinical MRI scanner (Philips Ingenia Elition X, Philips Medical Systems, the Netherlands). A 16-channel small extremity coil was wrapped around the stomach chamber. MRI scans were performed at baseline (before addition of the WPIS or SM), at  $t=0$  (right after addition) and every 10 min until  $t=60$  min or 80 min for WPIS or SM, respectively. During each scan, both the gastric secretion and circulating water bath were switched off to avoid artifacts caused by motion and influx of SGF.

For each timepoint CEST and WASSR data, a  $T_2$ -weighted image and a  $B_1$ -map were acquired. For both CEST and WASSR measurements, an  $S_0$  reference image (Eq. 4.1 in 4.2.8) at  $\Delta=450$  ppm was acquired. For CEST measurements,  $S_{sat}$  images (Equation 4.1 in 4.2.8) were acquired at  $\Delta = -2.7, 2.7$  and 10 ppm with a  $T_{sat}$  of 1 s and a  $B_1$  of 1.5 and 3  $\mu T$ . WASSR spectra were acquired using 21  $\Delta$  values ranging from -1.5 to 1.5 ppm, with a  $T_{sat}$  of 0.05 s and a  $B_1$  of 0.2  $\mu T$ . CEST and WASSR measurements were conducted using an RF pulse saturation module combined with a RARE sequence for pH mapping experiments. Five axial slices were acquired in an interleaved manner with a FOV of 120 mm x 120 mm, in-plane resolution of 0.94 mm x 0.94 mm, slice thickness of 3.5 mm and no interslice gap. SINC pulses were used for excitation and refocusing with an excitation flip angle of 90° and the first refocusing flip angle was 180° followed by 110° pulses.

A  $TR$  of 3.2 s, RARE factor of 38, and  $TE_{eff}$  of 80 ms were used, resulting in a total measurement time of 98.6 s and 44.6 s for  $B_1=1.5$  and 3  $\mu T$ , respectively. The

WASSR spectra were acquired using the same imaging parameters as described above, resulting in a measurement time of 164 s. For MT mapping of the coagulum, a Gradient Recalled Echo (GRE) sequence was used to acquire 33 axial slices with a slice thickness of 3.5 mm and no inter-slice gap to allow coverage of the whole gastric content. The FOV and in-plane resolution were the same as for the RARE measurements described above. A SINC excitation pulse with a flip angle of  $7^\circ$ ,  $TR$  of 4.4 ms, and  $TE$  of 2.1 ms were used, resulting in a measurement time of 71.4 s for a  $B_1$  of 3  $\mu\text{T}$ .

$T_2$ -weighted images were acquired using the RARE sequence with the same acquisition parameters as described above, but with a  $TR$  of 1 s, and a RARE factor of 43, resulting in a total acquisition time of 26 s. The  $B_1$  map was acquired using the dual refocusing echo acquisition mode (DREAM) sequence (Nehrke & Börnert, 2012) with a  $TR$  of 11 ms,  $TE$  of 3.32 and 6.55 ms, and  $TF$  of 136, resulting in a total acquisition time of 26.1 s.

#### 4.2.7. Protein concentration measurements

The total protein concentration in the supernatant of the gastric content samples was estimated by the Bicinchoninic Acid (BCA) method with the use of Pierce™ BCA Protein Assay Kit. The pH of the samples was adjusted to pH 7 using 0.1 or 1 M NaOH and the samples were centrifuged for 15 min at 4000  $g$ . The supernatant was collected and diluted 100x and 30x for the WPIS and SM samples, respectively. The calibration curve consisted of 25, 125, 250, 500, 750 and 1000  $\mu\text{g}/\text{mL}$  bovine serum albumin (BSA) standard solutions. For the measurement, 25  $\mu\text{L}$  of standard solution, sample or blank was pipetted in duplicate in a different well of a clear bottom 96-wells well-plate (Greiner Bio-One, the Netherlands).

To this 200  $\mu\text{L}$  of BCA reagent was added, the plate was mixed for 30 s using a well-plate mixer and incubated at 37  $^\circ\text{C}$  for 30 min. After cooling down to room temperature, the absorbance was measured at 562 nm using microplate reader (Spectramax M2, USA).

#### 4.2.8. MRI data processing and analysis

All processing and calculations were done in MATLAB R2019b (MathWorks, Massachusetts, USA). A WASSR  $B_0$  map was constructed and used for voxel-wise  $B_0$ -inhomogeneity correction of the 7 T CEST spectra as previously described (Mayar et al., 2023). Region-of-Interest (ROI) masks of the middle slice of the sample tube were drawn manually, and the mean signal intensity within the ROI was used to construct the CEST spectra, where  $S_{sat}/S_0$  is plotted as a function of  $\Delta$ . The  $MTR_{asym}$  was calculated according to Eq. 4.1.

$$MTR_{asym} = (S_{sat}(-\Delta) - S_{sat}(+\Delta))/S_0 \quad \text{Eq. 4.1}$$

The  $MTR_{asym}$  area was calculated as the area under the curve (AUC) between 1.2 and 4 ppm. To evaluate CEST MRI for pH mapping, the dual-power CEST method was used (Longo et al., 2014). This method involves measuring CEST at two  $B_1$  amplitudes to calculate the Ratio of RF Power Mismatch ( $RPM$ ). The CEST effect and, consequently, the  $MTR_{asym}$  depend on several factors, including the solute concentration, the chemical exchange rate ( $k_{ex}$ ), which in turn is linked to pH, the longitudinal relaxation rate of water ( $R_1^w$ ) and the saturation efficiency ( $\alpha$ ). We note that  $k_{ex}$  is also affected by temperature, which was therefore kept constant during the measurements on the 7 T NMR spectrometer. Moreover, the WPIS was brought to a temperature of 37 °C before the start of the digestion experiment for the *in situ* pH mapping measurements on the 3 T clinical MRI scanner. The  $\alpha$  can be approximated by  $\alpha \approx (\gamma B_1)^2 / ((\gamma B_1)^2 + k_{ex}^2)$ , where  $\gamma$  is the gyromagnetic ratio of  $^1\text{H}$  in  $\text{rad} \cdot \text{s}^{-1} \cdot \text{T}^{-1}$ . By calculating the ratio of the  $MTR_{asym}$  at two  $B_1$  values (Eq. 4.2), it is possible to compensate for the concomitant changes in concentration and  $R_1^w$ , which makes the  $RPM$  solely dependent on  $k_{ex}$ , and hence, pH. The  $RPM$  was calculated for amine protons ( $\Delta \pm 2.7$  ppm) using a  $B_1$  combination of 1.5/3  $\mu\text{T}$ .

$$RPM = \frac{[(1-MTR_{asym})/MTR_{asym}]_{1.5\mu\text{T}}}{[(1-MTR_{asym})/MTR_{asym}]_{3\mu\text{T}}} \quad \text{Eq. 4.2}$$



Linear calibration lines for the acid- and base-catalysed chemical exchange regimes were constructed by taking the logarithm of the *RPM* and were used to predict the pH of the validation and digestion samples.

For data acquired at 3 T, a WASSR  $B_0$  map was constructed in the same way as done for the 7 T data. However, a CEST spectrum could not be acquired during the *in situ* measurements at 3 T due to their long measurement time. Instead the  $MTR_{asym}$  was acquired using  $\Delta \pm 2.7$  ppm. Voxels-wise correction of  $MTR_{asym}$  values was performed using the regression-based fast  $B_0$ -inhomogeneity correction (Sun, 2020). In brief, the effect of  $B_0$  inhomogeneity on the  $MTR_{asym}$  was estimated using the polynomial function shown in Eq. 4.3.

$$MTR_{asym}(x, y) = A + [C_1 \cdot \delta B_0(x, y) - C_2 \cdot \delta B_0^2(x, y)] \quad \text{Eq. 4.3}$$

Here  $A$  is the dimensionless composite parameter, namely  $(f_s \cdot k_{ex})/R_1^w$ , in which  $f_s$  is the fraction of solute protons,  $k_{ex}$  is the solute-water  $^1\text{H}$  chemical exchange rate and  $R_1^w$  is the longitudinal relaxation rate of the bulk water pool.  $C_1$  and  $C_2$  are coefficients (in seconds squared) determined from the polynomial fitting, and  $\delta B_0$  is the  $B_0$  shift in Hz per voxel. The  $MTR_{asym}$  was voxel-wise corrected for  $B_0$ -inhomogeneity by subtracting the  $B_0$ -artifact from the  $MTR_{asym}$ , estimated as:

$$C_1 \cdot \delta B_0(x, y) - C_2 \cdot \delta B_0^2(x, y).$$

The  $B_0$ -corrected  $MTR_{asym}$  values obtained at a  $B_1$  of 1.5 and 3  $\mu\text{T}$  were corrected for  $B_1$ -inhomogeneity using the two-point contrast- $B_1$ -correction described by Windschuh et al. (2015). The resulting  $B_0$ - and  $B_1$ -corrected  $MTR_{asym}$  maps were used to calculate the *RPM* values for each voxel, which were subsequently used to determine the pH per voxel using the acid- or base-catalysed chemical exchange calibration lines.

For characterizing MP coagulation and breakdown, coagulum masks were obtained by intensity thresholding of the  $T_2$ -weighted images using the multithresh function (Otsu's method) with two levels in MATLAB. Otsu's method finds the optimal threshold value that groups the imaging voxels into separate classes for which the within-class variance is minimised. Threshold analysis was separately performed on the images of each digestion time and experiment. This thresholding method

allowed for the identification of low-intensity voxels belonging to the coagulum. Using the coagulum mask, the volume of the coagulum was calculated by multiplying the voxel volume by the total number of coagulum voxels. The mask was also applied to the  $S_{sat}$  and  $S_0$  images to construct *MTR* maps of the coagulum at  $\Delta = 10$  ppm (Eq. 4.4) and to calculate the mean *MTR* value for the coagulum voxels at each digestion time point.

$$MTR = 1 - (S_{sat}/S_0) \quad \text{Eq. 4.4}$$

#### 4.2.9. Storage and loss modulus measurements

The storage ( $G'$ ) and loss ( $G''$ ) modulus of the coagulum were measured for the at  $t = 20, 40$  and  $70$  mins of semi-dynamic digestion. For each rheological measurement, carried out in duplicate, the coagulum was removed from the beaker and any excess liquid was discarded. The coagulum samples were measured within 2.5 hours after their preparation. A 25 mm circular sample was cut out from the center of the coagulum. The samples were stored at  $5^\circ\text{C}$  until 30 min before the measurements, after which they were kept at room temperature. Measurements were performed using an Anton Paar Rheometer (MCR 302, Anton Paar, Germany) equipped with a sandblasted parallel plate geometry. The development of  $G'$  and  $G''$  was monitored at a frequency of 1 Hz and strain of 0.1-10%.

#### 4.2.10. Confocal Laser Scanning Microscopy (CLSM)

The microstructure of the coagulum was studied using a Rescan Confocal Microscope (RCM) (Confocal.nl, The Netherlands). Rhodamin B (fluorescent dye) was used to stain proteins with an excitation line at 561 nm. The coagulum was collected after 20, 40 and 70 min of digestion, and a small piece of approximately 10 mm x 5 mm was cut from the centre of the coagulum. The samples were stained with 1% (w/v) of Rhodamine B for 5 min, placed on a glass microscope slide and examined with a 63x water immersion objective lens. Images were recorded using MicroManager 2.0.

#### 4.2.11. Statistical analysis

All statistical analysis was performed in MATLAB 2019b. The error bars in the figures represent the standard deviation (SD). In the case of duplicate experiments, the pooled SD over the time or pH series was calculated (Eq. 4.5) and reported in the figure captions. This calculation relies on the assumption that the variances over the measurement series are homoscedastic. This assumption holds true for our data since no systematic trends in the variances were observed.

$$S_{pooled} = \sqrt{\frac{\sum_i^k S_i^2}{k}} \quad \text{Eq. 4.5}$$

where  $S_i^2$  is the variance for each measurement point (time or pH) and  $k$  is the total number of measurement points.

The normalized root mean square deviation (NRMSD) (Eq. 4.6) was used to evaluate the agreement between the pH values estimated using the CEST MRI approach and those measured with a pH electrode.

$$NRMSD = \frac{1}{\bar{y}^m} \sqrt{\frac{\sum_{i=1}^n (y_i^m - y_i^e)^2}{n}} \quad \text{Eq. 4.6}$$

where  $\bar{y}^m$  is the mean of the pH values measured by a pH electrode;  $y_i^m$  are the pH values measured by a pH electrode for each measurement point  $i$ ;  $y_i^e$  are the pH values estimated using the CEST MRI approach for each measurement point  $i$ ; and  $n$  is the total number of measurement points.

### 4.3. Results and discussion

#### 4.3.1. *In vitro* gastric digestion of WPIS, LPSM and HPSM

For 12% WPIS, a transition from a homogeneous solution to a system with small insoluble particles was found to start around 30 min when the pH reached 4.5 (Fig. S4.2), which is close to the iso-electric point (pI) of  $\alpha$ -lactalbumin (4.2) and  $\beta$ -lactoglobulin (5.1), causing protein aggregation and precipitation (Nicolai et al., 2011; Pederson et al., 2006). These small insoluble aggregates are difficult to observe in the top-view photographs (Fig. 4.1a), but can be discerned at  $t = 60$  min. They were removed from the stomach chamber with the syringe used to mimic gastric emptying due to their size of less than 2 mm (the inner diameter of the syringe tip). For LPSM and HPSM, coagulation was observed (Fig. 4.1a). Based on visual inspection, the coagulum of LPSM was compact and became smaller in volume as digestion progressed, while HPSM showed a softer and looser coagulum. The consistency of the coagulum depends on the extent of WP denaturation, as denatured WPs can form s-s bridges with  $\kappa$ -casein, resulting in WP-casein aggregates. The formation of these aggregates results in a softer and looser MP coagulum during gastric digestion (Ye et al., 2019), which explains the observed difference in the consistency of the MP coagulum between LPSM and HPSM. In the case of LPSM, only the supernatant was removed by gastric emptying starting from  $t = 20$  min, while for HPSM, small and soft coagulated proteins were removed until the end of digestion.

The area under the  $MTR_{asym}$  curve ( $AUC_{MTR_{asym}}$ ) of the gastric content samples, obtained from the  $^1H$  CEST spectra, is shown in Fig. 4.1b. During 80 min of digestion, the  $AUC_{MTR_{asym}}$  decreased by 90%, 80% and 50% for LPSM, HPSM and 12% WPIS, respectively. The  $MTR_{asym}$  is influenced by changes in protein concentration and pH, as described previously (Mayar et al., 2023). Both protein concentration and pH (Fig. S4.2) decreased during semi-dynamic digestion due to the removal of soluble or small aggregated proteins, and due to the secretion of acidic SGF. The 2D scatter plots in Figs. 4.1c-e show that the  $AUC_{MTR_{asym}}$  decreased in accordance with the decrease in protein concentration and pH observed during digestion.

For 12% WPIS, protein concentration and pH gradually decreased, resulting in a continuous decrease in the AUC  $MTR_{asym}$ . In the case of LPSM and HPSM, the protein concentration decreased from  $t = 0$  to 20 min, followed by small fluctuations until 80 min. These fluctuations may be attributed to proteins and polypeptides being released from the coagulum into the liquid phase as digestion progressed. A similar trend was reported for the protein concentration during semi-dynamic gastric digestion of MP powder (Mulet-Cabero et al., 2020). Whereas the start and end pH were similar for all test products, the variations during digestion were different. The pH decreased rapidly for LPSM, while for HPSM the decrease was slower and the pH remained higher throughout the digestion. The trend observed for HPSM was more similar to that of 12% WPIS, particularly in the first 40 mins of digestion. This difference can be attributed to the difference in coagulation behaviour between the differently heated milk products. In the case of LPSM, the majority of the caseins were incorporated into the coagulum, resulting in a liquid phase with a low amount of proteins and, hence, limited buffering capacity. This resulted in a more rapid decrease in pH, and hence, AUC  $MTR_{asym}$ . On the other hand, HPSM did not exhibit a clear phase separation, leading to a higher buffering capacity in the liquid phase and a slower decrease in pH, similar to WPI.

Overall, these results demonstrate that the  $MTR_{asym}$  reflects variations in pH and protein concentration that occur during semi-dynamic digestion, and is sensitive to differences in gastric digestion among products with different protein composition and heat treatment.

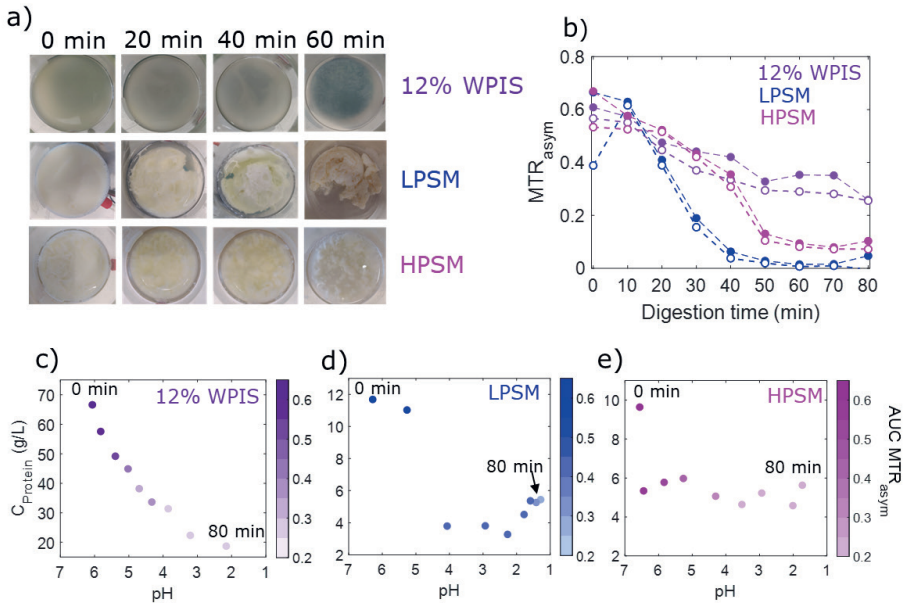


**Figure 4.1.** For 12% WPIS, LPSM and HPSM: (a) Photographs from the top of the stomach chamber at increasing digestion time from left to right; (b) evolution of the AUC  $MTR_{asym}$  for the gastric content samples during semi-dynamic *in vitro* digestion measured on a 7 T NMR spectrometer. The filled and empty symbols represent repeats of the same experiment. The pooled SD over the time series was 0.04, 0.07 and 0.04, respectively, for WPIS, LPSM and HPSM. 2D scatter plots for (c) 12% WPIS, (d) LPSM and (e) HPSM showing the AUC  $MTR_{asym}$  as a function of pH and protein concentration during semi-dynamic *in vitro* gastric digestion. The pH axis is inverted to follow the digestion time. The colour of the datapoints is weighted by the AUC  $MTR_{asym}$  value. The values represent the mean of the duplicate experiments, and the individual datasets can be found in Fig. S4.1. The pooled SD for the pH and concentration was 0.07 and 6.5, 0.3 and 0.4, 0.2 and 1.3, respectively, for WPIS, LPSM and HPSM.

#### 4.3.2. CEST MRI pH mapping of gastric digestion

In the previous section we found that the  $MTR_{asym}$  followed the variations in pH that occur during gastric digestion. Therefore, we further explored the use of CEST MRI for pH mapping under gastric digestion conditions. First, a validation was performed using standard WPIS and gastric content samples using the 7 T NMR spectrometer, followed by a proof-of-concept experiment for *in situ* pH mapping during semi-dynamic *in vitro* gastric digestion on a 3 T clinical MRI scanner.

#### 4.3.2.1. Validation of CEST MRI for pH mapping at 7 T

The  $MTR_{asym}$  curves showed a clear dependence on the  $B_1$  amplitude (Fig. 4.2a), and were used to calculate the  $RPM$  values of amines to construct the acid- (Fig. 4.2b) and base-catalysed (Fig. 4.2c) chemical exchange calibration lines. The  $^1H$  chemical exchange between amines and water can occur through both acid, base, and buffer catalysis, leading to a pH-dependent “v-shaped” pattern of the chemical exchange, as described before (Bai et al., 1993). However, the amine-water  $^1H$  chemical exchange is predominantly base-catalysed at  $pH > 5$ , and increasing exchange rates have been observed with increasing pH values for amino acids (Liepinsh & Otting, 1996; Wermter et al., 2022). The  $RPM$  value for the base-catalysed region showed a good linear correlation with pH ( $R^2 = 0.94$ ), while the correlation for the acid-catalysed region was lower ( $R^2 = 0.78$ ). This is likely due to the slower chemical exchange at low pH for amines, resulting in lower measured  $MTR_{asym}$  values, especially at  $B_1 = 1.5 \mu T$ . Consequently, the CEST MRI approach is less sensitive at low pH values.

The calibration lines were used to estimate the pH of a set of validation samples of 12% WPIS ranging from pH 3-7. A Bland-Altman plot was used to assess the agreement between the pH values estimated by CEST MRI and those measured with a pH electrode (Fig. 4.2d). The mean difference was around 0.34, which indicates a systematically higher pH estimated by the CEST MRI approach. The individual data points are scattered around the mean difference line, and are within the limits of agreement (LoA) except for the WPIS at pH 4.2. The difference appears to increase at lower pH values, indicating an overestimation of the pH in the lower pH range ( $< 4.5$ ), which may be attributed to the lower sensitivity of CEST at low pH as explained above. Overall, there was a good agreement between the pH estimated by CEST MRI and the pH values measured with an electrode within the pH range of 4.5-7 (NMRSD = 0.04). To assess whether the pH estimation is independent of protein concentration, we measured 6%, 8%, and 10% (wt%) WPI samples at pH 3.5 and 6.5. The obtained pH values were accurate and independent of protein concentration, as depicted in Fig. 4.2e. Subsequently, we used the calibration lines to estimate the pH of gastric content samples from the semi-dynamic digestion of 12% WPIS (Fig. 4.2f). The estimated pH values followed the same trend as the pH values measured by an electrode (grey line).

However, the agreement between the two methods was lower (NMRSD = 0.14) compared to the data of the validation samples. Larger deviations were observed at later digestion time points, consistent with previous observations for the validation samples at low pH. Based on these findings, we established that the pH range where CEST MRI can provide accurate pH estimates is pH 4.5 to 7; this can potentially aid *in vivo* mapping of the pH distribution throughout the stomach and determining the activation time of pepsin occurring at  $\sim$ pH 5.5 (Gray et al., 2014).

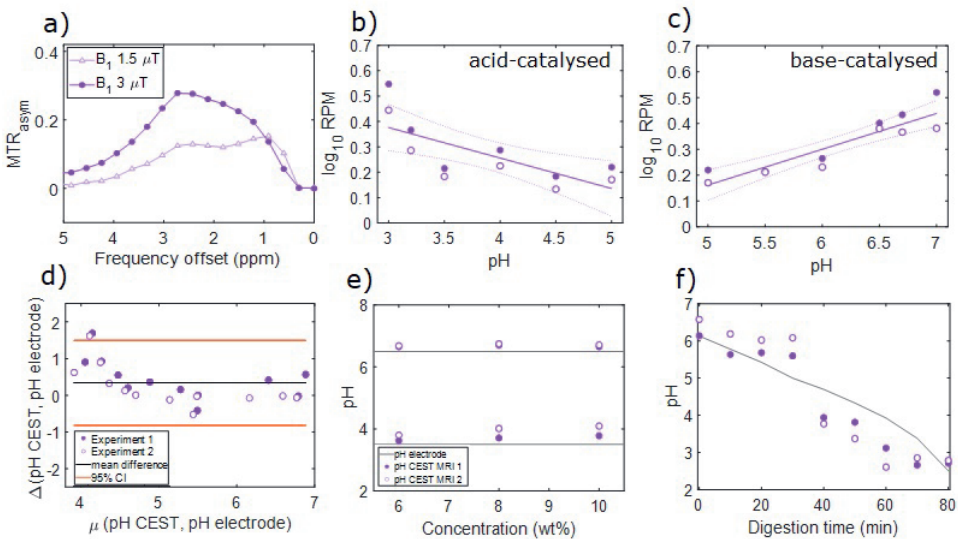


**Figure 4.2.** Validation of CEST for pH estimation on a 7 T NMR spectrometer using 12% (wt%) WPIS. (a)  $MTR_{asym}$  curves at pH 6 obtained with a  $B_1$  amplitude of 1.5 and 3  $\mu$ T. The filled and empty symbols in b-f represent repeats of the same experiment. pH calibration lines for (b) acid- ( $\log_{10} RPM = -0.21 \cdot pH + 1.4$ ;  $R^2 = 0.78$ ) and (c) base- ( $\log_{10} RPM = 0.25 \cdot pH - 0.9$ ;  $R^2 = 0.94$ ) catalysed chemical exchange. The solid and dotted lines represent the linear fit and the 95% confidence bounds of the fit, respectively. The pooled SD was 0.05 for both the acid- and base-catalysed calibration lines. (d) Bland-Altman plot of the pH estimated by CEST MRI vs. the pH measured with an electrode for a set of validation samples with a pooled SD of 0.15. (e) pH at different concentrations showing stable pH estimates upon varying concentrations with a pooled SD of 0.1. (f) pH of the gastric content samples estimated by CEST MRI and measured by the pH electrode. The pooled SD of the pH estimated by CEST MRI was 0.3.



#### 4.3.2.2. Proof-of-concept *in situ* pH mapping during gastric digestion

To further evaluate the feasibility of CEST MRI for *in vivo* pH mapping, CEST measurements were conducted on a 3 T clinical MRI scanner at 37 °C. The 12% WPIS at varying pH were measured to construct calibration curves for the acid- and base-catalysed chemical exchange (respectively,  $R^2 = 0.77$  and  $R^2 = 0.74$ ) (Fig. S4.3). It is worth noting that the  $R^2$  value for the base-catalysed calibration line is lower at 3 T compared to that at 7 T. This can be attributed to a shift in the chemical exchange peak observed in the CEST spectrum from  $\Delta = 2.7$  ppm at pH 3-6.5 to  $\Delta = 3.5$  ppm at pH  $\geq 6.5$  (Fig. S5.4). This leads to lower  $MTR_{asym}$  and  $RPM$  values at  $\Delta = 2.7$  ppm for pH 6.5-7. This shift in the  $\Delta$  is most likely caused by the higher temperature (37 °C) used for the 3 T measurements, resulting in a downfield shift of the chemical shift of amine protons. For comparison, CEST spectra of 12% WPIS at pH 4, 5.5 and 7 were also measured on a 7 T MRI scanner at 37 °C, and a similar shift was observed in the chemical exchange peak at pH 7 (Fig. S4.4).

The  $B_0$  correction of the  $MTR_{asym}$  using the method introduced by Sun (2020), yielded results consistent with the standard WASSR approach (Fig. S4.5). The corrected maps were then used to generate  $RPM$  maps. The calibration lines were used to obtain a pH map as a function of the digestion time (Fig 4.3a). Specifically, the calibration line for base- and acid-catalysed chemical exchange was used for the time periods  $t = 0-20$  min and 30-60 min, respectively.

The pH maps for  $t = 0 - 20$  mins were homogeneous, which is in line with the homogeneous gastric content observed in the corresponding photographs of the gastric compartment (Fig 4.3a). Additionally, the pH values estimated by CEST MRI were in close agreement with the mean pH measured by a pH electrode at 9 locations inside the beaker (Fig 4.3b). After  $t = 30$  min, the pH map becomes heterogeneous, consistent with visual observation of protein precipitation near the pI from  $t = 30$  min onwards. Consequently, voxels containing these aggregates have lower  $MTR_{asym}$  values, due to the reduced accessibility of chemically-exchangeable protons. This ultimately leads to lower  $RPM$  values, resulting in an overestimation of the pH by the acid-catalysed chemical exchange calibration line. This is also apparent in Fig. 4.3b, where the mean pH estimated by CEST MRI at

$t > 30$  mins is higher than the pH measured by the electrode. Therefore, this approach allows accurate estimation of pH up to the pI of the proteins under study and it is sensitive to the aggregation phenomena occurring near the pI. Notably, the CEST MRI method holds potential for detecting the formation of small aggregates during gastric digestion that cannot be detected in  $T_2$ -weighted MRI images (Fig. S4.6). Whereas most applications of pH mapping using CEST MRI focus solely on a narrow pH range, typically pH 6-7 (Boyd et al., 2022; Chen et al., 2017; Tang et al., 2020), our findings demonstrate that for WPIS the method can cover a broader pH range from pH 4.5-7. This is the relevant range for gastric digestion of proteins, and therefore this approach is worth pursuing in *in vivo* MRI studies. We acknowledge that the sensitivity and specificity of the method could be enhanced by utilizing a 7 T clinical MRI scanner. At this higher field strength we observed 1.5-2x higher  $MTR_{asym}$  values, depending on the pH and  $B_1$  amplitude (Fig. S4.7). Additionally, a better separation between the exchange peak and water could be obtained (Fig S4.4).

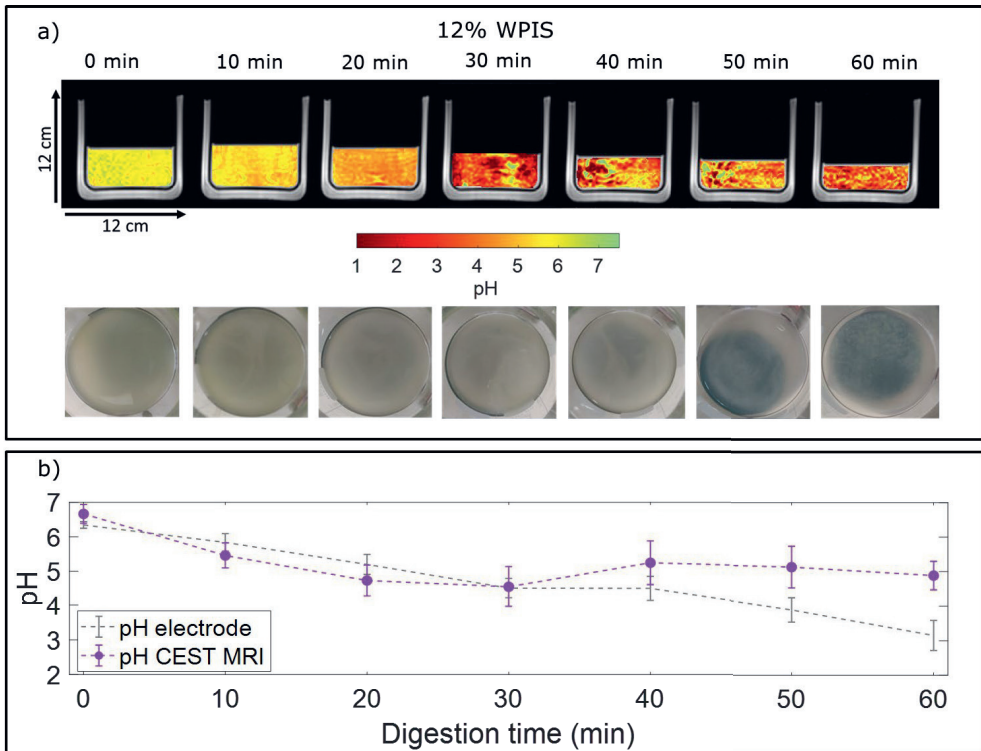


**Figure 4.3.** (a) pH maps during semi-dynamic *in vitro* gastric digestion of 12% WPI obtained using the dual power CEST MRI approach on a 3T clinical MRI scanner (top) and photographs of the beaker content during digestion (bottom). (b) Mean estimated pH of the gastric content (purple circles) and the mean pH measured by an electrode at 9 locations across the beaker content (gray line). The error bars for pH CEST MRI correspond to the SD of the pH across all the voxels ( $n=2058-3248$ ) in the gastric content. The error bars for pH electrode correspond to the standard deviation of the pH measured at 9 different locations across the beaker.

#### 4.3.3. Quantitative assessment of MP coagulation at 3T

In our previous work, we successfully applied  $T_2$ -weighted and MT MRI to monitor MP coagulation in static *in vitro* digestion samples using a 7 T NMR spectrometer (Mayar et al., 2023). In the present study, we set out to assess the feasibility of using these methods for *in situ* assessment of MP coagulation and breakdown under semi-dynamic conditions on a 3 T clinical MRI scanner.

#### 4.3.3.1. $T_2$ -weighted MRI of MP coagulation and breakdown

Phase separation between high- and low-intensity MRI components in  $T_2$ -weighted images as a result of gastric MP coagulation was observed from  $t = 10$  min and 20 min onwards for LPSM and HPSM, respectively (Fig. 4.4a). The high-intensity voxels correspond to the liquid phase consisting of SGF and dissolved proteins and peptides, having long  $T_2$ -values. The low-intensity MRI voxels correspond to the coagulum within which water protons undergo rapid  $T_2$  relaxation due to diffusional averaging and chemical exchange with immobile proteins. We note that the protons covalently bound to coagulated proteins have sub-ms  $T_2$ -values and, thus, are invisible in the conventional  $T_2$ -weighted MRI measurements performed here.

For LPSM, the coagulum was visible in the  $T_2$ -weighted images until the last digestion time point measured, while for HPSM, it was nearly completely solubilized or the soft coagulated proteins were completely removed by gastric emptying after  $t = 50$  min. It should be noted that in some of the other slices than the presented MRI slice of the gastric beaker coagulated proteins were observed at  $t > 50$  min. The measurements were conducted until  $t = 80$  min, but here we only show the images up until  $t = 70$  min because for HPSM, the volume of gastric content was too low for visualization and quantification at  $t > 70$  min.

The changes in the coagulum volume, estimated from the  $T_2$ -weighted images, varied as a function of the digestion time (Fig. 4.4b). The largest coagulum volume was observed at  $t = 10$  min and 20 min for LPSM and HPSM, respectively. Subsequently, the coagulum volume decreased for both milk products, with a consistently higher volume observed for LPSM at  $t \geq 30$  min. While, the  $T_2$ -weighted images proved useful for both visualizing and quantifying the changes in the coagulum volume, they do not provide information on the consistency of the coagulum. For that purpose, MT measurements were used as a complementary method.

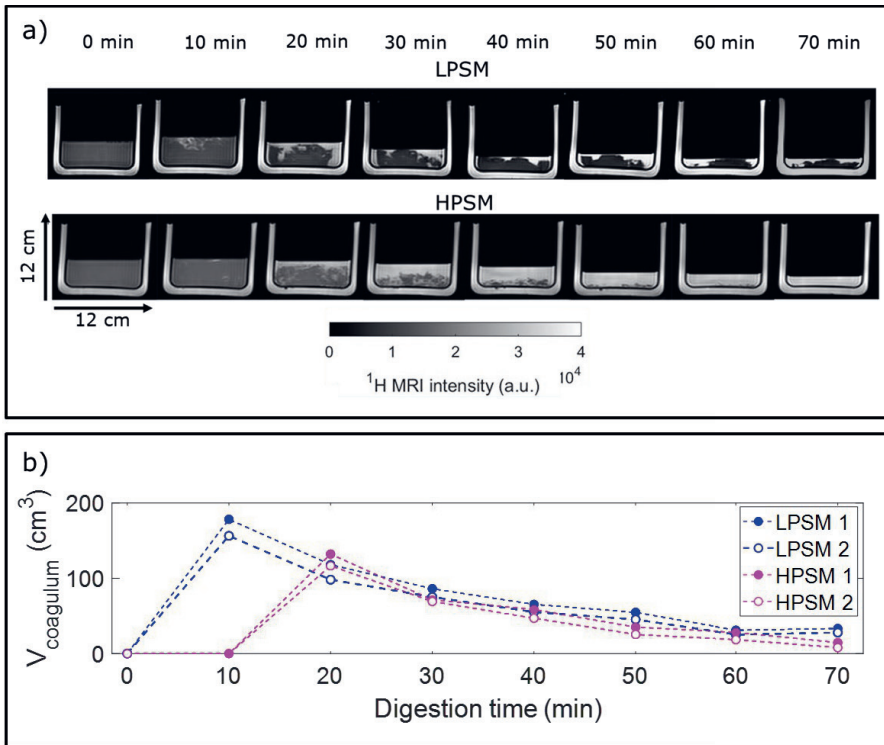


**Figure 4.4.** (a)  $T_2$ -weighted MRI images of LPSM and HPSM during semi-dynamic in vitro gastric digestion measured on a 3 T clinical MRI scanner. (b) Coagulum volume as a function of the digestion time obtained by intensity thresholding of the  $T_2$ -weighted images. The filled and empty symbols represent repeats of the same experiment. The pooled SD was 9 and 6, respectively, for LPSM and HPSM.

#### 4.3.3.2. MT MRI of MP coagulation

*MTR* maps of the coagulum (Fig. 4.5a, top) were obtained by applying the coagulum mask obtained from the  $T_2$ -weighted images to the MT data of the gastric beaker content. As digestion progressed, the *MTR* value within the coagulum increased, and a notable difference in the *MTR* maps of LPSM and HPSM was observed. The coagulum exhibited a greater spatial variability in the *MTR* values at later digestion time points, with the *MTR* maps of HPSM appearing more heterogeneous. The *MTR* values on the surface of the coagulum are lower, which might be due to partial-volume effects, and appear as a black/red edge.

The *MTR* distribution for the gastric content within each image (Fig. 4.5a, bottom) was unimodal and symmetric for both LPSM and HPSM at  $t = 0-10$  min, indicating high spatial homogeneity within the gastric content regions. However, from  $t = 20$  min onwards, the spatial *MTR* distributions for LPSM and HPSM began to differ. For LPSM, the peak shifted to higher *MTR* values, while for HPSM it remained nearly constant. The distribution for LPSM became asymmetric and appeared bimodal, while a broadened unimodal symmetric distribution was observed for HPSM. The bimodal nature of the *MTR* histogram for LPSM became more pronounced at later digestion time points.

As shown in Fig. 4.5b, the mean *MTR* of the coagulum increased with digestion for LPSM. This increase was 55% from  $t = 0$  to 70 mins. For HPSM, the *MTR* increased by 24% from  $t = 20 - 40$  mins followed by a decrease until 70 min. An increase in the *MTR* can be attributed to variations in the macromolecular content and mobility, and in the magnetization transfer dynamics (Henkelman et al., 2001). We have previously shown that the *MTR* depends on the composite parameter  $R_{ex}M_0^{ss}/R_1^w$ , which includes the rate of magnetization transfer ( $R_{ex}$ ), the population of semi-solid protons ( $M_0^{ss}$ ) and the longitudinal relaxation rate of water ( $R_1^w$ ) (Mayar et al., 2022). In our previous work, we observed that the  $R_1^w$  did not change during *in vitro* digestion. Therefore, the increased *MTR* observed for the MP coagulum during gastric digestion could be the result of a decrease in macromolecular mobility and an increase in the protein content within the coagulum. Constrained macromolecular mobility results in stronger inter- and intra-molecular dipolar interactions, which are the drivers of magnetization transfer (van Zijl et al., 2018; Zhou et al., 2023). This increase in dipolar interactions yields greater efficiency in magnetization transfer between the two proton pools and, hence, a higher *MTR*.

To better understand the increase in the *MTR* of the coagulum,  $G'$  and  $G''$  of the LPSM coagulum at  $t = 20, 40$  and 70 min were measured (Fig. S4.8). The  $G'$  and  $G''$  values at  $t = 20$  and 40 min are similar. However, a clear increase in both parameters was observed from  $t = 40$  up to 70 min. This observation is in line with the *MTR* data, where little variation was observed between  $t = 20$  and 40 min, followed by an increase from  $t = 40$  to 70 min. The  $G'$  represents the ability of a material to store and recover elastic energy and can be used to quantify its

ability to resist deformation. On the other hand, the  $G''$  represents the viscous component of a material's response to cyclic deformation and can be used to quantify a material's ability to dissipate energy and flow or deform plastically (Macosko, 1996). These observations are consistent with previous studies that demonstrated an increase in the  $G'$  and  $G''$  during acid and rennet coagulation of milk (Le Feunteun et al., 2012; Le Feunteun & Mariette, 2008). Moreover, Roy et al. (2022) showed an increase in the complex modulus ( $G^*$ ), a parameter that describes the complete viscoelastic behaviour of a material by combining the  $G'$  and  $G''$ , during *in vivo* gastric digestion of raw cow's milk in piglets. Both the increase in  $G'$  and  $G''$  point to a protein network that is becoming more dense and non-covalently crosslinked. The concomitant decrease in molecular mobility and increase in dipolar interactions within the protein network is reflected in the increase in the  $MTR$ . We acknowledge that the variability in the rheology data is large due to the inherent heterogeneity of the coagulum.

CLSM was used to assess changes in the coagulum at the micron-scale (Fig. S4.9). For both LPSM and HPSM, at  $t = 20$  min the micron-scale protein network within the coagulum appeared to be porous with void spaces filled with liquid entrapped within the protein network. The coagulum appeared more compact as digestion progressed, and minimal variation was observed in the microstructure of the coagulum between 40 and 70 min. Overall, both the CLSM and rheology data indicate that changes in protein network density and mobility within the coagulum are reflected in the  $MTR$  values.

Overall, these results demonstrate that CEST and MT combined with  $T_2$ -weighted imaging can be used to probe pH and MP coagulation under semi-dynamic *in vitro* gastric digestion conditions. This integrated approach may offer a more comprehensive overview of gastric digestion compared to the use of only  $T_2$ -weighted imaging for measuring GE and visual assessment of phase separation or coagulation. The measurements presented here are fast enough to be feasible for monitoring gastric digestion over time in *in vivo* human studies. The primary challenge of *in vivo* measurements is the presence of motion due to breathing and peristaltic contractions of the stomach. Breathing-related motion artifacts can be minimized by performing each scan within one breath-hold, which is common practice in clinical MRI of the abdominal area. Furthermore, motion-induced

artifacts in the calculated  $MTR$  and  $MTR_{asym}$  maps can be reduced through image registration of the  $S_0$  and  $S_{sat}$  images. In this study, our primary focus was gastric digestion, as it is the first step in MP digestion. Gastric digestion involves structuring and de-structuring of milk to facilitate further breakdown of MPs in the intestines. Consequently, gastric digestion may influence intestinal digestion, thereby affecting absorption of amino acids in the bloodstream. In future works, it would be interesting to link gastric digestion to the absorption of amino acids in the bloodstream.

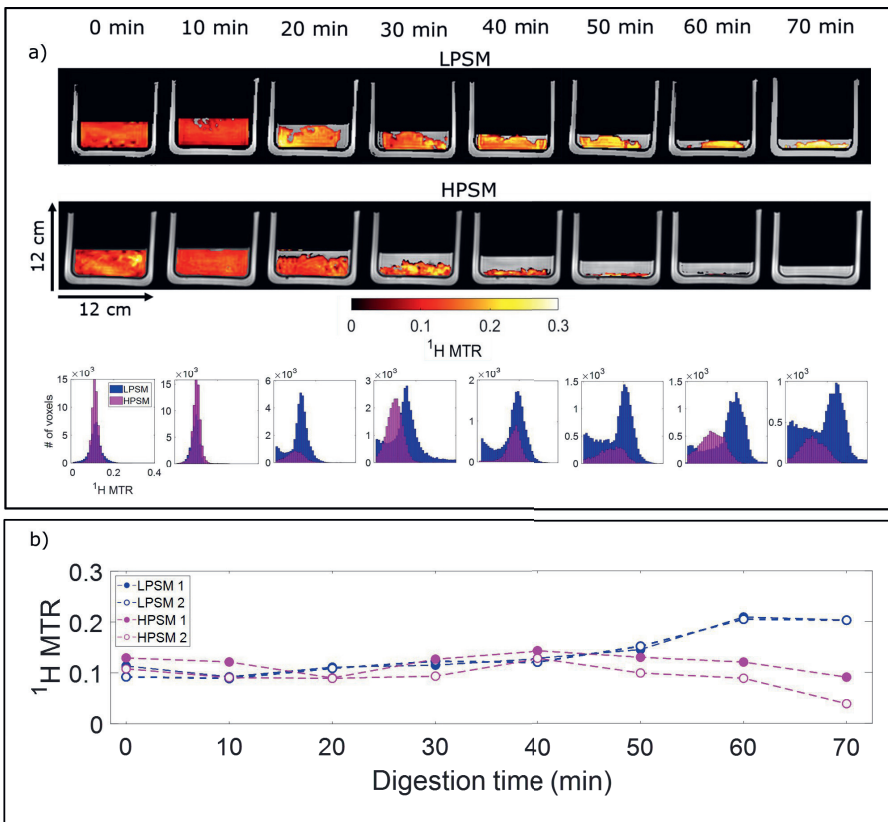


**Figure 4.5.** (a)  $^1H$  MTR MRI maps of the coagulum for LPSM and HPSM during semi-dynamic *in vitro* gastric digestion measured on a 3T clinical MRI scanner (top) and histograms with a bin width of 0.01 of the MTR inside the coagulum (bottom). (b) Mean MTR of the coagulum voxels as a function of the digestion time. The empty and filled symbols refer to repeats of the same experiment. The pooled SD was 0.01 and 0.02, respectively, for LPSM and HPSM.



## 4.4. Conclusions

In this work, we explored the use of CEST and MT MRI for monitoring pH and MP coagulation during semi-dynamic *in vitro* gastric digestion using 12% WPIS, LPSM and HPSM as test products. Our results demonstrate that the  $MTR_{asym}$  can be used to monitor concomitant pH and protein concentration changes during gastric digestion, and is sensitive to the effect of heat treatment on these changes. The dual-power CEST method was successfully validated on a 7 T NMR spectrometer as an indirect method for measuring pH using the 12% WPIS. The method demonstrated good agreement with measurements obtained via a pH electrode (NRMSD = 0.04 for pH 4.5-7). Accurate pH mapping was achieved on a 3 T clinical MRI scanner until  $t = 20$  min of digestion, but heterogeneities and inaccuracies in the estimated pH arose from 30 min onwards due to protein aggregation near the pI. Moreover, a combination of  $T_2$ -weighted images and  $MTR$  maps obtained *in situ* during semi-dynamic digestion on a 3 T clinical MRI scanner, proved to be valuable for assessing changes in coagulum volume and consistency, and for revealing differences in gastric coagulation behavior between differently heated milk products.

In summary, our findings demonstrate that the combined use of CEST, MT, and  $T_2$ -weighted MRI can be used to effectively capture the variations in pH and coagulation dynamics, allowing for the investigation of the impact of different heat treatments on gastric MP digestion. These findings are a significant advancement towards future assessment of *in vivo* gastric MP digestion in humans using MRI.

### Authorship contribution statement

Morwarid Mayar: Conceptualization, Methodology, Formal analysis, Investigation, Data curation, Visualization, Validation, Writing – original draft; Mart de Vries: Investigation, Methodology, Formal analysis, Writing – review; John van Duynhoven, Paul Smeets and Camilla Terenzi: Conceptualization, Methodology, Validation, Writing – review & editing, Supervision.

## Acknowledgements

Lucas van Grootveld is gratefully acknowledged for performing the CEST measurement of LPSM on the 7 T NMR spectrometer. We also acknowledge the MAGNEFY centre which was supported by the uNMR-NL Grid: A distributed, state-of-the-art Magnetic Resonance facility for the Netherlands (NWO grant 184.035.002). John Philippi is thanked for expert technical support on the 7 T NMR spectrometer. The use of the 3 T MRI facility has been made possible by Wageningen University & Research Shared Research Facilities. Paul de Bruin is thanked for his expert support with setting up the measurements on the 3 T clinical MRI scanner. Jeanine Prompers and Hans Hoogduin are thanked for their help with the measurements on the 7 T clinical MRI scanner.

## References

- Bai, Y., Milne, J. S., Mayne, L., & Englander, S. W. (1993). Primary structure effects on peptide group hydrogen exchange. *Proteins: Structure, Function, and Genetics*, *17*(1), 75–86. <https://doi.org/10.1002/prot.340170110>
- Balaban, R.S., & Ceckler, T. (1992). Magnetization transfer contrast in magnetic resonance imaging. *Magn Reson Q*, *8*(2), 116–137.
- Bornhorst, G. M., & Paul Singh, R. (2014). Gastric Digestion In Vivo and In Vitro: How the Structural Aspects of Food Influence the Digestion Process. *Annual Review of Food Science and Technology*, *5*(1), 111–132. <https://doi.org/10.1146/annurev-food-030713-092346>
- Boyd, P. S., Breitling, J., Korzowski, A., Zaiss, M., Franke, V. L., Mueller-Decker, K., Glinka, A., Ladd, M. E., Bachert, P., & Goerke, S. (2022). Mapping intracellular pH in tumors using amide and guanidyl CEST-MRI at 9.4 T. *Magnetic Resonance in Medicine*, *87*(5), 2436–2452. <https://doi.org/10.1002/mrm.29133>
- Brodkorb, A., Egger, L., Alminger, M., Alvito, P., Assunção, R., Ballance, S., Bohn, T., Bourliou-Lacanal, C., Boutrou, R., Carrière, F., Clemente, A., Corredig, M., Dupont, D., Dufour, C., Edwards, C., Golding, M., Karakaya, S., Kirkhus, B., Le Feunteun, S., ... Recio, I. (2019). INFOGEST static in vitro simulation of gastrointestinal food digestion. *Nature Protocols*, *14*(4), 991–1014. <https://doi.org/10.1038/s41596-018-0119-1>
- Carver, J. P., & Richards, R. E. (1972). A general two-site solution for the chemical exchange produced dependence of T<sub>2</sub> upon the carr-Purcell pulse separation. *Journal of Magnetic Resonance (1969)*, *6*(1), 89–105. [https://doi.org/10.1016/0022-2364\(72\)90090-X](https://doi.org/10.1016/0022-2364(72)90090-X)
- Chen, M., Chen, C., Shen, Z., Zhang, X., Chen, Y., Lin, F., Ma, X., Zhuang, C., Mao, Y., Gan, H., Chen, P., Zong, X., & Wu, R. (2017). Extracellular pH is a biomarker enabling detection of breast cancer and liver cancer using CEST MRI. *Oncotarget*, *8*(28), 45759–45767. <https://doi.org/10.18632/oncotarget.17404>
- Deng, R., Janssen, A. E. M., Vergeldt, F. J., Van As, H., de Graaf, C., Mars, M., & Smeets, P. A. M. (2020). Exploring in vitro gastric digestion of whey protein by time-domain nuclear magnetic resonance and magnetic resonance imaging. *Food Hydrocolloids*, *99*(August 2019), 105348. <https://doi.org/10.1016/j.foodhyd.2019.105348>
- Deng, R., Mars, M., Janssen, A. E. M., & Smeets, P. A. M. (2023). Gastric digestion of whey protein gels: A randomized cross-over trial with the use of MRI. *Food Hydrocolloids*, 108689. <https://doi.org/10.1016/j.foodhyd.2023.108689>

- Deng, R., Seimys, A., Mars, M., Janssen, A. E. M., & Smeets, P. A. M. (2022). Monitoring pH and whey protein digestion by TD-NMR and MRI in a novel semi-dynamic in vitro gastric simulator (MR-GAS). *Food Hydrocolloids*, *125*, 107393. <https://doi.org/10.1016/j.foodhyd.2021.107393>
- Dupont, D., & Mackie, A. R. (2015). Static and dynamic in vitro digestion models to study protein stability in the gastrointestinal tract. *Drug Discovery Today: Disease Models*, *17–18*, 23–27. <https://doi.org/10.1016/j.ddmod.2016.06.002>
- Gottwald, A., Creamer, L. K., Hubbard, P. L., & Callaghan, P. T. (2005). Diffusion, relaxation, and chemical exchange in casein gels: A nuclear magnetic resonance study. *The Journal of Chemical Physics*, *122*(3). <https://doi.org/10.1063/1.1825383>
- Gray, V. A., C. Marques, M. R., Cole, E., Riva Toma, J. M. D., Ghidorsci, L., Guo, J.-H., Han, J.-H., Han, F., Hosty, C. T., Kochling, J. D., Kraemer, J., Langdon, T., Leinbach, S. R., Martin, G. P., Meyerhoffer, S. M., Moreton, R. C., Raghaven, K. S., Shneyvas, E., Suggett, J. A., ... Eranui, T. (2014). Use of Enzymes in the Dissolution Testing of Gelatin Capsules and Gelatin-Coated Tablets-Revisions to Dissolution & 711&gt; and Disintegration and Dissolution of Dietary Supplements & 2040&gt; *Dissolution Technologies*, *21*(4), 6–18. <https://doi.org/10.14227/DT210414P6>
- Henkelman, R. M., Stanisz, G. J., & Graham, S. J. (2001). Magnetization transfer in MRI: A review. *NMR in Biomedicine*, *14*(2), 57–64. <https://doi.org/10.1002/nbm.683>
- Hills, B. P., Takacs, S. F., & Belton, P. S. (1990). A new interpretation of proton NMR relaxation time measurements of water in food. *Food Chemistry*, *37*(2), 95–111. [https://doi.org/10.1016/0308-8146\(90\)90084-H](https://doi.org/10.1016/0308-8146(90)90084-H)
- Hinrichs, R., Bulca, S., & Kulozik, U. (2007). Water mobility during renneting and acid coagulation of casein solutions: a differentiated low-resolution nuclear magnetic resonance analysis. *International Journal of Dairy Technology*, *60*(1), 37–43. <https://doi.org/10.1111/j.1471-0307.2007.00290.x>
- Huppertz, T., & Chia, L. W. (2021). Milk protein coagulation under gastric conditions: A review. *International Dairy Journal*, *113*, 104882. <https://doi.org/10.1016/j.idairyj.2020.104882>
- Kim, M., Gillen, J., Landman, B. A., Zhou, J., & Van Zijl, P. C. M. (2009). Water saturation shift referencing (WASSR) for chemical exchange saturation transfer (CEST) experiments. *Magnetic Resonance in Medicine*, *61*(6), 1441–1450. <https://doi.org/10.1002/mrm.21873>
- Le Feunteun, S., & Mariette, F. (2008). Effects of Acidification with and without Rennet on a Concentrated Casein System: A Kinetic NMR Probe Diffusion Study. *Macromolecules*, *41*(6), 2079–2086. <https://doi.org/10.1021/ma702248z>
- Le Feunteun, S., Ouethrani, M., & Mariette, F. (2012). The rennet coagulation mechanisms of a concentrated casein suspension as observed by PFG-NMR diffusion measurements. *Food Hydrocolloids*, *27*(2), 456–463. <https://doi.org/10.1016/j.foodhyd.2011.09.008>
- Liepinsh, E., & Otting, G. (1996). Proton exchange rates from amino acid side chains—implications for image contrast. *Magnetic Resonance in Medicine*, *35*(1), 30–42. <https://doi.org/10.1002/mrm.1910350106>
- Longo, D. L., Sun, P. Z., Consolino, L., Michelotti, F. C., Uggeri, F., & Aime, S. (2014). A general MRI-CEST ratiometric approach for pH imaging: Demonstration of in vivo pH mapping with iobitridol. *Journal of the American Chemical Society*, *136*(41), 14333–14336. <https://doi.org/10.1021/ja5059313>
- Mackie, A., Mulet-Cabero, A.-I., & Torcello-Gómez, A. (2020). Simulating human digestion: developing our knowledge to create healthier and more sustainable foods. *Food & Function*, *11*(11), 9397–9431. <https://doi.org/10.1039/D0FO01981J>
- Macosko, C. W. (1996). *Rheology: Principles, Measurements, and Applications* (1st ed.). Wiley-VCH.

- Mayar, M., Miltenburg, J. L., Hettinga, K., Smeets, P. A. M., van Duynhoven, J. P. M., & Terenzi, C. (2022). Non-invasive monitoring of in vitro gastric milk protein digestion kinetics by <sup>1</sup>H NMR magnetization transfer. *Food Chemistry*, *383*(February), 132545. <https://doi.org/10.1016/j.foodchem.2022.132545>
- Mayar, M., Smeets, P., Duynhoven, J., & Terenzi, C. (2023). In vitro <sup>1</sup>H MT and CEST MRI mapping of gastro-intestinal milk protein breakdown. *Food Structure*, *36*, 100314–100324.
- Ménard, O., Bourlieu, C., De Oliveira, S. C., Dellarosa, N., Laghi, L., Carrière, F., Capozzi, F., Dupont, D., & Deglaire, A. (2018). A first step towards a consensus static in vitro model for simulating full-term infant digestion. *Food Chemistry*, *240*(2017), 338–345. <https://doi.org/10.1016/j.foodchem.2017.07.145>
- Mulet-Cabero, A. I., Egger, L., Portmann, R., Ménard, O., Marze, S., Minekus, M., Le Feunteun, S., Sarkar, A., Grundy, M. M. L., Carrière, F., Golding, M., Dupont, D., Recio, I., Brodkorb, A., & Mackie, A. (2020). A standardised semi-dynamic: in vitro digestion method suitable for food-an international consensus. *Food and Function*, *11*(2), 1702–1720. <https://doi.org/10.1039/c9fo01293a>
- Mulet-Cabero, A. I., Mackie, A. R., Wilde, P. J., Fenelon, M. A., & Brodkorb, A. (2019). Structural mechanism and kinetics of in vitro gastric digestion are affected by process-induced changes in bovine milk. *Food Hydrocolloids*, *86*, 172–183. <https://doi.org/10.1016/j.foodhyd.2018.03.035>
- Musse, M., Le Feunteun, S., Collewet, G., Ravilly, M., Quellec, S., Ossemond, J., Morzel, M., Challoy, S., Nau, F., & Lucas, T. (2023). Quantitative magnetic resonance imaging of in vitro gastrointestinal digestion of a bread and cheese meal. *Food Research International*, *169*, 112821–112833.
- Nehrke, K., & Börner, P. (2012). DREAM—a novel approach for robust, ultrafast, multislice B1 mapping. *Magnetic Resonance in Medicine*, *68*(5), 1517–1526. <https://doi.org/10.1002/MRM.24158>
- Nicolai, T., Britten, M., & Schmitt, C. (2011).  $\beta$ -Lactoglobulin and WPI aggregates Formation, structure and applications. *Food Hydrocolloids*, *25*, 1945–1962.
- Pederson, J. B., Fojan, P., Sorensen, J., & Petersen, S. B. (2006). Towards Control of Aggregational Behaviour of  $\alpha$ -Lactalbumin at Acidic pH. *Journal of Fluorescence*, *16*, 611–621.
- Roy, D., Moughan, P. J., Ye, A., Hodgkinson, S. M., Stroebinger, N., Li, S., Dave, A. C., Montoya, C. A., & Singh, H. (2022). Structural changes in milk from different species during gastric digestion in piglets. *Journal of Dairy Science*, *105*(5), 3810–3831. <https://doi.org/10.3168/jds.2021-21388>
- Smeets, P. A. M., Deng, R., Van Eijnatten, E. J. M., & Mayar, M. (2020). Monitoring food digestion with magnetic resonance techniques. *Proceedings of the Nutrition Society*, *3*, 1–11. <https://doi.org/10.1017/S0029665120007867>
- Sun, P. Z. (2020). Fast correction of B0 field inhomogeneity for pH-specific magnetization transfer and relaxation normalized amide proton transfer imaging of acute ischemic stroke without Z-spectrum. *Magnetic Resonance in Medicine*, *83*(5), 1688–1697. <https://doi.org/10.1002/mrm.28040>
- Tang, Y., Xiao, G., Shen, Z., Zhuang, C., Xie, Y., Zhang, X., Yang, Z., Guan, J., Shen, Y., Chen, Y., Lai, L., Chen, Y., Chen, S., Dai, Z., Wang, R., & Wu, R. (2020). Noninvasive Detection of Extracellular pH in Human Benign and Malignant Liver Tumors Using CEST MRI. *Frontiers in Oncology*, *10*. <https://doi.org/10.3389/fonc.2020.578985>
- Tome, D. (2012). Criteria and markers for protein quality assessment – a review. *British Journal of Nutrition*, *108*(S2), S222–S229. <https://doi.org/10.1017/S0007114512002565>
- Tunick, M. H., Ren, D. X., Van Hekken, D. L., Bonnaillie, L., Paul, M., Kwoczek, R., & Tomasula, P. M. (2016). Effect of heat and homogenization on in vitro digestion of milk. *Journal of Dairy Science*, *99*(6), 4124–4139. <https://doi.org/10.3168/jds.2015-10474>

- van Lieshout, G. A. A., Lambers, T. T., Bragt, M. C. E., & Hettinga, K. A. (2019). How processing may affect milk protein digestion and overall physiological outcomes: A systematic review. *Critical Reviews in Food Science and Nutrition*, *0*(0), 1–24. <https://doi.org/10.1080/10408398.2019.1646703>
- Van Obberghen, E., Mchinda, S., le Troter, A., Prevost, V. H., Viout, P., Guye, M., Varma, G., Alsop, D. C., Ranjeva, J.-P., Pelletier, J., Girard, O., & Duhamel, G. (2018). Evaluation of the Sensitivity of Inhomogeneous Magnetization Transfer (ihMT) MRI for Multiple Sclerosis. *American Journal of Neuroradiology*, *39*(4), 634–641. <https://doi.org/10.3174/ajnr.A5563>
- van Zijl, P. C. M., Lam, W. W., Xu, J., Knutsson, L., & Stanisiz, G. J. (2018). Magnetization Transfer Contrast and Chemical Exchange Saturation Transfer MRI. Features and analysis of the field-dependent saturation spectrum. *NeuroImage*, *168*, 222–241. <https://doi.org/10.1016/j.neuroimage.2017.04.045>
- Wang, X., Ye, A., Lin, Q., Han, J., & Singh, H. (2018). Gastric digestion of milk protein ingredients: Study using an in vitro dynamic model. *Journal of Dairy Science*, *101*(8), 6842–6852. <https://doi.org/10.3168/jds.2017-14284>
- Ward, K. M., Aletras, A. H., & Balaban, R. S. (2000). A New Class of Contrast Agents for MRI Based on Proton Chemical Exchange Dependent Saturation Transfer (CEST). *Journal of Magnetic Resonance*, *143*(1), 79–87. <https://doi.org/10.1006/jmre.1999.1956>
- Weiger, M., & Pruessmann, K. P. (2019). Short-T2 MRI: Principles and recent advances. *Progress in Nuclear Magnetic Resonance Spectroscopy*, *114–115*, 237–270. <https://doi.org/10.1016/j.pnmrs.2019.07.001>
- Welsch, G. H., Trattinig, S., Scheffler, K., Szomonanyi, P., Quirbach, S., Marlovits, S., Domayer, S., Bieri, O., & Mamsch, T. C. (2008). Magnetization transfer contrast and T2 mapping in the evaluation of cartilage repair tissue with 3T MRI. *Journal of Magnetic Resonance Imaging*, *28*(4), 979–986. <https://doi.org/10.1002/jmri.21516>
- Wermter, F. C., Bock, C., & Dreher, W. (2022). Characterization of amine proton exchange for analyzing the specificity and intensity of the CEST effect: from humans to fish. *NMR in Biomedicine*, *35*(2). <https://doi.org/10.1002/nbm.4622>
- Windschuh, J., Zaiss, M., Meissner, J. E., Paech, D., Radbruch, A., Ladd, M. E., & Bachert, P. (2015). Correction of B1-inhomogeneities for relaxation-compensated CEST imaging at 7T. *NMR in Biomedicine*, *28*(5), 529–537. <https://doi.org/10.1002/nbm.3283>
- Wolff, S. D., & Balaban, R. S. (1989). Magnetization transfer contrast (MTC) and tissue water proton relaxation in vivo. *Magnetic Resonance in Medicine*, *10*(1), 135–144. <https://doi.org/10.1002/mrm.1910100113>
- Wu, B., Warnock, G., Zaiss, M., Lin, C., Chen, M., Zhou, Z., Mu, L., Nanz, D., Tuura, R., & Delso, G. (2016). An overview of CEST MRI for non-MR physicists. *EJNMMI Physics*, *3*(1). <https://doi.org/10.1186/s40658-016-0155-2>
- Wu, R., Longo, D. L., Aime, S., & Sun, P. Z. (2015). Quantitative description of radiofrequency (RF) power-based ratiometric chemical exchange saturation transfer (CEST) pH imaging. *NMR in Biomedicine*, *28*(5), 555–565. <https://doi.org/10.1002/nbm.3284>
- Ye, A., Weilin, L., Cui, J., Kong, Z., Roy, D., Kong, Y., Han, J., & Singh, H. (2019). Coagulation behaviour of milk under gastric digestion: Effect of pasteurization and ultra-high temperature treatment. *Food Chemistry*, *286*, 216–225.
- Zhou, Y., Bie, C., van Zijl, P. C. M., & Yadav, N. N. (2023). The relayed nuclear Overhauser effect in magnetization transfer and chemical exchange saturation transfer MRI. *NMR in Biomedicine*, *36*(6). <https://doi.org/10.1002/nbm.477>

## 4.5. Supplementary Information

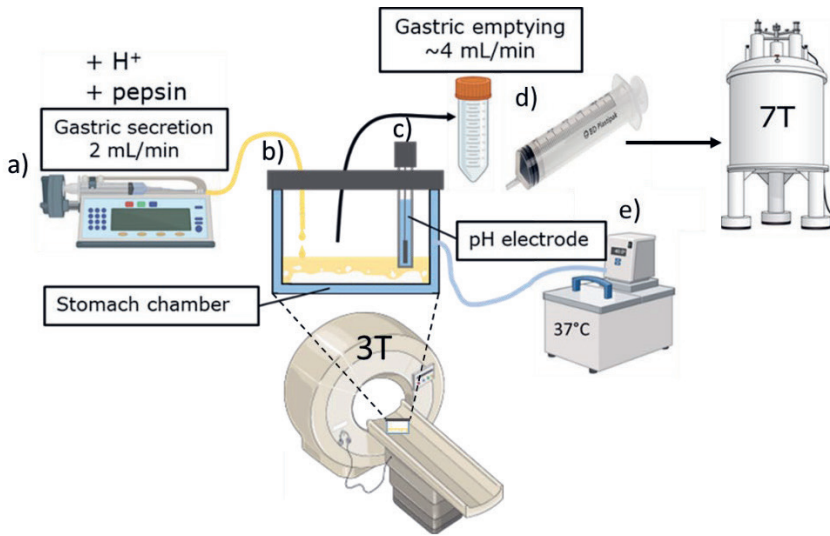


**Figure S4.1.** Schematic representation of the semi-dynamic MRI compatible in vitro gastric digestion model used in this work adapted from (Deng et al., 2022), consisting of (a) syringe pump used for gastric secretion, (b) a water-jacketed beaker serving as the stomach chamber, (c) a pH meter used to monitor the pH during experiment conducted outside of the MRI scanner, (d) a syringe used for manual removal of gastric content to mimic gastric emptying, (e) a circulating water bath to keep the temperature of the stomach chamber at 37 °C.

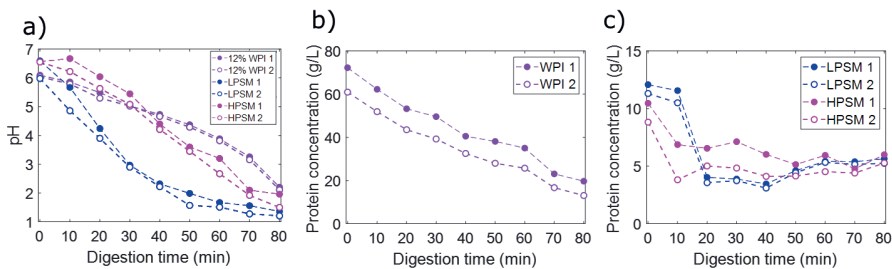


**Figure S4.2.** For WPI, LPSM and HPSM: Evolution of the (a) pH and (b,c) protein concentration during semi-dynamic in vitro gastric digestion. The empty and filled symbols represent repeats of the same experiment.

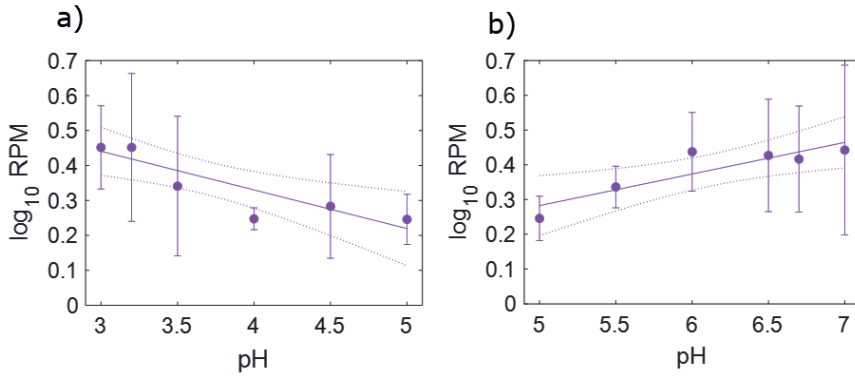


**Figure S4.3.** Calibrations line for (a) the acid- and (b) base-catalysed chemical exchange obtain on the 3T clinical MRI scanner at 37 °C. The error bars correspond to the standard deviation across the gastric content voxels, and the data is represented as mean $\pm$ SD. The solid and dotted lines represent the linear fit and the 95% confidence bounds of the fit, respectively.

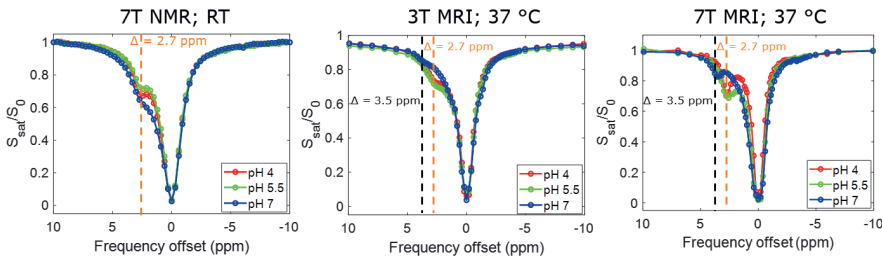


**Figure S4.4.** CEST spectra of 12% WPI at pH 4, 5.5, 7 measured at room temperature on a 7T NMR spectrometer (a), and at 37 °C on 3T (b) and 7T (c) clinical MRI scanners. The spectra show the shift in the chemical exchange peak for pH 7 at 37 °C.

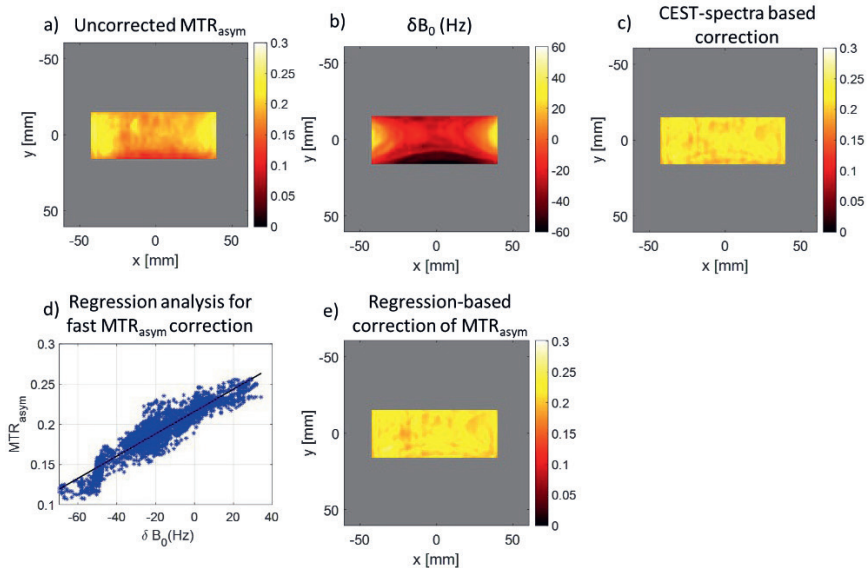


**Figure S4.5.** (a) Uncorrected  $MTR_{asym}$  map of 12% WPI solution at pH 6.7 showing spatial variations in the  $MTR_{asym}$  caused by  $B_0$  inhomogeneities as shown in the corresponding (b)  $B_0$  map. The standard approach realigns the minimum of the CEST spectra to  $\Delta = 0$  ppm to correct for  $B_0$  inhomogeneities, resulting in less spatial variations in (c) the corrected  $MTR_{asym}$  map. (d) The regression analysis for the  $MTR_{asym}$  vs.  $\delta B_0$  (Hz) used for fast  $B_0$ -inhomogeneity correction of the  $MTR_{asym}$  values. (e) The corrected  $MTR_{asym}$  map using the fast  $B_0$ -inhomogeneity correction yielding similar results as the standard CEST-spectra based approach.

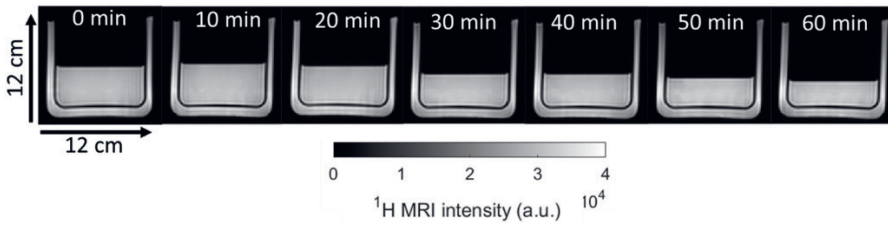


**Figure S4.6.**  $T_2$ -weighted MRI images of 12% WPIS during semi-dynamic *in vitro* gastric digestion on a 3T clinical MRI scanner.



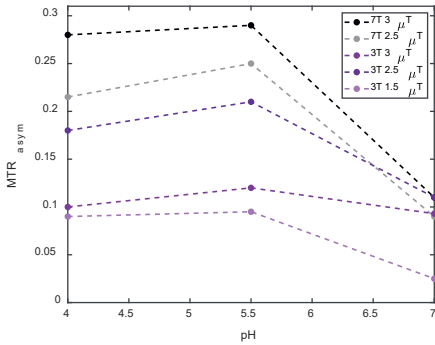


**Figure S4.7.**  $MTR_{asym}$  at  $\Delta = 2.7$  ppm for 12% WPI at pH 4, 5.5, 7 obtained at 7T and 3T using different  $B_1$  amplitudes, showing the higher sensitivity of the method at higher magnetic field strength.

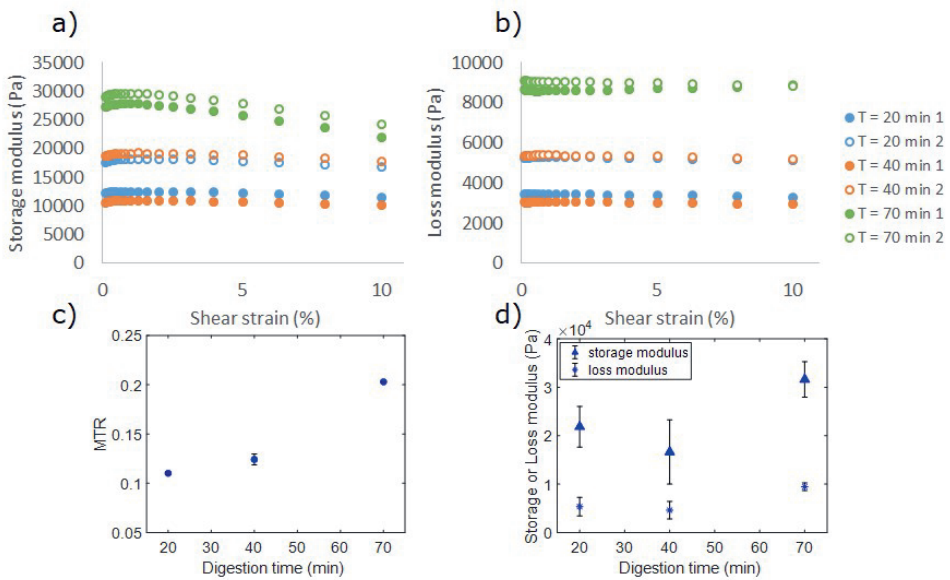


**Figure S4.8.** (a) Storage and (b) loss modulus of the coagulum of LPSM measured after 20, 40 and 70 min of semi-dynamic in vitro gastric digestion. The filled and empty symbols represent repeats of the same experiment. (c) The MTR of the coagulum of LPSM at  $t = 20, 40$  and  $70$  min, along with the corresponding (d) storage or loss modulus at a shear strain of 1%, showing the similar trend in the MTR and storage and loss modulus. The error bars in c and d correspond to the standard deviation of two repeated experiments.

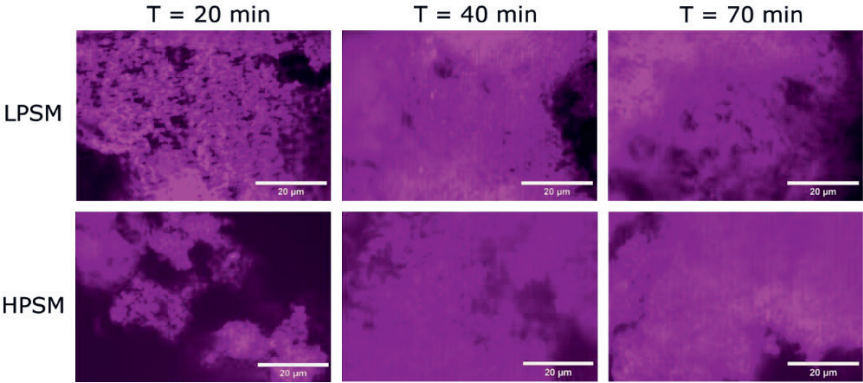


**Figure S4.9.** CLSM micrographs of the coagulum of LPSM (top) and HPSM (bottom) after 20, 40 and 70 min of semi-dynamic *in vitro* gastric digestion.



**CHAPTER**

# 5

# Magnetization Transfer MRI of intra-gastric milk digestion: a feasibility study in humans

This chapter is in preparation as:

Mayar, M. Terenzi, C., van Duynhoven, J.P.M., & Smeets, P.A.M., Magnetization Transfer MRI of intra-gastric milk digestion: a feasibility study in humans.

## Abstract

To develop food products and processing methods for optimal health benefits, it is necessary to understand the behavior of foods in our digestive system. The digestion of milk, a source of high-quality proteins, has been extensively studied using both *in vitro* and *in vivo* animal models. However, it is essential to validate these findings with *in vivo* data obtained from humans. Previously, we demonstrated the performance of Magnetization Transfer (MT) MRI in investigating gastric milk protein (MP) coagulation in a semi-dynamic model. In this study, we aimed to assess the feasibility of using MT MRI for monitoring gastric MP coagulation in humans.

A total of 12 healthy adults were enrolled. Participants underwent gastric MRI scans at baseline and after consumption of 300 g of either low- or high-pasteurized skim milk (LPSM and HPSM, respectively). We evaluated coagulation and gastric emptying (GE) dynamics using the  $^1\text{H}$  MT Ratio ( $^1\text{H}$  *MTR*), total gastric content (TGC), semi-solid, and liquid volumes.

The *MTR* increased with the digestion time for both LPSM and HPSM ( $p < 0.001$ ), indicating an increase in the degree of coagulation. There was no effect of heat treatment on the *MTR* with a mean difference (MD) of 16% (95% CI [10-21]) ( $p = 0.15$ ). The TGC volume over time for HPSM was higher than that of LPSM with an MD of 40.3 mL (95% CI [25.5-55.1]) ( $p = 0.044$ ). Furthermore, the AUC of the TGC and liquid volume were also higher for HPSM ( $p = 0.021$  and  $p = 0.017$ , respectively), and a trend towards a significantly higher AUC was found for the semi-solid volume of HPSM ( $p = 0.078$ ).

MT MRI enables monitoring of gastric MP coagulation in humans. By combining standard  $T_2$ -weighted anatomical MRI images with MT data, GE of total, semi-solid and liquid gastric content, as well as the coagulum consistency could be assessed *in vivo*. This approach opens the way to assessing intra-gastric digestion of a variety of protein-rich foods in humans.

## 5.1. Introduction

There is an increasing socio-economical demand in linking food with health. To aid the development of innovative food products and processing methods for optimal health benefits, one of the necessary requirements is to understand the behavior of foods in our digestive system (Bornhorst & Paul Singh, 2014). To this purpose, various static and (semi)-dynamic *in vitro* digestion models (Dupont & Mackie, 2015) have been developed, which simulate digestion in the human gastrointestinal (GI) tract. Such models have found widespread use because they are simple to use, well controlled and do not pose ethical concerns. However, even sophisticated dynamic *in vitro* models do not fully capture the complexity of *in vivo* digestion, which includes neural and hormonal regulation as well as feedback controls. Therefore, *in vivo* data from humans is needed to gain a better understanding of food digestion, and to verify and inform *in vitro* digestion models. This requires the development of non-invasive methods that can be used to study food digestion both *in vitro* and *in vivo* in humans.

We have previously demonstrated that Magnetization Transfer (MT)  $^1\text{H}$  MRI is a powerful imaging approach for assessing structural changes that occur during static (Mayar et al., 2022, 2023) and semi-dynamic (Chapter 4) *in vitro* gastric digestion using cow's milk, a widely consumed source of high-quality proteins, as a test case.

Cow's milk contains approximately 3.5% protein, with caseins and whey proteins (WPs) constituting 80% and 20%, respectively (Bhat et al., 2016). Gastric digestion of cow's milk involves acid- and pepsin-induced aggregation of casein micelles, which results in the formation of a semi-solid coagulum (Huppertz & Chia, 2021). The coagulation process results in reduced macromolecular mobility as liquid milk undergoes a transition into a semi-solid mass.

In our prior *in vitro* work (Chapter 4), we demonstrated that this transition can be monitored using the  $^1\text{H}$  MT ratio (*MTR*) as an MRI marker of the coagulum consistency, and that differences in the coagulation behaviour resulting from heat treatment can be unraveled.

Knowledge of the effect of heat treatment on gastric milk digestion is crucial because it can potentially be used to tune the gastric coagulation properties, and the kinetics of the subsequent breakdown and absorption in the intestines, for milk proteins (MPs). Therefore, gastric MP coagulation has been studied extensively with *in vitro* models (Li et al., 2022; Mulet-Cabero et al., 2019; Ye et al., 2016) and *in vivo* in animals (Ahlborn et al., 2023; Ye, Liu, et al., 2019). These studies have shown that heat treatment results in a looser and softer coagulum structure under gastric conditions, due to aggregation of WPs on the surface of casein micelles, resulting in reduced casein-casein interactions (Kethireddipalli & Hill, 2015). Moreover, a study in humans reported a difference in the time courses of dietary nitrogen (N) transfer into serum amino acids (AAs), urea, and protein pools, using  $^{15}\text{N}$  labelled milk for pasteurized and UHT milk and suggested that these effects may have been caused by a looser and softer coagulum structure and faster gastric emptying (GE) (Lacroix et al., 2008).

To date there are no *in vivo* studies in humans that have assessed intra-gastric MP coagulation, and the effect of heat treatment on this process. As demonstrated by our *in vitro* results,  $^1\text{H}$  MT MRI holds great potential for bridging this research gap (Mayar et al., 2022, 2023). However, studying gastric digestion with MRI is more challenging *in vivo* than *in vitro*, due to motion related to breathing and gastric motility, as well as to large biological variation. Therefore, the first aim of this study was to assess the performance of  $^1\text{H}$  MT MRI for assessing gastric MP coagulation in humans using low and high-pasteurized skim milk (LPSM and HPSM, respectively) as test products. Since the consistency of the coagulum may also affect GE, the secondary objective was to compare GE dynamics (changes in total, semi-solid and liquid gastric content volume) of LPSM and HPSM using  $T_2$ -weighted anatomical MRI images.



## 5.2. Materials and methods

### 5.2.1. Study design

The study was a single-blind randomized crossover trial in which healthy, normal-weight adults underwent gastric MRI scans at baseline and after consumption of two differently heated skim milk products. The primary outcome was the  $^1\text{H}$  *MTR* of the gastric content over time. Secondary outcomes were total gastric content (TGC), semi-solid and liquid volume fractions over time. Other outcomes were subjective ratings of appetite (hunger, fullness, thirst, desire to eat) and well-being (nausea and bloating). The study procedures were approved by a Medical Ethical Committee (METC Oost-Nederland) and were in accordance with the Helsinki declaration of 1975 as revised in 2013. The trial was registered with [clinicaltrials.gov](https://clinicaltrials.gov) under number NCT05854407. All participants provided written informed consent.

### 5.2.2. Participants

The study was conducted between June 2023 and September 2023 with 12 healthy (self-reported) adults ( $n = 6$  males and  $n = 6$  females, age  $24 \pm 4$  years, BMI  $22 \pm 2$  kg/m<sup>2</sup>; Fig. S5.1). The sample size estimation can be found in the Supplementary Information (SI). Participants were recruited in the Ede and Wageningen area, in The Netherlands, via digital advertisements (email and Wageningen University website). The inclusion criteria were: age between 18-45 years; BMI between 18.5 and 25 kg/m<sup>2</sup>; self-reported good general health. The main exclusion criteria were: lactose and milk protein intolerance or allergy; use of medication that may alter the normal functioning of the digestive system; having a gastric disorder or regular gastric complaints ( $\geq 1$  per week) and having a contra-indication for MRI including, but not limited to, pacemakers and defibrillators, ferromagnetic implants, or claustrophobia. Potential participants were informed about the details of the study via an online information meeting, followed by a screening session which involved tasting of the milk products, getting accustomed to undergoing MRI scans in a dummy MRI scanner, practicing drinking milk in a supine position and practicing the breath holds required for the MRI scans. Volunteers that were still interested in participation after this were

asked to sign the informed consent form followed by filling in the screening questionnaire.

### 5.2.3. Milk products

Commercial pasteurized skim milk (typically heated at 72 °C for 15 s) was purchased from the grocery store, and is referred to as LPSM. HPSM was prepared from the LPSM by heating the latter in a water bath for 30 min after reaching a temperature of 80 °C. The WP level in the milk products was measured using SDS-PAGE (data not shown), and were 3% and 90% for LPSM and HPSM, respectively. The milk products were purchased or prepared within one week prior to the test session and stored at 4 °C. The milk was kept at room temperature 30 min before the start of the test session. LPSM from the same brand was used throughout the study.

### 5.2.4. Study procedures

The participants visited Hospital Gelderse Vallei in Ede, the Netherlands, twice in the morning between 7.30 and 9.30 am, in fasted state. There was a minimum of 1 and a maximum of 4 weeks between the two visits. Eating and drinking was allowed until 8:00 pm the night before, and drinking water was allowed up to 1 hour before the start of the test session. A schematic overview of the study session is shown in Fig. 5.1. Upon arrival, participants completed an MRI screening form. After that, a baseline abdominal MRI scan was conducted and the participants provided baseline verbal ratings of their appetite and well-being. Subsequently, participants drank 300 g (291 mL) of either LPSM or HPSM through a tube (similar to drinking from a straw), while lying in a supine position on the scanner bed. The mean ingestion time, with its standard deviation (SD), was  $1.2 \pm 1.1$  min. MRI scans of the abdomen were performed at  $t = 5$  min and subsequently at intervals of 15 mins up until 95 min after the start of ingestion. The participants were asked to verbally rate their appetite and well-being, over a scale between 0 and 100, after the MRI scanning at each digestion time. The participants remained in a supine position for the full duration of the MRI scanning. After this, they exited the scanner and were offered a takeaway breakfast.

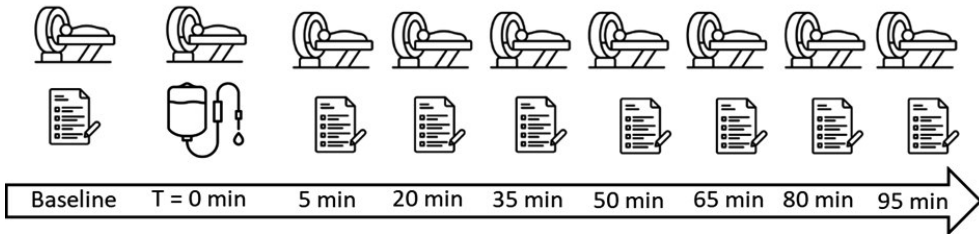


**Figure 5.1.** Schematic overview of a test day consisting of MRI baseline measurements, drinking 300 g (291 mL) of milk in a supine position through a tube (similar to drinking from a straw), followed by MRI measurements after 5 min from milk ingestion, repeated at intervals of 15 min up to 95 min.

### 5.2.5. MRI scans

Participants were scanned using a 3 T MRI scanner with the dStream torso coil (Philips Ingenia Elition X, Philips Medical Systems, the Netherlands). All scans were performed during breath-holds. Participants were asked to hold their breath on expiration to minimize motion. The breath hold duration was at most 21 s. At each timepoint, Saturation Transfer (ST) and  $T_2$ -weighted measurements were conducted. The spatial variation in the radio frequency (RF) field ( $B_1$ ) was determined by measuring a flip angle map, using the dual refocusing echo acquisition mode (DREAM) sequence (Nehrke & Börner, 2012). A map of the relative irradiation amplitude ( $rB_1(x, y)$ ) was obtained by dividing the flip angles by the nominal flip angle. The  $^1\text{H}$  MT MRI measurements were conducted using a saturation RF pulse combined with a Rapid Acquisition with Refocusing Echoes (RARE) sequence. A reference unsaturated MRI image ( $S_0$ ) and a saturated image ( $S_{sat}$ ) were acquired at frequency offsets ( $\Delta$ ) of 450 ppm and 10 ppm, respectively to obtain the  $MTR$ . In addition,  $S_{sat}$  images were acquired at  $\Delta \pm 2.7$  ppm to obtain the  $MTR_{asym}$ , and Water Saturation Shift Referencing (WASSR) spectra were acquired to construct a  $B_0$ -map (data not shown in this chapter). The saturation pulse consisted of a train of pulses with a total duration ( $T_{sat}$ ) of 1 s and a saturation pulse amplitude ( $B_1$ ) of 3  $\mu\text{T}$ . Three sagittal slices with a field-of-view (FOV) of 400 mm x 352 mm, in-plane resolution of 1 mm x 1 mm, slice thickness of 4 mm, inter-slice gap of 2 mm were acquired. SINC pulses were used for excitation and refocusing. The excitation flip angle was  $90^\circ$  and the first refocusing

flip angle was  $180^\circ$  followed  $110^\circ$  pulses. A repetition time ( $TR$ ) of 6.6 s, effective echo time ( $TE_{eff}$ ) of 80 ms, and a RARE factor of 82 were used, resulting in a total measurement time of 79.5 s. To assess TGC, semi-solid and liquid volumes,  $T_2$ -weighted anatomical images were acquired using a RARE sequence with 28 axial slices, FOV of 400 mm x 400 mm, in-plane resolution of 0.625 mm x 0.625 mm, slice thickness of 4 mm and inter-slice gap of 1.4 mm. The excitation and refocusing RF pulse angles were the same as for the ST scans. The adopted MRI acquisition parameters, namely  $TR$  of 755 ms,  $T_{eff}$  of 80 ms, and RARE factor of 65, resulted in a total measurement time of 21 s. Shimming and pulse calibrations were conducted before the MT and  $T_2$ -weighted scans at each measured digestion timepoint. Shimming was performed on the stomach area using pencil beam volume with higher order shims.

### 5.2.6. MRI data processing and analysis

The gastric content was manually delineated in the  $S_0$  and  $S_{sat}$  MT MRI images for each slice and at each timepoint using the Medical Image Processing And Visualization (MIPAV) software 11.0.3. (National Institute of Health, Bethesda, Maryland, USA) and stored as binary masks. All further image processing and calculations were conducted in MATLAB 2019b (MathWorks, Massachusetts, USA). The imaging masks were used to extract the gastric content. Rigid (translation and rotation) and non-rigid (deformation) motion of the stomach were corrected for by using the robust principal component analysis (RPCA) approach (Bie et al., 2019), combined with affine image registration (Fig. S5.2). The image registration was performed after applying the gastric content mask on the images because this provided better spatial alignment of the gastric content between the reference  $S_0$  and  $S_{sat}$  MRI images compared to performing the correction on the whole FOV. In short, RPCA was used to decompose the  $S_0$  and  $S_{sat}$  (including at  $\Delta \pm 2.7$  ppm) images into a low-rank and sparse component of the image to separate the contrast from the motion. The motion-free low-rank component was recomposed into the  $S_0$  and  $S_{sat}$  images, which were averaged over the  $\Delta$  to obtain a motion-free reference image. The reference image was used for re-alignment of the original motion-corrupted images. The re-aligned gastric content images were used to obtain masks of the low- and high-intensity image voxels, attributed to

the semi-solid and liquid components, respectively. This segmentation was achieved via automatic intensity-thresholding using the multi-thresh function (Otsu's method) with two levels in MATLAB similar to the approach used in Chapter 4. Otsu's method finds the optimal threshold value that groups the imaging voxels into separate classes for which the within-class variance is minimised. Threshold analysis was separately performed on the images of each digestion time and scan session. Imaging voxels with intensities below or above the second threshold value, which represented 40-50% of the maximum image intensity, were respectively categorized as low- or high-intensity voxels, and attributed to semi-solid or liquid fractions (Fig. S5.3). The low-intensity voxels were saved as a binary mask and applied to the re-aligned MT images to construct the *MTR* maps of semi-solid gastric content for each slice using Eq. 5.1, from which we can see that the *MTR* ranges between 0 and 1.

The *MTR* values of the semi-solid content were corrected by omitting values that were  $<0$  and  $\geq 1$ , in turn likely caused by gastric content mixing. The corrected data for each slice was used to calculate the mean and SD of the *MTR* over all the low-intensity (semi-solid) voxels for each time point and participant. The *MTR* of only the low-intensity voxels was calculated as the *MTR* of the high-intensity liquid fraction is negligible because of its high proton mobility. The SD of the *MTR* map was calculated as a measure of the spatial variation in *MTR* values across the semi-solid gastric content.

$$MTR = 1 - (S_{sat}/S_0) \quad \text{Eq. 5.1}$$

Gastric content masks of the  $T_2$ -weighted scans in the transverse direction were obtained in the same way as described for the MT scans. These masks were used to calculate the TGC volume by multiplying the total number of voxels by the voxel volume, taking into account the slice thickness and inter-slice gap. GE was defined as the decrease in TGC volume over time. The semi-solid and liquid masks were obtained in the same manner as for the MT data, which were subsequently used to calculate the corresponding volumes.

### 5.2.7. Statistical analysis

Data are reported in the form mean  $\pm$  SD unless stated otherwise. All statistical analysis were performed using RStudio 4.3.1 (PBC, Boston, MA). The threshold for statistical significance was set to  $p = 0.05$ . Normality of the data was checked with quantile-quantile plots of the residuals. A Sidak-adjusted Linear Mixed Model (LMM) was used to test for effects of time, treatment and a treatment-by-time interaction on the *MTR* of the gastric content. Time and treatment (milk products) were added as fixed effects and participants were included as a random effect. Outliers in the MT data were identified and removed using the 3\*IQR (interquartile range) criterion method (Fig. S5.4). A LMM was also used to test the effect of time, treatment and treatment-by-time interaction on the TGC, semi-solid and liquid volumes with the inclusion of baseline GC volumes as a covariate. For the appetite and well-being ratings, baseline ratings were included as a covariate. In the case of a significant treatment effect, Tukey HSD-corrected post-hoc t-tests were used to compare individual time points. As an exploratory analysis, the effect of sex on the outcomes was tested using a LMM with time and sex as fixed factors and participants as a random factor. To test for the effect of sex on TGC, semi-solid and liquid volumes, the baseline GC volume was included as a covariate. The two treatments were grouped per sex. The analysis was conducted with and without the inclusion of body size, approximated as weight times height of the participant, as a covariate. Paired t-tests were used to compare LPSM and HPSM with the following measures: the incremental area under the curve (AUC) of the *MTR*, TGC, semi-solid and liquid volume, as well as the  $MTR_{max}$  and the change in the *MTR* between  $t = 5$  min and  $t = 95$  min ( $\Delta MTR$ ).

## 5.3. Results

### 5.3.1. TGC, semi-solid and liquid volume vs. digestion time

The axial  $^1\text{H}$  MRI  $T_2$ -weighted images were used to quantify the volume of the TGC and semi-solid or liquid fractions over time (Fig. 5.2). At baseline, there was only gastric juice present and, at  $t = 12$  min, the milk was still in the liquid state. As digestion progressed, low-intensity voxels at the center surrounded by high-intensity voxels at the stomach wall were observed, respectively, corresponding to the semi-solid coagulum and gastric fluid, indicated in the insets in red and blue, respectively.

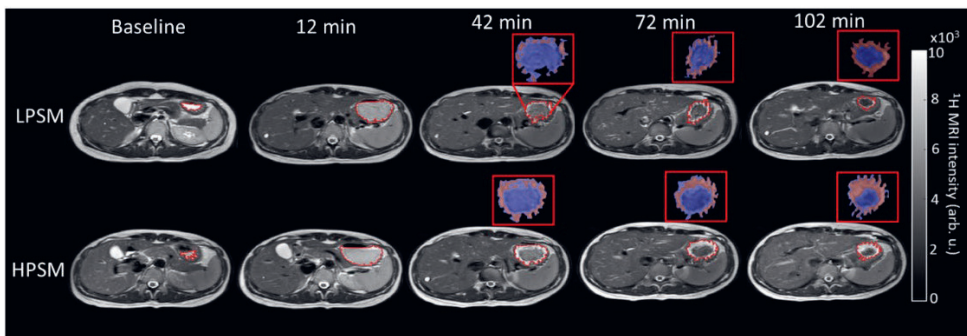


**Figure 5.2.** Example of axial  $^1\text{H}$  MRI  $T_2$ -weighted images at baseline and during digestion, showing the emptying of the stomach and the changes in liquid (red) and semi-solid (blue) fractions as shown in the insets on the top right.

The baseline GC volume was  $31 \pm 18$  mL and  $35 \pm 12$  mL for LPSM and HPSM treatments, respectively ( $p = 0.69$ ). After milk ingestion, the TGC volume increased to  $267 \pm 44$  mL and  $288 \pm 40$  mL for LPSM and HPSM, respectively, followed by a decrease over time (Fig. 5.3a). There was a significant effect of treatment on the TGC volume, with lower volumes for LPSM ( $p = 0.044$ , MD = 40.3 mL 95% CI [25.5 – 55.1]). This effect was significant at most timepoints ( $t = 27$  and  $57 - 102$  min, all  $p < 0.05$ ). There was no treatment-by-time interaction effect ( $p = 0.49$ ). The semi-solid volume (Fig. 5.3b) decreased linearly with time for both LPSM and HPSM. The treatment effect tended to be significant ( $p = 0.057$ ) with lower volumes for LPSM (MD = 31.8 mL 95% CI [19.9–43.8]), and the treatment-by-time interaction effect was not significant ( $p = 0.26$ ). The liquid volume (Fig. 5.3c) for LPSM decreased with a similar trend as the TGC volume,

with lower volumes compared to HPSM from 57 min onwards. The liquid volume for HPSM showed little variation over time. There was no main effect of treatment on the liquid volume ( $p = 0.68$ ), but the treatment-by-time effect tended to be significant with higher liquid volumes for HPSM at  $t \geq 57$  min ( $p = 0.065$ , MD = 65.8 mL 95% CI [43.4 – 88.2]).

The AUC of the TGC (Fig. 5.3d) and liquid volume (Fig. 5.3f) were lower for LPSM compared to HPSM ( $p = 0.021$  and  $p = 0.017$ ). There was a trend towards a lower semi-solid volume for LPSM ( $p = 0.078$ ) (Fig. 5.3e).

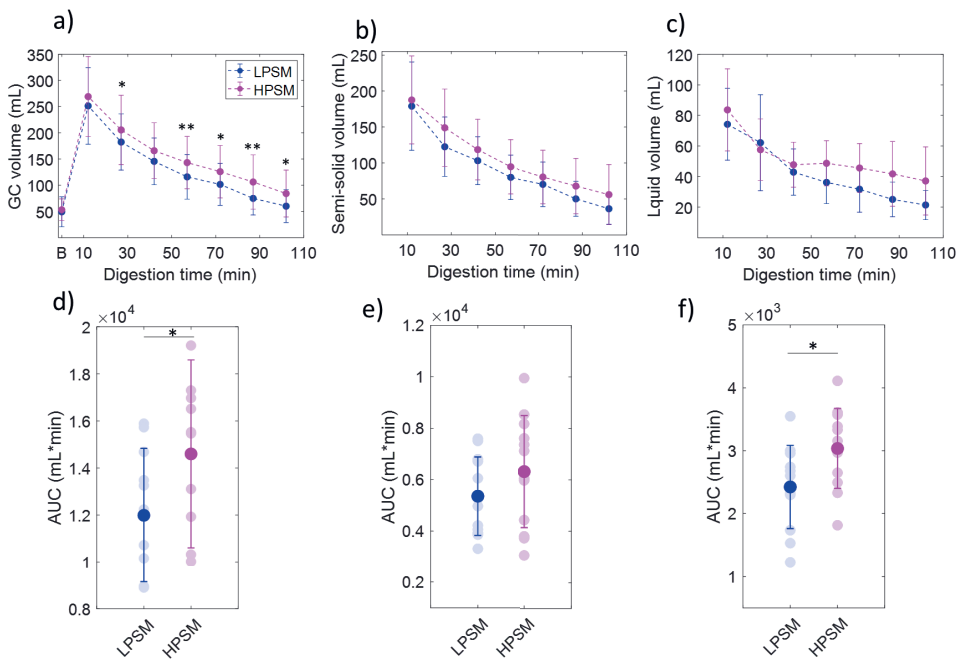


**Figure 5.3.** (a) TGC, (b) semi-solid and (c) liquid volumes vs. digestion time for LPSM and HPSM estimated from the  $T_2$ -weighted MRI images, along with the respective AUC of the (d) TGC, (e) semi-solid and (f) liquid volumes. Symbols \*\* and \* stand for  $p < 0.01$  and  $p < 0.05$ , respectively. Data are plotted as mean  $\pm$  SD over all participants. In d-f individual data for each participant are also shown.



### 5.3.2. $^1\text{H}$ MT MRI during gastric digestion

The sagittal  $T_2$ -weighted images of the abdomen (top), and the corresponding  $MTR$  maps overlaid on the  $T_2$ -weighted images (middle), are shown in Fig. 5.4. At  $t = 5$  min, the gastric content appeared homogeneous in the  $T_2$ -weighted images (Fig. 5.4a) for both LPSM and HPSM. As digestion progressed, the size of the stomach decreased due to GE and the semi-solid coagulum and liquid components could be observed. The  $MTR$  maps (Fig. 5.4b) show an increase in the  $MTR$  values of the gastric content over time for both LPSM and HPSM. The histograms of the  $MTR$  values are characterized by a narrow unimodal distribution at  $t = 5$  min, followed by a broadening of the distribution and a shift to higher  $MTR$  values at longer digestion times.

The mean  $MTR$  increased over time for both LPSM and HPSM ( $p < 0.001$ , Fig. 5.5a). The MD between LPSM and HPSM was 16% (95% CI [10-21]). The  $MTR$  values of HPSM appeared higher than those of LPSM from 35 to 65 min. However, no significant treatment or treatment-by-time interaction effects were found ( $p = 0.15$  and  $p = 0.58$ , respectively). The spatial variation of the  $MTR$  values also increased with time, which may indicate an increase in the heterogeneity of the semi-solid gastric content with digestion (Fig. 5.5b), in agreement with the observations from the histograms in Fig. 5.4. In contrast to the  $MTR$  values, the average  $rB_1$  and its spatial variation over the voxels used for calculating the  $MTR$  maps, decreased with the digestion time from  $100 \pm 15\%$  at  $t = 5$  min to  $87 \pm 9\%$  at  $t = 95$  min (Fig. S5.5 of SI). As demonstrated in Fig. 5.5c-e and Fig. S5.6 of the SI, the inter-individual variation in the  $MTR$  values was large, and there was no significant difference in the  $\Delta MTR$  ( $p = 0.29$ ),  $AUC_{MTR}$  ( $p = 0.48$ ) and  $MTR_{max}$  ( $p = 0.15$ ) between LPSM and HPSM.

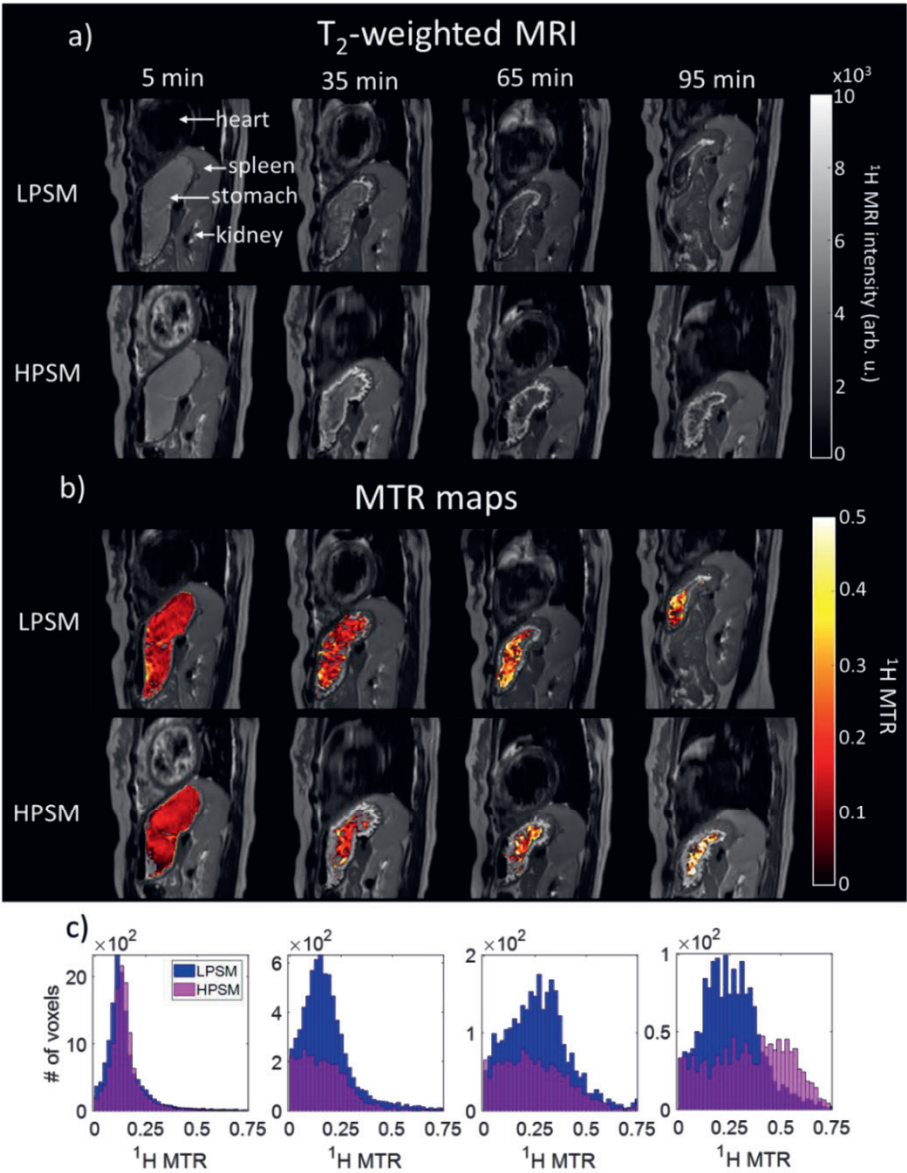


**Figure 5.4.** (a) T<sub>2</sub>-weighted sagittal MRI images of the abdomen at t = 5 min after ingestion of 300 g of LPSM or HPSM and at 30 min intervals until t = 95 min. Corresponding (b) color-coded MTR maps and (c) MTR histograms are also shown. Data are from one randomly selected female participant.

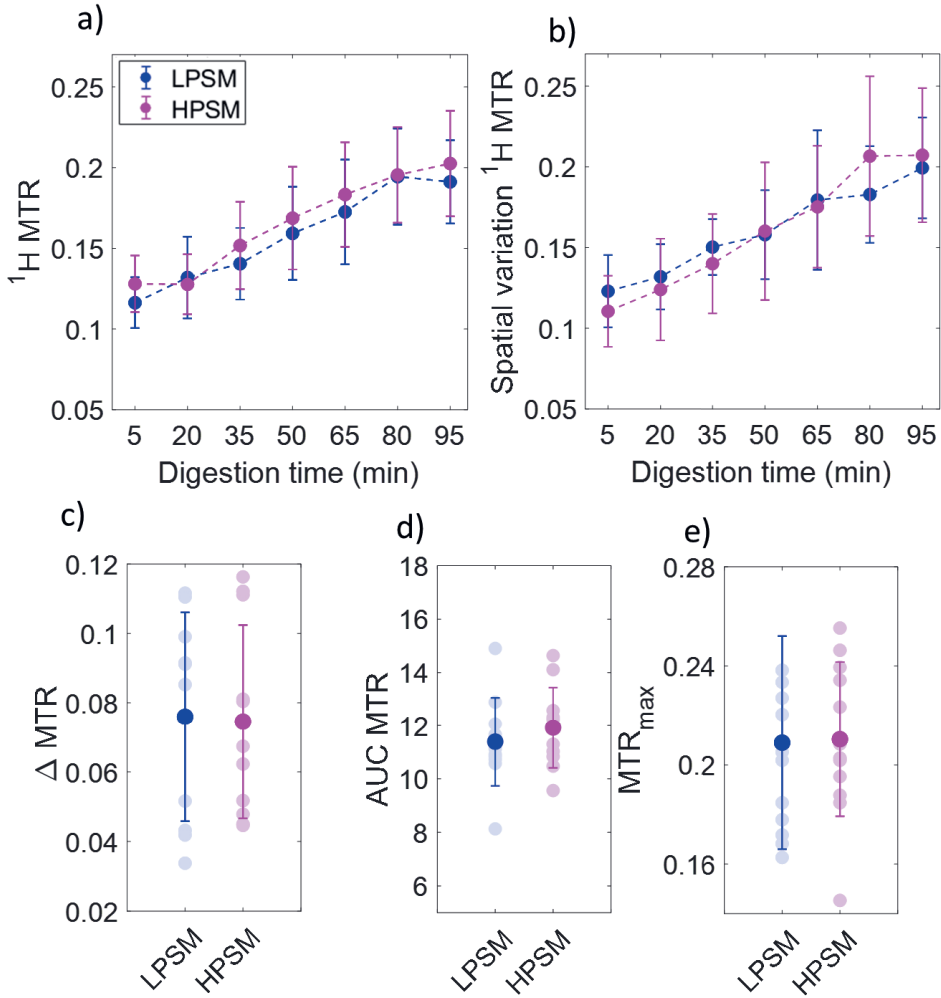


**Figure 5.5.** (a) Mean  $^1\text{H MTR}$  and (b) spatial variation, determined by the SD of the  $^1\text{H MTR}$  values of the semi-solid voxels over time (c) The change in MTR from 5 to 95 min after milk ingestion ( $\Delta\text{MTR}=\text{MTR}(t=95)-\text{MTR}(t=5)$ ), (d) the AUC MTR and (e) the  $\text{MTR}_{\text{max}}$ . The data in a and b are plotted as the mean  $\pm$  SD over all participants. In c-e individual data for each participant are also shown.

### 5.3.3. Exploratory analysis on the effect of sex on the outcomes

Exploratory analysis showed that the *MTR*, TGC volume and liquid volume over time were higher for females compared to males ( $p < 0.001$ ,  $p = 0.025$ ,  $p = 0.026$ , respectively, Fig. S5.7 of the SI). There was no difference in the semi-solid volume between males and females ( $p = 0.12$ ). The male and female participants had an average body size, estimated as weight times the height, of  $(1.4 \pm 1.7) \cdot 10^4$  and  $(1.1 \pm 0.9) \cdot 10^4$  kg\*cm, respectively.

After accounting for the effect of body size, the effect of sex on the *MTR*, TGC volume and liquid volume was no longer significant ( $p = 0.46$ ,  $0.28$ ,  $0.74$ , respectively).

### 5.3.4. Appetite and well-being ratings

The appetite and well-being ratings over time are reported in Fig. S5.8 of the SI. Participants reported a higher level of hunger ( $p < 0.01$ ) and appetite ( $p < 0.001$ ), and a lower level of fullness ( $p < 0.05$ ) for HPSM compared to LPSM. For hunger and appetite, the effect was driven by most time points ( $p < 0.05$ ), whereas for fullness, the effect was driven by time points 42 min and 57 min ( $p = 0.020$  and  $p = 0.048$ , respectively). There was no treatment effect on thirst, bloating or nausea ( $p = 0.31$ ,  $p = 0.29$  and  $p = 0.90$ , respectively). There was a significant treatment-by-time effect with higher ratings of nausea at  $t \geq 57$  min for HPSM compared to LPSM ( $p = 0.04$ ). However, this effect was mainly driven by 2 participants who reported nausea scores of 20 points higher for HPSM compared to LPSM, whereas the other participants reported nausea scores of around 0 throughout the digestion and for both milk products. Therefore, no conclusions can be drawn from this.

## 5.4. Discussion

The objective of this study was to assess the feasibility of using  $^1\text{H}$  MT MRI for monitoring gastric milk protein coagulation *in vivo* in humans using LPSM and HPSM as test-products. The TGC, semi-solid and liquid volumes were compared between the two products to investigate the effect of heat treatment on the GE dynamics. To the best of our knowledge, this is the first study in humans that investigated the effect of heat treatment on gastric coagulation of milk. Moreover, the same heat treatments and MRI data acquisition and analysis were used as in our *in vitro* study from Chapter 4, enabling a direct comparison between the *in vitro* digestion model and digestion in humans.

### 5.4.1. GE dynamics

We found that the TGC volume remained higher for a longer duration for HPSM compared to LPSM. This suggests a slower GE with more extensive heat treatment. Additionally, the semi-solid and liquid volumes vs. digestion time appeared to be higher for HPSM compared to LPSM, although these differences were not statistically significant.

These findings contradict our initial expectation, as previous *in vitro* (Li et al., 2022; Mulet-Cabero et al., 2019) and *in vivo* animal (Ahlborn et al., 2023; Ye et al., 2019) studies have demonstrated that heat treatment typically results in a coagulum with a looser and softer consistency during gastric digestion, which has been suggested to potentially lead to a faster GE. Ahlborn et al. (2023) showed that, for a 500 mL load of milk, the TGC, coagulum, total protein and coagulated protein emptied faster for UHT compared to pasteurized milk during gastric digestion in pigs. These differences were attributed to the weaker and more open coagulum structure observed in UHT milk. In contrast, Ye et al. (2019) reported that the wet and dry weight of the coagulum were higher for UHT compared to pasteurized milk in rats at 30 and 120 min after milk ingestion, but slightly lower at 240 min. This suggests that the volume and moisture content of the coagulum from UHT milk is higher in the first 120 min of digestion, aligning with the higher

appearing semi-solid and liquid volume found for HPSM in the present study. The higher liquid volume for HPSM may indicate a higher moisture content which, in turn, could be attributed to a coagulum microstructure with more abundant and larger voids (Ye et al., 2016). Barbé et al., (2013) found that the mean retention time of chromium in the stomach in pigs was longer for heated (10 min at 90 °C) compared to unheated rehydrated ultra-low heat skim milk powder, which may suggest a slower emptying of milk upon heat treatment. Overall, *in vitro* and *in vivo* studies in animals have shown that high temperature or prolonged heat treatment result in a looser and softer milk protein coagulum during gastric digestion. However, currently there is no consistent picture on the effect of heat treatment on the GE of the total or semi-solid gastric content.

*In vivo* studies in humans (Horstman et al., 2021; Lacroix et al., 2008) did not report a difference in AA concentrations in blood following the consumption of UHT or pasteurized milk, but Lacroix et al. (2008) did report an enhanced transfer of dietary nitrogen into serum AA, urea, and protein pools for UHT compared to pasteurized milk. They proposed that a softer coagulum and more rapid GE could explain the observed difference. However, as shown in the present study, more extensive heat treatment resulted in higher TGC over time, indicating that the effect of heat treatment may be different in humans compared to in animals or *in vitro* models.

#### 5.4.2. Interpretation of MT MRI data

Following ingestion, the *MTR* was initially low but, as digestion progressed, a notable increase in the *MTR* was observed for both LPSM and HPSM. Right after ingestion, the milk is in a liquid state and, consequently, the macromolecular mobility is still high, resulting in a low *MTR* (Henkelman et al., 2001; van Zijl et al., 2018). As digestion proceeds, a transition from a liquid to semi-solid state occurs, primarily driven by the aggregation of caseins induced by pepsin and stomach acid (Huppertz & Chia, 2021). This transition to a semi-solid state causes a decrease in the macromolecular mobility, leading to stronger inter- and intra-molecular dipolar interactions, which are the drivers of the  $^1\text{H}$  MT effect in MRI

(Henkelman et al., 2001; van Zijl et al., 2018; Zhou et al., 2023). In Chapter 4, a similar increase in the *MTR* was observed for LPSM during semi-dynamic *in vitro* gastric digestion. The *in vitro MTR* data was compared with visual and rheological assessment of the coagula, which confirmed that the increase in *MTR* corresponded to an increase in the storage modulus and, hence, stiffness of the coagulum. The agreement between the *in vitro* and *in vivo* data for LPSM, alongside the significant *MTR* variation vs. digestion time, confirm the suitability of MT MRI for monitoring gastric milk protein coagulation *in vivo*. However, we did not observe an effect of heat treatment on the *MTR* over time. Interestingly, this is in contrast with our *in vitro* findings from Chapter 4, where based on visual assessment, the coagulum of HPSM appeared more loose compared to that of LPSM. This difference was also reflected in the *MTR*, which was lower for HPSM compared to LPSM beyond 50 min of gastric digestion.

The *MTR* and GE data altogether may suggest that the effect of heat treatment on gastric coagulation is different in humans compared to what has been observed in *in vitro models* and *in vivo* animal models. Gastric coagulation of milk is highly affected by pH and pepsin activity, which can vary both between and within individuals (Fadda et al., 2022). Furthermore, gastric fluid volume in the fasted state also varies between and within individuals (Grimm et al., 2018), and has previously been shown to affect the formation of a fat layer during gastric milk digestion (Camps et al., 2021). Accordingly, the gastric fluid volume may also affect gastric milk coagulation. Variations in gastric fluid volume and secretion can lead to large variations in the *MTR* values during digestion, making it more challenging to detect subtle differences in coagulation resulting from heat-induced changes to protein structure. Consequently, additional research using a larger sample size may be necessary to provide more insights into this complex process. Furthermore, conducting *in vitro* experiments under varying gastric conditions (pH and pepsin activity) and for different milk heat treatments may be necessary to investigate more thoroughly the sensitivity of the *MTR* parameter to heat-induced alterations in gastric coagulation of MPs.

A recent study assessed gastric milk coagulation in women experiencing gastro-intestinal (GI) complaints and in a control group after milk consumption by calculating image texture measures, namely homogeneity, contrast, busyness,

and coarseness, for the  $T_2$ -weighted anatomical images (van Eijnatten et al., 2023). The decrease in homogeneity, and increase in contrast and coarseness, were associated with the coagulation process. While such image texture measures show promise for monitoring gastric MP coagulation, they need to be verified with MRI data of *in vitro* digestion samples, in analogy to what we have done so far for the *MTR*.

### 5.4.3. Challenges in acquisition and quantification

Conducting MT measurements *in vivo* in humans is challenging due to breathing motion and gastric motility. To construct the *MTR* maps, the  $S_0$  and  $S_{sat}$  images were acquired separately in different breath holds. Although breath holding minimizes breathing-related motion artifacts within an image, it does not account for differences between the  $S_0$  and  $S_{sat}$  images. Differences in both the position and shape of the stomach were observed, with the latter being caused by gastric contractions. These differences were corrected for using rigid and non-rigid image registration. However, in certain cases, gastric contractions and mixing resulted in differences in the content of individual voxels between the  $S_0$  and  $S_{sat}$  images. For example, some voxels contained low-intensity components in the  $S_0$  image, arising from semi-solid fractions, but high-intensity (liquid) components in the  $S_{sat}$  image, leading to negative *MTR* values. These values were excluded from the *MTR* maps and from the corresponding calculation of the mean *MTR* over the semi-solid voxels. In future applications it is preferable to work on reducing the acquisition time of the scans to enable acquisition of both the  $S_0$  and  $S_{sat}$  images in one breath hold. This could help minimize the sensitivity to mixing effects, and to improve the accuracy of the *MTR* measurements.

In this work, the  $^1\text{H}$  MT MRI scans were acquired using a RARE sequence with a  $90^\circ$  RF excitation flip angle and  $T_2$ -weighting, with an acquisition time of around 19 s per image. In humans the stomach typically contracts about three times per minute (Lu et al., 2022), which suggests that the  $S_0$  and  $S_{sat}$  scans may have been acquired during two different contractions. The acquisition can be accelerated by replacing the RARE sequence with a faster image acquisition sequence, such as a



Gradient Recalled Echo (GRE) sequence. However, faster image acquisition schemes often come at the cost of lower signal-to-noise ratios (SNR) and poorer contrast. This could make it challenging to accurately delineate the gastric content and to separate liquid and semi-solid components using intensity thresholding. Therefore, further optimization of the scan parameters is required to achieve faster measurements, while maintaining a high SNR and good contrast. Faster measurements are also beneficial for covering a whole stomach volume. In this study, with a scan time of 19 s, only three sagittal slices could be acquired with a thickness and interslice gap of 4 and 2 mm, respectively, covering 16 mm in the left-to-right direction. This might not be representative of the whole gastric content, and is a potential limitation of the study.

As demonstrated in Fig. 5.4 and 5.5, both the  $MTR$  and the spatial variation in the  $MTR$  values increased vs. digestion. This trend might be attributed to an increase in the degree of coagulation, and heterogeneity of the coagulum, though  $B_1$ -inhomogeneity could also play a role. While, the acquired  $rB_1$ -map could not be used to correct the  $MTR$  values, due to gastric mixing effects between the MT and  $B_1$ -map acquisitions, they could be used to assess changes in the  $B_1$  strength and variation over time. The  $rB_1$  and its spatial variation decreased vs. digestion. Specifically, in the voxels used to calculate the  $MTR$ , this decrease was from  $100 \pm 15\%$  at  $t = 5$  min to  $87 \pm 9\%$  at  $t = 95$  min. Given that a decrease in the  $B_1$  amplitude of the saturation pulse is expected to result in a decrease in the  $MTR$ , it appears unlikely that the observed increase in the  $MTR$  and its spatial variation vs. digestion were caused by changes in the  $B_1$  over time. However, further research is necessary to explore the effect of  $B_1$ -inhomogeneity, and different correction methods for MT MRI of gastric digestion.

In this study, the intensity thresholding method that we previously applied to *in vitro*  $T_2$ -weighted MRI images (Chapter 3 and 4) was used to identify low- and high-intensity voxels in *in vivo* images. The low- and high-intensity voxels were attributed to more semi-solid and liquid gastric content, respectively and were used to quantify their respective volumes over time. It is worth noting that with this approach a threshold value is determined even within 12 min after milk ingestion when milk is still in a liquid state. This stems from the lack of direct mixing between ingested milk and the baseline gastric content, primarily

composed of gastric juice. This leads to the formation of a thin layer of baseline gastric content on top of the milk. The baseline gastric content likely comprises gastric juice, based on its higher intensity compared to the ingested milk in the  $T_2$ -weighted MRI images. The intensity thresholding will then separate the liquid milk from this high-intensity layer. Therefore, in this study, the obtained semi-solid and liquid volumes from the second timepoint onwards, where coagulation became clearly visible, were considered.

A potential limitation of MRI is that it usually requires participants to be in a supine position, which affects the position of the stomach due to gravity. This could lead to a difference in fluid dispersion throughout the stomach, thereby affecting gastric coagulation and emptying (Holwerda et al., 2016). However, relative differences are expected to remain the same (Camps et al., 2018).

#### 5.4.4. Inter-individual variation

This study included both male and female participants for better generalizability. The *MTR*, *TGC*, and liquid volumes were higher in females compared to males. However, after accounting for body size, no significant differences remained. This indicates that these differences are related to body size and may not be inherently sex-specific. Previous studies have demonstrated slower GE in females compared to males (Camps, de Graaf, et al., 2018; Gill et al., 1987; Hermansson & Sivertsson, 1996). However, none of these studies included body size as a factor in their statistical analysis. Camps et al. (2018) did find a weak correlation ( $r=0.266$ ,  $p < 0.05$ ) between body size and *TGC* volume, but they concluded that this was not strong enough to explain the effect of sex on the *TGC* volume. Previous research has reported differences in pepsin activity and gastric pH between males and females (Lindahl et al., 1997), which could also influence gastric coagulation and emptying. Therefore, more research is warranted to better understand the effect of different factors, including body size and hormones, on gastric digestion.

## 5.5. Conclusions

We have demonstrated the potential of  $^1\text{H}$  MT MRI as a novel non-invasive method for monitoring gastric MP coagulation in humans. The *MTR*, which is a marker of coagulum consistency, can be obtained from two rapid scans of less than 20 s each. By combining conventional  $T_2$ -weighted anatomical images with MT measurements, the GE of total, semi-solid and liquid gastric content, as well as changes in the coagulum consistency, could be assessed *in vivo*.

The *MTR* of LPSM increased during gastric digestion, which reflected milk protein coagulation and was in agreement with previous data from a semi-dynamic *in vitro* model. Interestingly, contrary to the *in vitro* data, no difference was found in the *MTR* between LPSM and HPSM *in vivo*. Moreover, gastric content volumes over time were higher for HPSM compared to LPSM, indicating a slower GE upon heat treatment. These findings demonstrate that the effect of heat treatment on gastric milk protein digestion may be different in humans compared to what has been observed in *in vitro* and animal models. This highlights the importance of conducting *in vivo* studies in humans when investigating effects of heat treatment on gastric milk digestion. Our innovative approach holds promise for investigating the effect of various heat treatments or the presence of lipids on gastric milk protein coagulation and emptying dynamics. Moreover, it opens the way for exploring gastric digestion of a variety of (semi-)solid foods, including yoghurt, cheeses and protein-rich foods with different micro- and macrostructures. Insights from such studies can not only improve our understanding of how food processing, composition, and structure affect gastric digestion, but may also contribute to the improvement of *in vitro* digestion models.

## Authorship contribution statement

Morwarid Mayar: Conceptualization, Methodology, Formal analysis, Investigation, Data curation, Visualization, Validation, Writing – original draft; Camilla Terenzi; John van Duynhoven and Paul Smeets: Conceptualization, Methodology, Validation, Writing – review & editing, Supervision.

## Acknowledgement

Rosalind Vivia Tansy is gratefully acknowledged for her help with the data collection and analysis. The use of the 3 T MRI facility has been made possible by Wageningen University & Research Shared Research Facilities. Paul de Bruin is thanked for his expert support with setting up the measurements on the 3 T clinical MRI scanner.

## References

- Ahlborn, N. G., Montoya, C. A., Hodgkinson, S. M., Dave, A., Ye, A., Samuelsson, L. M., Roy, N. C., & McNabb, W. C. (2023). Heat treatment and homogenization of bovine milk loosened gastric curd structure and increased gastric emptying in growing pigs. *Food Hydrocolloids*, *137*, 108380. <https://doi.org/10.1016/j.foodhyd.2022.108380>
- Barbé, F., Ménard, O., Le Gouar, Y., Buffière, C., Famelart, M.-H., Laroche, B., Le Feunteun, S., Dupont, D., & Rémond, D. (2013). The heat treatment and the gelation are strong determinants of the kinetics of milk proteins digestion and of the peripheral availability of amino acids. *Food Chemistry*, *136*(3–4), 1203–1212. <https://doi.org/10.1016/j.foodchem.2012.09.022>
- Bie, C., Liang, Y., Zhang, L., Zhao, Y., Chen, Y., Zhang, X., He, X., & Song, X. (2019). Motion correction of chemical exchange saturation transfer MRI series using robust principal component analysis (RPCA) and PCA. *Quantitative Imaging in Medicine and Surgery*, *9*(10), 1697–1713. <https://doi.org/10.21037/qims.2019.09.14>
- Bornhorst, G. M., & Paul Singh, R. (2014). Gastric Digestion In Vivo and In Vitro: How the Structural Aspects of Food Influence the Digestion Process. *Annual Review of Food Science and Technology*, *5*(1), 111–132. <https://doi.org/10.1146/annurev-food-030713-092346>
- Camps, G., Mars, M., Witteman, B. J. M., de Graaf, C., & Smeets, P. A. M. (2018). Indirect vs direct assessment of gastric emptying: A randomized crossover trial comparing C-isotope breath analysis and <sup>13</sup>C-MRI. *Neurogastroenterology & Motility*, *30*(7). <https://doi.org/10.1111/nmo.13317>
- Camps, G., van Eijnatten, E. J., van Lieshout, G. A., Lambers, T. T., & Smeets, P. A. (2021). Gastric Emptying and Intra-gastric Behavior of Breast Milk and Infant Formula in Lactating Mothers. *The Journal of Nutrition*, *151*(12), 3718–3724. <https://doi.org/10.1093/jn/nxab295>

- Fadda, H. M., Hellström, P. M., & Webb, D.-L. (2022). Intra- and inter-subject variability in gastric pH following a low-fat, low-calorie meal. *International Journal of Pharmaceutics*, 625, 122069. <https://doi.org/10.1016/j.ijpharm.2022.122069>
- Grimm, M., Koziolok, M., Kühn, J.-P., & Weitschies, W. (2018). Interindividual and intraindividual variability of fasted state gastric fluid volume and gastric emptying of water. *European Journal of Pharmaceutics and Biopharmaceutics*, 127, 309–317. <https://doi.org/10.1016/j.ejpb.2018.03.002>
- Henkelman, R. M., Stanisz, G. J., & Graham, S. J. (2001). Magnetization transfer in MRI: A review. *NMR in Biomedicine*, 14(2), 57–64. <https://doi.org/10.1002/nbm.683>
- Holwerda, A., Lenaerts, K., Bierau, J., & van Loon, L. (2016). Body Position Modulates Gastric Emptying and Affects the Post-Prandial Rise in Plasma Amino Acid Concentrations Following Protein Ingestion in Humans. *Nutrients*, 8(4), 221. <https://doi.org/10.3390/nu8040221>
- Horstman, A. M. H., Ganzevles, R. A., Kudla, U., Kardinaal, A. F. M., van den Borne, J. J. G. C., & Huppertz, T. (2021). Postprandial blood amino acid concentrations in older adults after consumption of dairy products: The role of the dairy matrix. *International Dairy Journal*, 113, 104890. <https://doi.org/10.1016/j.idairyj.2020.104890>
- Lacroix, M., Bon, C., Bos, C., Léonil, J., Benamouzig, R., Luengo, C., Fauquant, J., Tomé, D., & Gaudichon, C. (2008). Ultra High Temperature Treatment, but Not Pasteurization, Affects the Postprandial Kinetics of Milk Proteins in Humans. *The Journal of Nutrition*, 138(12), 2342–2347. <https://doi.org/10.3945/jn.108.096990>
- Li, S., Pan, Z., Ye, A., Cui, J., Dave, A., & Singh, H. (2022). Structural and rheological properties of the clots formed by ruminant milks during dynamic in vitro gastric digestion: Effects of processing and species. *Food Hydrocolloids*, 126, 107465. <https://doi.org/10.1016/j.foodhyd.2021.107465>
- Lindahl, A., Ungell, A., Knutson, L., & Lennernäs, H. (1997). Characterization of fluids from the stomach and proximal jejunum in men and women. *Pharmaceutical Research*, 14(4), 497–502. <https://doi.org/10.1023/A:1012107801889>
- Lu, K., Liu, Z., Jaffey, D., Wo, J. M., Mosier, K. M., Cao, J., Wang, X., & Powley, T. L. (2022). Automatic assessment of human gastric motility and emptying from dynamic 3D magnetic resonance imaging. *Neurogastroenterology & Motility*, 34(1). <https://doi.org/10.1111/nmo.14239>
- Mayar, M., Miltenburg, J. L., Hettinga, K., Smeets, P. A. M., van Duynhoven, J. P. M., & Terenzi, C. (2022). Non-invasive monitoring of in vitro gastric milk protein digestion kinetics by <sup>1</sup>H NMR magnetization transfer. *Food Chemistry*, 383(February), 132545. <https://doi.org/10.1016/j.foodchem.2022.132545>
- Mayar, M., Smeets, P., Duynhoven, J., & Terenzi, C. (2023). In vitro <sup>1</sup>H MT and CEST MRI mapping of gastro-intestinal milk protein breakdown. *Food Structure*, 36, 100314–100324.
- Mulet-Cabero, A. I., Mackie, A. R., Wilde, P. J., Felon, M. A., & Brodkorb, A. (2019). Structural mechanism and kinetics of in vitro gastric digestion are affected by process-induced changes in bovine milk. *Food Hydrocolloids*, 86, 172–183. <https://doi.org/10.1016/j.foodhyd.2018.03.035>
- Nehrke, K., & Börnert, P. (2012). DREAM—a novel approach for robust, ultrafast, multislice *B*<sub>1</sub> mapping. *Magnetic Resonance in Medicine*, 68(5), 1517–1526. <https://doi.org/10.1002/mrm.24158>
- van Eijnatten, E. J. M., Camps, G., Guerville, M., Fogliano, V., Hettinga, K., & Smeets, P. A. M. (2023). Milk coagulation and gastric emptying in women experiencing gastrointestinal symptoms after ingestion of cow's milk. *Neurogastroenterology & Motility*. <https://doi.org/10.1111/nmo.14696>

- van Zijl, P. C. M., Lam, W. W., Xu, J., Knutsson, L., & Stanisz, G. J. (2018). Magnetization Transfer Contrast and Chemical Exchange Saturation Transfer MRI. Features and analysis of the field-dependent saturation spectrum. *NeuroImage*, *168*, 222–241. <https://doi.org/10.1016/j.neuroimage.2017.04.045>
- Ye, A., Cui, J., Dalgleish, D., & Singh, H. (2016). The formation and breakdown of structured clots from whole milk during gastric digestion. *Food & Function*, *7*(10), 4259–4266. <https://doi.org/10.1039/C6FO00228E>
- Ye, A., Roy, D., & Singh, H. (2019). Structural changes to milk protein products during gastrointestinal digestion. In *Milk Proteins: From Expression to Food* (3rd ed.). Elsevier Inc. <https://doi.org/10.1016/B978-0-12-815251-5.00019-0>
- Zhou, Y., Bie, C., van Zijl, P. C. M., & Yadav, N. N. (2023). The relayed nuclear Overhauser effect in magnetization transfer and chemical exchange saturation transfer MRI. *NMR in Biomedicine*, *36*(6). <https://doi.org/10.1002/nbm.4778>

## 5.6. Supplementary Information

### 5.6.1. Flow diagram of the study

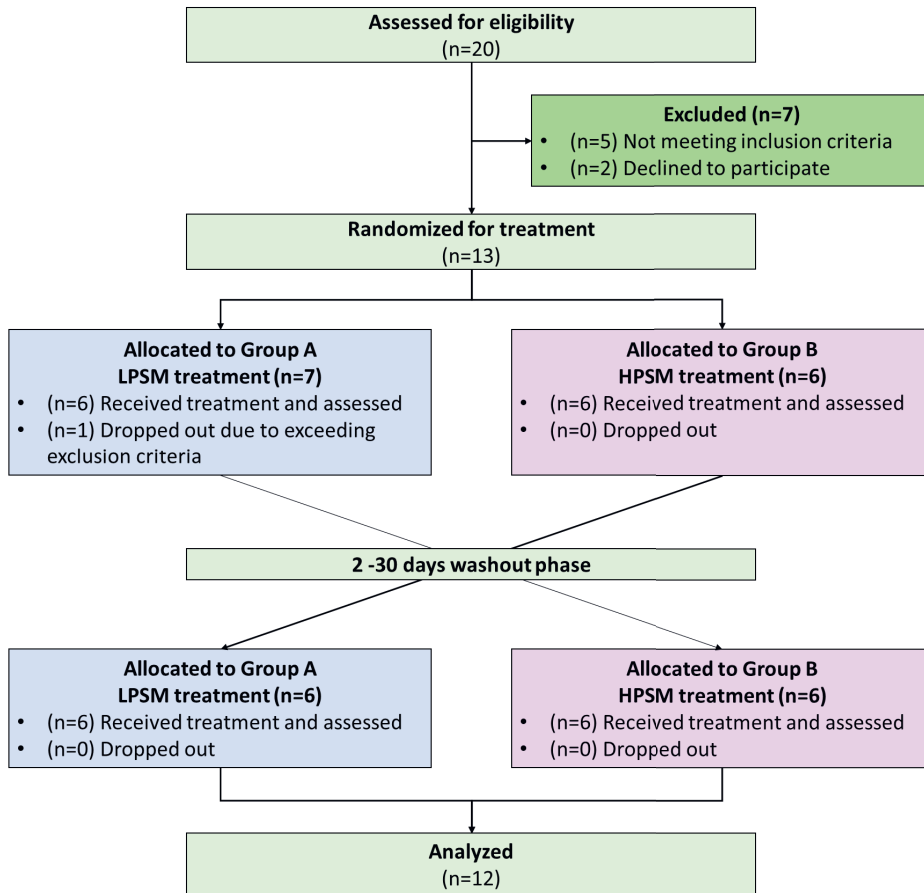


**Figure S5.1.** Flow diagram for inclusion, treatment allocation and analysis.

### 5.6.2. Sample size estimation

This is the first study in which MT MRI will be applied to study *in vivo* gastric protein digestion, and hence, the expected differences and population variance are unknown. Therefore, we use our *in vitro* findings of the evolution in semi-solid MTR during semi-dynamic *in vitro* digestion to estimate the expected difference and variance. The standard deviation (SD) *in vitro* was 0.0032 and, assuming that the SD *in vivo* will be at least 30 times higher due to physiological noise and movement-related distortions, we estimate a SD of 0.096. A repeated measures ANOVA will be used to determine if there is significant effect of time and treatment on the MTR. With a power of 90%, and a significance level of 0.05, a total of at least 9 or 12 complete datasets is required for the time and treatment effect, respectively (calculated using: <https://glimmpse.samplesizeshop.org/>). Therefore, a total of 12 participants will be recruited to be able to evaluate both the time and treatment effect. Participants will be replaced in case of dropouts up until a maximum of 14 participants.



5.6.3. Image registration and intensity thresholding

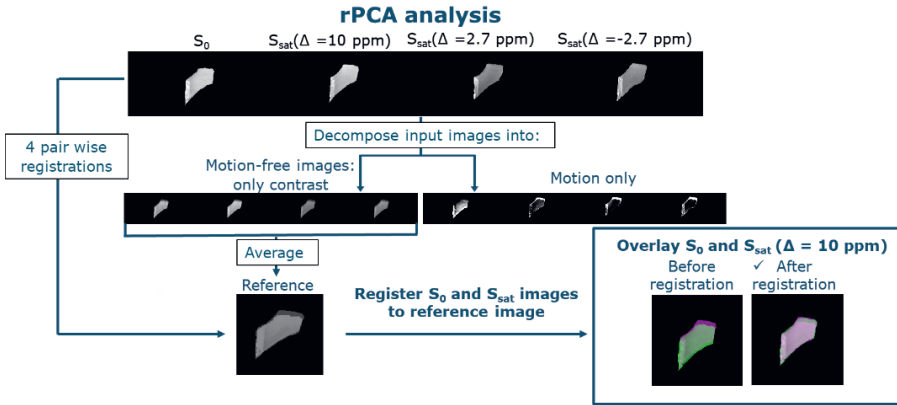


**Figure S5.2.** Schematic overview of the image registration process of the masked gastric content images, consisting of decomposing the MT images into a low-rank and sparse component, containing the motion-free contrast and motion information, respectively. The average of the low-rank images is used as a reference image for alignment of the original motion-corrupted images, resulting in well-aligned  $S_0$  and  $S_{sat}$  images.

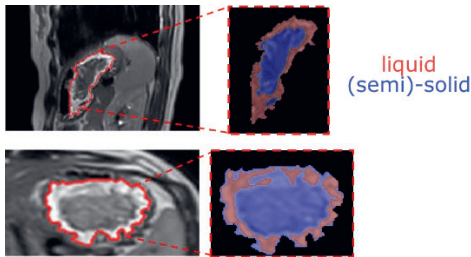


**Figure S5.3.** Liquid and semi-solid masks obtained by intensity thresholding of the sagittal (top) and axial (bottom)  $T_2$ -weighted MRI images.

5.6.4. MTR data

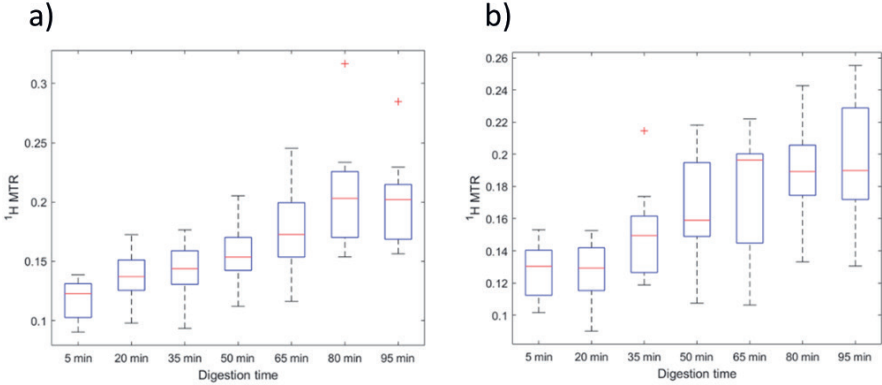


**Figure S5.4.** Boxplots of the MTR over time for (a) LPSM and (b) HPSM. Outliers are marked with a red symbol (+).

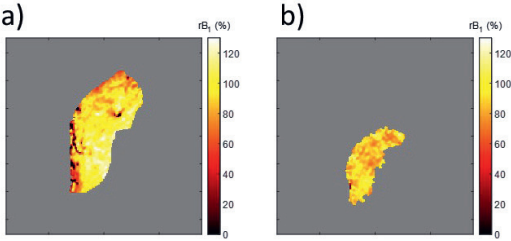


**Figure S5.5.**  $rB_1$  maps of the gastric content at (a)  $t = 5$  min and (b)  $t = 95$  min after the ingestion of 300 g HPSM are depicted for the same participant as shown in Fig. 5.4 in the main text. These maps illustrate a decrease in  $rB_1$  in the gastric content from  $t = 5$  to 95 min. Specifically, for the voxels used to calculate the MTR, this decrease was from  $100 \pm 15\%$  at  $t = 5$  min to  $87 \pm 9\%$  at  $t = 95$  min.

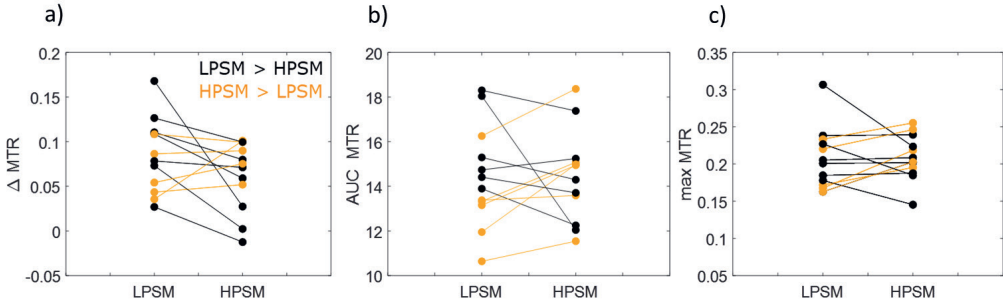


**Figure S5.6.** (a)  $\Delta$ MTR between T5-95 min, (b) AUC MTR and (c) max MTR per participant for LPSM and HPSM.

5.6.5. Effect of sex on digestion outcomes

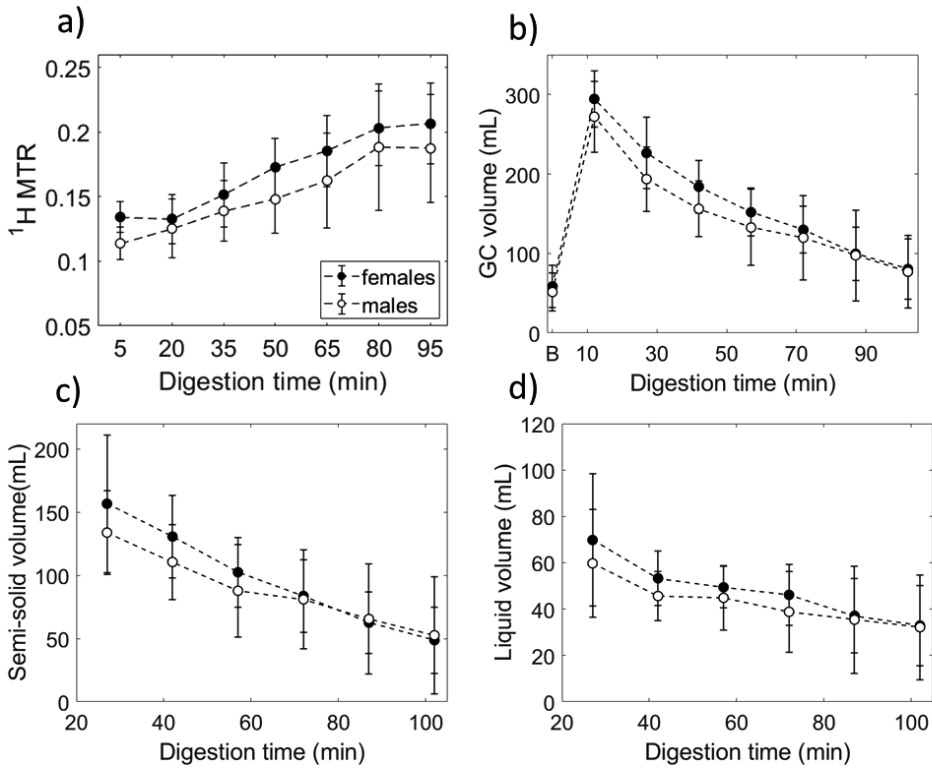


**Figure S5.7.** (a) MTR, (b) GC volume, (c) semi-solid volume and (d) liquid volume for female and male participants. The data of LPSM and HPSM were grouped per sex. Data are shown as mean  $\pm$  SD.

### 5.6.6. Appetite and well-being ratings

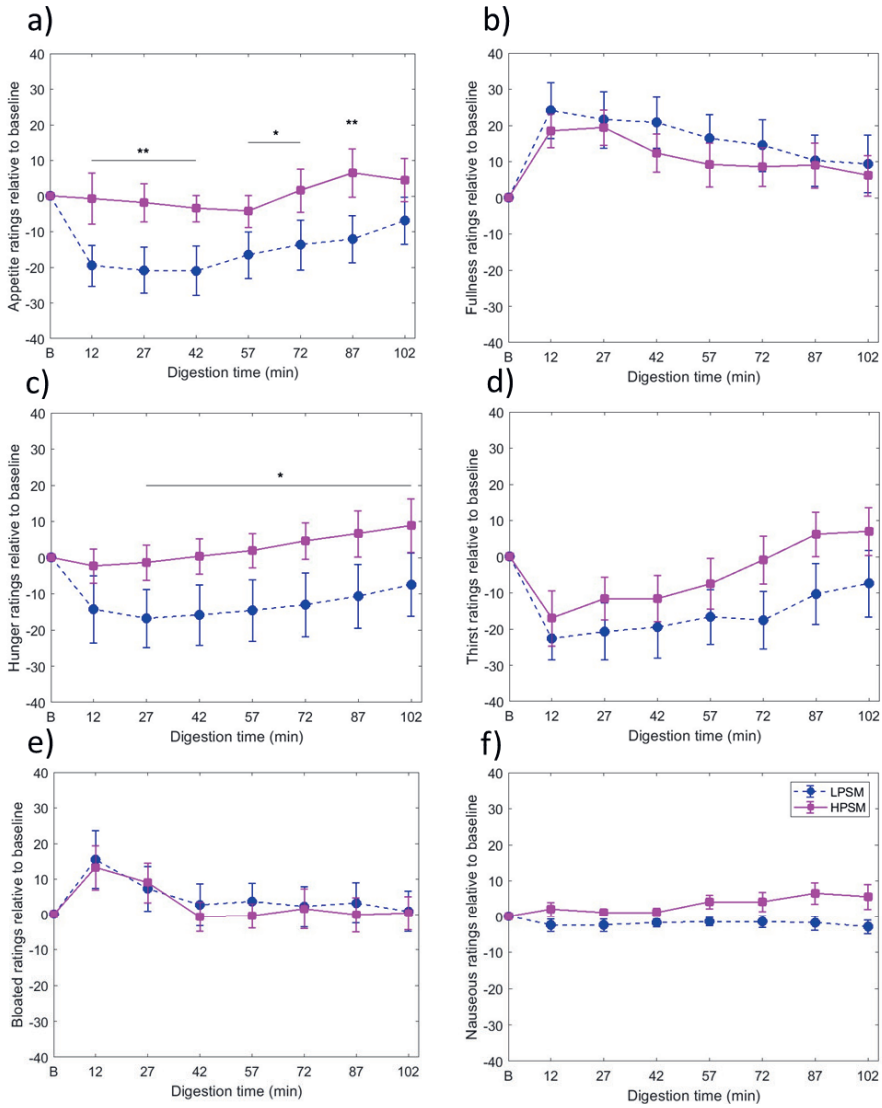


**Figure S5.8.** Changes relative to baseline in ratings (0-100 points) of the subjective feeling of hunger, fullness, appetite, thirst, bloating, and nausea over time. All values are presented as mean  $\pm$  SEM ( $n = 12$ ). \* $p < 0.05$  and \*\* $p < 0.01$ .



# CHAPTER

# 6

# General discussion





## 6.1. Main findings

The aim of this thesis work was to bridge the gap between *in vitro* digestion models and *in vivo* digestion in humans by developing  $^1\text{H}$  MRI markers for the assessment of intra-gastric milk protein digestion. To this aim  $^1\text{H}$  saturation transfer techniques, Magnetization Transfer (MT) and Chemical Exchange Saturation Transfer (CEST) were explored to probe the digestion of milk proteins.

In **Chapter 2**, MT NMR was implemented on a 7 T vertical bore NMR spectrometer for monitoring gastric milk protein digestion of raw and heated skim milk in static *in vitro* digestion samples. The composite exchange rate parameter,  $\frac{R_{ex}M_0^B}{R_1^A}$ , obtained from multiparameter fitting of MT spectra, and the semi-quantitative *MTR* parameter rapidly acquired at one saturation offset frequency ( $\Delta$ ), were shown to be potential markers of gastric milk protein coagulation, and of its subsequent solubilization. These markers also showed high sensitivity for the effect of heat treatment on the gastric coagulation of milk proteins. Given that the acquisition of the *MTR* is 46-fold faster than the  $\frac{R_{ex}M_0^B}{R_1^A}$ , and does not require data fitting, it was proven more feasible for *in vivo* studies. Consequently, it was further explored in the following chapters.

To build on this, in **Chapter 3**, spatially-resolved  $T_2$ -weighted MT and CEST measurements were implemented on the 7 T vertical bore NMR spectrometer to monitor changes in both the semi-solid and soluble protein fractions of static *in vitro* digestion samples. Specifically, the  $MTR_{asym}$  was established as a marker of protein hydrolysis and changes in protein/peptide concentration in the liquid phase of the digestion samples. Additionally, intensity thresholding of  $T_2$ -weighted images was used to estimate the semi-solid (coagulum) volume, and to construct *MTR* and  $MTR_{asym}$  maps of the semi-solid and liquid phases, respectively. By integrating MT and CEST MRI with  $T_2$ -weighted imaging, both macroscopic and molecular-level changes occurring during static *in vitro* gastric digestion could be monitored.

To move towards the dynamic complexity of *in vivo* gastric digestion, in **Chapter 4** the previously developed markers, namely  $MTR$ ,  $MTR_{asym}$  and the semi-solid (coagulum) volume were further explored for monitoring gastric digestion in a semi-dynamic *in vitro* model using low- and high-pasteurized skim milk (LPSM and HPSM, respectively) as test products. The supernatant of the digesta was measured with MT and CEST on the 7 T vertical bore NMR spectrometer. Moreover, *in situ* monitoring of the digestion was conducted using a 3 T clinical MRI scanner. Variations in pH and protein concentration were the dominant factors affecting the  $MTR_{asym}$  under semi-dynamic gastric conditions. Given the critical role of pH in gastric digestion, CEST MRI was used as an indirect method for pH mapping. Additionally,  $T_2$ -weighted images combined with  $MTR$  maps obtained *in situ* during digestion, proved to be valuable for assessing changes in the semi-solid volume and coagulum consistency. The  $MTR$  parameter was sensitive to differences in the intra-gastric coagulation behaviour from differently heated milk products. The findings of **Chapter 4** demonstrated the capability of CEST, MT and  $T_2$ -weighted MRI to capture the variations in pH and coagulation dynamics during gastric digestion.

**Chapter 5** expanded on the promising results of the *in vitro* work with an *in vivo* study in humans. The aim of the study was to assess the feasibility of utilizing MT MRI for *in vivo* monitoring of gastric milk protein coagulation, using LPSM and HPSM as test products. The findings demonstrated that the  $MTR$  parameter can serve as a suitable marker for monitoring milk protein coagulation during gastric digestion in humans. The observed trend in the  $MTR$  for LPSM was consistent with what was observed in the semi-dynamic model of **Chapter 4**. Interestingly, no differences were found in the  $MTR$  of LPSM and HPSM during gastric digestion suggesting a different effect in coagulation behaviour of HPSM *in vivo* in humans compared to the behaviour observed in the semi-dynamic model. In addition to the  $MTR$ , total, semi-solid and liquid gastric content volumes were determined. These indicated a slower gastric emptying for HPSM compared to LPSM. **Chapter 5** underscored the potential of MRI as a valuable tool for non-invasive monitoring of gastric milk protein digestion in humans.

In the remainder of this chapter, the findings from the previous chapters are jointly discussed and put into a broader perspective. First, the strengths and limitations of  $^1\text{H}$  MT and CEST MRI in digestion research are discussed and suggestions for improvements are provided. Next, a direct comparison between the semi-dynamic *in vitro* and human *in vivo* data is presented. Possible explanations for the observed differences are discussed and suggestions for designing a more physiologically relevant gastric digestion model are provided. Lastly, directions for future research regarding the application of the developed MRI markers for studying gastric digestion of different foods, and in different populations are proposed.

## 6.2. Strengths and limitations of $^1\text{H}$ ST MRI in digestion research

Gastric digestion involves breakdown of the food matrix, which may result in phase separation of the chyme. Conventional  $T_2$ -weighted anatomical MRI images have previously been used to visualize phase separation of milk into a fat and aqueous layer in the stomach (Camps et al., 2017, 2021). Gastric cow's milk digestion involves a separation into a semi-solid and liquid phase as a result of milk protein coagulation. In **Chapter 3**, we introduced intensity thresholding of these images as a tool to estimate the volume of the semi-solid (coagulum) fraction within static digestion samples, and demonstrated its application to images obtained during gastric digestion in a semi-dynamic *in vitro* model (**Chapter 4**) and *in vivo* in humans (**Chapter 5**). However, the volume of the different fractions alone does not provide a quantitative direct measure of the consistency of the coagulum. MRI offers various quantitative methods capable of providing specific parameters that contain information about the local micro- and macro-structural as well as the chemical environment of protons. Saturation Transfer techniques (MT and CEST) are examples of quantitative MRI methods, which provide molecular information, on semi-solid macromolecules and low-abundant solute molecules, that is not accessible by liquid-state spectroscopy or relaxometry measurements due to the short  $T_2$  relaxation times or low concentrations of such molecular components.

At the start of this thesis work, the potential of MT and CEST for monitoring structural- and molecular-level changes during gastric digestion had not been explored yet.

### 6.2.1. MTR: marker of gastric milk protein coagulation

The MT MRI method explored in this thesis can be used to monitor the transition of liquid milk into a semi-solid coagulum during gastric digestion. This coagulation process is characterized by a gradual reduction in the protein molecular mobility as the caseins aggregate to form a semi-solid mass. As digestion progresses, syneresis takes place, during which liquid whey is expelled from the semi-solid mass, resulting in a denser and more solid coagulum and, hence, a further reduction in protein molecular mobility (Daviau et al., 2000; Huppertz & Chia, 2021; Le Feunteun et al., 2012). Magnetization transfer takes place via through-space dipolar coupling between semi-solid macromolecular protons and mobile water protons. The strength of the dipolar coupling, and hence the extent of magnetization transfer, depends on the mobility and number of macromolecular protons (Henkelman et al., 2001; van Zijl et al., 2018; Wolff & Balaban, 1989). As demonstrated in **Chapter 2**, the *MTR* can be used to assess changes in the protein content of the coagulum. Furthermore, the *MTR* of the coagulum increased during gastric digestion in both a semi-dynamic *in vitro* model (**Chapter 4**) and *in vivo* in humans (**Chapter 5**), reflecting the progressive coagulation of the milk proteins. Therefore, the *MTR* has been proven to be a suitable marker of changes in the coagulum consistency over time. The information obtained on the consistency of the coagulum provides complementary information with respect to the gastric content and semi-solid volumes.

$T_2$  mapping is a quantitative MRI technique that has been used to study gastric digestion of whey protein gels (Deng et al., 2022, 2023) and a bread and cheese meal (Musse et al., 2023). The main advantage of MT compared to  $T_2$  mapping is that MT gives access to the semi-solid macromolecular protons with short  $T_2$ -values, invisible in  $T_2$ -maps. Moreover,  $T_2$ -mapping requires multiple measurements at varying echo times, to cover the full decay curve of the magnetization, whereas to obtain the *MTR* only two measurements, namely a

reference scan and a saturation scan, are required. Moreover, the range of measurement echo times that can be selected on clinical scanners is limited to about 20-120 ms and, for dynamic *in vivo* applications, the number of acquired echoes typically cannot exceed 5. As a result, neither the shortest or longest  $T_2$  components can be accurately captured. Moreover,  $T_2$ -mapping requires voxel-wise fitting of the echo amplitudes by mono- or multi-exponential decay functions, which introduces analysis errors and model assumptions absent in the calculation of the  $MTR$  (Dekkers & Lamb, 2018). In **Chapter 5**, the two required scans were obtained within a measurement time of 39 s using a RARE image readout to cover a volume of 352x400x16 mm with an in-plane resolution of 1 mm x 1 mm, and slice thickness and interslice gap of 4 mm and 2 mm, respectively. This acquisition time can be further reduced to 25.6 s for the same FOV and resolution conditions by using a gradient-recalled echo (GRE) sequence, but at the cost of image SNR and contrast.

The specificity of MT MRI measurements to semi-solid macromolecules can also be seen as a potential limitation of their accessible dynamic range, as they do not provide any information on proteins and peptides in solution. However, to overcome the latter pitfall, MT and CEST measurements can be mutually combined. This only requires the acquisition of two additional saturated images, and will be discussed in more detail in the following section. Moreover, the  $MTR$  parameter is only semi-quantitative, as it depends on the  $B_1$  strength and saturation frequency offset used for the acquisition. However, as long as these parameters are kept constant throughout the study, the  $MTR$  values corresponding to different digestion time points and treatments can be compared. The sensitivity of the  $MTR$  parameter to different coagulum consistencies warrants a more detailed investigation. This can be achieved by using casein gels with varying stiffness and coagula prepared from milk heated at different temperatures. Additionally, the association of denatured WPs with casein micelles in the coagulum of heated milk might influence the  $MTR$ . This influence could stem not only from increased proton mobility, as a result of a looser coagulum, but also from its impact on the total number of protons within the coagulum. Ideally, mapping the macromolecular proton fraction should be included to enable better interpretation of  $MTR$  data during gastric digestion of differently heated milk products. However, this would require time-consuming measurements of MT

spectra at different  $\Delta$  values and  $B_1$  amplitudes, as well as complex multiparameter fitting of the data, as conducted in **Chapter 2**. While this approach might not be feasible for *in vivo* studies, it could be used to understand the effects in more detail for *in vitro* samples.

### 6.2.2. CEST MRI: pH, protein concentration and hydrolysis

As mentioned in the previous section, CEST can complement MT measurements by providing information on the solute proteins and peptides. As demonstrated in **Chapter 3**, the  $MTR_{asym}$  parameter obtained from CEST measurements is sensitive to changes in pH, protein concentration, and protein hydrolysis. The latter is a result of the cleavage of peptide bonds leading to an increase in the number of exchangeable  $-NH_2$  and  $-OH$  protons. We showed that, for a WP concentrate, a degree of hydrolysis of  $26 \pm 1\%$  resulted in a  $35 \pm 1\%$  increase in the  $MTR_{asym}$ . This suggests that, under constant protein concentration and pH, the  $MTR_{asym}$  parameter could serve as a marker of protein hydrolysis. However, as shown in **Chapter 4**, under semi-dynamic gastric digestion conditions large variations in pH and protein concentration occur, which dominate over protein hydrolysis. Generally, protein hydrolysis in the stomach is quite limited as it mainly occurs in the small intestine. Therefore, under semi-dynamic digestion conditions, the  $MTR_{asym}$  parameter is mainly affected by changes in pH and protein concentration. As demonstrated in **Chapter 4**, the dual-power CEST MRI method could be used as an indirect way of measuring pH in standard WPI solutions and in digestion samples. The pH values obtained by CEST MRI at room temperature on a 7 T vertical bore NMR spectrometer showed excellent agreement with the values measured by a pH electrode. However, some challenges were faced for the measurements at 37 °C on a clinical 3 T scanner. Firstly, the CEST spectra at 37 °C contained an exchange relayed NOE (rNOE) signal at  $\Delta = -3.5$  ppm (Fig. 6.1.), likely resulting from a two-step process in which magnetization of non-exchangeable protons is transferred via through-space dipolar coupling towards neighboring exchangeable protons, and then to water via  $^1H$  chemical exchange (Jones et al., 2013; Zhou et al., 2023). Whereas dipolar coupling is expected to decrease with temperature due to increased molecular motion, the

chemical exchange rate is expected to correspondingly increase. The latter is a result of an increase in the force and frequency of collisions between the reacting species, facilitating the chemical exchange of protons (Wermter et al., 2022).

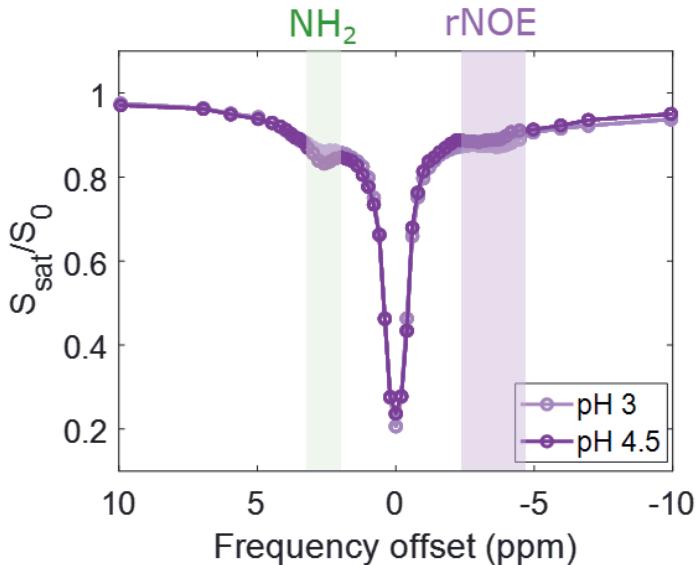


**Figure 6.1.** CEST spectra of 12% WPIS at pH 3 and 4.5 obtained with a  $B_1$  of  $1.5 \mu T$  for  $37^\circ C$  on a 3T clinical MRI scanner.

Secondly, a shift in the  $^1H$  chemical shift difference from water for the chemical exchange peak at  $pH \geq 6.5$  was observed from  $\Delta \sim 2.7$  ppm at room temperature to  $\sim 4$  ppm at  $37^\circ C$  (Fig. S4.4). This complicated the quantification of the  $MTR_{asym}$  for *in situ* pH mapping, where data was only obtained at  $\Delta = \pm 2.7$  ppm. Thirdly, protein aggregation near the pI of WP resulted in inhomogeneities in the *in situ* pH maps from 30 min onwards. The chemical exchange rate for proteins in solution is higher than that of aggregated proteins due to a reduced water accessibility of the exchangeable protons in the latter. This resulted in lower  $MTR_{asym}$ , and consequently lower  $RPM$  values for the aggregated particles, leading to an overestimation of the pH. Therefore, the application of CEST pH mapping during gastric digestion requires further development and validation.

Generally, it is recommended to measure saturated images at multiple  $\Delta$  values to construct a CEST spectrum instead of images obtained at only one set of negative and positive  $\Delta$ . This could enable more accurate quantification of the chemical exchange through multipool Lorentzian fitting (Zaiß et al., 2011). However, for gastric digestion studies, this would necessitate a significant acceleration of the measurement time per offset.

### Sensitivity to field inhomogeneities

One limitation of CEST is its strong sensitivity to magnetic field inhomogeneities. In MRI scanners, the amplitude of the main magnetic field ( $B_0$ ) and the applied RF field ( $B_1$ ) vary across the field of view (FOV) due to inherent challenges in achieving a perfectly uniform  $B_0$ - and  $B_1$ -field and tissue-related magnetic susceptibility variations throughout the imaging volume. The asymmetry analysis most commonly used for CEST quantification only works well if the water chemical shift is exactly known and can be referenced to 0 ppm. Due to the steep slope of the direct saturation curve, even a small shift in the  $B_0$ -field and the concomitant shift in the CEST spectrum can result in errors in the quantification of the  $MTR_{asym}$ .

These effects can be reduced by improving the shimming, which is challenging *in vivo* due to the large volumes that need to be shimmed, variable tissue compositions resulting in different magnetic susceptibilities, and time constraints. Therefore, the water saturation shift per voxel can be used to construct a  $B_0$ -shift map by either separately measuring the direct water saturation spectra per voxel, known as the WASSR approach, and used in **Chapter 3** and **4** for measurements of WP solutions and digesta samples (Kim et al., 2009), or by using the measured CEST spectrum itself (Stancanello et al., 2008). The resulting  $B_0$ -shift map was used for prospective voxel-wise correction of the CEST spectra, to enable reliable quantification of the  $MTR_{asym}$ .

However, for *in situ* measurements during gastric digestion in the semi-dynamic model and *in vivo*, it was not possible to acquire CEST spectra due to their long measurement times. Instead saturated images were obtained at  $\Delta \pm 2.7$  ppm along with a reference unsaturated image to obtain the amine  $MTR_{asym}$ . The  $MTR_{asym}$  values were voxel-wise corrected using the fast  $B_0$ -inhomogeneity



correction approach that uses regression to describe the effect of the  $B_0$ -artifact on the CEST effect. This approach performed well for the measurements of the semi-dynamic model in **Chapter 4**, and showed excellent agreement with the conventional CEST-spectrum interpolation-based correction (Fig. S4.5).

Quantification of the chemical exchange is also influenced by  $B_1$ -field inhomogeneities, which result in spatial variations in the saturation efficiency and consequently errors in the  $MTR_{asym}$  values. To correct for  $B_1$ -inhomogeneity, a relative  $B_1$ -map ( $rB_1$ ) can be acquired to determine the exact  $B_1$  amplitude of the saturation pulse per voxel. The  $rB_1$ -map can subsequently be used for voxel-wise interpolation of the  $B_0$ -corrected CEST spectra or  $MTR_{asym}$  values (Windschuh et al., 2015). The latter was used in **Chapter 4** to correct the  $MTR_{asym}$  values obtained for the 3 T measurements of the semi-dynamic model.

The effect of  $B_0$ - and  $B_1$ -inhomogeneity on the  $MTR_{asym}$  was also visible in the data from the *in vivo* study (Fig. 6.2). However, applying the fast  $B_0$ -correction method on the *in vivo* data of the stomach was not possible because the delay between the acquisition of the  $MTR_{asym}$  and WASSR  $B_0$ -map caused a difference in the voxel contents between the two maps, especially at later time points during digestion. Moreover, at  $t = 35$  min (Fig. 6.2, middle) the gastric mixing caused a mismatch in the voxel contents between the individual saturated images obtained to construct the WASSR  $B_0$ -map, resulting in inaccurate  $\delta B_0$  values. To assess the validity of the measurements and correction methods, data from the kidney, a static organ in the abdomen, was used (Fig. 6.2, bottom row). This shows that the  $B_0$ - and  $B_1$ -inhomogeneity were smaller in the kidney, and that the  $B_0$ - and  $B_1$ -inhomogeneity corrections used for the *in vitro* data of **Chapter 4** also worked well *in vivo* for a static organ, but not for a dynamic organ like the stomach and its contents.

The large  $B_0$ -inhomogeneity across the stomach highlights the need for better shimming of this region and for another correction approach. For the *in vivo* scans, shimming was performed before the acquisition of the CEST measurement for each time point using the so called "pencil beam volume" shimming, with the shim volume placed on the stomach to optimize the magnetic field specifically in that region. This approach performed better than the default approach, which is to

shim over the whole imaging volume. It is important to mention that obtaining good shims within the stomach volume is challenging because of its close proximity to other organs, presence of air leading to susceptibility artifacts, and motion of both the stomach and organs around it. Therefore, it is worth exploring more advanced shimming approaches in future works. One example would be to explore real-time shim corrections using Double-volumetric Navigators (Simegn et al., 2019), which has the added advantage of offering real-time motion correction.

Alternatively, CEST spectra could be measured to allow construction of an internal  $B_0$ -map, thereby mitigating gastric mixing effects between the CEST and the WASSR  $B_0$ -map acquisition. As mentioned in the previous section, the number of  $\Delta$  values should be optimized for speed, and different sequences that may allow faster CEST spectra acquisition should be explored. Since the long acquisition times of CEST spectra are the primary factor limiting its widespread clinical application, a plethora of acquisition schemes have been developed to accelerate CEST measurements (Zhang et al., 2023). Some examples of image readout schemes that are faster than the RARE readout used in this thesis include echo-planar imaging (EPI), Gradient-Recalled Echo (GRE), Gradient Echo and Spin Echo (GRASE), and optimized turbo spin echo (TSE, also known as RARE) with different flip angle evolutions (SPACE) (Zhang et al., 2020). However, these methods have their own limitations and suffer from susceptibility-related image distortions and low SNR. An alternative approach is to adjust the saturation scheme. For example, Scheidegger et al. (2011) proposed a method called saturation with frequency alternating RF irradiation (SAFARI), in which chemical exchange contrast can be obtained from four images without the need for  $B_0$ -correction. This includes the acquisition of a SAFARI image with saturation alternating between the positive label and negative control  $\Delta$ , e.g. at  $\Delta \pm 3.5$  ppm for amides, along with standard CEST images obtained at the label and control  $\Delta$ , and an unsaturated image. This approach is robust towards both  $B_0$ -inhomogeneity effects, and asymmetry effects, such as the rNOE contributions described in the previous section.

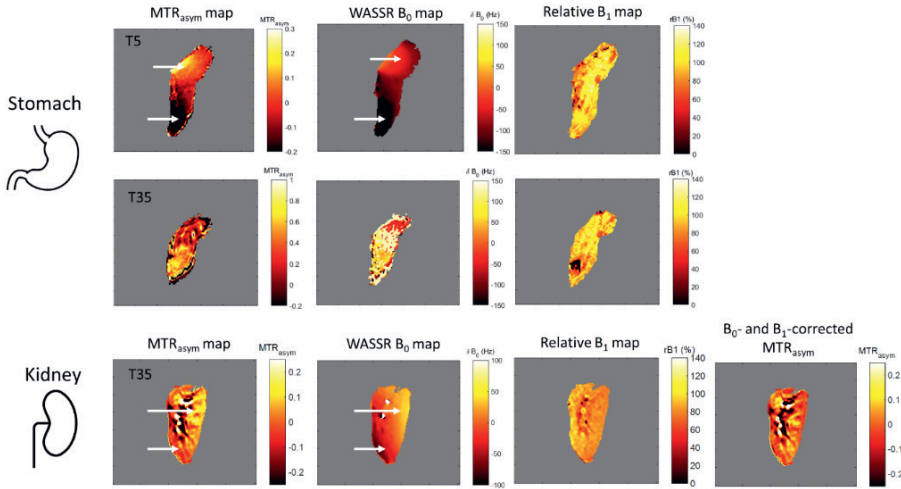


**Figure 6.2.**  $MTR_{asym}$ , WASSR  $B_0$ - and relative  $B_1$ -maps of the stomach contents of a female participant at  $t = 5$  min (top) and  $t = 35$  min (middle) after ingestion of 300 g LPSM. The white arrows point at areas of high or low  $MTR_{asym}$  corresponding to regions with large  $B_0$ -inhomogeneity. The same is shown in the bottom row for the kidney at  $t = 35$  min to assess the validity of the measurements and the corrections for a static organ. The  $MTR_{asym}$  map was obtained from CEST measurements at  $\Delta = \pm 2.7$  ppm with a  $B_1$  amplitude of 3  $\mu$ T and saturation time of 1 s.

In **Chapter 1**,  $T_{1\rho}$  and  $T_2$ -dispersion were also introduced as potential MRI techniques that can provide markers of protein content, structure and pH. However, both of these techniques are also susceptible to  $B_0$ - and  $B_1$ -inhomogeneities, and require long acquisition times (Leforestier et al., 2021; Shaffer et al., 2020; Witschey et al., 2007). Hence, they do not offer an advantage over CEST and MT MRI in the context of digestion research.

### 6.3. Effect of heat treatment on gastric milk protein digestion

A sub-aim of this thesis was to investigate the effect of heat treatment on the gastric digestion of milk proteins. In **Chapter 2** and **3**, the gastric digestion of unheated skim milk (USM) and heated skim milk (HSM) under static *in vitro* conditions simulating gastric digestion in infants were compared using the  $MTR$ ,  $MTR_{asym}$  and semi-solid volume. In these static digestion conditions, the pH is fixed at 5.3, and pepsin activity remains constant at 268 U/mL from the start of digestion, resulting in rapid ( $\leq 1$  min) formation of the coagulum. The  $MTR$  of USM

decreased rapidly during digestion due to solubilization of the initially formed coagulum. Heating of SM resulted in a slower decrease in the *MTR*, indicating a casein coagulum that is correspondingly more resistant to solubilization (**Chapter 2**). This observation is in agreement with results from Sánchez-Rivera et al. (2015) and Miltenburg et al. (2024) who showed that caseins are more resistant to gastric digestion after heat treatment.

In **Chapter 4** and **5**, the USM and HSM were replaced by commercial LPSM (typically heated at  $\sim 72$  °C for 15s) and in-house prepared HPSM (heated at 80 °C for 30 min), respectively. Moreover, in **Chapter 4**, a semi-dynamic *in vitro* model with adult gastric digestion conditions was used (Deng et al., 2022; Mulet-Cabero et al., 2020) to enable comparison with the data from the *in vivo* study of **Chapter 5**. During semi-dynamic *in vitro* gastric digestion, the semi-solid volume was higher for LPSM compared to HPSM. This indicates that the coagulum of LPSM remained intact and emptied more slowly than that of HPSM. Moreover, the *MTR* of the LPSM coagulum continuously increased with digestion, whereas that of HPSM decreased from 50 min onwards. These observations are in agreement with previous (semi)-dynamic *in vitro* studies (Mulet-Cabero et al., 2019; Ye et al., 2016), which showed that heat treatment results in a looser and softer coagulum during gastric digestion. An *in vivo* study in growing pigs (Ahlborn et al., 2023) showed that the coagulum dry weight and stiffness was lower for UHT compared to pasteurized milk, which is in agreement with the *in vitro* observations. Another study in rats (Ye et al., 2019) showed that the coagula for both pasteurized and UHT milk were soft and watery, while that of unheated milk was solid. They also reported a higher wet and dry weight as well as moisture content up to 120 min of digestion for UHT compared to pasteurized milk, in contrast to the findings of Ahlborn et al. (2023). It is important to note that a higher temperature was used for the pasteurized milk in the rat study (85 °C for 15 s) compared to that in the pig study (75 °C for 15 s). This difference in heating temperature could potentially have impacted the coagulation process.

Another study in pigs reported a slower emptying of heated (90 °C for 10 min) compared to unheated skim milk determined by the mean retention time of chromium in the stomach (Barbé et al., 2013). Overall, there is no consistent picture in the literature on the effect of heat treatment on gastric emptying and coagulation of milk, partially due to the different heat treatments used in each study.

The data from the human study in **Chapter 5** showed that gastric emptying of the total gastric content was slower for HPSM compared to LPSM, and that of the semi-solid and liquid content tended to be slower as well. Moreover, in contrast to the *in vitro* data of **Chapter 4**, the *MTR* for HPSM increased until the last digestion time point measured ( $t = 95$  min), with the same trend observed for LPSM. This indicates a different gastric coagulation behavior of HPSM *in vivo* in humans compared to *in vitro*. In the next section, a direct comparison of the *in vitro* and *in vivo* data is provided and potential explanations for the differences are discussed.

## 6.4. Bridging the gap between *in vitro* models and *in vivo* digestion in humans

### 6.4.1. Comparison of *in vivo* and *in vitro* semi-solid and liquid fractions

The gastric emptying *in vitro* was mimicked by manually removing gastric content with a syringe at 4.3 mL/min. This, coupled with a gastric secretion rate of 2 mL/min, resulted in a decrease of 2.3 mL/min in gastric content, a rate comparable to the overall emptying rate estimated from the *in vivo* data, which was 2.2 mL/min for both milk products. However, the emptying of the semi-solid and liquid fractions differed between *in vitro* and *in vivo* for HPSM as shown in Fig. 6.3. For LPSM (Fig. 6.3a,b), the variation over time in the semi-solid and liquid fractions is small for both the semi-dynamic *in vitro* and *in vivo* data. The mean difference between the *in vitro* and *in vivo* data was  $4.6 \pm 4.3\%$  and  $8.0 \pm 9.5\%$  for the semi-solid and liquid fractions, respectively. This small difference between the *in vitro* and *in vivo* data along with the overall similar trend with the digestion time, indicates that gastric digestion of LPSM is realistically mimicked in the semi-dynamic *in vitro* model. For HPSM (Fig. 6.3c,d), a strong decrease in the semi-

solid fraction, and a strong increase in the liquid fraction was observed during *in vitro* digestion. However, very little variation with the digestion time was observed in the *in vivo* data, and both the trend and values were similar to those of LPSM. The mean difference between the *in vitro* and *in vivo* data was  $40\pm 18\%$  and  $39\pm 17\%$  for the semi-solid and liquid fractions, respectively. This suggests that the semi-solid fraction of HPSM is removed more rapidly during semi-dynamic *in vitro* digestion compared to *in vivo* digestion in humans. During *in vitro* digestion, the coagulum of HPSM appeared loose and soft compared to that of LPSM, which can be observed in both the photographs of the digesta, and in the  $T_2$ -weighted MRI images (Fig. 6.3e). This loose and soft coagulum was easily disrupted and removed by the syringe used to mimic gastric emptying. However, the *in vivo*  $T_2$ -weighted MRI images do not point to a more loose and soft coagulum for HPSM compared to LPSM. Instead, what can be observed is that the liquid phase for HPSM is more abundant compared to that of LPSM (see also Figure 5.2 and 5.3). This suggests that the coagulum from HPSM may have a higher water holding capacity compared to that of LPSM, which is supported by observations of a higher water holding capacity for denatured WPs compared to their native counterparts (Kethireddipalli & Hill, 2015). Additionally, it has been shown that the gastric coagulum from UHT milk has a higher moisture content compared to that from pasteurized milk (Ye et al., 2019). This can be explained by the formation of casein-whey protein aggregates upon heat treatment of milk, which have a microstructure with large voids that can hold water (Lucey et al., 1997). The slower emptying of milk during *in vivo* gastric digestion could induce more coagulation because the milk proteins will be exposed to pepsin and acid for a longer time. This should be verified *in vitro*, for example, by performing static digestion experiments at different pH around the pI of caseins (e.g. pH 3,4 and 5), or by repeating the semi-dynamic digestion with a slower gastric emptying rate.

It should be noted that from the  $T_2$ -weighted images, it is not possible to distinguish gastric juice from the liquid fraction of the meal. Therefore, the higher liquid volume for HPSM could be the result of higher gastric juice production. Hoad et al. (2015) showed that labelling the meal with gadolinium, to decrease its longitudinal relaxation time compared to that of gastric juice, can be used to estimate gastric secretion volumes with  $T_1$ -mapping (Hoad et al., 2015). In future

works, it could be useful to include such measurements in MRI studies of milk digestion to quantify the gastric juice secretion in response to different milk products.

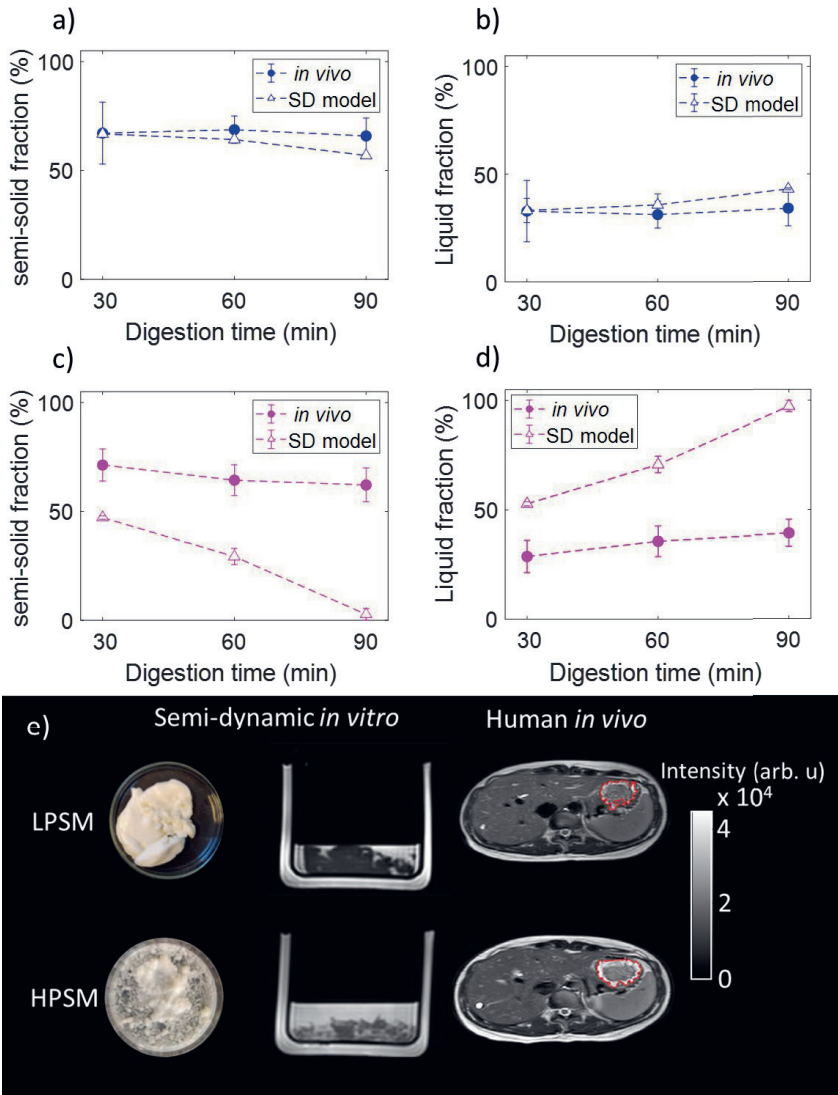


**Figure 6.3.** Comparison of (a,c) semi-solid and (b,d) liquid gastric content, estimated from the  $T_2$ -weighted MRI images, between *in vivo* in humans and the semi-dynamic (SD) *in vitro* model for LPSM (top) and HPSM (bottom). (e) Photographs of the *in vitro* coagulum at  $t = 40$  min along with the corresponding *in vitro* and *in vivo*  $T_2$ -weighted MRI images. The gastric content is outlined in red in the *in vivo* MRI images.

### 6.4.2. Comparison of *in vivo* and *in vitro* $^1\text{H}$ MTR

The difference in semi-solid and liquid fractions observed between the *in vitro* and *in vivo* data was further supported by the MT data (Fig. 6.4). The mean difference in the *MTR* between *in vitro* and *in vivo* was small for LPSM, around  $12\pm 6\%$ , while for HPSM it was  $40\pm 35\%$  and especially large (90%) at  $t = 80$  min. Interestingly, for HPSM, the *in vivo* *MTR* value increased by 15% between  $t = 50$  and 80 min, whereas *in vitro* a large decrease by 80% was observed. As mentioned in the previous section, the coagulum of HPSM was rapidly removed during *in vitro* digestion due to its soft and loose structure and, hence, at  $t = 80$  min there was almost no coagulated milk left in the gastric compartment. However, the *in vivo* data showed that even after 80 min of digestion, there was still a substantial amount of coagulum present in the stomach, as can be observed in both the  $T_2$ -weighted images (Fig. 6.3e) and the *MTR* maps (Fig. 6.4c). These findings suggest that the effect of heat treatment on gastric milk protein coagulation may not be accurately mimicked in the semi-dynamic *in vitro* model. Two factors possibly responsible for this finding are given below.

**1. Gastric emptying and secretion:** *in vitro* gastric emptying and secretion were fixed at, respectively, 2.3 mL/min and 2 mL/min for both milk products. The emptying rate was based on the caloric content of skim milk as suggested by (Mulet-Cabero et al., 2020). *In vitro*, both the semi-solid and liquid fractions of HPSM were removed with the syringe used for gastric emptying whereas, for LPSM, only the liquid fraction was removed. The rapid removal of the milk proteins for HPSM resulted in less coagulation as digestion progressed, thus explaining the low *MTR* at the later digestion time points. However, *in vivo* gastric emptying and secretion is a more complex process driven by the interaction between neural and hormonal factors (Camilleri, 2019; Murray & Abell, 2018). The hormone gastrin, plays an important role during gastric digestion and is responsible for enhancing gastric motility and release of gastric acid (Duan et al., 2021; Mori et al., 2022). The release of gastrin is regulated by gastric distension, presence of proteins/peptides in the stomach, and pH of the stomach. Based on the results shown in Fig. 6.3, the semi-solid fraction emptied slower *in vivo* compared to *in vitro* for HPSM, which results in a slower decrease of the protein concentration in



the stomach. A high protein concentration is expected to result in a high stomach pH due to the high buffering capacity of milk proteins. This combined effect of elevated protein concentration and pH levels could potentially trigger an enhanced release of gastrin. Consequently, this heightened gastrin release may contribute to further coagulation of milk proteins due to an increase in gastric juice production. This could explain the increase in *MTR* observed for HPSM until the latest digestion time, and the discrepancy with the *in vitro* data. Future *in vivo* work could include measurements of the gastrin concentrations in blood (Malagelada et al., 1976; Rehfeld, 2008; Rehfeld et al., 2012) to aid in interpreting the gastric coagulation and emptying data. This can be achieved by taking blood samples at baseline and postprandially, which can easily be done while the participant remains in the MRI scanner and has previously been done for measuring blood hormone or AA concentrations (Aliyu et al., 2023; Eijnatten et al., 2023; Roelofs et al., 2023).

**2. Intra-subject variability:** The pH of the simulated gastric fluid was the same for all semi-dynamic *in vitro* experiments, while *in vivo* there may be considerable intra-subject variability in gastric pH (Fadda et al., 2022). Differences in the gastric pH between the two visits would have affected pepsin activity and, hence, milk protein coagulation. It would be interesting to assess intra-subject variability in gastric coagulation by repeating the test session with the same participant and milk product on different days. This could be complemented by static and semi-dynamic *in vitro* experiments in which the pH or pepsin activity is varied. For example, a previous study showed that, under static *in vitro* conditions, a 50% lower pepsin activity resulted in a higher coagulum dry weight and firmness after 5 min but not after 30 min of digestion (van Eijnatten et al., 2023).

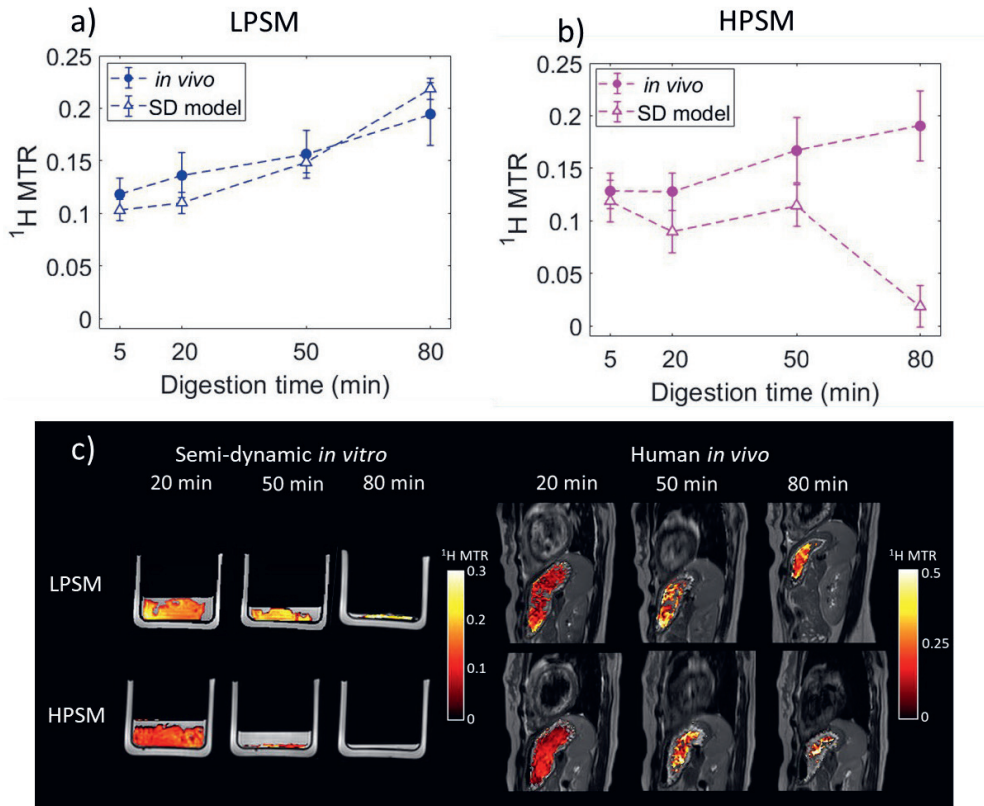


**Figure 6.4.** Comparison between semi-dynamic *in vitro* and human *in vivo*  $^1\text{H MTR}$  values vs. gastric digestion time for (a) LPSM and (b) HPSM. (c) The corresponding  $^1\text{H MTR}$  maps during semi-dynamic *in vitro* (left) and human *in vivo* (right) gastric digestion.

### 6.4.3. Towards more physiologically relevant models of digestion

#### ***In vitro* digestion models**

The semi-dynamic *in vitro* model used in this thesis was based on the MR-GAS model (Deng et al., 2022), which is relatively simple (Fig. 6.5a), as it only included gradual addition of SGF and removal of the chyme at intervals of 10 min to simulate gastric secretion and emptying, respectively. The set-up was kept simple to ensure MRI-compatibility and ease of use. However, the simplified setup had several key limitations that still require improvements to better simulate *in vivo*

gastric digestion. In the following, the limitations and suggestions for improvement are discussed.

Most of the suggestions are based on the human gastric simulator (HGS) (Kong & Singh, 2010), the *in vitro* distal gastric simulator (DGS) (Donis-Rabanales et al., 2022), and the artificial stomach response kit (ARK)(Payal et al., 2021) with recommended adjustments to ensure MRI-compatibility.

- **Shape and material of the gastric compartment:** the gastric compartment consisted of a water-jacked beaker made of glass, which is very different from the J-shape and tissue of the stomach. In future work, the gastric compartment could be 3D printed from a flexible material such as silicon rubber similar to the *in vitro* gastric simulator shown in Fig. 6.5b (Donis-Rabanales et al., 2022) or the ARK model (Payal et al., 2021), which is especially important for mimicking stomach contractions.
- **Gastric emptying:** this was manually performed from the top of the beaker through a syringe with a tip that had an inner diameter of 2 mm to mimic the emptying of small particles. *In vivo*, gastric emptying occurs through the pylorus, which connects the stomach to the duodenum. As mentioned in the previous section, *in vivo* gastric emptying of the semi-solid fraction was different from *in vitro*. Therefore, performing gastric emptying from the top using a syringe is not representative of the real situation. Instead the gastric compartment should be lined with a mesh bag that has a pore size of ~2 mm. Emptying can be performed from the bottom of the gastric compartment using a peristaltic pump, as done in the HGS model (Kong & Singh, 2010) and MR-GAS model (Deng et al., 2022). The peristaltic pump should be placed outside the MRI scanner room, but can be connected to the gastric compartment with long tubing, similar to what was done for the tubing of the water bath and gastric secretion in **Chapter 4**.
- **Gastric secretion:** simulated gastric fluid was added from the top of the beaker at one location, whereas *in vivo* gastric juice is secreted from the stomach wall. This can be improved by connecting multiple small tubes to the gastric compartment through which gastric juice is secreted. The end tips could be placed at different elevations to simulate uniform distribution of the simulated gastric fluid.

- **Gastric mixing:** the current setup did not include the peristaltic contractions of the stomach and instead manual stirring was used. Simulating gastric contractions in a MRI-compatible manner is challenging. One approach could be to use double-acting pneumatic pistons, in which air is used to push and retract the piston, similar to what has been used in the ARK model by Payal et al. (2021). The pistons can be used to apply pressure on specific parts of the flexible gastric compartment wall to simulate gastric contractions. Most MRI scanner rooms contain pressurized air-outlets, which can be used for this purpose. The main challenge would be to make the pistons from non-magnetic materials: polyether ether ketone (PEEK) could be a suitable MRI-compatible material. Another challenge would be holding the pistons in place, and applying different pressures on different parts of the stomach. For example, the pressure on the proximal stomach should be lower than on the distal stomach to simulate the strong antral contraction waves in the distal part (Brandstaeter et al., 2019). Another approach would be to use water to induce pressure on the stomach wall in a hydro-pneumatic chamber as done by (Donis-Rabanales et al., 2022) and shown in Fig. 6.5b, in which the water inlet/outlet ports are indicated with the number 5.
- **Temperature control:** temperature control through the use of a water-jacketed beaker worked well in the current setup, and a similar approach is used in the model of Donis-Rabanales et al. (2022) in which the hydro-pneumatic chamber surrounding the stomach is filled with water kept at 37 °C.

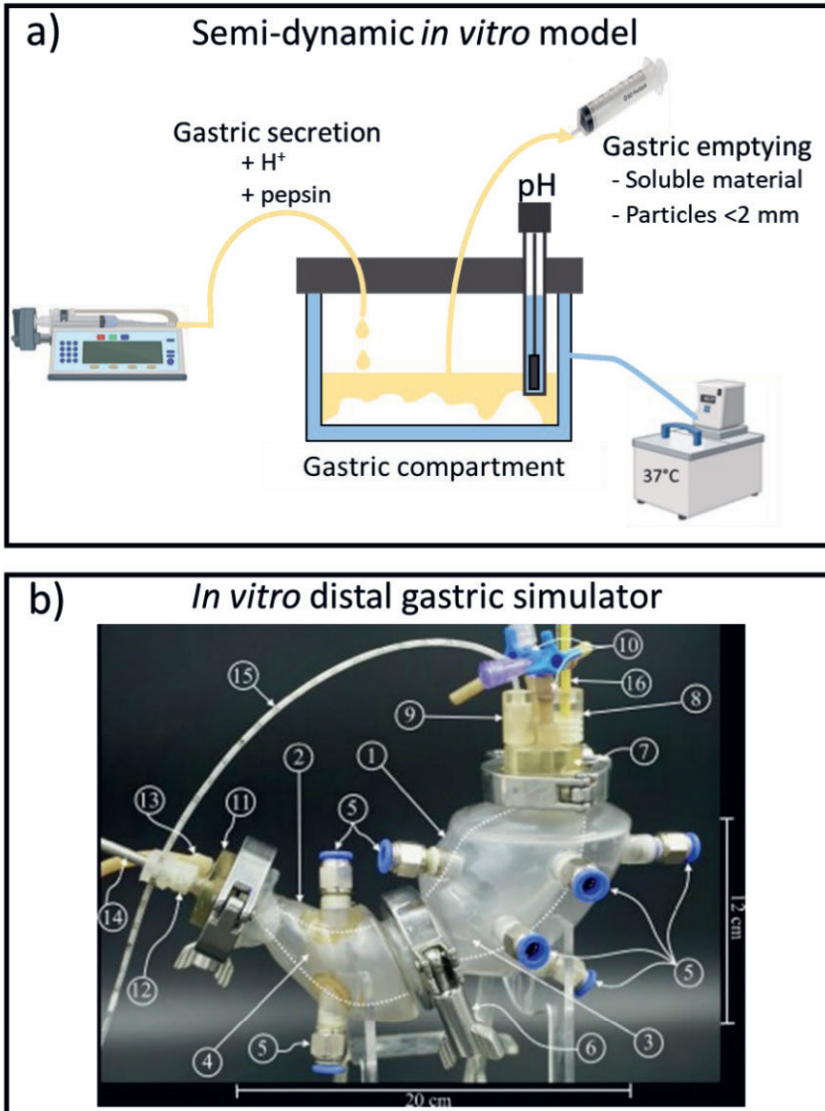


**Figure 6.5.** (a) semi-dynamic *in vitro* gastric digestion model used in this thesis. (b) *in vitro* distal gastric simulator adapted from Donis-Rabanales et al. (2022) with permission. (1) and (2) distal stomach chambers; (3) and (4) silicon rubber membranes simulating the gastric walls; (5) Water Inlet/Outlet Ports; (6) Sanitary stainless-steel clamp; (7) Upper cap; (8) Thermometer port; (9) Catheter port; (10) Food/gastric juice port; (11) Lower cap; (12) pH-meter port; (13) Emptying port; (14) pH probe; (15) Manometry catheter; (16) Thermometer.

The development and validation of physiologically relevant *in vitro* models is an ongoing effort (<https://www.cost-infogest.eu/>). Several *in vitro* models have been compared with *in vivo* data from either humans or animals. Vardakou et al. (2011) showed that the mean breaking time of agar gel beads in a dynamic gastric simulator was similar to *in vivo* human data from Marciani et al. (2001).

The digestion of skim milk proteins in the consensus static *in vitro* and the dynamic DIDGI model (Egger et al., 2019) has been validated against digestion in pigs. The gastric transit of infant formula in the DIDGI system showed similar results as in piglets (Ménard et al., 2014). Additionally, gastric emptying and intra-gastric pH in the HGS and *in vivo* in pigs showed similar results (Dupont et al., 2019). However, measurements of the pH distribution in the stomach in humans is an ongoing challenge. Ingestible pH sensor capsules can be used to monitor gastric pH, but are limited by their uncontrollable location. MRI has the potential to map the pH inside the stomach through either CEST, as demonstrated for *in vitro* digestion in **Chapter 4**, or through relaxometry as demonstrated by Deng et al. (2023). However, further *in vitro* development and validation of these techniques is necessary to make *in vivo* pH mapping during gastric digestion possible. Additionally, it is essential to acknowledge that validating an *in vitro* model with *in vivo* data for a particular food or nutrient does not guarantee its accuracy for other food types. Hence, validation of *in vitro* models across various food categories against human *in vivo* data is crucial.

### ***In silico* modelling of digestion**

A limitation of *in vitro* digestion models is that neural and hormonal regulation, as well as feedback loops, cannot be incorporated. Furthermore, as *in vitro* models become more physiologically relevant, their complexity increases, resulting in more complex experiments. This increases the time, cost, and challenges associated with conducting such experiments. *In silico* digestion models could potentially address these limitations and complement both *in vitro* models and *in vivo* studies.

The primary advantage of *in silico* models is their cost-effectiveness, high flexibility, and absence of ethical concerns. Although the field of *in silico* models is relatively new, it has proven potential in comprehensively simulating digestion. For instance, multicompartmental models can simulate the digestion and absorption of various foods or nutrients, incorporating hormonal responses and feedback mechanisms (Le Feunteun et al., 2020, 2021). MRI can play an important role in the development and validation of these models by providing *in vivo* data on gastric emptying, (semi-)solid and liquid volumes, gastric motility, as well as structural changes.

## 6.5. Directions for future research

The exploratory work in this thesis focused on applying  $^1\text{H}$  MT and CEST MRI for monitoring gastric digestion, using skim milk products as test foods. As mentioned in section 6.2., there is still considerable room for improving the MRI measurements, especially with regards to the acquisition times. While the *in vivo* MT measurements in **Chapter 5** provided reliable results, validated against the *in vitro* data of **Chapter 4**, the measurement time of  $\sim 38$  s (2 breath holds) to obtain both a reference and a saturated image ideally should be reduced to a maximum of 20 s (1 breath hold) to mitigate gastric motion and mixing effects. This adjustment could improve the *MTR* quantification.

Both the acquisition and analysis of *in vivo* MT data are relatively simple and could be within reach of researchers interested in studying gastric digestion of a variety of foods. It would be interesting to study the digestion of model foods with different micro- and macrostructure, such as protein gels also of plant-based origin, which undergo structural breakdown during gastric digestion and, as a result, could lead to changes in the *MTR* of the gastric content. Additionally, the effect of the food matrix, such as the presence of lipids and carbohydrates, on the intra-gastric behaviour of food proteins could be studied. This would require separate *in vitro* validation of the *MTR* parameter for such different food products before an *in vivo* MT study, similar to that described in this thesis for skim milk.

The sample size calculation for the *in vivo* study in **Chapter 5** was derived from the *in vitro* data due to the absence of relevant *in vivo* data to estimate the effect

size or variability. The mean difference found between LPSM and HPSM was 0.022 (95% CI [0.018-0.027]), indicating a small and potentially irrelevant difference. A retrospective sample size calculation, using the same approach as in **Chapter 5**, showed that with a power of 90%, and a significance level of 0.05, a sample size of  $n = 101$  is required to detect a difference between LPSM and HPSM *in vivo*. Such requirement for a large sample size suggests that there might be hardly any discernible difference between the products. However, data from **Chapter 5** could be used for sample size calculations in future studies using MT MRI to study digestion of similar products.

In the *in vivo* study of **Chapter 5**, only healthy normal-weight adults were included. However, factors such as age, sex, ethnicity and health status can influence digestion. Understanding food digestion across different populations is crucial for facilitating the development of foods adapted to their specific nutritional needs. For instance, gastric pH is higher and gastric enzyme activities are lower in infants compared to adults (Ménard et al., 2018). Consequently, intra-gastric behaviour of milk and subsequent intestinal digestion are expected to differ significantly from adults. Similarly, in older adults (>65 years) the rate of gastric emptying is slower, gastric pH is higher, and gastric enzyme activities are lower (Menard et al., 2023). While conducting *in vivo* MRI studies in infants may not be feasible, it might be possible to simulate higher pH and lower pepsin activity in adult participants using proton-pump inhibitors. Such data could be used to improve *in vitro* models that simulate digestion in infants.

An exploratory analysis of the data from **Chapter 5** demonstrated differences in gastric digestion of skim milk between male and female participants. For example, the gastric content over time remained higher in females compared to males, indicating a potentially slower gastric emptying in females. While this finding is consistent with observations from previous studies in which slower gastric emptying was found for females compared to males (Bennink et al., 1998; Camps et al., 2018), definitive conclusions cannot be drawn given the exploratory nature of our study and the limited sample size. The effect of sex-based differences on digestion is a topic of increasing interest, and an *in vitro* model that accounts for these differences has been introduced (Lajterer et al., 2022). However, it is important to note that in our work we showed that the differences are driven by



body size and, hence, may not be sex-specific. Therefore, further research is needed to shed light on the underlying factors contributing to these differences, and to separate the effects of body size from sex-related factors.

Although this thesis primarily focused on gastric digestion, it is important not to overlook the oral and intestinal phases. Oral processing, encompassing salivation and mastication, is important for (semi-)solid foods, and influences the structure of the food bolus and subsequently impacts gastric and intestinal digestion, but is less important for liquid foods. The breakdown of proteins into di- and tri-peptides occurs primarily in the small intestines, which is pivotal for AA absorption. While studying intestinal digestion with MRI poses challenges due to extensive intestinal motility, complementing gastric MRI data with data on postprandial blood AA concentrations can provide a more comprehensive understanding of the impact of food processing on digestion (Eijnatten et al., 2023; Roelofs et al., 2023). Studying the different phases of digestion is essential for achieving a detailed understanding of food digestion and the influence of food processing on digestion. This can aid the development of innovative food products and processing methods for optimal health benefits.

## References

- Ahlborn, N. G., Montoya, C. A., Hodgkinson, S. M., Dave, A., Ye, A., Samuelsson, L. M., Roy, N. C., & McNabb, W. C. (2023). Heat treatment and homogenization of bovine milk loosened gastric curd structure and increased gastric emptying in growing pigs. *Food Hydrocolloids*, *137*, 108380. <https://doi.org/10.1016/j.foodhyd.2022.108380>
- Aliyu, A. I., Nixon, A., Hoad, C. L., Marciani, L., Corsetti, M., Aithal, G. P., Cordon, S. M., Macdonald, I. A., Alhussain, M. H., Inoue, H., Yamada, M., & Taylor, M. A. (2023). A comparative, randomised MRI study of the physiological and appetitive responses to gelling (alginate) and non-gelling nasogastric tube feeds in healthy men. *British Journal of Nutrition*, *130*(8), 1316–1328. <https://doi.org/10.1017/S0007114523000302>
- Barbé, F., Ménard, O., Le Gouar, Y., Buffière, C., Famelart, M.-H., Laroche, B., Le Feunteun, S., Dupont, D., & Rémond, D. (2013). The heat treatment and the gelation are strong determinants of the kinetics of milk proteins digestion and of the peripheral availability of amino acids. *Food Chemistry*, *136*(3–4), 1203–1212. <https://doi.org/10.1016/j.foodchem.2012.09.022>
- Bennink, R., Peeters, M., Van den Maegdenbergh, V., Geypens, B., Rutgeerts, P., De Roo, M., & Mortelmans, L. (1998). Comparison of total and compartmental gastric emptying and antral motility between healthy men and women. *European Journal of Nuclear Medicine and Molecular Imaging*, *25*(9), 1293–1299. <https://doi.org/10.1007/s002590050298>
- Brandstaeter, S., Fuchs, S. L., Aydin, R. C., & Cyron, C. J. (2019). Mechanics of the stomach: A review of an emerging field of biomechanics. *GAMM-Mitteilungen*, *42*(3). <https://doi.org/10.1002/gamm.201900001>
- Camilleri, M. (2019). Gastrointestinal hormones and regulation of gastric emptying. *Current Opinion in Endocrinology, Diabetes & Obesity*, *26*(1), 3–10. <https://doi.org/10.1097/MED.0000000000000448>
- Camps, G., de Graaf, K., & Smeets, P. A. M. (2018). Men and Women Differ in Gastric Fluid Retention and Neural Activation after Consumption of Carbonated Beverages. *The Journal of Nutrition*, *148*(12), 1976–1983. <https://doi.org/10.1093/jn/nxy230>
- Camps, G., Mars, M., de Graaf, C., & Smeets, P. A. M. (2017). A tale of gastric layering and sieving: Gastric emptying of a liquid meal with water blended in or consumed separately. *Physiology & Behavior*, *176*, 26–30. <https://doi.org/10.1016/j.physbeh.2017.03.029>
- Camps, G., van Eijnatten, E. J., van Lieshout, G. A., Lambers, T. T., & Smeets, P. A. (2021). Gastric Emptying and Intra-gastric Behavior of Breast Milk and Infant Formula in Lactating Mothers. *The Journal of Nutrition*, *151*(12), 3718–3724. <https://doi.org/10.1093/jn/nxab295>
- Daviau, C., Famelart, M.-H., Pierre, A., Gouderanche, H., & Maubois, J.-L. (2000). Rennet coagulation of skim milk and curd drainage: Effect of pH, casein concentration, ionic strength and heat treatment. *Le Lait*, *80*(4), 297–415.
- Dekkers, I. A., & Lamb, H. J. (2018). Clinical application and technical considerations of  $T_1$  &  $T_2$  (\*) mapping in cardiac, liver, and renal imaging. *The British Journal of Radiology*, *91*(1092), 20170825. <https://doi.org/10.1259/bjr.20170825>
- Deng, R., Mars, M., Janssen, A. E. M., & Smeets, P. A. M. (2023). Gastric digestion of whey protein gels: A randomized cross-over trial with the use of MRI. *Food Hydrocolloids*, *108689*. <https://doi.org/10.1016/j.foodhyd.2023.108689>
- Deng, R., Seimys, A., Mars, M., Janssen, A. E. M., & Smeets, P. A. M. (2022). Monitoring pH and whey protein digestion by TD-NMR and MRI in a novel semi-dynamic *in vitro* gastric simulator (MR-GAS). *Food Hydrocolloids*, *125*, 107393. <https://doi.org/10.1016/j.foodhyd.2021.107393>

- Donis-Rabanales, F., López-Ruiz, T., Ruiz-Huerta, L., Ascanio, G., Brito-de la Fuente, E., & Caballero-Ruiz, A. (2022). Development of an *in vitro* distal gastric simulator to mimic the mechanical action of the human stomach. *Food Research International*, *161*, 111902. <https://doi.org/10.1016/j.foodres.2022.111902>
- Duan, S., Rico, K., & Merchant, J. L. (2021). Gastrin: From Physiology to Gastrointestinal Malignancies. *Function*, *3*(1). <https://doi.org/10.1093/function/zqab062>
- Dupont, D., Alric, M., Blanquet-Diot, S., Bornhorst, G., Cueva, C., Deglaire, A., Denis, S., Ferrua, M., Havenaar, R., Lelieveld, J., Mackie, A. R., Marzorati, M., Menard, O., Minekus, M., Miralles, B., Recio, I., & Van den Abbeele, P. (2019). Can dynamic *in vitro* digestion systems mimic the physiological reality? *Critical Reviews in Food Science and Nutrition*, *59*(10), 1546–1562. <https://doi.org/10.1080/10408398.2017.1421900>
- Egger, L., Ménard, O., Baumann, C., Duerr, D., Schlegel, P., Stoll, P., Vergères, G., Dupont, D., & Portmann, R. (2019). Digestion of milk proteins: Comparing static and dynamic *in vitro* digestion systems with *in vivo* data. *Food Research International*, *118*, 32–39. <https://doi.org/10.1016/j.foodres.2017.12.049>
- Eijnatten, E. J. M. van, Roelofs, J. J. M., Camps, G., Huppertz, T., Lambers, T. T., & Smeets, P. A. M. (2023). Gastric coagulation and postprandial amino acid absorption of milk is affected by mineral composition: a randomized crossover trial. *MedRxiv*, 2023.09.13.23295475. <https://doi.org/10.1101/2023.09.13.23295475>
- Fadda, H. M., Hellström, P. M., & Webb, D.-L. (2022). Intra- and inter-subject variability in gastric pH following a low-fat, low-calorie meal. *International Journal of Pharmaceutics*, *625*, 122069. <https://doi.org/10.1016/j.ijpharm.2022.122069>
- Henkelman, R. M., Stanisz, G. J., & Graham, S. J. (2001). Magnetization transfer in MRI: A review. *NMR in Biomedicine*, *14*(2), 57–64. <https://doi.org/10.1002/nbm.683>
- Hoad, C. L., Parker, H., Hudders, N., Costigan, C., Cox, E. F., Perkins, A. C., Blackshaw, P. E., Marciani, L., Spiller, R. C., Fox, M. R., & Gowland, P. A. (2015). Measurement of gastric meal and secretion volumes using magnetic resonance imaging. *Physics in Medicine and Biology*, *60*(3), 1367–1383. <https://doi.org/10.1088/0031-9155/60/3/1367>
- Huppertz, T., & Chia, L. W. (2021). Milk protein coagulation under gastric conditions: A review. *International Dairy Journal*, *113*, 104882. <https://doi.org/10.1016/j.idairyj.2020.104882>
- Jones, C. K., Huang, A., Xu, J., Edden, R. A. E., Schär, M., Hua, J., Oskolkov, N., Zacà, D., Zhou, J., McMahon, M. T., Pillai, J. J., & van Zijl, P. C. M. (2013). Nuclear Overhauser enhancement (NOE) imaging in the human brain at 7T. *NeuroImage*, *77*, 114–124. <https://doi.org/10.1016/j.neuroimage.2013.03.047>
- Kethireddipalli, P., & Hill, A. R. (2015). Rennet Coagulation and Cheesemaking Properties of Thermally Processed Milk: Overview and Recent Developments. *Journal of Agricultural and Food Chemistry*, *63*(43), 9389–9403. <https://doi.org/10.1021/jf504167v>
- Kim, M., Gillen, J., Landman, B. A., Zhou, J., & Van Zijl, P. C. M. (2009). Water saturation shift referencing (WASSR) for chemical exchange saturation transfer (CEST) experiments. *Magnetic Resonance in Medicine*, *61*(6), 1441–1450. <https://doi.org/10.1002/mrm.21873>
- Kong, F., & Singh, R. P. (2010). A Human Gastric Simulator (HGS) to Study Food Digestion in Human Stomach. *Journal of Food Science*, *75*(9), E627–E635. <https://doi.org/10.1111/j.1750-3841.2010.01856.x>
- Lajterer, C., Levi, C. S., & Lesmes, U. (2022). An *in vitro* digestion model accounting for sex differences in gastro-intestinal function and its application to study differential protein digestibility. *Food Hydrocolloids*, *132*(June), 107850. <https://doi.org/10.1016/j.foodhyd.2022.107850>
- Le Feunteun, S., Al-Razaz, A., Dekker, M., George, E., Laroche, B., & van Aken, G. (2021). Physiologically Based Modeling of Food Digestion and Intestinal Microbiota: State of the

- Art and Future Challenges. An INFOGEST Review. *Annual Review of Food Science and Technology*, 12(1), 149–167. <https://doi.org/10.1146/annurev-food-070620-124140>
- Le Feunteun, S., Mackie, A. R., & Dupont, D. (2020). In silico trials of food digestion and absorption: how far are we? *Current Opinion in Food Science*, 31, 121–125. <https://doi.org/10.1016/j.cofs.2020.04.006>
- Le Feunteun, S., Ouethrani, M., & Mariette, F. (2012). The rennet coagulation mechanisms of a concentrated casein suspension as observed by PFG-NMR diffusion measurements. *Food Hydrocolloids*, 27(2), 456–463. <https://doi.org/10.1016/j.foodhyd.2011.09.008>
- Leforestier, R., Mariette, F., & Musse, M. (2021). Impact of chemical exchange on transverse relaxation at low and moderate magnetic field strengths for sugar solutions representative of fruit tissues analyzed by simulation and MRI experiments. *Journal of Magnetic Resonance*, 322, 106872. <https://doi.org/10.1016/j.jmr.2020.106872>
- Lucey, J. A., Teo Cheng Tet, Munro, P. A., & Singh, H. (1997). Rheological properties at small (dynamic) and large (yield) deformations of acid gels made from heated milk. *Journal of Dairy Research*, 64(4), 591–600. <https://doi.org/10.1017/S0022029997002380>
- Malagelada, J.-R., Longstreth, G. F., Summerskill, W. H. J., & Go, V. L. W. (1976). Measurement of Gastric Functions During Digestion of Ordinary Solid Meals in Man. *Gastroenterology*, 70(2), 203–210. [https://doi.org/10.1016/S0016-5085\(76\)80010-8](https://doi.org/10.1016/S0016-5085(76)80010-8)
- Marciani, L., Gowland, P. A., Fillery-Travis, A., Manoj, P., Wright, J., Smith, A., Young, P., Moore, R., & Spiller, R. C. (2001). Assessment of antral grinding of a model solid meal with echo-planar imaging. *American Journal of Physiology-Gastrointestinal and Liver Physiology*, 280(5), G844–G849. <https://doi.org/10.1152/ajpgi.2001.280.5.G844>
- Ménard, O., Bourlieu, C., De Oliveira, S. C., Dellarosa, N., Laghi, L., Carrière, F., Capozzi, F., Dupont, D., & Deglaire, A. (2018). A first step towards a consensus static *in vitro* model for simulating full-term infant digestion. *Food Chemistry*, 240(2017), 338–345. <https://doi.org/10.1016/j.foodchem.2017.07.145>
- Ménard, O., Cattenoz, T., Guillemin, H., Souchon, I., Deglaire, A., Dupont, D., & Picque, D. (2014). Validation of a new *in vitro* dynamic system to simulate infant digestion. *Food Chemistry*, 145, 1039–1045. <https://doi.org/10.1016/j.foodchem.2013.09.036>
- Menard, O., Lesmes, U., Shani-Levi, C. S., Araiza Calahorra, A., Lavoisier, A., Morzel, M., Rieder, A., Feron, G., Nebbia, S., Mashiah, L., Andres, A., Bornhorst, G., Carrière, F., Egger, L., Gwala, S., Heredia, A., Kirkhus, B., Macierzanka, A., Portman, R., ... Dupont, D. (2023). Static *in vitro* digestion model adapted to the general older adult population: an INFOGEST international consensus. *Food & Function*, 14(10), 4569–4582. <https://doi.org/10.1039/D3FO00535F>
- Miltenburg, J., Bastiaan-Net, S., Hoppenbrouwers, T., Wichers, H., & Hettinga, K. (2024). Gastric clot formation and digestion of milk proteins in static *in vitro* infant gastric digestion models representing different ages. *Food Chemistry*, 432, 137209. <https://doi.org/10.1016/j.foodchem.2023.137209>
- Mori, H., Verbeure, W., Schol, J., Carbone, F., & Tack, J. (2022). Gastrointestinal hormones and regulation of gastric emptying. *Current Opinion in Endocrinology, Diabetes & Obesity*, 29(2), 191–199. <https://doi.org/10.1097/MED.0000000000000707>
- Mulet-Cabero, A. I., Egger, L., Portmann, R., Ménard, O., Marze, S., Minekus, M., Le Feunteun, S., Sarkar, A., Grundy, M. M. L., Carrière, F., Golding, M., Dupont, D., Recio, I., Brodkorb, A., & Mackie, A. (2020). A standardised semi-dynamic: *in vitro* digestion method suitable for food-an international consensus. *Food and Function*, 11(2), 1702–1720. <https://doi.org/10.1039/c9fo01293a>
- Mulet-Cabero, A. I., Mackie, A. R., Wilde, P. J., Fenelon, M. A., & Brodkorb, A. (2019). Structural mechanism and kinetics of *in vitro* gastric digestion are affected by process-induced

- changes in bovine milk. *Food Hydrocolloids*, 86, 172–183.  
<https://doi.org/10.1016/j.foodhyd.2018.03.035>
- Murray, D., & Abell, T. (2018). Neural Control of the Gastrointestinal System. In *Neuromodulation* (pp. 1373–1378). Elsevier. <https://doi.org/10.1016/B978-0-12-805353-9.00114-5>
- Musse, M., Le Feunteun, S., Collewet, G., Ravilly, M., Quellec, S., Ossemond, J., Morzel, M., Challos, S., Nau, F., & Lucas, T. (2023). Quantitative magnetic resonance imaging of *in vitro* gastrointestinal digestion of a bread and cheese meal. *Food Research International*, 169, 112821–112833.
- Payal, A., Elumalai, A., Murugan, S. V., Moses, J. A., & Anandharamakrishnan, C. (2021). An investigation on gastric emptying behavior of apple in the dynamic digestion model ARK® and its validation using MRI of human subjects – A pilot study. *Biochemical Engineering Journal*, 175, 108134. <https://doi.org/10.1016/j.bej.2021.108134>
- Rehfeld, J. F. (2008). The art of measuring gastrin in plasma: A dwindling diagnostic discipline? *Scandinavian Journal of Clinical and Laboratory Investigation*, 68(5), 353–361.  
<https://doi.org/10.1080/00365510701771831>
- Rehfeld, J. F., Bardram, L., Hilsted, L., Poitras, P., & Goetze, J. P. (2012). Pitfalls in Diagnostic Gastrin Measurements. *Clinical Chemistry*, 58(5), 831–836.  
<https://doi.org/10.1373/clinchem.2011.179929>
- Roelofs, J. J. M., van Eijnatten, E. J. M., Prathumars, P., de Jong, J., Wehrens, R., Esser, D., Janssen, A. E. M., & Smeets, P. A. M. (2023). Gastric emptying and nutrient absorption of pea protein products differing in heat treatment and texture: A randomized in vivo crossover trial and *in vitro* digestion study. *Food Hydrocolloids*, 109596.  
<https://doi.org/10.1016/j.foodhyd.2023.109596>
- Sánchez-Rivera, L., Ménard, O., Recio, I., & Dupont, D. (2015). Peptide mapping during dynamic gastric digestion of heated and unheated skimmed milk powder. *Food Research International*, 77, 132–139.  
<https://doi.org/https://doi.org/10.1016/j.foodres.2015.08.001>
- Scheidegger, R., Vinogradov, E., & Alsop, D. C. (2011). Amide proton transfer imaging with improved robustness to magnetic field inhomogeneity and magnetization transfer asymmetry using saturation with frequency alternating RF irradiation. *Magnetic Resonance in Medicine*, 66(5), 1275–1285. <https://doi.org/10.1002/mrm.22912>
- Shaffer, J. J., Mani, M., Schmitz, S. L., Xu, J., Owusu, N., Wu, D., Magnotta, V. A., & Wemmie, J. A. (2020). Proton Exchange Magnetic Resonance Imaging: Current and Future Applications in Psychiatric Research. *Frontiers in Psychiatry*, 11.  
<https://doi.org/10.3389/fpsy.2020.532606>
- Simegn, G. L., Van der Kouwe, A. J. W., Robertson, F. C., Meintjes, E. M., & Alhamud, A. (2019). Real-time simultaneous shim and motion measurement and correction in glycoCEST MRI using double volumetric navigators (DvNavs). *Magnetic Resonance in Medicine*, 81(4), 2600–2613. <https://doi.org/10.1002/mrm.27597>
- Stancanello, J., Terreno, E., Castelli, D. D., Cabella, C., Uggeri, F., & Aime, S. (2008). Development and validation of a smoothing-splines-based correction method for improving the analysis of CEST-MR images. *Contrast Media & Molecular Imaging*, 3(4), 136–149.  
<https://doi.org/10.1002/cmimi.240>
- van der Meulen, P., Groen, J. P., Tinus, A. M. C., & Bruntink, G. (1988). Fast Field Echo imaging: An overview and contrast calculations. *Magnetic Resonance Imaging*, 6(4), 355–368.  
[https://doi.org/10.1016/0730-725X\(88\)90472-9](https://doi.org/10.1016/0730-725X(88)90472-9)
- van Eijnatten, E. J. M., Camps, G., Guerville, M., Fogliano, V., Hettinga, K., & Smeets, P. A. M. (2023). Milk coagulation and gastric emptying in women experiencing gastrointestinal

- symptoms after ingestion of cow's milk. *Neurogastroenterology & Motility*.  
<https://doi.org/10.1111/nmo.14696>
- van Zijl, P. C. M., Lam, W. W., Xu, J., Knutsson, L., & Stanisiz, G. J. (2018). Magnetization Transfer Contrast and Chemical Exchange Saturation Transfer MRI. Features and analysis of the field-dependent saturation spectrum. *NeuroImage*, *168*, 222–241.  
<https://doi.org/10.1016/j.neuroimage.2017.04.045>
- Vardakou, M., Mercuri, A., Barker, S. A., Craig, D. Q. M., Faulks, R. M., & Wickham, M. S. J. (2011). Achieving Antral Grinding Forces in Biorelevant *in vitro* Models: Comparing the USP Dissolution Apparatus II and the Dynamic Gastric Model with Human *in vivo* Data. *AAPS PharmSciTech*, *12*(2), 620–626. <https://doi.org/10.1208/s12249-011-9616-z>
- Wang, X., Ye, A., Lin, Q., Han, J., & Singh, H. (2018). Gastric digestion of milk protein ingredients: Study using an *in vitro* dynamic model. *Journal of Dairy Science*, *101*(8), 6842–6852. <https://doi.org/10.3168/jds.2017-14284>
- Wermter, F. C., Bock, C., & Dreher, W. (2022). Characterization of amine proton exchange for analyzing the specificity and intensity of the CEST effect: from humans to fish. *NMR in Biomedicine*, *35*(2). <https://doi.org/10.1002/nbm.4622>
- Windschuh, J., Zaiss, M., Meissner, J. E., Paech, D., Radbruch, A., Ladd, M. E., & Bachert, P. (2015). Correction of B1-inhomogeneities for relaxation-compensated CEST imaging at 7T. *NMR in Biomedicine*, *28*(5), 529–537. <https://doi.org/10.1002/nbm.3283>
- Witschey, W. R. T., Borthakur, A., Elliott, M. A., Mellon, E., Niyogi, S., Wallman, D. J., Wang, C., & Reddy, R. (2007). Artifacts in T1ρ-weighted imaging: Compensation for B1 and B0 field imperfections. *Journal of Magnetic Resonance*, *186*(1), 75–85.  
<https://doi.org/10.1016/j.jmr.2007.01.015>
- Wolff, S. D., & Balaban, R. S. (1989). Magnetization transfer contrast (MTC) and tissue water proton relaxation *in vivo*. *Magnetic Resonance in Medicine*, *10*(1), 135–144.  
<https://doi.org/10.1002/mrm.1910100113>
- Ye, A., Cui, J., Dagleish, D., & Singh, H. (2016). The formation and breakdown of structured clots from whole milk during gastric digestion. *Food & Function*, *7*(10), 4259–4266.  
<https://doi.org/10.1039/C6FO00228E>
- Ye, A., Liu, W., Cui, J., Kong, X., Roy, D., Kong, Y., Han, J., & Singh, H. (2019). Coagulation behaviour of milk under gastric digestion: Effect of pasteurization and ultra-high temperature treatment. *Food Chemistry*, *286*, 216–225.  
<https://doi.org/10.1016/j.foodchem.2019.02.010>
- Zaiß, M., Schmitt, B., & Bachert, P. (2011). Quantitative separation of CEST effect from magnetization transfer and spillover effects by Lorentzian-line-fit analysis of z-spectra. *Journal of Magnetic Resonance*, *211*(2), 149–155.  
<https://doi.org/10.1016/j.jmr.2011.05.001>
- Zhang, Y., Yong, X., Liu, R., Tang, J., Jiang, H., Fu, C., Wei, R., Hsu, Y., Sun, Y., Luo, B., & Wu, D. (2020). Whole-brain chemical exchange saturation transfer imaging with optimized turbo spin echo readout. *Magnetic Resonance in Medicine*, *84*(3), 1161–1172.  
<https://doi.org/10.1002/mrm.28184>
- Zhang, Y., Zu, T., Liu, R., & Zhou, J. (2023). Acquisition sequences and reconstruction methods for fast chemical exchange saturation transfer imaging. *NMR in Biomedicine*, *36*(6).  
<https://doi.org/10.1002/nbm.4699>
- Zhou, Y., Bie, C., van Zijl, P. C. M., & Yadav, N. N. (2023). The relayed nuclear Overhauser effect in magnetization transfer and chemical exchange saturation transfer MRI. *NMR in Biomedicine*, *36*(6). <https://doi.org/10.1002/nbm.4778>



**CHAPTER**





# Summary

## Samenvatting

## Summary

Proteins are indispensable building blocks of life, serving numerous structural and biochemical functions in our bodies. These vital molecules are synthesized in our cells from amino acids (AAs), categorized into essential and non-essential AAs. Essential AAs (EAAs) must be obtained from dietary proteins. The nutritional benefits of dietary proteins depend on how well the latter are broken down into absorbable AAs within our digestive tract. Milk is a widely consumed source of high-quality proteins, namely caseins and whey proteins (WPs). However, food processing, such as heat treatment, may affect the structure, and subsequent digestion of milk proteins (MPs).

The digestion of MPs starts in the stomach, which involves acid- and pepsin-induced aggregation of caseins, resulting in the formation of a semi-solid protein coagulum. This process regulates the gradual release of proteins into the intestinal tract, preventing an overload of the digestive capacity of the intestines. Gastric digestion of proteins is commonly studied using *in vitro* and *in vivo* animal digestion models. However, findings from these studies need to be verified with *in vivo* digestion data from humans, which is challenging due to the lack of non-invasive, spatially-resolved, methods to quantitatively measure changes in the gastric content during digestion. Magnetic Resonance Imaging (MRI) is a non-invasive technique that can be used to obtain detailed images, with imaging contrast based on the local composition and structure of tissues or food systems: this makes MRI highly promising for investigating gastric digestion. Hence, the aim of this thesis was to address the above-mentioned research gap by exploring  $^1\text{H}$  MRI techniques, namely Magnetization Transfer (MT), Chemical Exchange Saturation Transfer (CEST) and conventional  $T_2$ -weighted MRI, for assessing gastric MP digestion, both *in vitro* and *in vivo*.

To this aim, in **Chapter 2** and **3**, we first implemented  $^1\text{H}$  MT and CEST MRI measurements on a 7 T laboratory MRI scanner to optimize measurement parameters, and explore the sensitivity of MT and CEST to the structural and chemical changes that occur during gastric digestion using static *in vitro* samples. Furthermore, the sensitivity of MT and CEST to the effect of heat treatment on gastric MP digestion was assessed by comparing raw- and heated (30 min at 80 °C, 90% WP denaturation) skim milk.

This work showed that the  $^1\text{H}$  magnetization transfer between semi-solid macromolecules and water, quantified by the MT ratio ( $MTR$ ), is a marker of gastric MP coagulum formation and solubilization. Additionally, the assessment of the  $^1\text{H}$  chemical exchange between soluble proteins/peptides and water, quantified by the  $MTR_{asym}$  parameter, was established as a marker of protein hydrolysis, and changes in protein/peptide concentration under static *in vitro* conditions. The trends in the  $MTR$  and  $MTR_{asym}$  vs. digestion time were different for raw- and heated skim milk, thus demonstrating the sensitivity of these MRI markers to heat-induced changes in the gastric digestion of MPs. Furthermore, intensity thresholding of  $T_2$ -weighted images enabled estimating the semi-solid volume representing the coagulum, and monitoring its changes during digestion. By integrating MT and CEST MRI with  $T_2$ -weighted MRI, both macroscopic and molecular-level changes occurring during static *in vitro* gastric digestion could be monitored.

To move towards the dynamic complexity of *in vivo* gastric digestion, in **Chapter 4** the previously developed MRI markers were further explored for probing gastric digestion in a semi-dynamic *in vitro* model using WP isolate solution (WPIS), as well as low- and high-pasteurized skim milk (LPSM and HPSM, respectively). LPSM was a commercially available skim milk, which is typically heated for 15 s at 72 °C, resulting 3% WP denaturation. HPSM was prepared from LPSM by heating it for 30 min at 80 °C, resulting 90% WP denaturation.

Variations in pH and protein concentration were the dominant factors affecting the  $MTR_{asym}$  under semi-dynamic gastric conditions. Given the critical role of pH in gastric digestion, CEST MRI was further developed as an indirect method for pH mapping. This method enabled accurate estimation of the pH for WPIS within a pH range of 4.5-7. Additionally, *in situ* pH maps during gastric digestion could be

obtained using a 3 T clinical MRI scanner. Furthermore,  $T_2$ -weighted imaging, combined with respective  $MTR$  mapping of semi-solid proteins, enabled *in situ* assessment of the volume and consistency of the coagulum during digestion.

Overall, these results demonstrated the capability of MT, CEST and  $T_2$ -weighted MRI to capture the variations in pH and coagulation dynamics during gastric digestion.

**Chapter 5** expanded on the promising results of the *in vitro* work with an *in vivo* study in humans. The aim of the study was to assess the translatability of the optimized MT MRI measurements to *in vivo* monitoring of gastric MP coagulation. Participants ( $n = 12$ ) underwent gastric MRI scans at baseline and after consumption of 300 g of either LPSM or HPSM. The coagulation and gastric emptying dynamics were evaluated using the  $MTR$ , total gastric content (TGC), semi-solid, and liquid volumes.

The findings demonstrated that the  $MTR$  parameter can serve as a suitable marker for measuring MP coagulation during gastric digestion in humans. The observed trend in the  $MTR$  for LPSM was consistent with what was observed in the semi-dynamic model of **Chapter 4**. Interestingly, while no differences were found in the  $MTR$  between LPSM and HPSM, the TGC, semi-solid, and liquid volumes indicated a slower gastric emptying for HPSM compared to LPSM. **Chapter 5** underscored the potential of MRI as a valuable tool to non-invasively measure intra-gastric processes during digestion in humans. These findings demonstrate that the effect of heat treatment on gastric milk protein digestion may be different in humans compared to what has been observed in *in vitro* or animal models. This highlights the importance of conducting *in vivo* studies in humans when investigating the effects of heat treatment on digestion.

Finally, in **Chapter 6** the findings from the preceding chapters were jointly discussed and put into a broader perspective. First, a thorough discussion on the strengths and limitations of  $^1\text{H}$  MT and CEST MRI in the context of digestion research was provided, accompanied by suggestions for future improvements.

Next, a direct comparison between the semi-dynamic *in vitro* and human *in vivo* data was presented. This comparison showed that gastric digestion of LPSM is realistically mimicked in the semi-dynamic *in vitro* model, given that the differences between *in vitro* and *in vivo* results in terms of *MTR*, semi-solid or liquid volumes were relatively small ( $\leq 12\%$ ). Conversely, for HPSM, substantial differences around 40% were observed between the *in vitro* and *in vivo* data of the *MTR*, and semi-solid and liquid volumes. This discrepancy could potentially stem from an oversimplified representation of the gastric emptying, secretion and mixing within the *in vitro* model. Suggestions for improving these aspects of the *in vitro* model in the future were provided. Finally, an outlook towards future studies of gastric digestion with MRI was proposed, including studies across different populations and/or of different foods.

## Samenvatting

Eiwitten zijn belangrijke bouwstenen van het leven en hebben belangrijke structurele en biochemische functies in ons lichaam. Wij kunnen eiwitten verkrijgen uit onze voeding. De gezondheidsvoordelen van eiwitten hangen echter af van hoe goed ze worden afgebroken tot opneembare aminozuren in ons maag-darmkanaal. Melk is een bron van hoogwaardige eiwitten, namelijk caseïne en wei-eiwitten.

Voordat melk in de supermarkt terechtkomt, wordt het verhit om het veilig en lang houdbaar te maken. Dit proces kan de structuur van de eiwitten veranderen en daarmee de daaropvolgende vertering van melkeiwitten beïnvloeden.

De vertering van melkeiwitten begint in de maag, waarbij onder invloed van zuur en het enzym pepsine de caseïnes aan elkaar gaan kleven en stollen, een proces dat coagulatie wordt genoemd. Dit leidt tot de vorming van een eiwitgel in onze maag, die veel op kaas lijkt. Dit proces is belangrijk omdat het ervoor zorgt dat de eiwitten geleidelijk worden afgegeven aan het darmkanaal, waardoor een overbelasting van de verteringscapaciteit van de darmen wordt voorkomen. De vertering van eiwitten in de maag wordt vaak bestudeerd in het laboratorium of bij dieren. Dit is echter niet representatief voor hoe de vertering in het menselijke lichaam plaatsvindt. Om de vertering direct in het menselijke lichaam te kunnen meten, zijn niet-invasieve meettechnieken nodig waarmee veranderingen in de maaginhoud kwantitatief gevolgd kunnen worden.

Magnetic Resonance Imaging (MRI) is een niet-invasieve techniek die kan worden gebruikt om gedetailleerde beelden te verkrijgen van het menselijk lichaam, waarbij het contrast iets zegt over de lokale samenstelling en structuur van het weefsel of de inhoud van de maag of darmen. Dit maakt MRI veelbelovend voor onderzoek naar vertering. Het doel van dit proefschrift was dan ook om verschillende MRI-technieken te gebruiken om de vertering van melkeiwitten in de maag te volgen, zowel met laboratoriummodellen als direct in het menselijke lichaam.

De MRI-technieken die in dit proefschrift zijn gebruikt, waren conventionele  $T_2$ -gewogen anatomische MRI-beelden, magnetisatie-overdracht MRI, en chemische uitwisseling MRI

**$T_2$ -gewogen MRI:** In  $T_2$ -gewogen MRI-beelden worden weefsels of componenten met een lange  $T_2$ -relaxatietijd, zoals vloeistoffen, helder (wit) weergegeven, terwijl weefsels of andere componenten met een korte  $T_2$ -relaxatietijd, zoals orgaanweefsels of bot, donker (grijs tot zwart) verschijnen. Deze beelden worden gebruikt in onderzoek naar spijsvertering om de maaginhoud te onderscheiden van het omringende weefsel. Zo kan de maaginhoud over tijd gekwantificeerd worden als maatstaf voor maaglediging.

**Magnetisatieoverdracht MRI:** Met deze techniek kan de interactie tussen grote moleculen (macromoleculen), zoals eiwitten in een gel of vaste toestand, en water gemeten worden. De mate van magnetisatie-overdracht geeft een indicatie van hoe vast de matrix is waarin de macromoleculen zich bevinden.

**Chemische-uitwisselings-MRI:** Met deze techniek kan de chemische uitwisseling van protonen tussen water en mobiele moleculen, zoals eiwitten en peptiden in oplossing, worden gemeten. Dit dient als maatstaf voor de pH, de eiwit-concentratie en structuur.

Met dit doel hebben we in **hoofdstuk 2** en **3** eerst magnetisatieoverdracht- en chemische-uitwisselings-MRI-metingen opgezet en uitgevoerd op een 7T laboratorium-MRI-scanner. We wilden de meetparameters optimaliseren en de gevoeligheid van deze metingen voor de structurele en chemische veranderingen tijdens de vertering van melkeiwitten onderzoeken. Hiervoor hebben we gebruikgemaakt van een eenvoudig laboratoriummodel om de biochemische vertering van eiwitten in de maag na te bootsen. Dit werk toonde aan dat de ontwikkelde metingen geschikt waren om de coagulatie en afbraak van eiwitten, evenals veranderingen in pH en eiwitconcentratie, te volgen tijdens de vertering in een laboratoriummodel. We hebben ook aangetoond dat de vertering van rauwe en verhitte melk aanzienlijk verschilt onder deze verteringscondities.

Om meer inzicht te krijgen in de dynamische complexiteit van de vertering in het menselijk lichaam, werd in **hoofdstuk 4** een semi-dynamisch laboratoriummodel voor de maagvertering opgezet en gebruikt. In dit semi-dynamische model wordt de geleidelijke afscheiding van maagzuur en pepsine, evenals de lediging van de maaginhoud, nagebootst. Onder deze dynamische omstandigheden waren variaties in pH en eiwitconcentratie de dominante factoren die de chemische uitwisseling beïnvloedden. Gezien de kritieke rol van pH in de maag, werd chemische-uitwisselings-MRI verder ontwikkeld als een indirecte methode voor het in kaart brengen van de pH gedurende de vertering. Met deze methode was het mogelijk om de pH tijdens de vertering van een wei-eiwitdrink te volgen. Daarnaast ontdekten we dat onder de semi-dynamische verteringscondities de eiwitcoagulatie langzamer verliep vergeleken met die in het eenvoudige model van hoofdstuk 2 en 3. We maakten gebruik van een computer-algoritme om in de T<sub>2</sub>-gewogen MRI-beelden de gecoaguleerde melk (lage intensiteit, donker) en de vloeistof (hoge intensiteit, helder) van elkaar te onderscheiden op basis van hun intensiteit. Dit kon gebruikt worden om het volume van het eiwitcoagulaat gedurende de vertering te meten. Verder kon magnetisatieoverdracht-MRI ook hier gebruikt worden om de eiwitcoagulatie te volgen en om verschillen daarin tussen laag- en hoogverhitte melk in kaart te brengen.

**Hoofdstuk 5** breidde de resultaten van het laboratoriumwerk uit met een onderzoek bij mensen. Het doel van de studie was om de geoptimaliseerde MRI-metingen toe te passen om de eiwitvertering van laag- en hoogverhitte melk te onderzoeken. Twaalf vrijwilligers ondergingen MRI-scans van de maag na minstens 11 uur vasten en na consumptie van 300 g laag- of hoogverhitte melk. Magnetisatieoverdracht-MRI werd gebruikt om de coagulatie van melk te volgen, en T<sub>2</sub>-gewogen MRI-beelden werden gebruikt om de maaglediging te volgen.

De bevindingen toonden aan dat het meten van de magnetisatieoverdracht ook geschikt is voor het volgen van de melkeiwitcoagulatie in de maag direct bij mensen. Voor laag-verhitte melk was de trend in de magnetisatieoverdracht tijdens de vertering vergelijkbaar met die in het semi-dynamisch laboratoriummodel van hoofdstuk 4. Interessant genoeg werden in deze studie geen verschillen gevonden in de coagulatie van laag- en hoogverhitte melk, maar de maaglediging van laagverhitte melk was sneller dan die van hoogverhitte melk.



Dit is in tegenstelling tot de bevindingen uit dieronderzoeken bij varkens en ratten. Hoofdstuk 5 onderstreepte niet alleen het potentieel van MRI als waardevol hulpmiddel om processen tijdens de spijsvertering bij mensen op niet-invasieve wijze te meten, maar toonde ook aan dat het effect van verhitting op de vertering van melkeiwitten anders kan zijn bij mensen dan wat is waargenomen in laboratorium- of diermodellen.

Tot slot werden in **hoofdstuk 6** de bevindingen uit de voorgaande hoofdstukken gezamenlijk besproken en in een breder perspectief geplaatst. Eerst werden de sterke punten en beperkingen van de MRI-technieken in de context van verteringsonderzoek besproken, vergezeld van suggesties voor toekomstige verbeteringen. Vervolgens werd een directe vergelijking tussen spijsvertering in het semi-dynamische laboratorium model en in mensen gepresenteerd. Uit deze vergelijking bleek dat de maagvertering van laagverhitte melk realistisch wordt nagebootst in het laboratoriummodel. Voor hoogverhitte melk werden daarentegen substantiële verschillen waargenomen tussen het laboratoriummodel en mensen. Deze verschillen kunnen mogelijk het gevolg zijn van een te eenvoudige weergave van de maaglediging, de maagafscheidingen en menging binnen het laboratoriummodel. Er werden suggesties gegeven om deze aspecten van het laboratoriummodel in de toekomst te verbeteren. Tot slot werd een vooruitblik gegeven op toekomstige studies naar maagvertering met MRI, zoals studies bij verschillende leeftijdsgroepen en mensen met een spijsverteringsstoornis.







# Appendix

Acknowledgements

List of publications

Overview of completed training activities

About the author

## Acknowledgements

Eight years ago, I visited Wageningen for the first time to attend an event on the Wageningen University campus. My conclusion from that day was that I would never want to study, work, or live in Wageningen. Fast forward four years later and what do you know? I am unpacking my bags in Wageningen to start a PhD. I would like to take this opportunity to thank the wonderful people who have made Wageningen not just bearable, but enjoyable, and those who offered a nice distraction when I wanted to escape my PhD or Wageningen.

First, I would like to thank my co-promotors and promoter. **Camilla**, I am grateful for your thorough guidance and support, not only regarding the project but also concerning my well-being. I admire that you have created a group where constant learning and sharing of knowledge are encouraged, and I appreciate everything I have learned from you about NMR, MRI, giving presentations, writing and teaching. I also enjoyed all the lunches, dinners, conference parties, and escape room experiences.

**Paul**, I really appreciate the enthusiasm you showed for the project from day one. Thank you for all your guidance and patience, despite being so busy, and sometimes providing feedback even at 2 am. I enjoyed working with you, chatting about both scientific and non-scientific topics, and, of course, all your jokes.

**John**, we first met around 6 years ago at Unilever R&D, where I did my MSc thesis. Even then, I appreciated your supervision style, which encouraged me to pursue a PhD under your guidance. Thank you for giving me the freedom to become an independent researcher while always being there to provide guidance when I needed it. I also appreciate that you were always super quick with providing feedback on papers and thesis chapters, which was especially crucial for me in handing in my thesis on time.

To the original NMR group: **Raquel**, **Wouter**, and **Klausha**, I really enjoyed all our (online) coffee breaks after NMR meetings and the trips to Nijmegen and Hamburg. **Raquel**, thank you for making me feel welcome in the group during my MSc thesis and when I started my PhD. I also appreciate that I could always come to you with questions or to vent. **Wouter**, many of my questions during the NMR meetings were directed at you; thank you for helping me understand magnetization transfer NMR a bit better. **Klausha**, we started the PhD journey together, and I feel so fortunate to have you as my PhD/NMR sister. The whole PhD would have been much more difficult to get through if I didn't have you by my side. Thank you for being a fantastic colleague, an amazing paranymph, and a wonderful friend <3.

**Sasan**, thank you for the delicious Turkish food, for which I would also like to thank Esin. **Dmytro**, our time together in the NMR group was quite short but I really enjoyed it. Thank you for being so supportive and always checking up on me even after leaving Wageningen. **Baris**, I enjoyed teaching together with you and discussing relaxation. **Sam**, you have been a great addition to the NMR group. Thank you for the nice collaboration during which we measured your beautiful samples with my beautiful technique 😊. I also enjoyed the tea breaks, dinners, and playing Wingspan.

**Frank**, You might not remember this, but you helped me set up my very first inversion recovery measurement during my master's thesis when no one else was (avail)able to help me. Since then, you have helped me with setting up many more NMR/MRI experiments. Thank you for always being enthusiastic and willing to help when I ask questions or have a problem that needs solving. **John** (Philippi) and **Yanzhang** Thank you for ensuring that everything in MAGNEFY runs smoothly, and for all of your technical support.

To my original BIP office mates and colleagues: **Koen** (Martens), **Tatiana**, **Ahmad**, **Suyeon**, **Abbas**, **Benjamin**, **David**, **Christo**, **Peter** and **Ludo** thank you for the great atmosphere in the office and lab, and during all the fun labuitjes. **Bejamin**, I really enjoyed our chats in the office and lab when we were both working late. I am still waiting for that piano lesson :p. **Christo** and **Peter**, thank you for organizing all the awesome labuitjes and social activities. **Ludo**, we are the only two original pre-corona BIP-ers still in the BIP office. I really enjoyed your tiramisus, the trip to Rennes, trying to sing along to Bollywood and CHIPz songs, and moving random pieces of equipment to hidden rooms in Impulse.

To my new office and group mates: **Jarne**, **Cleo**, **Mariska**, **Keshav**, **Martijn**, **Francesco**, **Lennart** and **Dana**, thank you for making me feel welcome in the group when I returned to BIP. I really enjoyed our most recent board game night and hope we will have more of those soon.

**Cor** and **Ian**, thank you for keeping the lab organized and making sure that everything runs smoothly. **Cor**, I also enjoyed the many afternoons we spent teaching together in room P6010. **Emilie**, I enjoyed teaching the introductory physics practicals with you. Thank you for being so easy-going and patient, which made me less nervous about having to teach physics. **Arjen**, thank you for your help with the microscopy measurements. **Annelies**, I enjoyed our chats about teaching and careers, and your final tips before the deadline of my thesis were very handy, thank you!

**Laavanya**, the coffee breaks and walks around the campus or Wageningen were always a nice distraction. I also enjoyed our fun day trips and all the delicious Indian food, for which I would also like to extend my thanks to Siva.

**Centje** (Vincent), the most delicious pizzas that I have eaten in the Netherlands were at your house; thank you for those! I also really appreciate your energetic and easy-going personality, which made the long road trips to Rennes and Aarhus more fun.

**Gert-Jan, Ewoud, Niels, and Donny**, Thank you for introducing me to NMR and MRI. It is always nice running into you again in MAGNEFY or at conferences. **Gert-Jan** thank you for the nice conversations in MAGNEFY, and your help with NMR and MRI measurements. **Ewoud**, I suppose when we briefly shared an office at Unilever, you did not expect that years later you would still receive emails from me about statistics. Thank you for taking time out of your busy schedule to send elaborate answers to all my questions.

I would also like to thank **Herbert, Ciaran** and **Kees** for making me feel welcome in their research groups and for facilitating a nice atmosphere. **Brenda, Sjanneke, Jasmijn** and **Gea** thank you for all your help and quick replies to my emails.

To the TKI digestion team, **Julie, Kasper, Harry, Shanna** and **Tamara**, Thank you for the nice atmosphere during the internal monthly and consortium meetings. I really enjoyed working with you on this project. **Kasper**, thank you for sharing your in-depth knowledge of dairy proteins and digestion and for ensuring the project ran smoothly. I am also grateful that I could always meet with you to discuss new results that were hard to understand, often feeling more motivated after these meetings. **Julie**, I cannot imagine a better person to have at my side during this project. Thank you for all the chats and discussions about doing a PhD, digestion, and milk. I really appreciate your support over the past 4+ years!

To the consortium partners: **Tim, Carolien, Paulien, Evan, Tao, Paula, Gabriele** and **Ruth**, thank you for your valuable questions and suggestions during the consortium meetings.

**Jeanine**, Thank you for your help with the 7T MRI measurements and for always being open to discuss *in vivo* MRI measurements. **Paul** (de Bruin), thank you for your help with the 3T MRI measurements. I truly value all the early mornings and late evenings during which you helped me with setting up the CEST measurements or conducting pilot scans. I am grateful for everything I learned from you, and your support was crucial to the completion of my thesis.

To my MRI/digestion colleagues at HNH, **Ruoxuan, Elise, Julia, Dan** (Liu), **Louise**, and **Xinhang**, I enjoyed our lunch dates and all the chats about MRI, digestion, and beyond. **Louise**, I really appreciate that I could vent to you about the struggles of METC applications, and I also enjoyed spending time together at the MRI scanner.

**Corine**, thank you for your help with working in the kitchen. **Anne** (v/d Wiel), thank you for ordering almost every chemical I needed for my experiments and



for your help in recruiting participants. **Koen** (Manusama), thank you for your help in the research unit, especially with moving around a giant water bath. I also appreciate how you care for the well-being of all the PhD students in the division. In my opinion, you are one of the most valuable people in HNH.

To my friends at HNH: **Tesfaye, Pari, Tsitsi, Abisola, Marjolein, Taonga, Ismet, Dan** (Kirk), and **Romain**, I enjoyed all the fun coffee and lunch breaks and sharing the office with you! **Tesfaye**, thank you for all your wise advice, being open to talk about anything, and opening your home to me. I also appreciate the super delicious Ethiopian food, for which I would also like to thank your wife. **Pari** and **Tsitsi**, as the only girl in my family, I often missed having a sister. Thank you both for all your sisterly advice on both personal and professional matters. **Pari**, thank you for sharing your delicious Iranian food with me. I also appreciate your passionate and direct personality, and making me feel like I can come to you about anything. Thank you for being a wonderful friend. **Abisola**, I am sorry for distracting you from your work even after I left HNH. I don't have a good excuse other than that I really like you and need my daily dose of Abisola. Thank you for being a wonderful and kind friend. The last few months of the PhD were more bearable because of you! **Marjolein**, I admire your positive and energetic personality, and thank you for always being open to talk about anything. **Taonga**, thank you for being the best neighbour in office 1027, and it's always a nice surprise to see you pop up in Helix/Impulse again. **Ismet**, some of the best and most thought-provoking conversations I have had were with you. Thank you for always being up for a talk and encouraging me when I was doubting myself. **Dan**, I enjoyed playing Wordle and Heardl with you. Your discipline and work ethic always motivated me to stop complaining and overthinking and just get things done. Thank you. **Romain**, I enjoyed our talks about research and careers, and appreciate your calm nature, which luckily was contagious at times.

I would also like to thank my students, who were invaluable to this thesis. **Dirk**, I cannot imagine a better first student. You really impressed me with your independence and how quickly you learned everything. I am also happy that I inspired you to follow in my footsteps by participating in the COAST honours program and pursuing the analytical science master's in Amsterdam. I wish you all the best during your own PhD journey; I am sure you will do great! **Lucas**, I appreciate your enthusiasm for lab work, and I really enjoyed conducting digestion experiments with you, even when we had to start very early in the morning. **Mart**, thank you for all your hard work, which sometimes included staying in the hospital until very late to finish the MRI scans. I also enjoyed hearing about your basketball adventures and sharing stories about studying at the HBO. **Miel**, I appreciate the perseverance and growth you showed during your thesis project. I know it wasn't an easy topic, but you made it to the end, and the knowledge we gained from your project ended up being useful for the analysis of the *in vivo* data. I also enjoyed hearing about your rowing adventures and your plans for the future.

**Rosalind**, I also cannot imagine a better last student. Your independence, motivation, and enthusiasm made it fun to work with you. Thank you for sacrificing many of your weekend mornings to conduct the *in vivo* MRI scans with me. Honestly, I don't know how I would have finished in time without your help. I also enjoyed the Indonesian teas and chatting about food!

To my neighbours, who are really much more than just neighbours: **Parnian**, it was so nice to have another Afghan-Dutch person living so close to me. I enjoyed our dinners and the Dari lessons, for which I would also like to thank your mom, تشکر استاد نسرين. **Clementina** and **Nico**, thank you for making Wageningen feel like home with all the lovely BBQs, lunches, and dinners. **Nico**, you are an incredible cook and baker, and I am glad I got to enjoy so many of your delicious creations, including the best vegetarian burger I have ever eaten :p. **Clementina**, my volleyball buddy. While to some people, it might seem like we talked more about going to volleyball than actually going, I am glad we could encourage each other to do at least a little bit of sports during our PhD, even if we spent the first hour of training venting about our PhDs. Thank you for being a wonderful volleyball buddy, friend, and paranymp. **Ane**, I enjoyed all the dinners we shared. Thank you for always offering a listening ear and advice about my PhD.

**Mattia**, you have been supportive since day one of my PhD. Thank you for all the scientific advice, listening to me, challenging me, making me laugh and reminding me that there is life outside of the PhD. I enjoyed all of our mini adventures and look forward to many more of those.

**Sahar**, thank you for asking me a question in the train, and the friendship that followed. I loved our trip to Sicily, which came at the perfect moment to help me get over one of the most difficult moments of my PhD.

**Sanne** and **Insam**, we go waaaay back. I am very grateful that after the bachelor's and master's, we still remained friends even though our lives changed and became much busier. It is always a nice distraction to hang out with you in Leiden, especially at our favourite hotspot! I also want to thank you for all the times you have encouraged me to finish my PhD. **Nadia** and **Wasana**, We also go way back, and despite the many kilometers between us now, I am glad that we are still friends, and I love seeing how your lives have evolved. Thank you for all your support and encouragement.

**Nahid**, I love that I can talk to you about anything, and I am very grateful for your support. One of the perks of doing a PhD was that it allowed me to travel to Denmark for work and hang out with you. Thank you for being a wonderful cousin and friend. **Said**, I am glad there is another science nerd in the family. I really enjoyed chatting with you about research, academia, and career options during family gatherings. Thank you for your encouragement and advice.

**Marieke** en **Macy**, bedankt voor de gezelligheid en de nodige afleiding tijdens verjaardagen, Eid, Nowruz en kerst vieringen. **Nadim** en **Matin**, bedankt dat ik altijd op jullie kan rekenen, voor al jullie waardevolle inzichten en adviezen en hulp bij de verhuizingen in Wageningen. **Mobin**, je bent niet alleen mijn broertje maar ook mijn maatje. Ik kijk er altijd naar uit om tijd met jou door te brengen als ik weer in Boskoop ben, omdat ik met jou altijd de leukste en meest uitdagende gesprekken heb.

Lieve **mama** en **papa**, jullie hebben veel meegemaakt en veel moeten opofferen om ons een goede toekomst te geven. Ik ben enorm dankbaar voor jullie onvoorwaardelijke liefde en steun, en dat jullie mijn grootste supporters zijn! دارم دوستتان

**Merwarid**



## List of publications

### This thesis

**Mayar, M.**, de Vries, M. Smeets, P. A. M., van Duynhoven, J. P. M., & Terenzi, C. (2024) *In vitro*  $^1\text{H}$  MT and CEST MRI mapping of gastro-intestinal milk protein breakdown. *Food Hydrocolloids*, 152, 109866-109878

**Mayar, M.**, Smeets, P. A. M., van Duynhoven, J. P. M., & Terenzi, C. (2023) *In vitro*  $^1\text{H}$  MT and CEST MRI mapping of gastro-intestinal milk protein breakdown. *Food Structure*, 36, 100314-100324

**Mayar, M.**, Miltenburg, J. L., Hettinga, K., Smeets, P. A. M., van Duynhoven, J. P. M., & Terenzi, C. (2022) Non-invasive monitoring of in vitro gastric milk protein digestion kinetics by  $^1\text{H}$  NMR magnetization transfer. *Food Chemistry*, 383, 132545-132555

### Other publications

Smeets, P., Deng, R., Van Eijnatten, E., & **Mayar, M.** (2021) Monitoring food digestion with magnetic resonance techniques. *Proceedings of the Nutrition Society*, 80(2), 148-158

**Mayar, M.** (2020). Spijsvertering ontrafelen met MRI. *Nederlands Tijdschrift voor Natuurkunde* (Unraveling digestion with MRI, published in the Dutch Journal of Physics)

**Mayar, M.**, de Roo, N., Hoos, P., van Duynhoven, J.P.M. (2020).  $^{31}\text{P}$  NMR Quantification of Phospholipids and Lysophospholipids in Food Emulsions. *Journal of Agricultural Food Chemistry*, 68(17), 5009-5017

Zietek, B. **Mayar, M.**, Slagboom, J. et al (2018). Liquid chromatographic nanofractionation with parallel mass spectrometric detection for the screening of plasmin inhibitors and (metallo)proteinases in snake venoms. *Analytical and bioanalytical chemistry*, 410(23):5751-5763

## Overview of completed training activities

<b>Discipline specific activities</b>	<b>Organizer</b>	<b>Year</b>
<i>In vivo</i> NMR	Radboud UMC	2019
Dairy protein biochemistry	University of Aarhus	2019
Reaction kinetics in food science	VLAG	2021
Advanced food analysis	VLAG	2022
NMRdg	Dow Terneuzen	2019
NMRdg	Shell, Amsterdam	2022
Dutch Biophysics	NWO	2020
Dutch Biophysics	NWO	2022
FAST	TI-COAST	2021
MRfood	University of Aarhus	2022
Euromar	Utrecht University	2022
ISMRM & ISMRT annual meeting	ISMRM, Toronto	2023
<b>General courses</b>		
VLAG PhD week	VLAG	2019
Scientific writing	WGS	2021
Project and time management	WGS	2021
Presenting with impact	WGS	2022
Teaching lab practicals	Education Support Centre, WUR	2022
Career perspectives	WGS	2023
<b>Other activities</b>		
Preparation of research proposal	BIP	2019
NMR group meetings	BIP	2019-2023
Tasty talk (research group meeting)	SSEB-HNH	2019-2023

## About the author

Morwarid Mayar was born on April 15, 1995, in Kabul, Afghanistan. Her family moved to the Netherlands when she was 5 years old. After receiving her high school diploma from Coenecoop College in Waddinxveen, her keen interest in life sciences led her to pursue a degree in chemistry at Leiden University of Applied Sciences. She graduated with a BSc in 2017, completing her thesis titled "Screening and Identification of Plasmin Inhibitors and Metalloproteases in Snake Venoms" within the BioAnalytical Chemistry group at the Free University of Amsterdam.



She then pursued a MSc in Analytical Sciences, a joint degree offered by the Free University Amsterdam and the University of Amsterdam. During her master's, she also took part in the COAST MSc+ honours program, focusing on Analytical Technology. During her Master's thesis project, she developed a  $^{31}\text{P}$  NMR method for the quantification of (lyso)phospholipids in food emulsions at Unilever R&D, Vlaardingen.

In 2019, Morwarid embarked on a multidisciplinary PhD project at Wageningen University and Research, working in the laboratory of Biophysics and the division of Human Nutrition and Health. Under the guidance of prof. Dr. John van Duynhoven, Dr. Camilla Terenzi, and Dr. Paul Smeets, she investigated the *in vitro* and *in vivo* gastric digestion of milk proteins using NMR and MRI techniques. The findings of her research are presented in this thesis.

## **Colophon**

The research described in this thesis was performed at the Laboratory of Biophysics, Wageningen University & Research, The Netherlands, and at the division of Human Nutrition and Health, Wageningen University & Research, The Netherlands. This work was part of a public-private partnership supported by the Dutch Ministry of Economic Affairs Top Sector Agri&Food (grant number AF-18012)

Cover design by Lucile Michels and the author

Printed by proefschriftmaken.nl on FSC-certified paper.

Morwarid Mayar, 2024





